



BARD

FINAL REPORT

PROJECT NO. US-1848-90

המסד הלאומי
לנרטיב החקלאות
הישראלי

**Traction*Soil Compaction Tradeoffs as a Function of
Dynamic Soil Tire Interaction Due to Varying Soil and
Loading Conditions**

S.K. Upadhyaya, W.J. Chancellor, D. Wolf, I. Shmulevich, A. Hadas

1995

44592

Date: October 10, 1995

BARD Project NO.: 1848-90R

TITLE:

TRACTION SOIL COMPACTION TRADEOFFS AS A FUNCTION OF
DYNAMIC SOIL TIRE INTERACTION DUE TO VARYING SOIL AND
LOADING CONDITIONS.

Investigators' Name

Investigators Institutions

Shrini K. Upadhyaya

University of California, Davis, USA

William J. Chancellor

University of California, Davis, USA

Dan Wolf

Technion, Haifa, ISRAEL

Itzhak Shmulevich

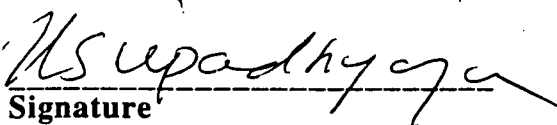
Technion, Haifa, ISRAEL

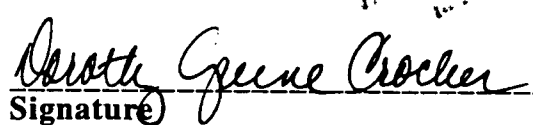
Amos Hadas

ARO, Bet-Dagan, ISRAEL

Project Starting Date: October 1, 1991

Type of Report: FINAL


Signature
Principal Investigator


Signature
Institution's Authorizing Official
Dorothy Greene Crocker
Director of Sponsored Programs

OCT 23 1995

630.72
BAR/UPA
2nd copy

TABLE OF CONTENTS

<u>ITEM</u>	<u>PAGE NO.</u>
I. COVER PAGE	
II. TABLE CONTENTS	1
III. ABSTRACT	3
IV. OBJECTIVES OF THE ORIGINAL RESEARCH	4
V. REVALANT DATA, METHODOLOGY, RESULTS AND DISCUSSION	9
V.1 MODELING TRACTION	9
V.1.1 WHEEL TRACTION PREDICTION ON HARD SOIL	10
V.1.2 THE EFFECT OF DYNAMIC VARYING VELOCITY ON WHEEL TRACTION	28
V.2 DEVELOPMENT OF IMPROVED MEASUREMENT TECHNIQUES RELEVANT SOIL PARAMETERS	38
V.2.1 A NEW FIELD SINGLE WHEEL TESTER	38
V.2.2 TIRE FOOTPRINT CHARACTERISTICS AS A FUNCTION OF SOIL PROPERTIES AND TIRE OPERATION	52
V.2.3 IN-SITU SOIL PROPERTIES MEASURING TECHNIQUES FOR SOIL-TIRE INTERACTION	67
V.2.4 INFLUENCE OF TIRE ACTION ON TOP SOIL COMPACTION	71
V.3 SOIL COMPACTION-CONCEPTS, MODELS, AND MEASUREMENTS	84
V.3.1 SIMULATION OF TIRE TRACTION VERSUS SOIL COMPACTION	84
V.3.2 COMAPRATIVE ANALYSIS OF SOME SOIL COMPACTION MEASUREMENT TECHNIQUES	101
V.3.3 SOIL COMPACTION CAUSED BY HEAVY AXLE LOADS - REVIEW OF CONCEPTS AND EXPERIMENTAL DATA	110

V.4	HYDRAULIC CONDUCTIVITIES OF SOIL AS A FUNCTION OF THEIR VOID RATIO	110
V.4.1	MEASUREMENTS OF HYDRAULIC CONDUCTIVITIES AS A FUNCTION OF VOID RATIOS	110
V.5	DETERMINATION OF ENGINEERING PROPERTIES OF SOIL IN-SITU USING A RESPONSE SURFACE METHODOLOGY	112
V.5.1	DETERMINATION OF ENGINEERING PROPERTIES OF SOIL IN-SITU	115
V.5.2	EXPERIMENTAL VERIFICATION OF THE RESPONSE SURFACE METHODOLOGY	184
V.5.3	MEASUREMENT OF SOIL PARAMETERS RELEVANT TO TRACTION AND TRACTION TESTS	202
V.5.4	DEVELOPMENT OF TRACTION SOIL COMPACTION MODEL	236
VI.	DESCRIPTION OF COOPERATION	287
VII	EVALUATION OF THE RESEARCH ACHIEVEMENT WITH RESPECT TO THE ORIGINAL RESEARCH PROPOSAL AND ITS OBJECTIVES	287
VIII	CONCLUSIONS	289
IX	LIST OF PUBLICATIONS	290

ABSTRACT

The objectives of this study were to investigate soil-pneumatic tire interaction and develop traction-soil compaction prediction model. We have developed an inverse solution technique that employs a response surface methodology to determine engineering properties of soil in-situ. This technique is useful in obtaining actual properties of soil in-situ for use in traction and soil compaction studies rather than using the values obtained in the laboratory by employing remolded and/or disturbed soil samples. We have conducted extensive field tests in the U. S. to develop semi-empirical traction prediction equation for radial ply tires. A user friendly traction-soil compaction program was developed to predict tractive ability of radial ply tires using several different techniques and to estimate soil compaction induced by these tires. A traction prediction model that incorporates strain rate effects on the tractive ability of tires was developed in Israel. A mobile single wheel tester and an in-situ soil test device were developed in Israel to significantly enhance the ability of Israeli investigators to conduct traction-soil compaction research. This project has resulted in close cooperation between UCD, Technion, and ARO, which will be instrumental in future collaboration.

IV. OBJECTIVES OF THE ORIGINAL RESEARCH PROPOSAL

Background: Over the past few decades, tractor sizes have steadily increased. With the growth in power, performance is restricted mainly by the limitations of the traction device(wheels or tracks) imposed by the terrain over which the tractors operate. The tractive efficiency (ratio of drawbar power to axle power) of pneumatic tires ranges from about 90% when operating on concrete to less than 50% on loose or sandy soils (Wulfsohn et al., 1988*). A conservative estimate of the annual fuel loss due to the poor tractive efficiency of agricultural tractors in the United States alone is 152 million gallons(Gill and VandenBerg, 1968). Even the increase in tractive efficiency by a percentage point, amounts to over 25 million dollars saved annually in the U. S. alone. Since drawbar is the most commonly used power outlet of agricultural tractors, the ability to provide draft to pull various types of implements is one of the measure of a tractor's performance. The tractive efficiency with which the pull is achieved is also of importance. Both the pull developed and tractive efficiency depend on the dynamic axle load, inflation pressure, tire type and geometry, and soil type and conditions (Upadhyaya and Wulfsohn, 1989; Wulfsohn, et al., 1988; Upadhyaya, 1988; Yong et al., 1984; Gill and VandenBerg, 1968). For a particular tire working in a given soil type and condition, tractive efficiency depends on dynamic axle load and inflation pressure. Numerous researchers have shown that increased dynamic load on the axle leads to increased tractive performance of the tire (Upadhyaya et al., 1989; Wulfsohn, et al., 1988; Yong, et al., 1984; Wong, 1980; Nowatski and Karafiath, 1978; and Bekker, 1956, 1960). It should be noted that the tractive efficiency does not continue to increase but attains a maximum and then decreases as the dynamic load increases due to increasing motion resistance.

* All references can be found in the body of the text.

Although, increased dynamic load on the axle leads to increased tractive performance, it also increases soil compaction. Soil compaction has been recognized as a major worldwide problem with serious implications for agricultural sustainability (Gupta and Allmaras, 1987). Increased weight of tractors, harvesting equipment and trucks in the past few decades are the main reason for traffic induced soil compaction (Daniel et al., 1988; Voorhees, et al., 1988; Taylor and Gill, 1984; Gameda, et al., 1988; Negi, et al., 1988). Increased soil compaction leads to a reduction in air-filled porosity critical to gaseous diffusion and exchanges in soil; reduced water infiltration and resultant increase in surface flow and soil erosion; collapse of natural structure leading to a coarse seedbed for subsequent crop; increased resistance to root penetration; increased tillage energy requirements; decreased biological activity in the soil (Trowse, 1971; Russel and Goss, 1974; Chancellor, 1977; Gupta and Larson, 1982; Grable, 1981; Bowen, 1982; Taylor and Arkin, 1982; Cannel and Jackson, 1982; Hadas, et al. 1983, 1985, 1988; Hadas and Wolf, 1984; wolf and Hadas, 1983, 1984; LAWR-Cooperative Extension, 1984; Braunack and Freebairn, 1988; Carter et al, 1988; Chamen et al., 1988; Dickson and Campbell, 1988; Raghavan et al, 1988). These factors lead to reduced crop yield, increased energy costs, machinery wear and tear culminating in increased cost and reduced profit (Raghavan, et al, 1979a,b; Negi, et al., 1981; Chamen, et al., 1988, 1990; Dickson and Campbell, 1988; Daniel, et al., 1988; Douglas and Campbell, 1988; Voorhees, et al., 1988). Voorhees(1990) pointed out that the problem of soil compaction has been of concern in the southeastern and south western United States. In recent years, this problem is getting increased attention in the midwest and northern region. The economic loss due to increased soil compaction is estimated to be \$157 million in Canada and \$12 million in Sweden. In the United States, the economic loss due to reduction in yield alone is estimated to be over one billion dollars! (Voorhees, 1990; Raghavan et. al., 1976). It should be noted that the adverse effect of soil compaction depends on soil type, crop type, and available moisture (Soane, 1985). There appears to exist an optimum level of soil compaction which is

beneficial to plant growth. This optimum is higher for monocotyledons grown in coarse textured soils in dry seasons, and lower for dicotyledons grown in fine textured soils in wet season (Soane, 1990). Yield reduction resulting from adverse effect of soil compaction may not always be noticeable. The adverse effect of soil compaction can often be offset by increased use of water and chemicals. However, this increased need for water and chemicals which has undesirable effect on agricultural sustainability should be charged to soil compaction (Poincelot, 1986). Taylor and Gill (1984), Taylor (1990), and Schafer (1990) have emphasized the need for "managing" soil compaction. Thus there is a need to compare the gains in traction due to increased dynamic load with the adverse effect of soil compaction due to heavy axle load. This BARD project was undertaken to address the traction-soil compaction tradeoffs as a function of dynamic load on the axle.

The major objectives of our study were:

1. Develop a comprehensive traction-soil compaction model that incorporates dynamic effects.
2. Develop improved techniques for measuring relevant soil parameters under dynamic loading conditions.
3. Experimentally validate the developed traction-soil compaction model in controlled laboratory trials (soil bins) and in the field.
4. Develop guidelines for agricultural equipment operators (charts and monographs) based on the validated traction-soil compaction model to optimize traction potential while reducing soil compaction.
5. Develop a model based expert system to assist farm equipment operators, dealers, and manufacturers of traction potential versus soil compaction hazards due to soil-pneumatic tire interaction. The knowledge base of the expert system includes a quantitative model to predict traction and soil compaction which employs tire geometric parameters, tire type and loading (vertical load, input axle torque, and inflation pressure) and soil type and condition.

The secondary (specific) objectives of this were:

1. Investigate tractive ability of pneumatic tires as affected by
 - a) tire type, tire geometry, inflation pressure and dynamic load on the axle at various levels of slip;
 - b) soil type and condition- soil density, moisture content, soil structure. Pertinent soil dynamic parameters, which relate the soil-tire interface stresses to the total normal and shear loads, and the rate at which they are applied, may include soil cone index, soil shear modulus, maximum shear stress at failure (cohesion and internal angle of friction), elastic and plastic moduli, and soil sinkage parameters measured under various load rates.
2. Derive quantitative relationship for the 3-D tire imprint dimensions based on soil and tire characteristics and loading.
3. Develop quantitative relationships between net traction, input torque, dynamic axle load (vertical and horizontal), soil condition and strength, and tire parameters as a function of wheel slip.
4. Develop quantitative relationships for compaction within the soil as a function of tire and soil parameters and applied dynamic shear and compressive loading.
5. Combine the above objectives into a rheological-mechanistic model or one based on constitutive laws (e.g. critical state based model) and verify the model experimentally.
6. Incorporate the model as a knowledge base into an expert system to advise farm equipment operators, dealers, and manufacturers of traction-compaction tradeoffs of various pneumatic tires in different soil conditions.

Modifications of the objectives: At the initial meeting between the U.S. and Israeli investigators we decided that U.S. investigators will concentrate on the determination of in-situ determination engineering soil properties (secondary objectives 1a and part of 1b), determination of 3-D soil-tire contact profile (secondary objective #2), development of traction prediction models (secondary objective #3), and the Israeli investigators will concentrate on the dynamic aspects of traction prediction (part of secondary objective #1b),

and developing a soil compaction model (secondary objective #4). At the end of second year of the study when Dr. Upadhyaya visited Israel the project status was evaluated and we decided that dynamic effects were extremely complex and would require much more time and effort to bring to meaningful conclusions. Since even the quasi-static aspects of traction and soil compaction are not well understood, it was thought to be worthwhile to concentrate on the quasi-static aspects. We felt that since most of the agricultural heavy draft operations fall under this category (0 to 5 kmph range), this is an appropriate compromise to make. In view of this, only limited studies were conducted in Israel on the effect of strain rate on soil-tire interaction. We decided that Israeli investigators will concentrate on the development of traction and soil property test devices (single wheel tester and in-situ soil sinkage and shear tester) and the development of a quasi-static soil compaction model. Rather than critical state concept based soil compaction model which requires a large computer to simulate, a simpler model that can be implemented on a PC would be developed by the U.S. researchers. Moreover, secondary objective #5 would be accomplished by integrating the traction model with the soil compaction. It was also felt that we would not have enough time to accomplish objective #6 as it stands (reduced budget compared to our original request limited our ability to hire additional people to accomplish objective#6). Instead of an expert system, an user friendly computer program that predicts tractive ability of pneumatic tires would be developed at U. C. Davis. When coupled with the soil compaction program, this results in a traction-soil compaction prediction program.

V. RELAVANT DATA, METHODOLOGY, RESULTS AND DISCUSSION:

The relevant data, methodology, results and discussion related to the various objectives of this study are presented in the form of journal articles, presented papers, preprints and experimental data sets. The results obtained the Israeli investigators are presented first followed by those of U. S. investigators. They are presented in the chronological order reflecting the implementation of various tasks and sub-tasks under the original/modified research plan. Each section is preceded by a short summary or some comments as to its content and its relevance to the objectives it addresses.

V.1 MODELING TRACTION

The work on the first major objective constituted the main thrust during this project duration. The problems that were analyzed were:

- a) traction losses by wheeled vehicles moving across fields with hard soil surfaces, and
- b) the effects of variations in moving vehicle velocity on the generated traction.

PART A

ACTIVITIES IN ISRAEL

V.1.1. WHEEL TRACTION PREDICTION ON HARD SOIL .

This paper presents a treatise on modeling traction generation by a moving vehicle across hard soil surface where wheel traction prediction models may be either limited or even fail since soil sinkage is practically zero and the cone-index readings are very high and irrelevant.

The results and conclusions reached show the shear characteristics of the soil surface and the wheel's peripheral flexibility to be the major parameters in the model developed. Traction was evaluated theoretically and experimentally.

WHEEL TRACTION PREDICTION ON HARD SOIL

D. Wolf, I. Shmulevich and U. Mussel
 Member Member
 ASAE ASAE

ABSTRACT

High traction is often required when operating tractors on hard field surface, such as compacted soils or dried irrigated semi arid areas. Existing wheel prediction models may be limited as soil sinkage under the tire load hardly exists and cone index readings are high and not relevant.

It was found that shear characteristics at the soil surface, together with wheel peripheral flexibility are well correlated to the wheel performance and should be considered as major affecting parameters. A tire traction model on hard soil surface, based on these parameters, was developed and studied numerically and experimentally.

INTRODUCTION

The conventional models for wheel performance prediction and soil -wheel relations, do not usually consider hard soils where tire sinkage into the surface is limited. The methodology of these models is aimed at softer soil conditions and as is the systematics in characterizing both wheels and soils. Some other works evaluate tractor operation on solid surface (de Souza and Milaneze, 1991. & Leviticus and Reyes, 1985). These works are important for wheel- field performance prediction out of concrete test results, but they do not simulate hard field surface operation.

Tractors are usually designed to operate optimally on softer soil conditions. On hard soil surface, especially when high traction is required, the tractor optimal performance is not well defined. The selection of the tractor major characteristics is not based on a proper model and analysis.

Bekker (1985) proposed a model for tire sinkage prediction for such conditions where the tire is supported only by its lugs and their sinkage is less deep than their height.

The sinkage of a driving wheel on hard soil is small and has little effect on the traction performance. On the other hand, under hard soil conditions, the tire circumferential flexibility becomes a major factor. The lugs of an agricultural tire are high and their deflection when interacting with hard surface may be significant.

The soil may be defined as hard when a footprint of the conventional agricultural tire is not deeper than the height of its lugs. In cone index terms, it can be found that the soil strength of hard soils, is above 1.5 MPa.

Hard soils penetrometer measurements are difficult and cannot be used to predict traction.

The model proposed in this work aim to predicts the traction performance of an agricultural pneumatic tire on hard soil surface. It uses measured wheel and soil parameters. The soil is characterized by simple in situ, portable direct shear. The tire is quantified by the dimensionless soil - tire factor circumferential flexibility which can be simply measure on rigid surface.

The work will present a tire-hard soil model for prediction of wheel performances. The model has been experimentally validated by a wheel tester in field conditions.

TIRE -HARD SOIL INTERACTION MODEL

The modeling assumptions

The development of tractive force causes the driving wheel slip, which may be a combined result of three sources:

- a. Sliding - relative motion between a tire and soil at the lug contact plane;
- b. Tire circumferential deformation. It is important as the construction of the agricultural tractor with high lugs and low inflation pressure causes high deflection when driving torque is applied.
- c. Soil longitudinal strain. This deformation is a result of the top layer displacement in relation to deeper layers when a horizontal traction force is applied.

The proposed model analyses the tractive stress along the tire and soil contact area. This area may generally be divided in two main regions: the adhesion region and the sliding region, according to Julien Model as defined by Wong (1978). The following analysis uses this definition:

- a. There is no sliding between the lug, supported surface and the ground in the adhesion region in the front end of the contact area. When the lug just touches the ground, shear stress does not yet exist in this front end. Behind the front end, along the contact area, tire circumferential deformation and shear stresses develop gradually and simultaneously.

The shear stress reaches its maximum value τ_m at a certain distance from the front end. This distance, named here the critical length, l_c , defines the boundary between the non-sliding and the sliding regions. The value of the maximum shear stress may be either the yield stress in the soil, τ_r , if soil shear does take place, or the dynamic soil - tire frictional stress, τ_f whichever is lower.

- b. There is a relative motion between the tire and the soil in the sliding region, from the critical point to the rear end of the contact area. This motion can occur in either the lug - soil contact area or in a deeper soil shear plane. It may be assumed that the shear stress exists all along the sliding region and has the maximum value τ_m . This shear stress is a function of the normal stress which can be assumed to be uniform in this region as well. At the end of this region the tractive effort, acting on the lug is released and the stress is zeroed.

It is difficult to define the contact area between the lugged tire and the hard surface. A rectangular area which includes both the lug footprint and the intermediate area is considered in this work .

The width of the contact area equals the tread width and is considered independent of the tire section width or the inflation pressure. It can be also assumed from the hard soils definition that the contact pressure at the tire intermediate areas is zero and that the ground resppure under the lugs can be taken as uniform.

Soil shear stress as a function of shear displacement

The soil behavior when shear loading is applied, may be described by an elasto - plastic model, as suggested by Grecenco (1967). The shear stress area can be divided into two linear zones :

- a. In the first zone the soil shear stress τ linearly increases with the shear displacement j . The linear constant k_s has stress units to unit length and can be defined by:

$$\tau = k_s j \quad (1)$$

The shear stress maximum value, τ_r , is reached for the critical displacement, j_c which depends on the soil type and conditions. This displacement is the boundary between the two zones.

$$\tau_r = k_s j_c \quad (2)$$

- b. In the second zone the shear stress is constant, independent of j and its value is τ_r .

The model schematics

The model assumption is that both the tire lugs and the soil act like a spring system. Each spring is loaded in the front end of the contact area and released at its rear end. The two spring systems are connected in series. In the adhesion region the increase of the tractive effort will be linear with the spring deformations, according to the equivalent spring constant. In the sliding region the tractive stress is constant and its value, as already mentioned, depends on the location of the sliding plane, either soil - soil or soil - tire.

The schematic description in Fig. 1, describes the geometry and the relation of the various system components on time basis. Subscript 0 and t note time. The time t is needed for a point

13



13

13

13

13

The longitudinal deflections cause a difference between the theoretical speed and actual ground speed of the wheel. The theoretical speed is ωr_e which is the circumferential speed for the rolling radius.

While the tire element $dx dy$ is in contact with the soil surface, (assuming constant contact width), the actual wheel advance is only $x-j$. At the same time the tire's theoretical advance is $x+e$.

Now the followings can be defined:

The actual wheel speed is
$$v_a = \frac{x-j}{t} \quad (4)$$

The theoretical wheel speed is
$$v_t = \omega r_e = \frac{x+e}{t} \quad (5)$$

The conventional definition of the driving wheel slip is:

$$s = 1 - \frac{v_a}{v_t} \quad (6)$$

Using the speed definitions, the slip is:

$$s = \frac{e+j}{x+e} \quad (7)$$

As $x \gg e$ and as e and j values can be replaced according to the tractive stress (Eq. 3), the slip can be modified into:

$$s = \frac{e+j}{x} = \frac{\frac{\tau}{k_t} + \frac{\tau}{k_s}}{x} = \frac{\tau}{x} \left(\frac{1}{k_t} + \frac{1}{k_s} \right) \quad (8)$$

The equivalent longitudinal flexibility of both the soil and the tire may be defined by a coefficient:

$$\frac{1}{k_{ts}} = \frac{1}{k_t} + \frac{1}{k_s} \quad (9)$$

By modifying the slip (Eq. 8) and by using the soil - tire flexibility coefficient definition (Eq. 9) the shear stress function is achieved:

$$\tau = k_{ts} s x \quad (10)$$

With the increase of x , from the front end of the contact area backward, the stress increases. It reaches its maximum value τ_m at the boundary of the adhesion region, at a distance l_c from the front end. (Eq. 10) is valid for this region only. The critical distance l_c is calculated according to (Eq. 10):

$$l_c = \frac{\tau_m}{k_{ts} s} \quad (11)$$

For the given tire and soil, the critical distance is a function of the wheel slip. The higher the slip the shorter l_c is. For low slip values, the critical distance may be equal or even longer than the length of the contact area $l_c > l_t$. In this case the contact area and the adhesion region are the same and (Eq. 10) is valid for the whole contact area.

Following the model assumptions, the tractive force in the adhesion region H_a is calculated by integrating the stress along the relevant contact area and multiplying it by the equivalent lug width- b :

$$H_a = b \int_0^{l_c} k_{ts} s dx \quad (12)$$

or:

$$H_a = \frac{1}{2} b k_{ts} s l_c^2 \quad (13)$$

It should be noticed that b is the equivalent lug width, defined as $b = n_l b_t$.

For the case mentioned before, when $l_c > l_t$, the tractive force will be calculated for l_t .

Let the critical slip s_c be defined for $l_t = l_c$. Eq. 13 will be valid as long as $s < s_c$.

The coefficient of traction (tractive force divided by the normal load on a tire), for the adhesion region is:

$$\frac{H_a}{W} = b k_{ts} s \frac{l_t^2}{2W} = \frac{s c_{ts}}{2} \quad (14)$$

When c_{ts} is a dimensionless soil - wheel factor, defined for simplification as:

$$c_{ts} = \frac{k_{ts} l_t}{p} = \frac{k_{ts} b l_t^2}{W} \quad (15)$$

The tire - soil relations in the sliding region

When higher tractive force is needed, the wheel slip increases and the critical distance decreases, as can be learnt from (Eq. 11).

The sliding region is formed when $s > s_c$ and $l_c > l_t$.

In the sliding region the tractive stress is constant and its value is τ_m . The tractive force H_s in the sliding region is the product of the equivalent lug width multiplied by the integral of the stress along the area:

$$H_s = b \int_{l_c}^{l_t} \tau_m dx = b \tau_m (l_t - l_c) \quad (16)$$

And by using the definition of τ_m from (Eq. 11) the tractive force will be:

$$H_s = bk_{ts}sl_c(l_t - l_c) \quad (17)$$

According to (Equations 11, 13 and 17) the tractive force H is the sum of the two separately calculated partial tractive forces. For $s > s_c$ the total tractive force is:

$$H = \tau_m bl_t \left(1 - \frac{\tau_m}{2k_{ts}sl_t} \right) \quad (18)$$

As mentioned before, the maximum stress equals to either the soil failure residual stress τ_r or the friction stress τ_f , whichever is lower.

The friction stress is defined as the friction force divided by the contact area. Its value is:

$$\tau_f = p\mu_f \quad (19)$$

The maximum soil shear stress is:

$$\tau_r = c + p \tan \phi \quad (20)$$

When the normal pressure is high, the relative value of the cohesion in the shear (Eq. 20), decreases. When c is relatively low, neglecting it will cause only a slight error, but will simplify the Equation:

$$\tau_r = p \tan \phi \quad (21)$$

The variable $\tan \Phi$, can be defined for the maximum stress value:

$$\tan \Phi = \frac{\tau_m}{p} \quad (22)$$

According to this definition ϕ can be called the equivalent angle of friction or the apparent angle of friction.

According to Equations 19, 20 and 21, the maximal stress τ_m , may take one out of three values.

The value of $\tan \phi$ will be according to the specific conditions:

$$\begin{aligned} \tan \Phi &= \tan \phi && \text{when } c=0 \text{ and } \tau_r < \tau_f \\ \tan \Phi &= c/p + \tan \phi && \text{when } c>0 \text{ and } \tau_r < \tau_f \\ \tan \Phi &= \mu_f && \text{when } \tau_r > \tau_f \end{aligned} \quad (23)$$

When (Eq. 22) is used while calculating (Eq. 18), the total tractive force can be calculated for the normal load on the wheel and the equivalent angle of friction:

$$H = W \tan \Phi \left(1 - \frac{W \tan \Phi}{2k_{ts}sl_t^2} \right) \quad (24)$$

When the soil - wheel factor is added, the coefficient of traction becomes:

$$\frac{H}{W} = \tan \Phi \left(1 - \frac{\tan \Phi}{2c_{ts}s} \right) \quad (25)$$

Tire traction on a solid surface as a means for predicting its field performance

When a tire operates on a solid surface, such as a paved road, the surface will not shear and its deflection may be considered negligible. In this case the constant k_s may be considered infinite and the equivalent soil - tire coefficient becomes the tire coefficient

$$k_{ts} \Rightarrow k_t$$

The wheel factor is achieved by inserting k_t in Equation 15. The maximum tractive stress is the tire to surface friction stress τ_f :

$$\tau_f = \frac{W\mu_f}{bl_t} = p\mu_f \quad (26)$$

For the adhesion region, by using k_t in Equation 14 the coefficient of traction is defined as:

$$\frac{H_a}{W} = bk_t s \frac{l_t^2}{2W} \quad (27)$$

By using Equation 27 and simple measurements on a hard surface, the tire can be characterized for predicting its performance on the field surface.

Rolling resistance

To predict the tire performance the rolling resistance force and coefficient are required:

$$P = H - R = W(\mu - f) \quad (28)$$

On a hard soil surface, the major component of resistance are the tire internal energy losses, resulting from its deflection and hysteresis. Researchers such as Dwyer (1987) and Wong (1978) analyzed and quantified rolling resistance on hard surface models. They determined the rolling resistance coefficient of the agricultural tire in the range of 3 - 5 %, with negligible effect of tire parameters or inflation pressure.

The working ranges

Following the proposed model, there are two working ranges. They correspond the two slip ranges $s < s_c$ and $s > s_c$.

A comprehensive prediction requires the calculation of the critical slip and the use of the proper Equation for both ranges. There is a continuity between the two ranges and continuous prediction is possible.

Practically, the critical slip is quite low and the actual traction is done in the higher slip range. This means that calculating the coefficient of traction according to Equation 25 yields more significant values.

Tractive efficiency

The tractive efficiency of a driving wheel is defined by ASAE S296.3 (1991) as the ratio between the output and the input power.

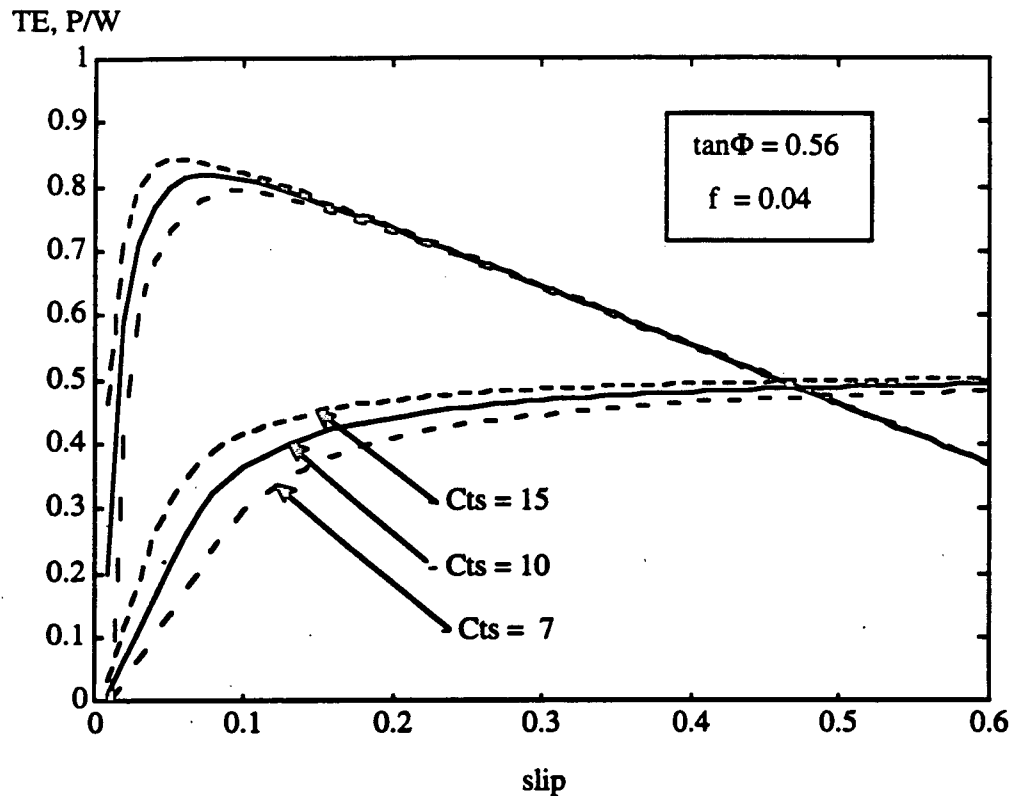


Fig. 2: - The effect of the soil - wheel factor c_{ts} on the traction performance

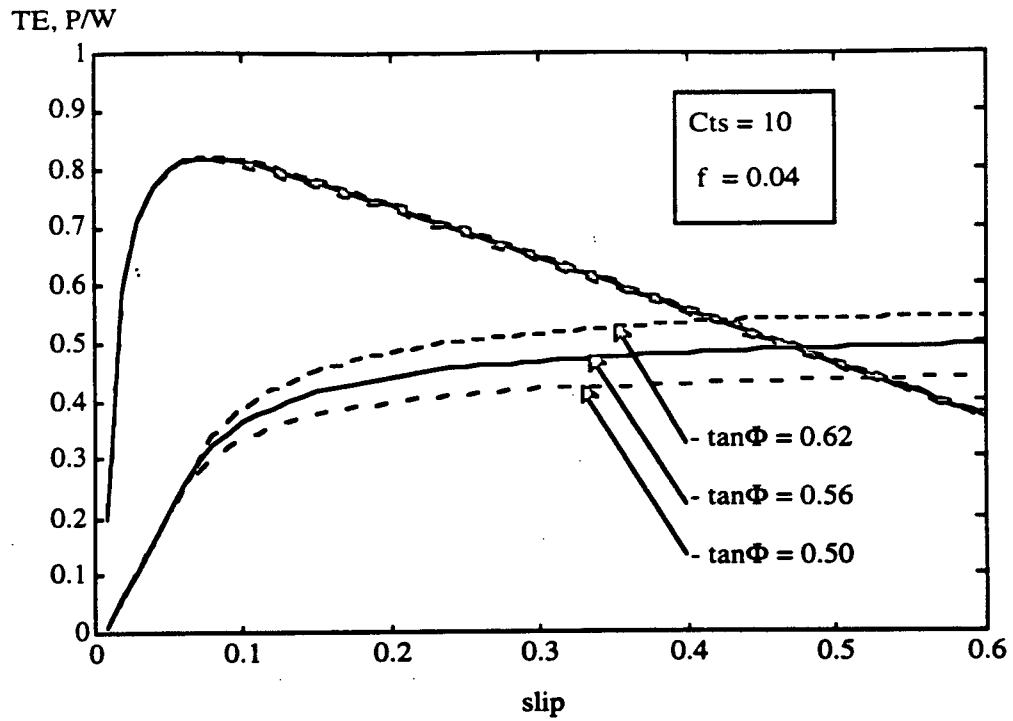


Fig. 3: - The effect of the soil internal friction $\tan\Phi$ on the traction performance

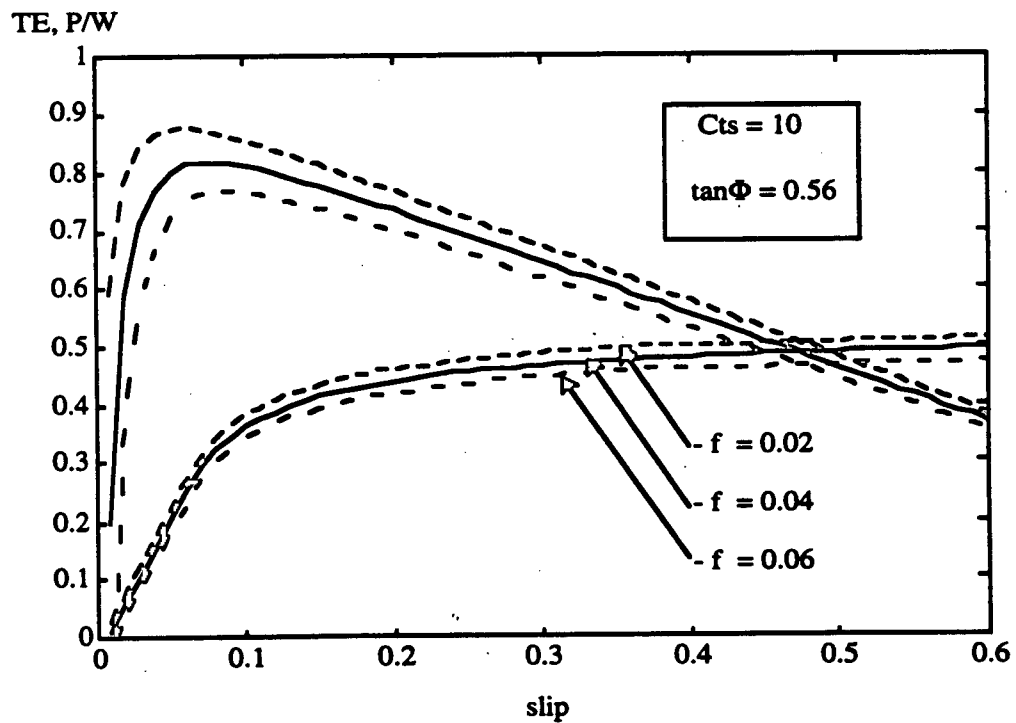


Fig. 4: - The effect of the coefficient of rolling resistance f on the traction performance

For the proposed model and low enough critical slip, using Equation 25, the tractive efficiency may be developed to the following form:

$$TE = \left[1 - \frac{f}{\tan \Phi \left(1 - \frac{\tan \Phi}{2c_{ts}} \right)} \right] (1 - s) \quad (29)$$

This Equation, like the tractive efficiency of the softer soil condition, has a maximum value. This point can be selected as optimal when considering the power efficiency of the wheel. Slip and efficiency values at this point are a function of the following variables: the coefficient of rolling resistance f , the soil - wheel factor c_{ts} and the soil internal friction $\tan \Phi$ variables.

The results of the parametric analysis of the model, computed with the objective of evaluating the effect of the three major variables, are presented in Figs 2, 3 and 4. The Figures show the coefficient of traction and tractive efficiency as a function of the wheel slip.

The central graph in each figure was calculated for the following values, based on the field experimental results: $f=0.04$, $\tan \Phi=0.56$, $c_{ts}=10$. The other graphs describe the effect of changing one variable in each figure.

EXPERIMENTAL SET-UP

Field experiments were carried out with two main objectives:

- To confirm the tire - hard soil prediction model.
- To generate a supporting quantitative database.

In order to reach these objectives, the experiment methodology was to characterize the tire performance as a function of tire variations, inflation pressure and hard surface conditions. This was done by testing and analyzing:

- Coefficient of rolling resistance.
- Coefficient of traction as a function of the wheel slip.
- Tractive efficiency, as a function of the wheel slip also.
- Tire characteristics by supplementary experiments. These include finding the effect of the normal load on the tire - surface contact area and the tire rolling radius as well as defining the tire k_t constant from solid surface experiments.

The field experiments were conducted in three sites:

- A solid concrete testing road.
- Field A: clay soil, wheat stubble, dense and dry surface, bulk density (dry basis) for depth of 0 - 200 mm was 1.31 t / m^3 , moisture content for the same depth range was 3 %, soil cohesion - almost negligible, $\tan \Phi = 0.47$ for disturbed and $\tan \Phi = 0.70$ for

non- disturbed zones (from in-situ shear tests), average of 15 hammer drops (of 3 kgm each) for 150 mm penetration of drop hammer penetrometer.

- c. Field B: clay soil, following irrigated industrial tomatoes, dense and dry surface, bulk density (dry basis) for depth of 0 - 200 mm was 1.23 t / m^3 , moisture content for depth of 0 - 100 mm was 12 % and for 100 - 200 mm - 19 %, soil cohesion - almost negligible, $\tan \Phi = 0.52$ for disturbed and $\tan \Phi = 0.66$ for non-disturbed zones (from in-situ shear tests), average penetration stress of 18 bar to reach depth of 270 mm with a conventional cone penetrometer.

The six tested tires were of the same model, same make (Aliance, IL), same lug type (R1, T-324 model), both bias-ply and radial-ply types and of a variety of sizes:

16.9-34 / 8, 16.9-30 / 8, 12.4-36 / 6, 12.4-28 / 6, 16.9R34 / 8 and 16.9R30 / 8.

All the tires were inflated to four inflation pressure levels: 0.8, 1.0, 1.3 and 1.7 bar.

The experiments were conducted in a single constant travel speed, 0.7 m / s.

A special single wheel traction tester, shown in Fig. 5, was used in the field experiments. The tester is built to apply vertical load, drawbar pull, input torque and controlled speed and slip. All the parameters are measured simultaneously.

EXPERIMENT RESULTS AND DISCUSSION

The soil in both fields B and C was hard enough, when the tires were tested, and the lugs did not sink to their full height as can be seen in Fig. 6. This may explain the minor, non significant difference in the tire rolling resistances:

- On the concrete road - 0.032
- On field A - 0.037
- On field B - 0.043

The P / W ratio is asymptotic to its ultimate value in hard soil conditions - 0.52.

The optimum slip for maximal tractive efficiency is between 5 to 10 %, for all the tires in these soils.

When the slip is low, the tire performance improves with the increase of the wheel factor c_t . This explains the advantage of the radial tires in this range. The longitudinal flexibility k_t of the radial tires was found to be higher (from the concrete road experiments):

For	16.9R34 and 16.9R30 tires	-	$k_t = 27.4 \text{ MPa / m}$
For	16.9-34 and 16.9-30 tires	-	$k_t = 20.0 \text{ MPa / m}$
For	12.4-36 and 12.4-28 tires	-	$k_t = 14.7 \text{ MPa / m}$

The inflation pressure did not show any significant effect on the tire performance (as shown in Fig. 7). The change of the length of the contact area. It is probably compensated by the change of the longitudinal flexibility k_t . As a result, the wheel factor c_t is not affected.

The normal load in the range of the tests did not show any significant effect on the coefficient of traction (as shown in Fig. 8).

No significant difference in the tire performance (TE and P / W) could be found in the high slip range, above 20 %. An example is presented in Fig. 9. According to the proposed model, the dominant factor affecting on the tire performance, in the high slip range, is $\tan\Phi$ which is a soil and not the tire characteristic.

When comparing the predicted tractive efficiency to the actual one (as presented in Figs 10 and 11) a very good correlation can be seen around the TE_{max} area. The actual efficiency decreases at a steeper slope comparing to the predicted one. The reason may be a higher rolling resistance when a driving torque is applied.

CONCLUSIONS

The developed prediction model of agricultural tire traction performances successfully covers the area of tire's operating under hard soil surface condition.

The presented tire-hard soil interaction model, based on analysis of the tractive stresses along the tire-soil contact area, as well as on the Julien's model, enabled prediction of tire motion resistance, coefficient of traction and tire tractive efficiency as a function of slip.

In order to confirm tire-hard soil surface prediction model, as well as to generate a supporting quantitative database, field experiments were carried out on a rigid concrete testing road and two types of compacted and dried clay soils, including six different agricultural tires and three different inflation pressures.

Reasonable correlation can be found comparing the predicted traction efficiency to the measured ones, around the maximum traction efficiency (TE_{max}) value. In addition, the actual efficiencies are some what lower compared to the predicted ones. A good prediction are obtained for coefficients of traction.

Based on analysis of predicted and measured tire traction parameters may be concluded that developed tire-hard soil traction model can be successfully applied for prediction of agricultural tire traction parameters on the hard soils.

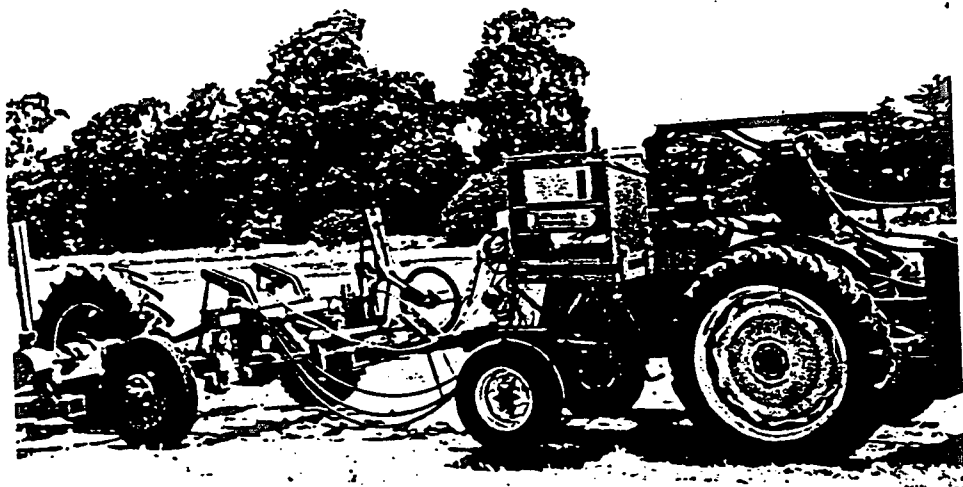


Fig. 5: - The single wheel traction tester

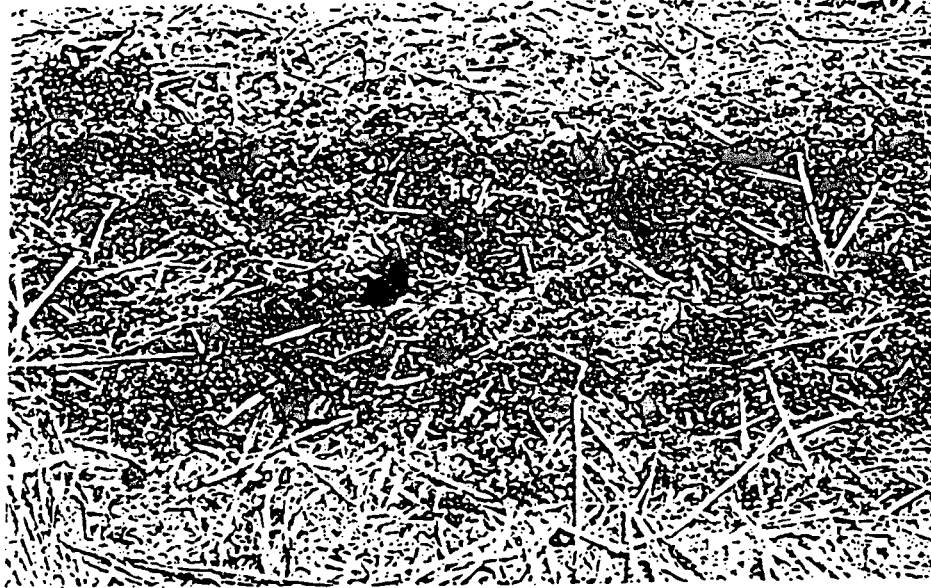


Fig. 6: - Typical tire print in field B after traction test at 20 % slip

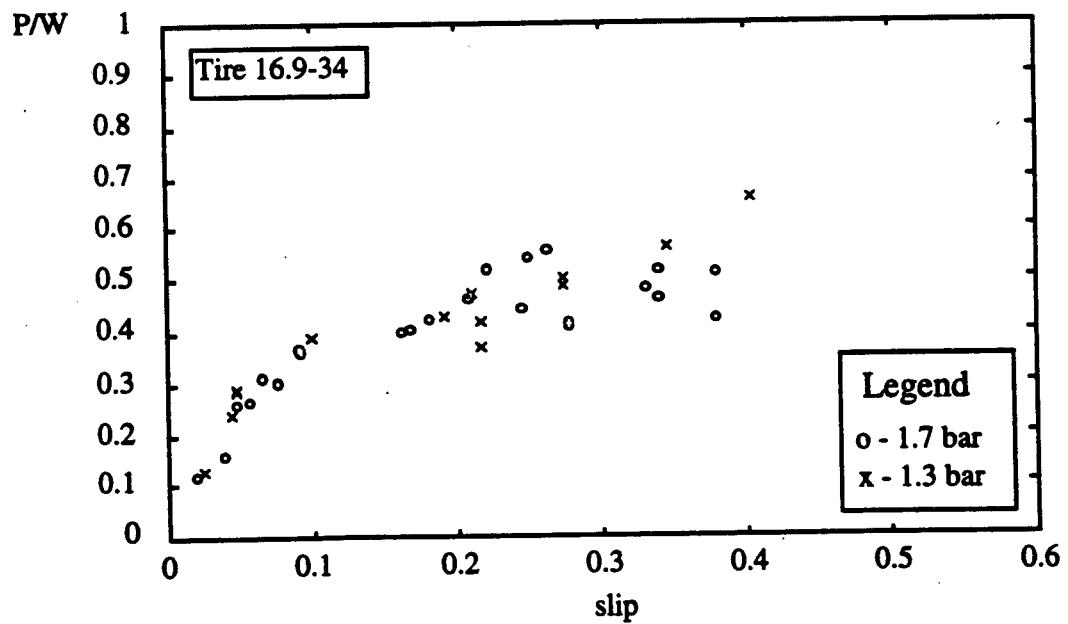


Fig. 7: - The effect of inflation pressure on the 16.9-34 tire performance

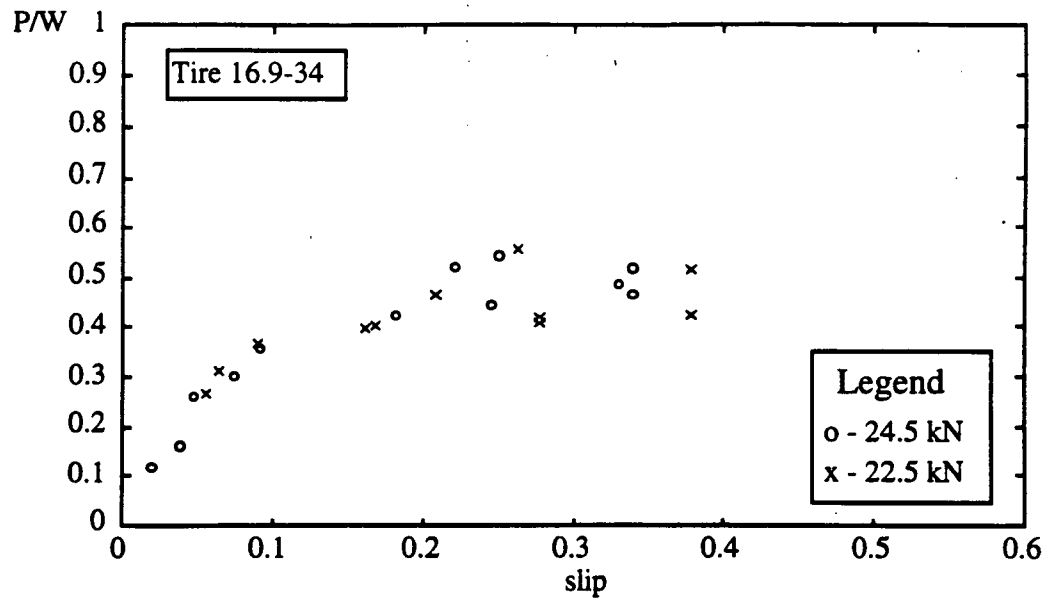


Fig. 8: - The effect of normal load on the 16.9-34 tire performance

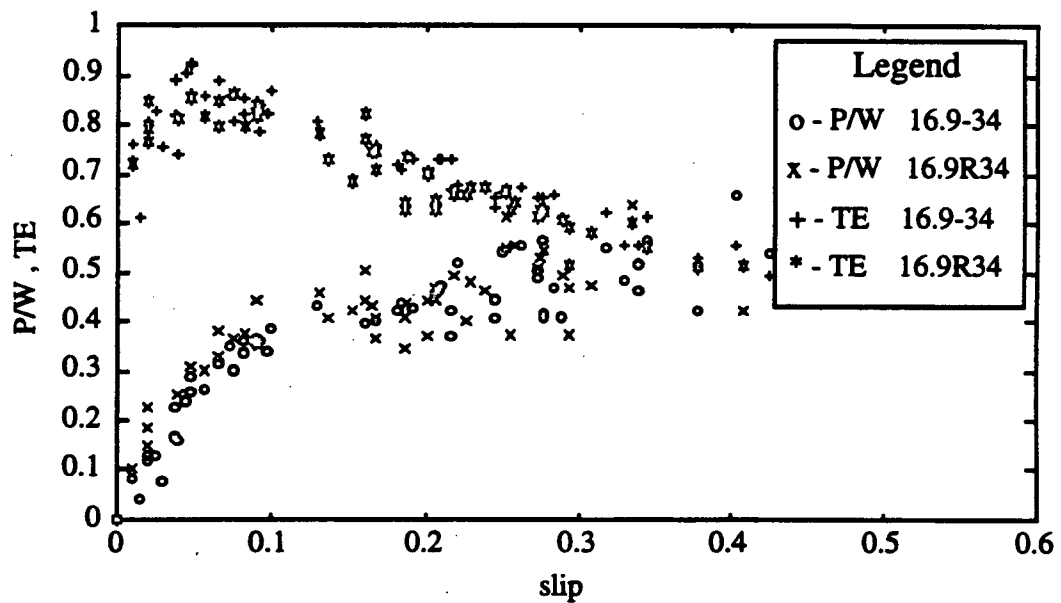


Fig. 9: - Comparing the performance of radial - ply and bias - ply tires- 21 -

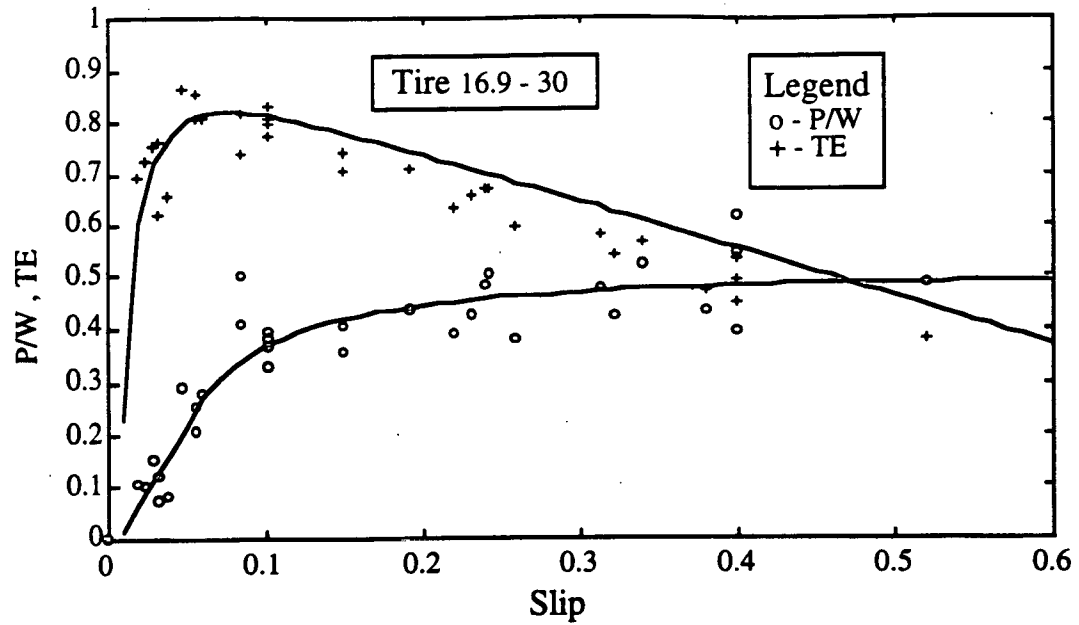


Fig. 10: - Comparison of predicted and measured performance of 16.9-30 bias - ply tire

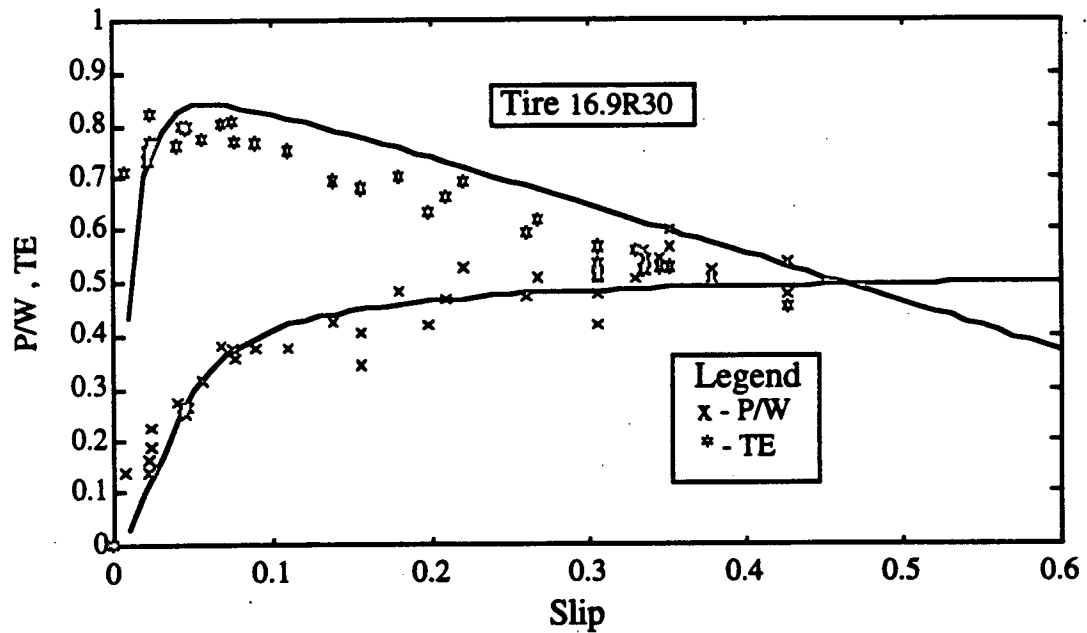


Fig. 11: - Comparison of predicted and measured performance of 16.9R30 radial - ply tire

Acknowledgements

This study was partially supported by Grant No.US-1848-90R of the United States-Israel Binational Agricultural Research and Development Foundation, Ltd.

REFERENCES

1. Bekker, M. G. 1985. The effect of tire tread in parametric analyses of tire - soil systems. National Research Council of Canada. NRCC No 24146, 34 p.
2. de Souza, E. G. and L. F. Milaneze. 1991. Predicting of tractor performance on concrete. Transaction of the ASAE 34(3):727-732.
3. Dwyer, M. J. 1987. Prediction of drawbar test performance. J. of Terramechanics. 24(2): 169-177.
4. Grecenco, A. 1967. Binomic slip - thrust equation for tractors on predominantly frictional soils. J. of Terramechanics 4(4):37-54.
5. Leviticus, L. I. and J. F. Reyes. 1985. Tractor performance on concrete. Transaction of the ASAE 28(5):1425-1429.
6. Wong, J. Y. 1978. Theory of ground vehicles. John Wiley & Sons, New York.
7. _____. 1991. ASAE Standard S296.3: Uniform terminology for traction of agricultural tractors, self-propelled implements and other traction and transport devices.

NOTATION

A_0, A_t	names of rim elements	m	coefficient of traction
B_0, B_t	names of tire elements at the lug tip	m_f	dynamic coefficient of fraction
B_f	location of B_t if no torque or load are applied	n_l	the ratio between the lug contact area and the total contact area
C_0, C_t	names of soil elements in the contact area	p	average lug contact ground pressure
D_0, D_t	soil elements in the non disturbed layer	P	drawbar pull
b	equivalent lug width	r_e	wheel rolling radius
b_t	contact width	R	wheel rolling resistance
c	cohesion	s	drive wheel slip
c_t	wheel factor	s_c	critical drive wheel slip
c_{ts}	soil - wheel factor	t	time
d	unloaded tire diameter	TE	tractive efficiency
d_r	rim diameter	τ	shear stress
dx, dy	elementary contact area	τ_f	frictional stress
e	longitudinal tire lug deflection, at the tip	τ_m	maximum tangential stress at the contact area
f	coefficient of rolling resistance	τ_r	residual shear stress
q_t	advance angle of the wheel	v_a	ground speed
f	soil angle of internal friction		theoretical wheel speed
F	equivalent angle of friction	w	angular velocity of the wheel
H	wheel tractive force	W	dynamic load on the wheel
H_a	tractive force in the adhesion region	x	distance from the front of the contact element
H_s	tractive force in the sliding region		
j	soil shear displacement		
j_c	critical soil shear displacement		
k_s	soil stress - strain ratio constant		
k_t	tire stress - longitudinal deflection constant		
k_{ts}	tire - soil constant		
l_c	critical length of contact area		
l_t	length of contact area		

V.1.2. THE EFFECT OF DYNAMICALLY VARYING VELOCITY ON WHEEL TRACTION.

This paper constitutes the main effort in developing a predictive model that will diverge from the currently available models in treating wheeled vehicles movement across highly variable soft and yielding soil surfaces where soil sinkage varies greatly, causing appreciable changes in the vehicle's speed and the traction it generates. A numerical model was developed which is based on numerical solutions of motion traction relations using instantaneous equilibria between wheel and soil elements. The soil-wheel elements are presented as deformation-force equations which account for the deformation rate. Calculations results obtained and comparisons made, point out, that velocity variations effects on wheel traction performance cannot be ignored.

THE EFFECT OF VELOCITY ON WHEEL PERFORMANCE

by

I. Shmulevich, U. Mussel, D. Wolf

Technion, Israel Institute of Technology, Haifa, Israel

1. Introduction

Throughout the years many models were developed to predict soil-wheel interaction for studying wheel performances at steady state condition. The existing models are limited and cannot predict well the variation in velocity and its influence on wheel performances. Motivation for this work came from difficulties in the previous studies of off-road tractor control according to existing soil-wheel interaction models which were reviewed by Upadhyaya and Wulfsohn (1990).

The most important information needed to predict soil-wheel performances is based on a knowledge of the distribution of stress at the interface. A study was carried out by Onafeko and Reece (1967) to measure the stress distribution under a rigid wheel. Wood and Burt (1987) reviewed and measured stress distribution under flexible tires. Wong and Reece (1967a,b) developed models to predict rigid wheel performances, verifying their findings using Onafeko's data. Many researchers used the experimental stress distribution reported by Krick (1969) for flexible tires. The reported investigations show the influence of drawbar pull, dynamic load variation, sizes of tires and soil conditions on stress distribution. In all these studies, velocity was not reported and its effect on stress distribution at the soil-wheel interface was neglected.

The velocity effects on soil-wheel interaction have received relatively little attention. The existing prediction models neglect the velocity, assuming that its influence on wheel performances is small. However, Pope (1971) studied the effect of velocity on the rolling resistance of a rigid wheel. A decrease of 9.3% in rolling resistance was reported for an increase of velocities from 0.01 to 0.076 m/s. Grahn (1990) investigated the influence of

velocity on sinkage and rolling resistance. He showed similar results of decrease in rolling resistance and sinkage, as velocity was increased from 0-4.6 m/s on sandy loam. Burt and Lyne (1985) addressed the issues of travel reduction and dynamic load which have significant effect on wheel performance and have not been carefully controlled during velocity investigations. Their results from a controlled tests showed that no effect of velocity on the net traction and tractive efficiency occurred within the velocity range of 0.1 to 0.6 m/s for flexible tires acting on two types of soil at constant travel reduction and wheel load. Gee-Clough et al. quoted by Burt and Lyne (1985) showed by practical field experiments that for velocities of 0.9 and 1.8 m/s the coefficient of traction at a 20% travel reduction was significantly higher at a higher velocity. Different testing techniques affect experimental results of wheel performances versus slip, as demonstrated by Upadhyaya et al. (1988). One source of variability in traction data is the necessity to keep constant velocity while changing wheel slip. While investigating the velocity effects there may be no significant difference between wheel performances at a range of constant slip. For flexible tires acting on the road Laib (1979) reported that increasing velocity from 3 to 5 m/s significantly decreased the coefficients of damping and spring. Similar results were reported by Kutzbach and Schrogl (1985) for velocities of 0 to 4 m/s.

The effect of penetration velocity to predict soil properties has been investigated by several studies. Results are contradictory and brought in detail by Mussel et al. (1992). However, the effect of shear rate on soil strength is clearer. Most of the studies showed that an increase in shear rate caused an increase in shear strength.

In an effort to suggest a better and more accurate method to predict soil-wheel interaction performances, a simulation model of soil-wheel interaction was developed, which simulates wheel performances subjected to variations in velocity, soil and wheel conditions. The simulation would provide a theoretical prediction to soil-wheel interaction studies.

2. Objectives

The goal of this research was to develop a new soil-wheel interaction model in order to investigate the effect of varying velocity on wheel traction.

The specific objectives of the research were:

- Formulation of a simulation soil-wheel interaction model based on the soil, wheel properties, interface behavior and their dependence on time and velocity.
- Verification of the simulation model to reported experimental data from a rigid wheel.
- Evaluation of the effect of forward velocity on the distribution of the stresses at the soil-wheel interface.
- Evaluation of the effect of forward velocity on wheel performances.

3. Soil-Wheel Interaction Model

The mathematical modeling of the wheel is based on general formulation of time-dependent wheel-soil interaction system. Wheel performances are calculated using the Newton-Euler equations of motion. In each time interval, dimensions of contact surface and stress distribution are obtained due to an instantaneous equilibrium between wheel element and soil which are in contact. Knowing the stress distribution in the contact surface, wheel acceleration, velocity and position can be determined as a function of the external forces and

moments acting on the wheel and the initial conditions of the wheel. The general formulation of equations used is given in detail in Mussel et al. (1992). The numerical solution of the equations has been achieved using the finite differences formulation. Wheel velocity and position were calculated in time steps, using the value of wheel acceleration in the same time step and value known from previous steps. The numerical formulation used was the known one-step algorithm for the semidiscrete equation of motion called the Family Newmark Method cited by Hughes (1987).

The calculation of stress distribution at the interface was performed in the presented study using instantaneous equilibrium between the external forces exerted by the soil and the internal forces in the wheel. Both types of forces are inflated by the deformations and deformation rates in the soil and the wheel, in addition to a geometric relationship existing between the wheel deformation and the deformation in the soil. The relationship between the deformations and stresses in each wheel element is based on existing models in the literature, which present the wheel, soil and the interface between them. The simulation model is very flexible to changes and could be modified using newer sub-models. In general the simulation needs 8 equations to solve the 4 deflections and forces both in normal and tangential directions in the soil and wheel.

An example of possible equations which expresses the normal and tangential forces acting on the wheel element and related to wheel and soil properties are given in Mussel et al (1992).

The predicted stress distribution was inserted in the general calculation to obtain wheel performances.

The simulation model calculates the following wheel performances as dependent on slip or wheel velocity and according to initial conditions:

DPC or F_x/W = net tractive ratio,
 GTC or $Q/(R W)$ = gross tractive ratio,
 z_0 / R = dimensionless wheel sinkage,
 F_x/W = free rolling force ratio at zero torque (towed wheel) and
 TE = tractive efficiency.

The tractive efficiency is calculated according to ASAE Standard:ASAE S296.3 (1991):

$TE = F_x v / Q\omega$, where the slip is calculated according to: $s = 1 - v / (\omega r)$ The algorithm of the calculation procedure and the described equations with the proper boundary and initial conditions are presented in the soil-wheel interaction model.

4.Method

4.1 Illustration of a Simulated Soil/Wheel Model

A computer program to simulate the soil-wheel interaction model was built according to the described equations and the flowcharts (see Mussel et al (1992)). The program used MatlabTM(1990) Language. The first part was dedicated to examine the effect of wheel element size on the accuracy and conversion of the solution. It was found that for a 1.25 m wheel diameter it would be appropriate to divide the wheel into 128 elements. For the influence of time interval, conversion criteria were examined first using a rigid wheel. In general the simulation model can be operated in several modes. One mode can choose the external forces (F_x , W) and wheel angular velocity (ω) as known inputs, assuming that the

wheel has unlimited torque, and the simulation program will run to get conversion. For these conditions the wheel performances are calculated including the wheel slip. Another mode can choose external forces (F_x , W) and wheel torque (Q) as known inputs, assuming that the wheel angular velocity (ω) is unlimited, and the simulation program will run to get conversion. At the conversion stage the slip and wheel performances are calculated. The effect of velocity on wheel performances for a rigid wheel was then investigated. In the second stage simulation results of a flexible tire are demonstrated.

5. Results and Discussion

5.1 Model Verification

Simulation results from the soil-wheel interaction model verified qualitatively and quantitatively with experimental data and with other prediction models reported in the literature for a rigid wheel. This comparison was made in order to examine firstly the correction of the simulation algorithm. A rigid wheel was chosen as a private solution where the geometry of the contact surface is known and for which the dynamic properties of the wheel are not taken into account. The height of the wheels axis from soil level was calculated by iterative calculation to achieve an equilibrium condition in the vertical direction. For these

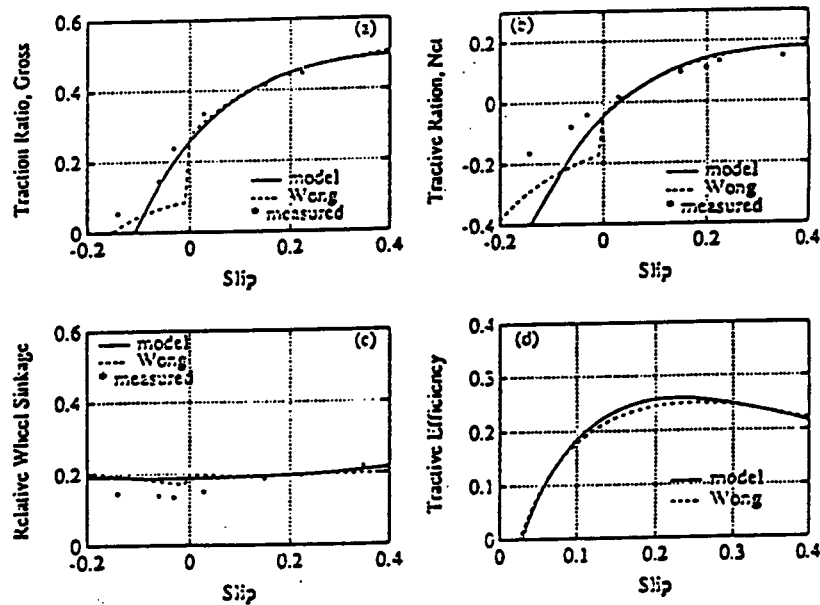


Fig. 1 Comparison of measured (Onafeko & Reece 1967) and predicted performances. by Wong and Reece (1967 a,b) and the suggested model, as affected by slip, for rigid driven wheel on compact sand and relative velocity $V/u_0=3$

equilibrium conditions: tractive ratio - net (F_x/W), traction ratio - gross ($Q/(R\omega)$). dimensionless wheel sinkage (z_0/R) and tractive efficiency (TE) values were determined. An example of wheel performances versus slip predicted from the simulation model for the following parameters are given in Fig. 1. Zero slip is specified according to - Zero conditions -ASAE S296.3 standard, where the zero slip accords on a rigid surface with zero drawbar pull.

The comparison results demonstrated the simulation prediction versus experimental data from Onafeko and Reece (1967) and predicted solution according to Wong and Reece(1967a,b) models for a driven and a towed rigid wheel. It can be seen that the simulation results are close to the experimental data and better than the predicted value according to Wong's model, especially around the zero slip whereas Wong's model has discontinuity.

5.2 Effect of Velocity on Wheel Performances

5.2.1 Rigid Wheel

The effect of velocity was examined by increasing by ten times the dimensionless velocity value ($v/u_0 = 30$). It can be seen in Figure 2 that as the velocity increased, the contact angular zone decreased and the maximum normal and tangential stresses significantly increased.

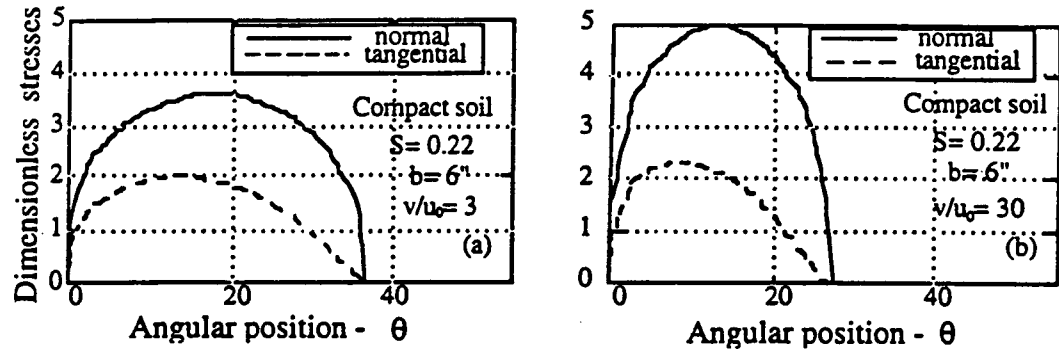


Fig. 2 - Predicted distributions of dimensionless normal(s^*) and tangential (t^*) stresses vs. angular position- q (a) for a 49.4X6 in. rigid driven wheel with an axle load 2,000 lb on compacted soil; (b) for a 49.4X12 in. rigid driven wheel with axle load 2,000 lb on loose sand; both for dimensionless velocity $v/u_0 = 30$ and at 22% slip

Three configurations of soil-rigid wheel conditions were predicted by the simulation model: first, 49.4X6 in. wheel on compacted soil, second, on loose sand (soil parameters as reported by Wong and Reece, 1967a,b) and last 49.4X12 in. wheel on loose sand where the vertical axial load kept constant 2,000 lb. Simulation results for investigating the effect of velocity on the towed wheel performances are presented. Free rolling wheel force ratio $-F_x/W$ both at zero torque versus dimensionless velocity v/u_0 are demonstrated in Fig.3. This agrees with results reported by Grahn (1990), and corroborates the fact that the velocity has a significant effect on wheel sinkage and free rolling forces. Increasing the velocity will reduce wheel sinkage and free rolling forces.

Simulation results for investigating the effect of velocity on the performances of driven wheel are presented. Maximum net tractive ratio F_x/W and net tractive ratio F_x/W at 20% slip, both versus dimensionless velocity v/u_0 , are demonstrated in Fig. 4 and 5, respectively. The maximum net tractive ratio significantly increased as dimensionless velocity v/u_0 decreased for all the three soil-wheel configurations. The increase in the compacted soil is more moderate compared to the increase in the loose sand. This phenomenon looks clearer in the maximum net tractive ratio presented in Fig.4, than in simulation results of net tractive ratio at constant slip presented in Fig. 5. Comparison between Fig.4 and 5 shows that for different

velocities the maximum wheel performances do not necessarily accord for the same range of slips. These results agree to some extent with the remarks and findings reported by Burt and Lyne (1985). As expected, the net tractive ratio is higher on compacted soil compared to the net tractive ratio on loose sand.

The tractive efficiency, demonstrated in Fig. 6 significantly increased as dimensionless velocity v/u_0 decreased for all the three soil-wheel configurations.

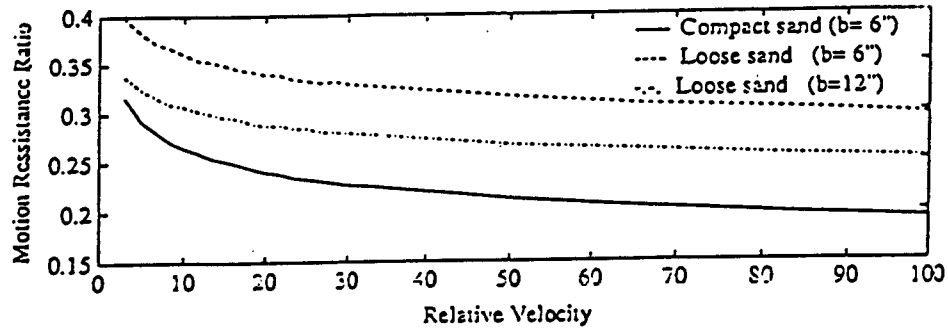


Fig. 3 Motion Resistance Ratio, at zero torque, as a function of relative velocity (V/u_0) for rigid towed wheel. For 6" wide wheel on compact and loose sand, and 12" wide wheel on loose sand

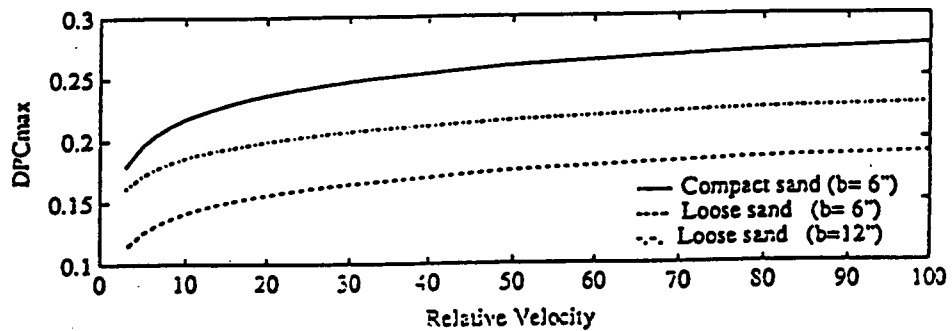


Fig. 4 Maximum Net Tractive Ratio as function of relative velocity (v/u_0) for rigid wheel. For 6" wide wheel on compact and loose sand, and 12" wide wheel on loose sand

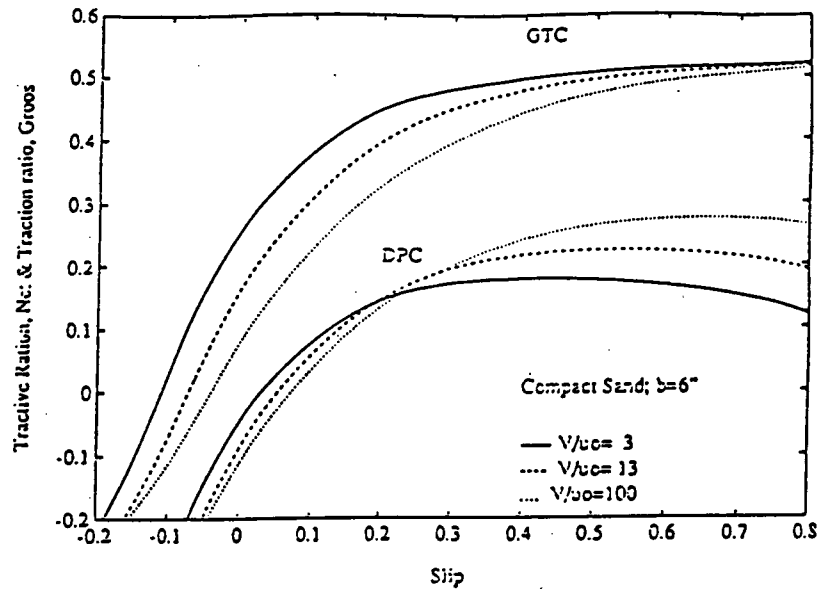


Fig. 5 - Net tractive ratio (DPC) and gross Traction Ratio (GTC) as a function of slip, for 6" wide rigid wheel on compact sand, for different velocities

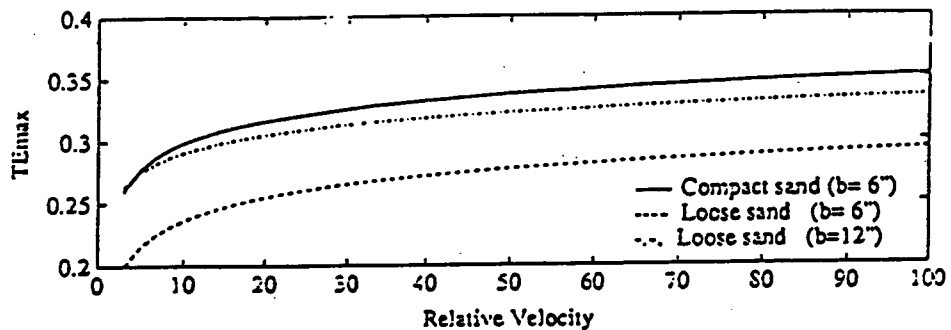


Fig. 6. - Maximal Tractive Efficiency as function of relative velocity. (v/u_0) for rigid wheel. For 6" wide wheel on compact and loose sand, and 12" wide on loose sand

5.2.2 Flexible Tire

Several soil-flexible wheel conditions were predicted by the simulation model. Net tractive ratio vs. slip for 16.9-30 tire on compacted soil and on Sandy loam (soil parameters as reported by Mussel 1993) for 4 different velocities are given in Fig. 7. Special experimental setup was built for measuring the radial damping and spring properties of a commercial agricultural tire of the same dimensions and inflation pressure

The simulation results demonstrated the effect of velocity on driven flexible tire and corroborates the fact that the velocity has a significant effect on wheel performances. Increasing the velocity will reduce wheel sinkage and free rolling forces and increase the net tractive ratio for a given slip.

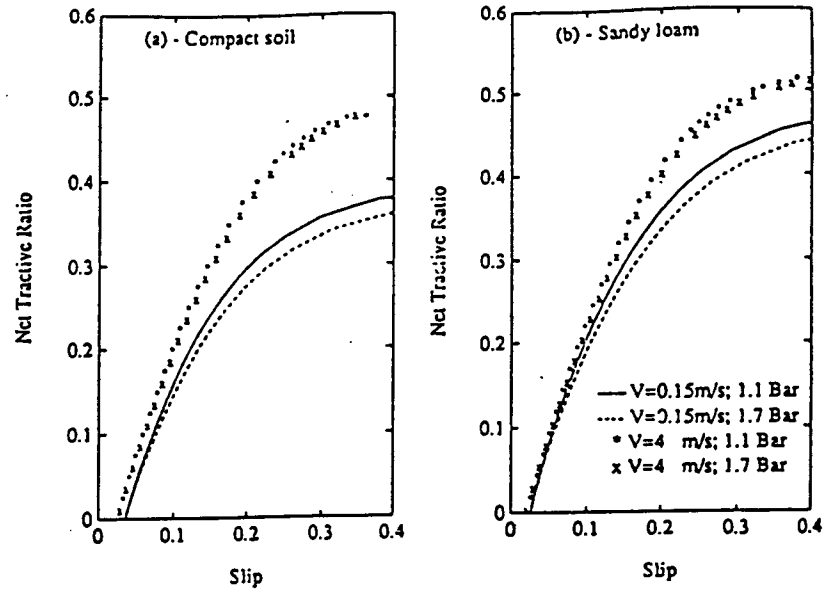


Fig. 7 Net tractive ratio vs. slip, for diagonal 16.9-30 tire at 1.1 Bar unflation pressure and different constant velocities of 0.15-4 m/s; (a) on Compact sand; (b) on Sandy loam

6. Conclusions

The following conclusions were drawn from this study:

1. The simulation study correlated well with experimental results reported by Onafeko and Reece (1967), and the predicted theoretical model suggested by Wong and Reece(1967a,b) for a rigid wheel.
2. The stress distribution under rigid wheel is effected by velocity. When increasing wheel velocity the maximum normal and tangential stresses increased and the front entry contact angle decreased.
3. The simulation results from several soil-wheel configurations corroborate that the effect of velocity cannot be neglected.
 - Wheel performances such as net tractive ratio and tractive efficiency increase with increasing dimensionless velocity.
 - Wheel sinkage and free rolling wheel force ratio, both at zero torque (towed wheel), showed significant decrease as dimensionless velocity increased.
4. Experimental work is needed to verify the theoretical simulation findings.

Acknowledgements

This study was partially supported by Grant No.US-1848-90R of the United States-Israel Binational Agricultural Research and Development Foundation, Ltd.

References

- 1) Burt, E. C. and P.W. Lyne. 1985. Velocity effects on traction performance. Transactions of the ASAE 28(6):1729-1730.
- 2) Hughes, T.J.R. 1987. The Finite Element Method, Linear Static and Dynamic Finite Element Analysis. Prentice-Hall, Inc. New Jersey U.S.A.
- 3) Grahn, M. 1990. Prediction of sinkage and rolling resistance for off-the-road vehicles considering penetration velocity. Proc. 10th International Conference of the ISTVS, Kobe, Japan, 371-381.
- 4) Krick, G. 1969. Radial and shear stress distribution under rigid wheels and pneumatic tires operating on yielding soils with consideration of tire deformation. Journal of Terramechanics, Vol.6, No. 3: 73-98.
- 5) Kutzbach, H. D. and H. Schrogl. 1987. Dynamic behaviour of rolling tractor tires. Proc. 9th International Conference of the ISTVS, Barcelona, Spain, 457-464.
- 6) Laib, L. 1979. On the dynamic behavior of agricultural tires. Journal of Terramechanics, Vol.16, No. 2: 77-85.
- 7) Mussel, U. Shmulevich, I. and Wolf, D. 1992 The effect of dynamically varying velocity on wheel traction. ASAE paper No. 92-1013. ASAE, St. Joseph, MI 49085
- 8) Mussel, U. 1993 The effect of varying velocity and load on wheel traction performance. P.Hd. Dissertation. Not published. Technion, Haifa.
- 9) Onafeko, O., and A.R. Reece. 1967. Soil stresses and deformations beneath rigid wheel. Journal of Terramechanics, Vol.4, No. 1: 59-80.
- 10) Pope, R.G. 1971. The effect of wheel speed on rolling resistance. Journal of Terramechanics, Vol.8, No. 1: 51-58.
- 11) Upadhyaya, S.K., W. J. Chancellor, D. Wulfsohn and J. L. Glancey. 1988. Sources of variability in traction data. Journal of Terramechanics, Vol.25, No. 4: 249-272.
- 12) Upadhyaya, S. K. and D. Wulfsohn. 1990. Review of traction prediction equations. ASAE Paper No.90-1573, Presented at 1990 International Winter meeting, Chicago, Illinois. 23p
- 13) Wood, R.K. and E.C. Burt. 1987. Soil-tire interface stress measurements. Transactions of the ASAE 30(5):1254-1258.
- 14) Wong, J. Y., and A. R. Reece. 1967. Prediction of rigid wheel performance based on the analysis of soil-wheel stresses. Part I performance of driven rigid wheel. Journal of Terramechanics, Vol.4, No. 1: 81-98.

- 15) Wong, J. Y., and A. R. Reece. 1967. Prediction of rigid wheel performance based on the analysis of soil-wheel stresses. Part II performance of towed rigid wheel. Journal of Terramechanics, Vol.4, No. 2: 7-25.
- 16) _____. 1990. Pro-Matlab™ for Sun workstations. User's Guide. The Math Works, Inc. Cochituate Place 24 Prime Park Way. Natick, MA. U. S. A.
- 17) _____. 1991. ASAE Standard: ASAE S296.3. Uniform terminology for traction of agricultural tractors, self-propelled implements, and other traction and transport devices.

V.2. DEVELOPMENT OF IMPROVED MEASUREMENT TECHNIQUES OF RELEVANT SOIL PARAMETERS

The following pre-prints and article drafts describe the general effort made to address the 2nd. major objective and the secondary objectives no. 1 to 4. The most difficult part was the design, construction and building-up the field wheel tester [1]. It required great engineering efforts and took too long a duration to make it ready to work (about two and a half years). Due the delay in getting this tester work on, previously obtained and collected data on tire footprints-soil properties-tire operation was carried-out [2].

V.2.1. A NEW FIELD SINGLE WHEEL TESTER

A field single wheel tester was designed, capable of performing off-road traction and determination of soil properties in situ. It is based on a heavy wheeled tractor on which a heavy duty bevameter and grouse-torque-meter are mounted and a wheel cage where vertical, horizontal and side forces can be measured.

A NEW FIELD SINGLE WHEEL TESTER

Ronai D., Shmulevich I., Wolf D.

Technion, Faculty of Agricultural Engineering, 32000 Haifa, Israel

Abstract

A field single wheel testing device (TWT) developed at the Department of Agricultural Engineering, Technion, Haifa, is a mobile testing unit capable to perform traction tests of agricultural or cross country tires in the field. The tire tester is based on heavy wheeled tractor which carries as well a unique bevameter mounted on the front side. The vertical, horizontal and side forces are measured inside the main cage, while the torque is measured by the separate linkage system. The tire testing device is capable to test tires up to 2 m in diameter, to apply vertical force up to 50 kN, and torque up to 31 kNm.

1. Introduction

Currently, 15 to 20 million agricultural tractors are active in the USA and Europe only (McKee, 1992 [5]), and the loss of fuel caused by inadequate choice of agricultural tires in the USA alone costs the country 575 million liter of fuel per year (Gill and Vanden Berg, 1968 [4]). Thus, lack of an adequate tires choice recommendations necessitated the buildup of tire testing devices that could ultimately contribute to energy saving. Excessive soil compaction caused by tire action was also one of the leading reasons for development, control and adequate choice of agricultural tires. Reported crop yield reductions caused by

the increase of soil bulk density, which influences root growing, soil aeration and water movement ranged between 10% and 20% depending on soil type and technology applied. Better choice of tractor tires, beside other influences, can greatly improve the present situation. Tire design is almost entirely determined by experimental methods, so, more than 90 testing facilities have been developed worldwide. Most of them (80%) are an indoor soil bin devices (Wismer, 1984 [7]).



Fig. 1. The Technion mobile soil and tire testing device

Indoor soil bin facilities can provide well controlled testing conditions but, it requires the remolding of the soil mass after each test run, thus it generates certain problems related to natural soil conditions. Instrumented tractors are often used for tire traction tests, but control of dynamic vertical load has certain influence on the test results and is very difficult during test run. Some single wheel testers have been developed mostly by government agencies in the USA and other countries (e.g. single wheel testing devices developed at the National Soil Dynamic Laboratory (NSDL, Auburn, USA), Silsoe Institute, England, and University of California, Davis, are typical of actual tire testing devices).

Table 1: Basic performances of build wheel testers

	NSDL	NIAE	DAVIS, CA
Tire range	from 12.4-28 to 30.5-32	from 11.2 - 28 to 18.4 - 38	from 0.46 m to 2 m diameter
Vertical load	up to 71.2 kN	Dead weight	up to 26.7 kN
Draft force	up to 44.5 kN	up to 25 kN	up to 13.2 kN
Draft control	Yes	Yes	Yes
Slip control	Yes	Yes	Yes
Load control	Yes	Dead weight	Yes
Test distance	80 m	Infinite	12.2 m

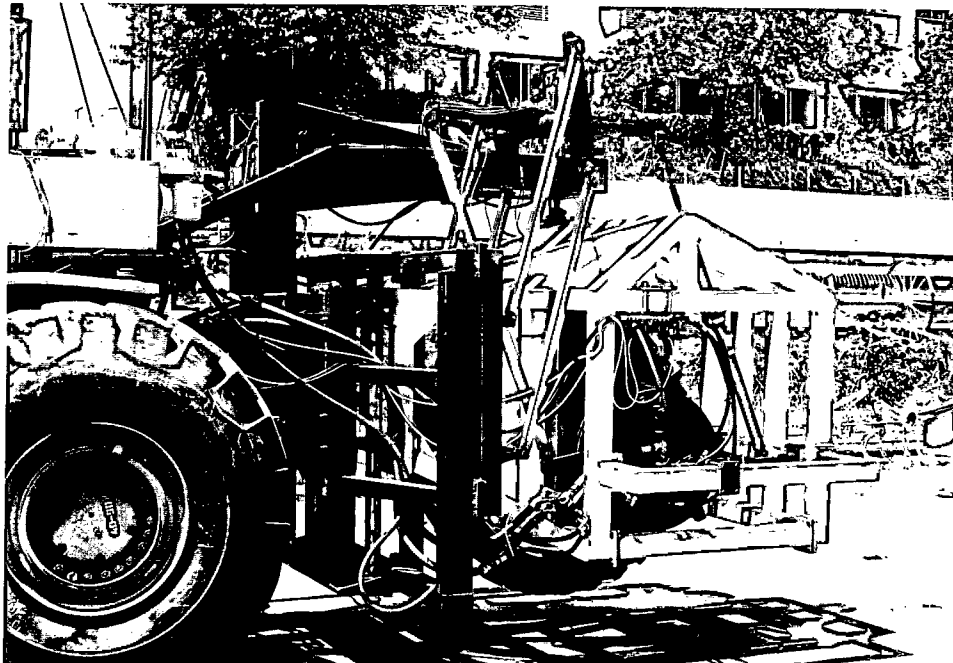


Fig. 2: Closer view of tire testing device

The NSDL single wheel tester (Burt, et al. 1980, [3]) was developed as an indoor and outdoor soil bin device capable of performing either variable travel reduction tests (while keeping the dynamic load constant) or variable dynamic load tests, (while maintaining travel reduction constant). Each major function, such as vertical load, angular velocity of tested tires and car's forward velocity, has its own control system. Some performances of NSDL wheel tester are given in Table 1. The NSDL unit is able to perform all necessary tire tests with very high level of control, but is limited to work in soil bin facilities, i.e., under remolded soil conditions.

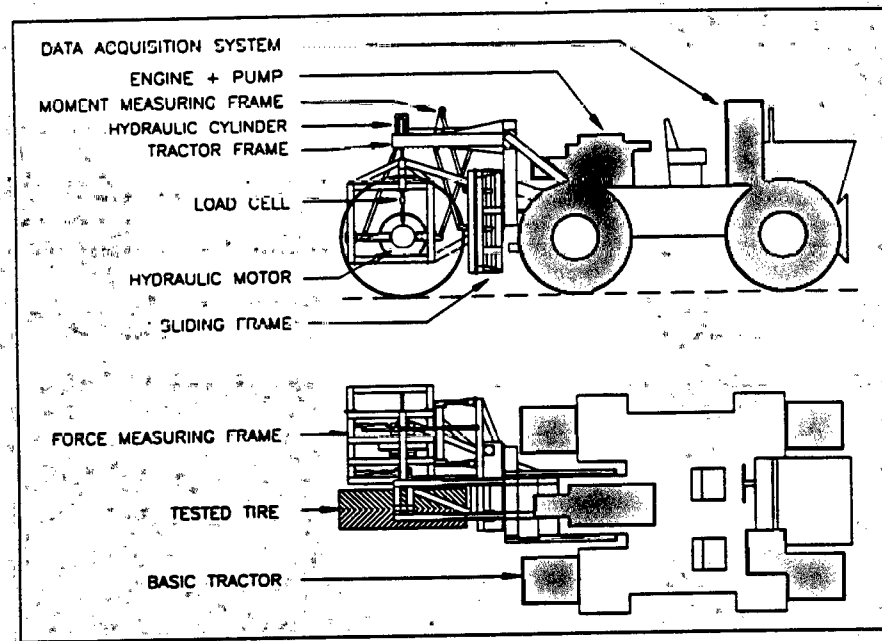


Fig. 3: Schematic view of the TWT

The NIAE Mk-2 single wheel tester (Billington, 1973, [1]) allows tests to be carried out either at constant forward speed or constant test wheel speed under field conditions. The unit is based on FC 1004 tractor and designed to cover a wide range of agricultural tires (Table 1). The tester gives continuous readings of the forward wheel's speed, tractive force and torque. The vertical load on NIAE Mk II wheel tester can be varied by adding weights to the rack fitted on the top of the test wheel carriage, which excludes possibilities to perform experiments with continuously varied dynamic load.

The single wheel tester developed at the University of California, Davis (Upadhyaya et al, 1986, [6]), is essentially a mobile soil bin unit that can be used to perform controlled field experiments (Table 1). The Davis, CA field single wheel tester is a certain combination of both, soil bin and field testing devices. It means that its operation is performed in the field but the length of test run is limited.

The Technion's tire tester allows free movement over the field and tire tests with continuously varying vertical load and slip, as well. In addition, it is able to measure and process all the requested traction data in real time. The same basic tractor carries the soil penetration and shear device on the front side, as shown in Fig. 1, thus allowing collection of all necessary data for tire traction analysis in the field. The closer view of tire testing device is given on Fig. 2.

2. The units' Design

The Technion's field single wheel tester (TWT), shown schematically in Fig. 3, is built around a M.R.S tractor, Model I-110. The weight of 17 tons of the basic unit allows testing of a full range of agricultural tires specified in the ASAE Standard S220.4 (SAE J711). That means that TWT is able to test tires up to 2 meters in diameter as well as to apply the recommended vertical loads.

The TWT consists of two frames for force and torque measurements, a hydraulic motor, a loading cylinder, measuring devices, sliding connection frame and tractor connection frame, shown in Fig. 3.

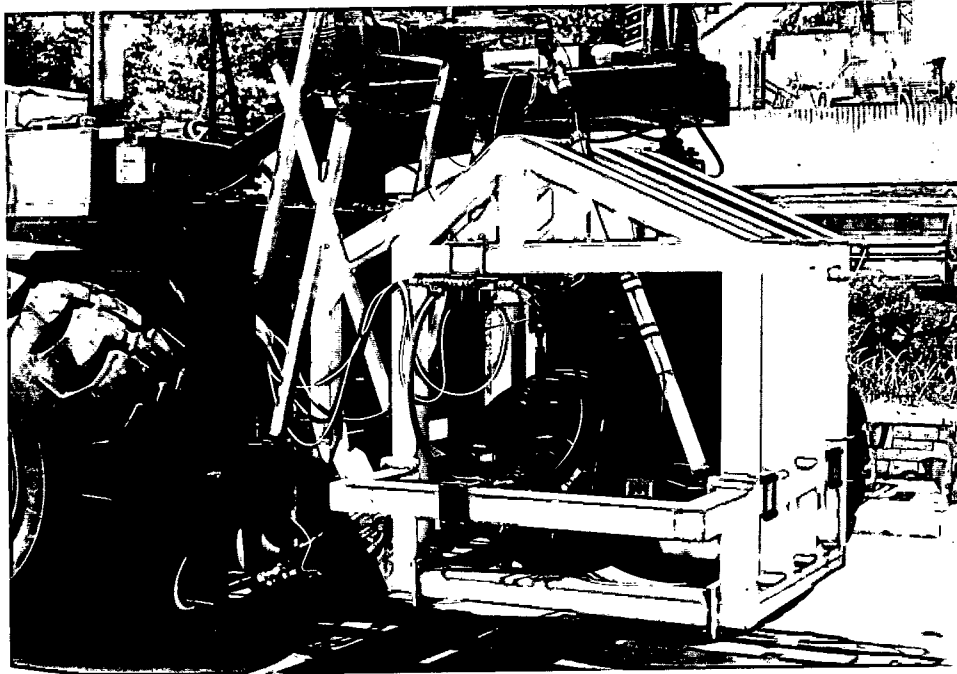


Fig. 4: Location of the hydraulic motor

The drawing unit consists of a low-speed hydraulic motor located inside of the measuring frame (Fig. 4), produced by Hagglunds, type 4071, with a maximum RPM of 38 (which, with two speed valves, increases up to 65). The maximum torque per 100 kPa is 140 Nm and maximum peak pressure is 20 MPa that gives about 28 KNm torque.

The Hagglunds 4071 is able to perform constant torque for a given pressure throughout the speed range and full starting torque. Also, it permits low RPM without loss of smooth running, two speed ranges with the same oil supply, and instant reversing. The hydraulic motor and power shaft are connected to the force measuring frame, via load cell assemblies (Fig. 5).

The hydraulic motor is supported by a separate frame (upper part of the motor supporting frame is given on Fig. 6). The object of dividing the mainframe in two parts is to exclude the influence of the developed torque and related circumferential forces, from the measuring units for dynamic load and draft force. A finite element model of the device helped to exclude undesirable influences of torque on force measurement and prevent the interdependence between horizontal and vertical force measurements.

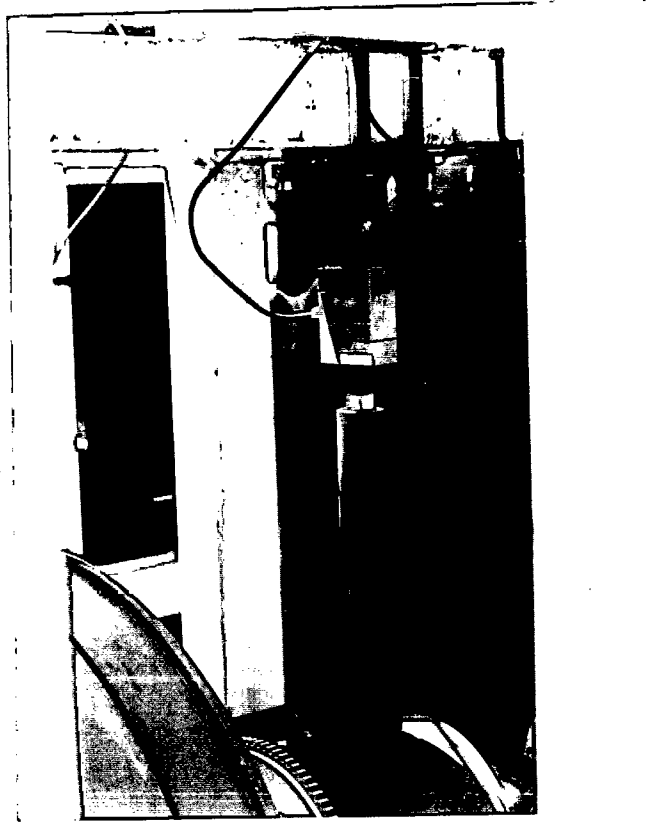


Fig.5: Detail of load cell assembly

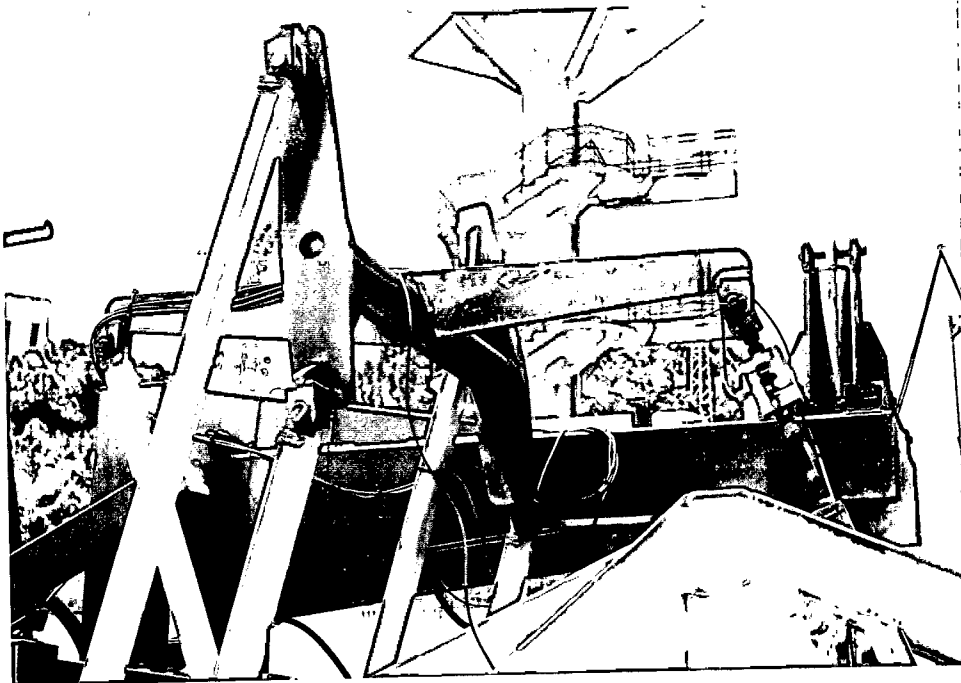


Fig. 6. Detail of the motor supporting frame

The torque frame, formed as a parallel linkage mechanism, is able to move vertically and prevent rotation of the stator part of the hydraulic motor. To calculate developed torque the force can be measured in one of the linkages by the HBM USB 5K load cell assembly. All the torque frame linkages are mutually connected by pin joints, and the whole torque frame is directly supported by the basic tractor.

The force measuring frame is connected to the sliding frame which allows for free movement along the vertical axes. This important possibility prevents both weight transfer from basic tractor to the measuring units and existence of vertical component of draft force that can affect the vertical load measurement reliability. The sliding frame is connected to the basic tractor body by a separate construction which supports the vertical hydro-cylinder which applies vertical load.

The range of vertical load is 0 to 50 kN with the possibility of continuous variation during the test. In addition, the conceptual solution of the testing device allows for easy changing of tested wheels.

The basic scheme of TWT hydraulic system is given on Fig. 7. The hydraulic system is divided in two separate parts with respect to power supply. The first part with hydraulic motor is fed by an additional engine and a pump mounted on the rear tractor side (Fig. 8). The system includes fine regulation of oil flow using adequate control chart, thus allowing regulation of RPM of tested wheel. The second part of the hydraulic system is supplied by a built-in tractor oil pump. This system serves as a power source for vertical loading of the tested wheel (Fig. 9). The system controls the oil pressure in the vertical cylinder, and acts as compensation of the field roughness influence on the applied load.

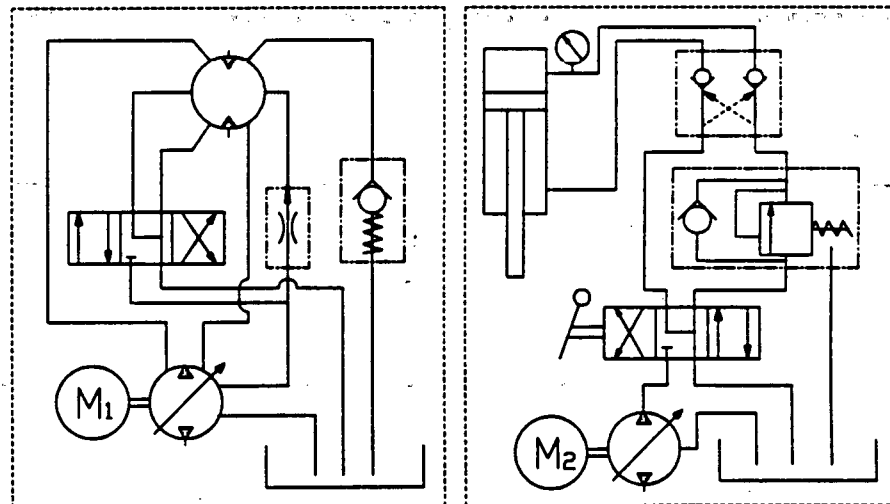


Fig. 7. Basic hydraulic system of the TWT

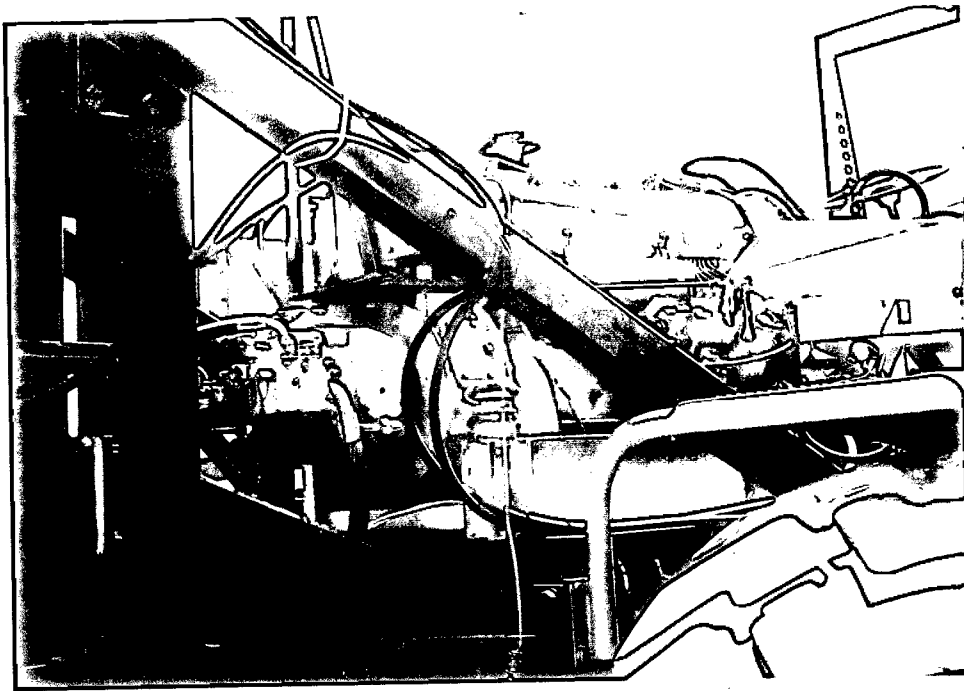


Fig.8: Detail of additional engine and a pump mounted on the rear tractor side

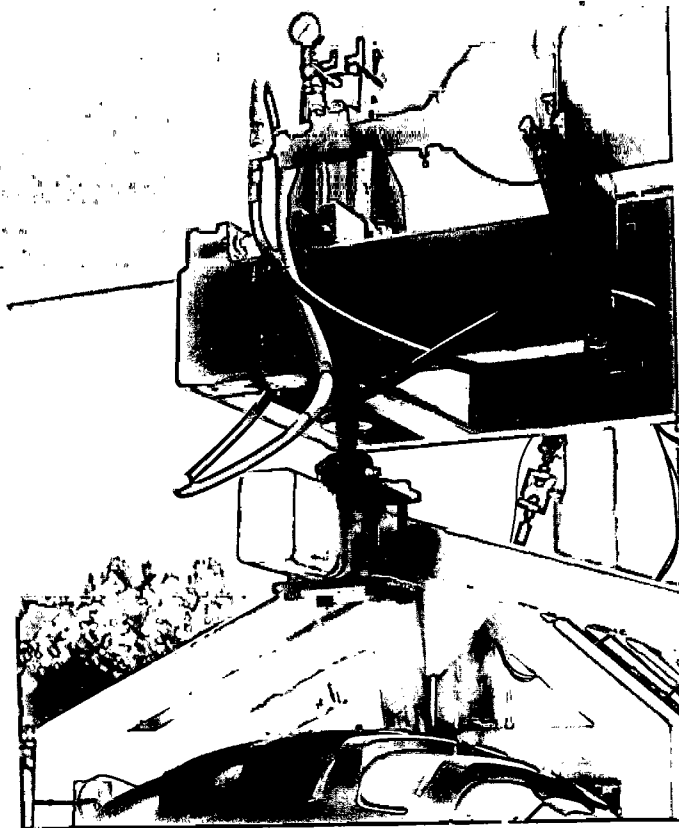


Fig. 9: Wheel loading assembly

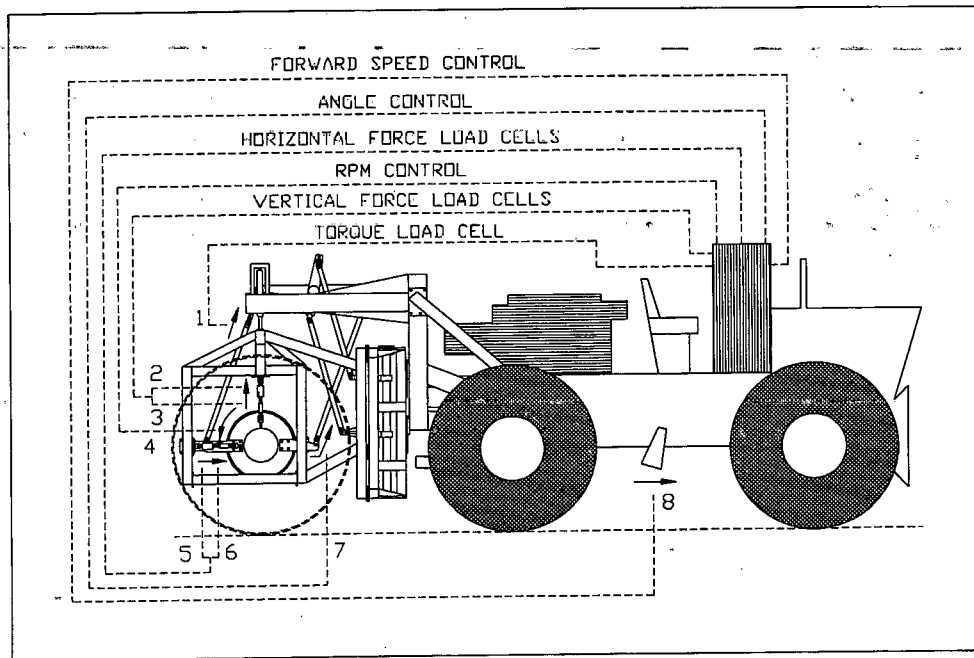


Fig. 10. Schematic view of measuring positions on the TWT

Vertical load is measured by means of two load cells (HBM USB 10K and HBM USB 5K) which are connected between the force measuring frame and power assembly by the universal joints and length adjusters. Likewise, two horizontally positioned load cells are mounted (Fig. 10).

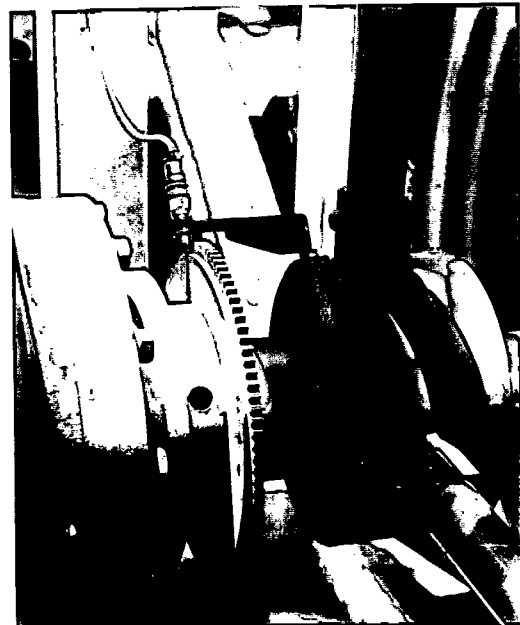


Fig. 11: Forward tractor speed (left) and wheel RPM (right) measuring assemblies

In addition, the side force is supported by two universal rod ends, which are located between the hydraulic motor and the force measuring frame.

Besides the measuring of horizontal and vertical forces, the testing device is instrumented to give continual readings of both forward tractor speed and angular velocity of the tested wheel (Fig.11). In addition, developed torque is measured by measuring of force in one of the moment frame linkages and accompanied angle between the linkage and the horizontal axle. All collected signals for forces and speeds are analog to digital, converted and processed by a PC located on the basic tractor (Fig. 12). Overall scheme of data acquisition system is given on Fig. 13.

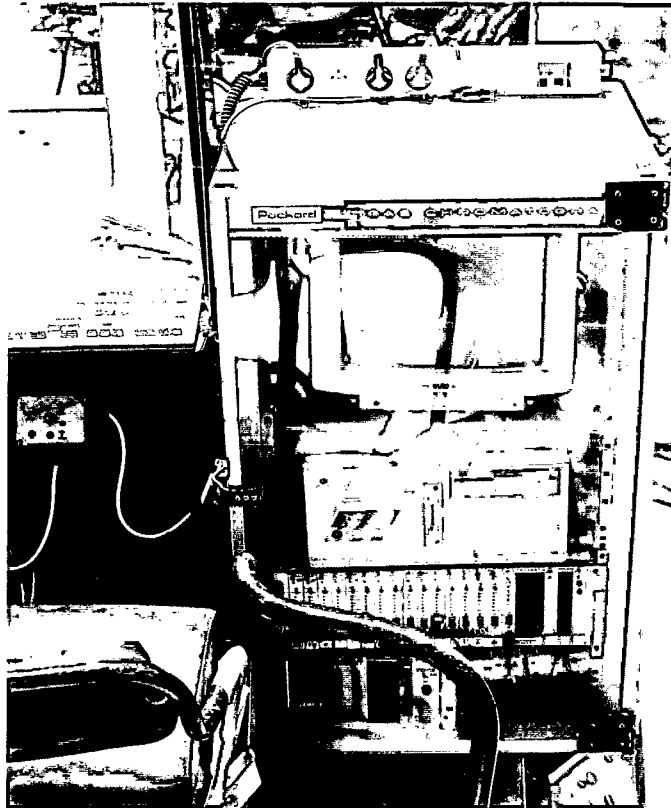


Fig. 12: Data acquisition system located on the basic tractor

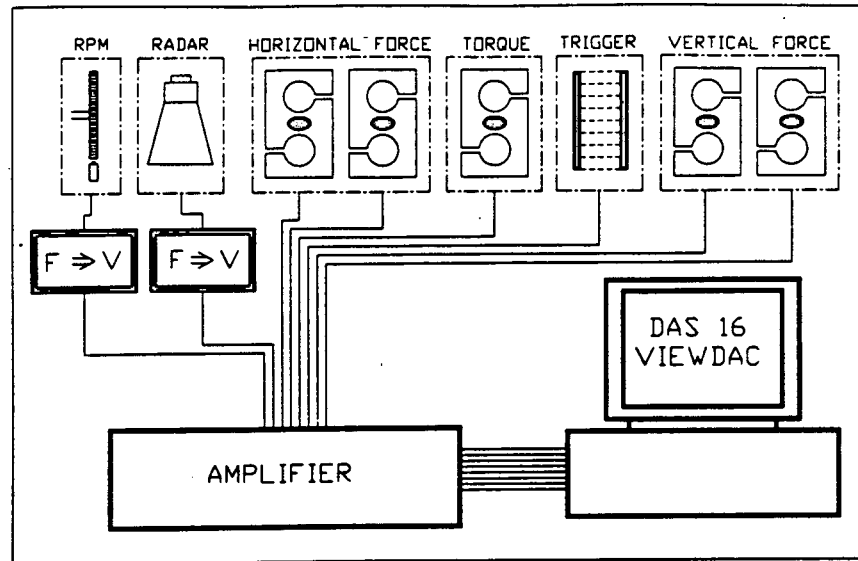


Fig. 13. Scheme of the measuring, conditioning and data processing system of the TWT

3. Testing capabilities

The TWT is designed to perform all requested tests related to complete characterization of traction characteristics of agricultural and cross-country tires, namely, to perform all three possible tire rolling conditions, such as: towed mode, self-propelled mode and driving mode, which are necessary for defining all traction characteristics including definition of optimal slip value, where developed draft force is maximal. Also, basic tire data, such as dynamic rolling radius, can be defined either from towed or self-propelled testing modes. To measure dependencies of either the developed draft force or torque of the tested tire on tire slip, thus enabling us to understand the tire traction capabilities for certain test conditions, as shown in Fig 14. (Brixius and Wismer, 1978, [2]).

As a result of tire traction tests which TWT is able to produce are relations of coefficient of traction (k) versus slip (Eq. 1) and tractive efficiency (TE) versus slip (Eq. 2) for defined test conditions, as shown in Fig 15,

$$\text{Coefficient of traction:} \quad k = P/W \quad \dots(1)$$

$$\text{Traction efficiency:} \quad TE = PV_t / Q\omega \quad \dots(2)$$

where (ω) is angular wheel speed.

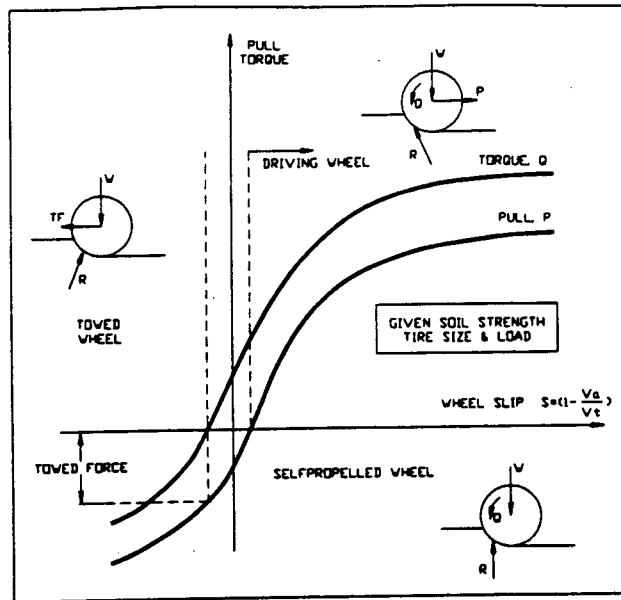


Fig. 14: Pull-Torque-Slip relation; Wheels on soil [2]. (W-Load, Q-Torque, R-Motion Resistance, S-Slip, V_a -Wheel speed, V_t -Travel speed, P-Pull, TF-Towed force) /2/

The TWT allows to perform tire tests in slip and vertical load mode, which means that the device is able to control input torque, vertical load and wheel speed.

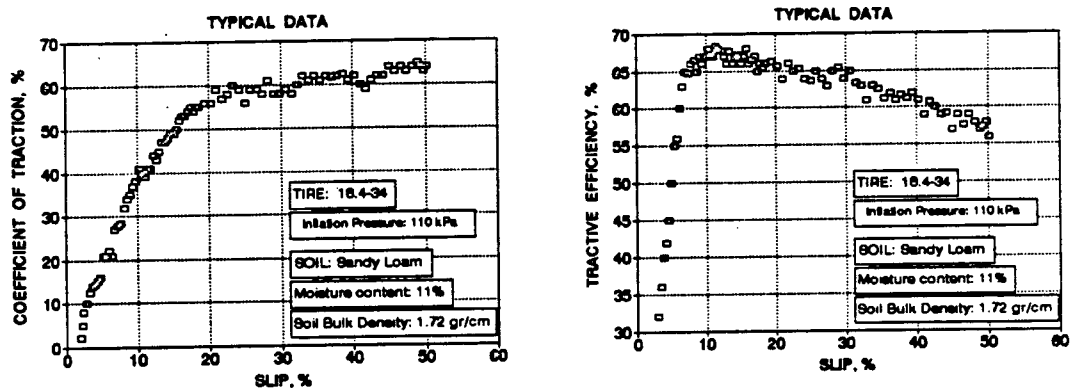


Fig. 15: Typical results of tire traction test

Generally, the flow chart of the TWT performance capabilities in tire tests, is shown in Fig. 16. The first is related to definition of tested tire's dynamic rolling radius which is necessary for further calculation of traction values. This type of test is performed on the rigid surface and can be done either in the towed or self-propelled tire mode. The TWT allows for both mentioned procedures. The constant load test includes control of constant forward speed of vehicle and constant level of vertical load. The torque increases during the test generating an increase of tire slip and draft force.

4. Conclusion

The TWT is a unique testing unit allowing to test a wide range of agricultural tires in accordance with ASAE S220.4 standard.

The TWT performs tests with variable draft force, vertical load and travel reduction in the range recommended in the Standard.

The main advantage of the designed solution is a very close measurement of draft force and dynamic load on the tested wheel, as well as separate measurement of

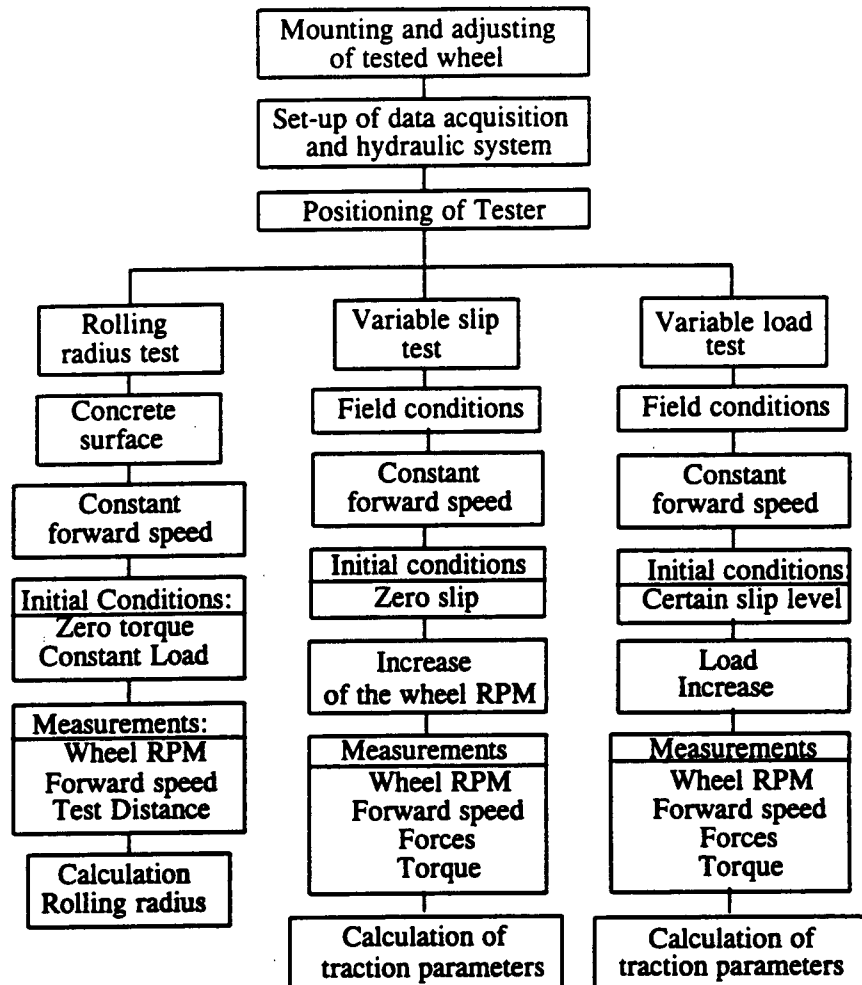


Fig. 16. Testing possibilities of the TWT

applied torque. At the same time, easy manipulation with tested wheel in the field is fully accomplished by the use of semi driven axle.

5. Acknowledgment

This study was done within the scope of BARD Project No. US-1848-90R titled: Traction-Soil Compaction Tradeoffs as a Function of Dynamic Soil-Tire Interaction Due to Varying Soil and Loading Conditions.

6. References

- 1) Billington P. W ,*The NIAE Mk II single wheel tester*, J. Agricultural Engineering Research, 1973, No.(18), pp 67-70;
- 2) Brixius W.W., Wismer R.D., *The role of slip in traction*, ASAE Paper No 78-1538, 1978;
- 3) Burt E. C, Reaves C. A, Bailey A. C, Pickering W. D., *A Machine for testing tractor tires in soil bins*, Transaction of the ASAE, 1980, Vol. 23(3), pp 546-547;
- 4) Gill W. R, Vanden Berg G. E, *Soil Dynamics in Tillage and traction*, Agricultural Handbook No. 316, ARA, USDA, 1968, p 511;
- 5) McKee A., *The role of the conventional tractor*, Presented at the Institution's Scottish Branch Conference "Tractors for Tomorrow", Edinburgh, 1992;
- 6) Upadhyaya S. K., Mehkschau J., Wulfson D., Glancey J. L., *Development of a unique, mobile, single wheel traction testing device*, Transaction of the ASAE, 1986, Vol. 29 (5), pp 1243-1246;
- 7) Wismer R. D, *Soil bin facilities: Characteristics and utilization*, Proc. of the First Int. Conference of ISTVS, 1984, Vol. III, pp 1201-1213;

V.2.2. TIRE FOOTPRINT CHARACTERISTICS AS A FUNCTION OF SOIL PROPERTIES AND TIRE OPERATION.

Results collected previously for two soils and two different transport tires operated under various tire loads, inflation pressures, and soil moisture contents were analyzed. It was found that tire footprints(e.g. contact area, length, width, sinkage)can be reliably predicted from established linear, multi-variety regression.

TIRE FOOTPRINT CHARACTERISTICS AS A FUNCTION OF SOIL PROPERTIES AND TIRE OPERATIONS

Ronai D*., Shmulevich I.*

Summary -The main objective of the following presentation is to examine the possibility of predicting agricultural tire footprint parameters under different operational conditions. The experimental part involved two agricultural transport tires operated on two soils, under variations of tire load inflation pressures and soil moisture contents. Results obtained show that tire footprint parameters, named contact area, length, width and sinkage, can be reliably predicted by using multifactorial linear and total regressions, within the range of recommended tire loads, inflation pressures and soil moisture contents around the plastic limit.

INTRODUCTION

Compaction of agricultural soils is mainly caused by field traffic. Field traffic includes operations such as basic tillage, secondary cultivation, spraying and harvesting, as well as traffic of transport equipment. Transport equipment activity over the field often causes greater soil damage than machinery for basic tillage. The reason is that axle loads of transportation equipment are usually very high while tires and their inflation pressures are often inadequately chosen to prevent soil compaction. In addition, the traffic paths of transportation vehicles over the field are more or less random and the field compacted area is usually very large after harvesting. Therefore, there is a need, to examine properly the influence of transportation activities and the activities of basic agricultural machinery on soil compaction phenomena, in order to predict seasonal soil compaction. Since compaction results from contact pressure or stresses, it is of great interest to examine the possibilities for prediction of geometrical parameters of tire-soil contact area of agricultural transport tires as a part of soil compaction phenomena. The mentioned relations can then be used as one of the inputs into more complex tire-soil system models.

The shape and dimensions of tire footprint area are very important soil-tire interactive characteristics which affect the pressure distribution at the boundary level, as well as the stress-strain relation deeper at the soil mass, and can be very helpful as an input data for a more complex tire-soil compaction model.

In order to analyze and predict soil compaction in the sub soil, the tire-soil system can be divided three following subsystems which require specific analyses, such as:

- Analysis of tire-soil contact area;
- Analysis of applied forces and their distribution over the contact area;
- Analysis of stress-strain distribution in soil mass under moving tires includes relations between stresses imposed and the relevant resultant compaction indices, such as, for example, tire sinkage and soil density.

The tire-soil interactive characteristics were explored and studied, but have not yet have been entirely understood and described. Studies by Sohne [1] showed the effects of tire footprint area shape on pressure distribution on hard and soft surfaces, for different tire characteristics, inflation pressures and vertical loads. It was one of the first researches

which introduced the tire footprint area as an important part of tire-soil modeling. Ageikin [2] attempted to give an analytical description of tire footprint area. The area was described as a combination of two ellipses, and since tire and soil elastic parameters were taken into account, fairly useful results were obtained.

Various models have been developed to describe tire contact area on rigid surface for certain tire characteristics such as carcass stiffness and inflation pressure (Karafiath, [3]). Komandy [4] developed empirical equations for tire loading capacity, footprint parameters and tire deflection. In addition, the highest permissible load as a function of tire geometry and construction was defined in his work. The tire tread "painting technique" was used by Plackett [5], with particular attention on tire lugs action and tire lug tread stiffness. He established a linear relationship between load and tire deflection. Upadhyaya and Wulfson [6] showed that contact area for small tire deflection is elliptical, and that the increase of the contact area width during the increase of tire deflection is limited. In addition, they developed analytical expressions for contact length, width and area, on rigid surface. Kolbov [7] discussed the changes of load position in relation to contact area, while Fujimoto [8] studied an elastic tire as a rigid wheel of larger diameter.

The main objective of the study presented is to develop a relation between certain agricultural transport tire parameters such as vertical loads and inflation pressures, and tire footprint characteristics, such as footprint area, length, width and sinkage, for some typical agricultural soils with variable moisture contents.

EQUIPMENT AND PROCEDURE

The tests included two agricultural tires used for transport 13/65-18 12PR and 7.50-20 12PR that are usually used on trucks and trailers in many countries. According to preliminary observation of typical agricultural transport vehicles in use, inflation pressures

Table 1. Texture of tested soils

Variety of soil	Sand > 0.2 mm	Sand 0.2-0.02	Silt 0.02-0.002	Clay < 0.002	Total Sand	Total Clay
Chernozem	0.8	37.44	30.56	31.20	38.24	61.76
Black soil	1.6	27.66	34.64	36.00	29.36	70.64

for the above mentioned tires range among 100 and 500 kPa, and the vertical load among 8 and 20 kN. Thus, dependent variables during the test activities, were:

- Tire 13/65-18:

Inflation pressure: 100, 200 and 300 kPa
Vertical load: 8, 14 and 20 kN

- Tire 7.50-20:

Inflation pressure: 100, 250 and 400 kPa
Vertical load: 8, 14 and 20 kN

Both tires have been tested on two cohesive soils e.g. clayey-loam (variety of Chernozem) and clay (variety of black soil) with 4.5 to 6% organic matter. The closer characteristics of the soils are given in Table 1:

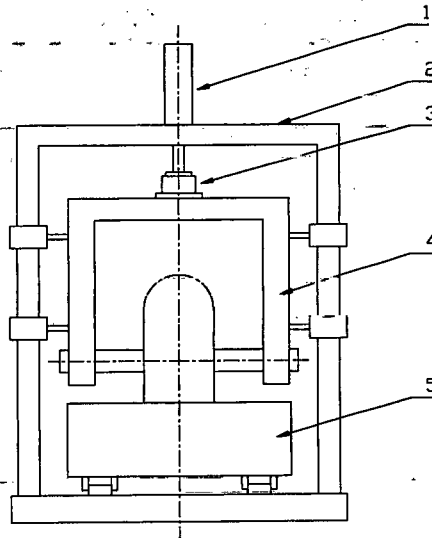


Fig. 1: Scheme of static tire testing device.

Moisture contents of the mentioned soils varied around plastic limits, or, around moisture content commonly observed during basic tillage operations. The moisture content

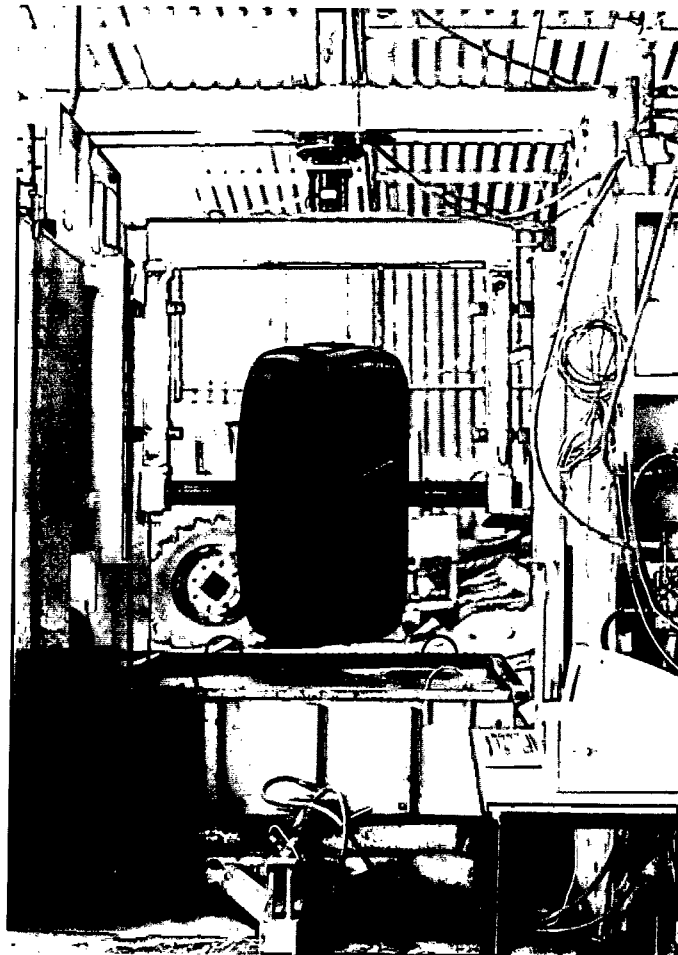


Fig. 2: Measuring device

range for Chernozem was between 15 and 27%, and for Black Soil between 23 and 35%. Both soils were precompacted in a soil bin until usual field condition was reached (porosity 55% *vol* for Chernozem and 65% *vol* for Black soil).

Tire footprint characteristics were measured by a special device, schematically given in Fig. 1, while the closer view is given on Fig. 2. This device consisted of a mainframe (2) with a loading cylinder (1) and a load transducer (3), given closer on Fig. 3.

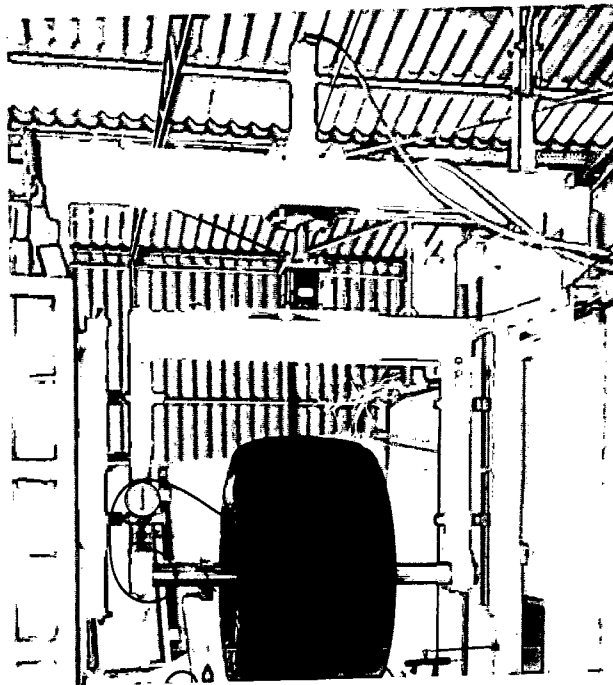


Fig. 3: Closer view of main frame, sliding frame, loading cylinder and load cell

The tested tires (5) was mounted on a sliding frame (4), while the soil was located in the moving carriage (6). The dimensions of the carriage excluded "side effects" but the depth of soil (50 cm) simulated the presence of a commonly existing hard pan.

The moving carriage is placed on the set of rollers, as it is shown on Fig. 4. The second, horizontal, hydraulic cylinder enables movement of the carriage.

Besides of the measuring of vertical load, the device is also equipped with horizontal load cell, given on the Fig. 4. The horizontal load cell enables measuring motion resistance of the carriage. Knowing the resistance of unloaded carriage filled by soil, the reading of the horizontal force necessary to move loaded carriage, can give information about motion resistance of the loaded tire under the given soil conditions.

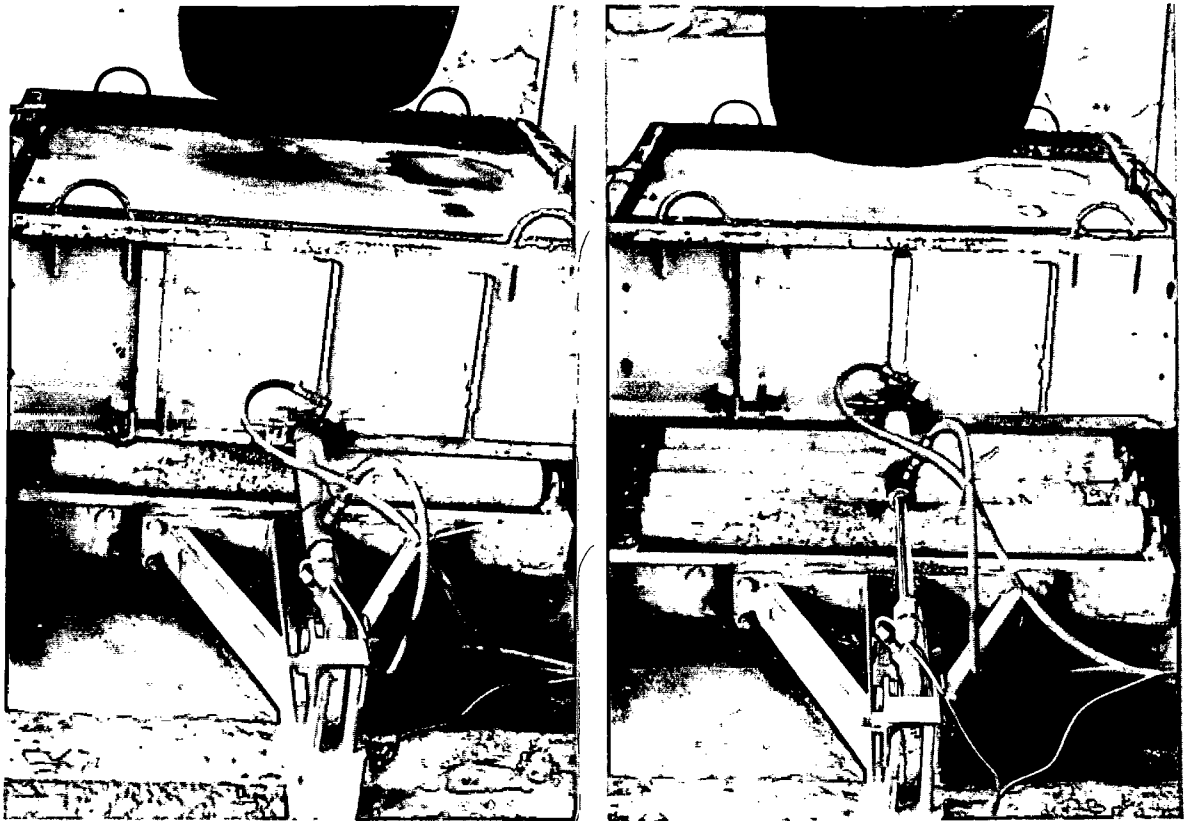


Fig. 3: Two position of the moving carriage

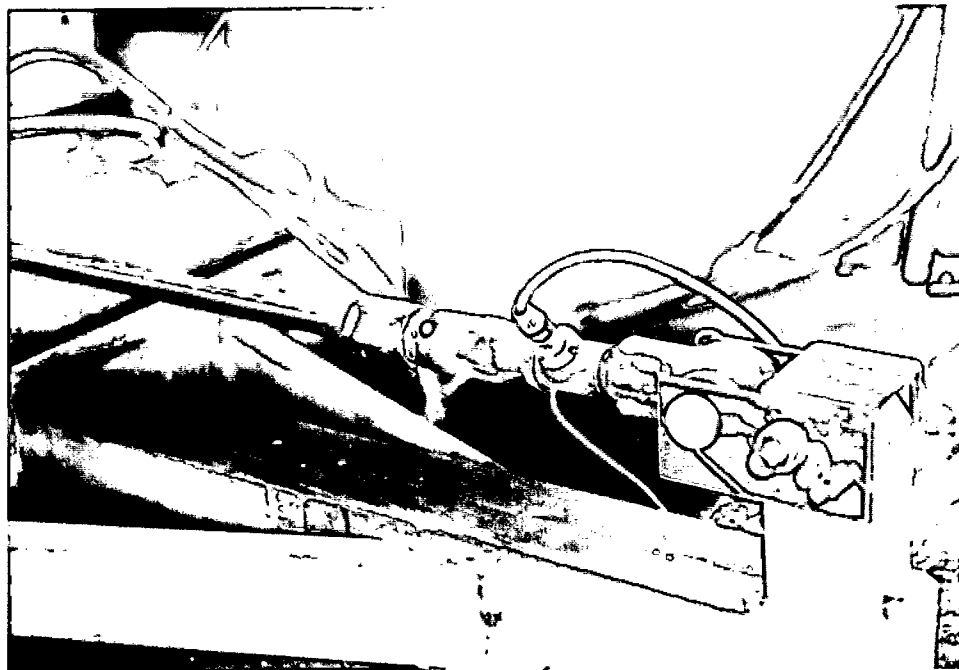


Fig. 4: Horizontal load cell

The device is equipped by regulated hydraulic power supply enables to keep constant amount of vertical force during the carriage movement.

Data collection, condition and acquisition system enable, Fig. 5, enables continual measuring of vertical and horizontal forces, as well as, vertical and horizontal displacement of the loaded tire body.

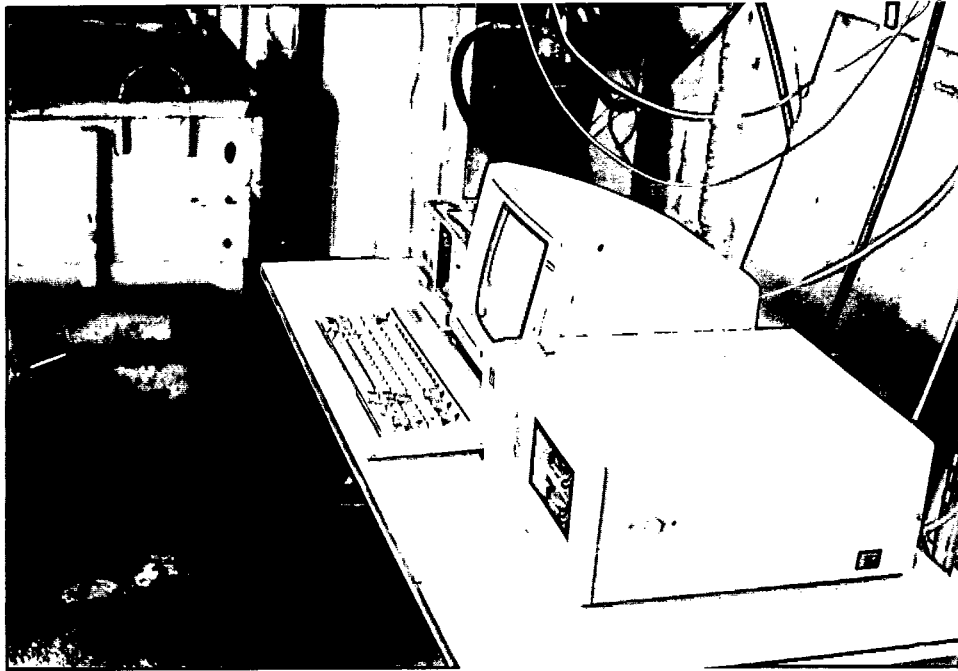


Fig. 5: Data acquisition system

The soils were first moistened, then placed in the bin's carriage and precompacted to the mentioned level. After the soil preparation stage, the tire, loaded up to the specific amount, was rolled over the soil by pulling the carriage for about 70 cm. Therefore, the carriage forward movement initiated the tire rolling. The rear side of the tire footprint was marked by special nails and the tire was unloaded and lifted after the marking was finished. An example of taken footprint in sand is given on Fig. 6.

After unloading, the footprint characteristics were measured using a 50x50 mm grid, shown schematically in Fig. 7. The sinkage was measured through holes drilled, in the grid corners, at 50 mm distances.

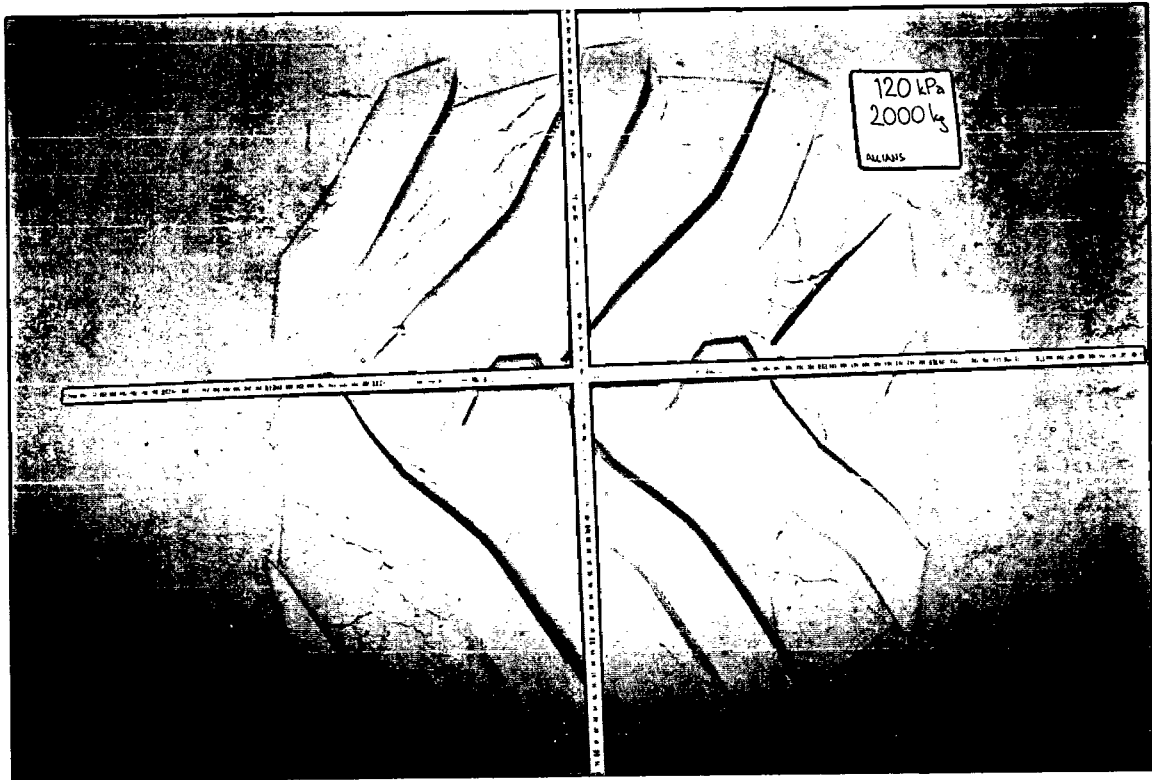


Fig. 6: Tire footprint in sand

RESULTS AND DISCUSSION

The examples of measured footprint area for the tire 13/65-18 in both tested soils are given in Fig. 8.

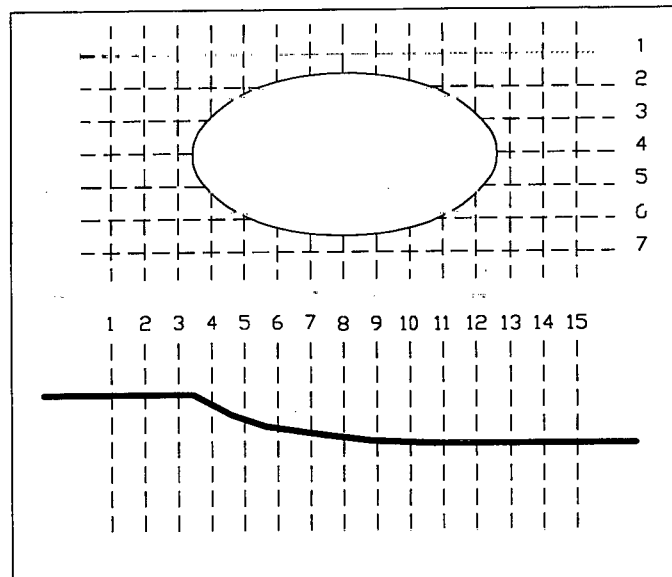


Fig. 7. Footprint measurement.

All footprint parameters, as expected, depended on load, inflation pressure and soil moisture content changes. Higher values of all independent variables (area, width, length and sinkage) were mostly obtained throughout the whole range of moisture contents in heavier Black Soil. The independent variables given in Fig. 3, show some regularity related to the changes of dependent variables, though, as it seems, only footprint width, especially for tire 7.50-20 shows some irregularity. Negligible or irregular changes of tire footprint width were also found by the other researchers [5].

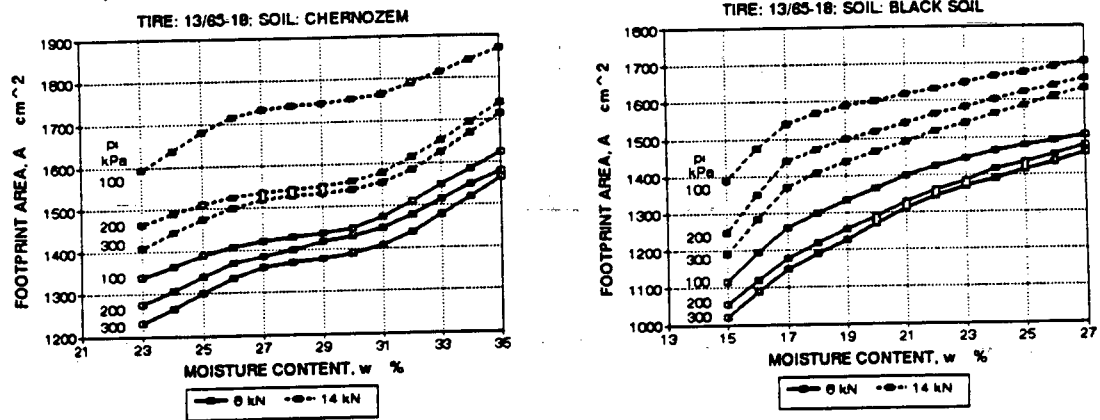


Fig. 8: The examples of measured values

The measured data for area (A), width (b), length (l) and sinkages (z) were fitted to a polynome of the third degree, using equations (1 to 4), i.e.:

$$A = k_{01} + k_{11}w + k_{21}w^2 + k_{31}w^3 \quad \dots (1)$$

$$b = k_{02} + k_{12}w + k_{22}w^2 + k_{32}w^3 \quad \dots (2)$$

$$l = k_{03} + k_{13}w + k_{23}w^2 + k_{33}w^3 \quad \dots (3)$$

$$z = k_{04} + k_{14}w + k_{24}w^2 + k_{34}w^3 \quad \dots (4)$$

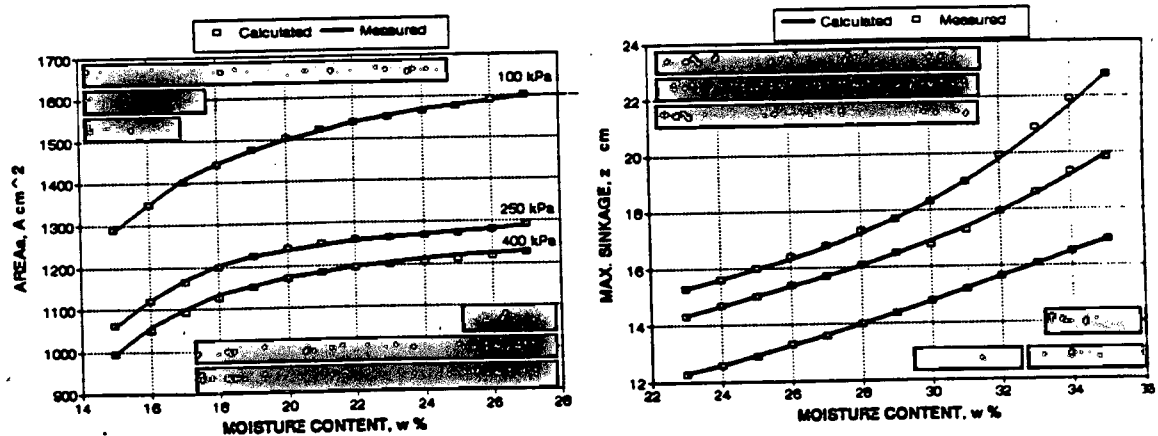


Fig. 9: The example of measured and fitted data.

where (w) is the soil moisture content and (k_{0i} , k_{1i} , k_{2i} and k_{3i}) are constants.

Examples of fitted data are given in Fig. 9 and the R-square values for all curve fitting have been very close to one.

The analysis of variances done by SAS computer statistical package for fitting data is given in Table 2. The analysis of variance was done in order to determine whether the treatment variations were the main source of variation or an experimental error.

Table 2. The analysis of variance

ANALYSIS OF VARIANCE						
Soil Type	Variable	F-VALUE				
		Model	Load	Press.	Moist.	C.V.
Chernoz. 13/65-18	Area	186**	820**	168**	83**	2.64
	Width	95**	412**	227**	20**	1.13
	Length	235**	1179**	198**	84**	1.62
	Sinkage	438**	462**	235**	528**	3.31
Black soil 13/65-18	Area	184**	1032**	210**	39**	2.33
	Width	191**	931**	318**	30**	0.66
	Length	242**	1283**	292**	60**	1.55
	Sinkage	191**	404**	360**	127**	3.78
Chernoz. 7.50-20	Area	128**	444**	389**	32**	3.63
	Width	74**	118**	464**	1.5ns	2.25
	Length	397**	1375**	454**	225**	1.17
	Sinkage	1052**	1122**	545**	1125**	2.03
Black soil 7.50-20	Area	369**	1515**	1081**	60**	2.03
	Width	85**	308**	371**	0.4ns	2.27
	Length	597**	2013**	1285**	246**	.98
	Sinkage	124**	216**	94**	115**	4.37
** Indicates significance at $\alpha=0.01$						
ns Indicates nonsignificance						

The data given in the Table 2 show a "highly significant" relation between all measured values (Area, Width, Length and Sinkage) to the tire loads and inflation pressures. In addition, for the 7.50-20 tire no significant influence of soil moisture content on footprint width change can be noticed. The analysis of C.V. shows that the obtained results are reliable.

Regression analyses of three-factorial sets of experiments were performed and empirical relation between tire footprint characteristics as independent variables, and tire load, inflation pressure and soil moisture content as dependent variables, were established.

SAS program allowed analyses of optimal regression procedure. The values of R-square are used as an estimation factor for four different regression procedures, i.e.:

Linear:

$$y = a_{0i} + a_{1i}F_n + a_{2i}P_i + a_{3i}w \quad (5)$$

Table 3. R-square values for regression procedures

Soil Type	Variable	R-SQUARE			
		Linear	Quadr.	Cross	Total
Chernoz. 13/65-18	Area	0.9425	0.0211	0.0277	0.9913
	Width	0.9009	0.0335	0.0537	0.9881
	Length	0.9457	0.0244	0.0191	0.9891
	Sinkage	0.9856	0.0003	0.0077	0.9935
Black soil 13/65-18	Area	0.9517	0.0088	0.0183	0.9856
	Width	0.9585	0.0088	0.0537	0.9881
	Length	0.9659	0.0045	0.0211	0.9913
	Sinkage	0.9246	0.0216	0.0301	0.9836
Chernoz. 7.50-20	Area	0.8931	0.0576	0.0378	0.9836
	Width	0.8464	0.0661	0.0496	0.9618
	Length	0.9493	0.0159	0.0103	0.9761
	Sinkage	0.9354	0.0578	0.0031	0.9962
Black soil 7.50-20	Area	0.9335	0.0497	0.0093	0.9925
	Width	0.8934	0.0367	0.0621	0.9931
	Length	0.9569	0.0318	0.0014	0.9902
	Sinkage	0.9448	0.0068	0.0413	0.9931

Table 4. Parameters of Linear regression

Soil Type	Variable	LINEAR REGRESSION			
		a ₀₁	a ₁₁	a ₂₁	a ₃₁
Chernoz. 13/65-18	Area	614.06	30.390	-0.820	30.090
	Width	30.600	0.2100	-0.009	0.1400
	Length	29.620	0.7200	-0.018	0.5800
	Sinkage	-9.870	0.2600	0.0101	0.8100
Black soil 13/65-18	Area	760.04	32.370	-0.846	19.840
	Width	31.220	0.1900	-0.008	0.1100
	Length	39.720	0.7500	-0.021	0.5200
	Sinkage	-7.310	0.2800	0.0157	0.4800
Chernoz. 7.50-20	Area	632.04	23.410	-0.846	18.810
	Width	24.870	0.1600	-0.012	0.0100
	Length	31.720	0.6100	-0.014	0.7600
	Sinkage	-8.460	0.2600	0.0077	0.8700
Black soil 7.50-20	Area	609.27	26.090	-0.830	16.410
	Width	22.990	0.2600	-0.011	0.020
	Length	30.960	0.6700	-0.020	0.7400
	Sinkage	-7.960	0.2600	0.0071	0.6200
$y = a_{01} + a_{11}F_n + a_{21}p_i + a_{31}w$ $F_n \text{ [kN]}, p_i \text{ [kPa]}, w \text{ [%]}, a_{ij} \text{ [cm}^2\text{] or [cm]}$					

Quadratic:

$$y = a_{02} + a_{12}F_n^2 + a_{22}p_i^2 + a_{32}w^2 \quad (6)$$

Cross product:

$$y = a_{03} + a_{13}F_n p_i + a_{23}F_n w + a_{33}p_i w \quad (7)$$

Total:

$$y = a_{04} + a_{14}F_n + a_{24}p_i + a_{34}w + a_{44}F_n^2 + a_{54}p_i^2 + a_{64}w + a_{74}F_n p_i + a_{84}F_n w + a_{94}p_i w \quad (8)$$

where, (y) is an independent variable, (F_n) is dynamic load, (p_i) inflation pressure, and (a_{0i} to a_{9i}) are coefficients of analytical expressions. The calculated R-square values for equations (5) to (8) are given in the Table 3.

These values given in Table 3 enable one to conclude, that linear and total regression procedure (Equations 5 and 8) can generate acceptable prediction of independent variable. The equations' parameters for linear, Eq.(5) and total regression, Eq (8), for all tested tires and soils are given in the tables 4 and 5.

Analysis of data given in Table 4 shows that footprint characteristics for tire 13/65-18 are more predictable. It means that variations of footprint characteristics of this tire for load, inflation pressure and soil moisture content changes are more regular, compared with 7.50-20. Presented equations with given parameters are valid only for the range of tire loads and inflation pressures recommended by the manufacturer and the soil moisture content range around the soils plastic limit.

Table 5: Parameters for Total regression

Soil Type	Variable	TOTAL REGRESSION				
		a ₀₄	a ₁₄	a ₂₄	a ₃₄	a ₄₄
Chernoz. 13/65-18	Area	-462.95	67.0832	-1.3411	115.95	-0.5430
	Width	24.0235	0.18234	-0.0084	0.7685	0.0117
	Length	0.28234	1.37423	-0.0095	2.9436	-0.0073
	Sinkage	-5.7742	0.04344	-0.0063	0.7143	-0.0015
Black soil 13/65-18	Area	879.586	64.6185	-1.8154	0.8603	-0.0973
	Width	22.4912	0.42643	-0.0113	0.6219	-0.0003
	Length	26.3074	1.60362	-0.0228	0.3436	-0.0105
	Sinkage	19.7356	0.07541	-0.0179	-1.0705	-0.0122
Chernoz. 7.50-20	Area	-293.78	30.0262	-1.4048	106.76	0.3012
	Width	29.9968	0.37473	-0.0371	0.0021	0.0021
	Length	13.7846	0.94589	-0.0118	2.2750	-0.0139
	Sinkage	-37.803	1.11145	-0.0072	3.4020	-0.0283
Black soil 7.50-20	Area	-68.527	16.0379	-1.8051	72.662	0.5975
	Width	21.758	0.29147	-0.0333	0.2425	0.0034
	Length	20.3105	0.46575	-0.0494	1.7500	0.0049
	Sinkage	1.50921	-0.0287	-0.0329	-0.1062	-0.0099

Soil Type	Variable	TOTAL REGRESSION				
		a ₅₄	a ₆₄	a ₇₄	a ₈₄	a ₉₄
Chernoz. 13/65-18	Area	-0.0788	0.00206	-0.2726	0.0381	-2.1345
	Width	-0.0008	0.00002	-0.0069	0.0002	-0.0134
	Length	-0.0015	0.000011	-0.0075	0.0004	-0.0556
	Sinkage	-0.0005	0.000008	0.0066	0.0006	-0.0029
Black soil 13/65-18	Area	-0.0683	0.00405	-0.5471	0.0118	0.4187
	Width	-0.0003	0.00001	-0.0059	0.0001	-0.0078
	Length	0.0016	0.00005	-0.0080	0.0001	0.0046
	Sinkage	0.0010	0.00004	0.0115	0.0002	0.0235
Chernoz. 7.50-20	Area	-0.0007	0.00325	-0.0366	-0.1104	-2.0107
	Width	-0.0005	0.00004	-0.0073	0.0005	0.0091
	Length	-0.0007	0.00002	-0.0051	0.0003	-0.0605
	Sinkage	0.0002	0.00001	-0.0051	0.0003	-0.0605
Black soil 7.50-20	Area	-0.0270	0.00352	0.00271	-0.0140	-0.9102
	Width	-0.0007	0.00003	0.00167	0.0005	-0.0066
	Length	-0.0002	0.00008	0.00351	-0.0003	-0.0168
	Sinkage	0.0004	-0.00005	0.01648	-0.0010	0.0128

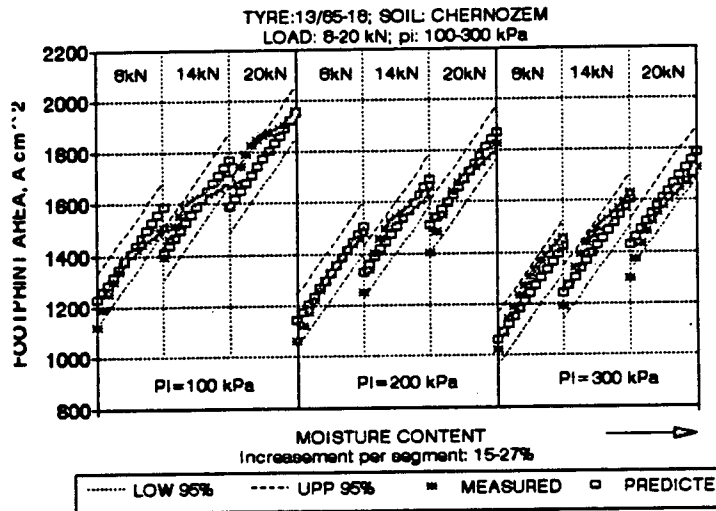


Fig. 10. Linear regression for footprint area ; Confidence level is 95 %; Conditions are listed in the figures.

The R-square values are higher for all regression equations calculated by total regression compared to the linear. This leads to the conclusion that the total regression procedure, equation (8), yields much better prediction of tire footprint characteristics than the linear one.

The mentioned conclusion is also illustrated in Figs. 10 and 11, where the measured and the predicted values for tire footprint area and width are shown for linear and total regression procedures, respectively.

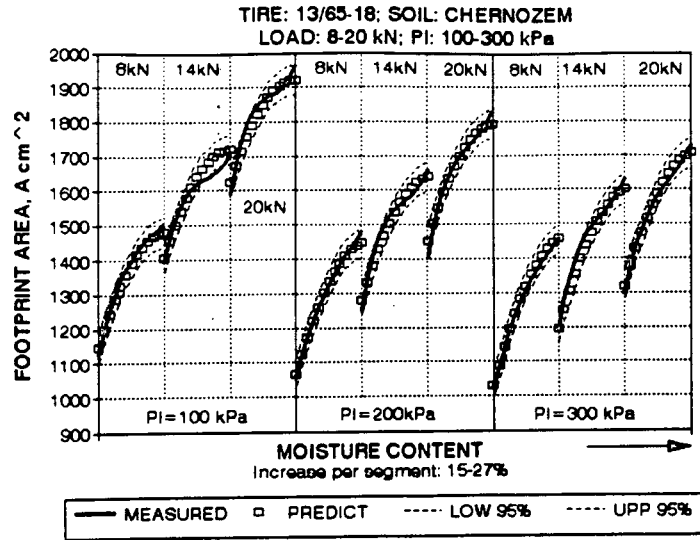


Fig.11: Total regression for footprint area ; Confidence level is 95 % and conditions are listed in the figures.

The analysis of the results obtained from linear regression procedure (Fig. 10) shows that the differences between measured and predicted values are higher for tire footprint width than for other observed parameters,. This can be also observed from R square values given on the Fig. 12. Moreover, it may be observed that footprint width changes are quite small in comparison to the other footprint characteristics. This means that tire footprint width can be taken as a constant value with no significant estimation error.

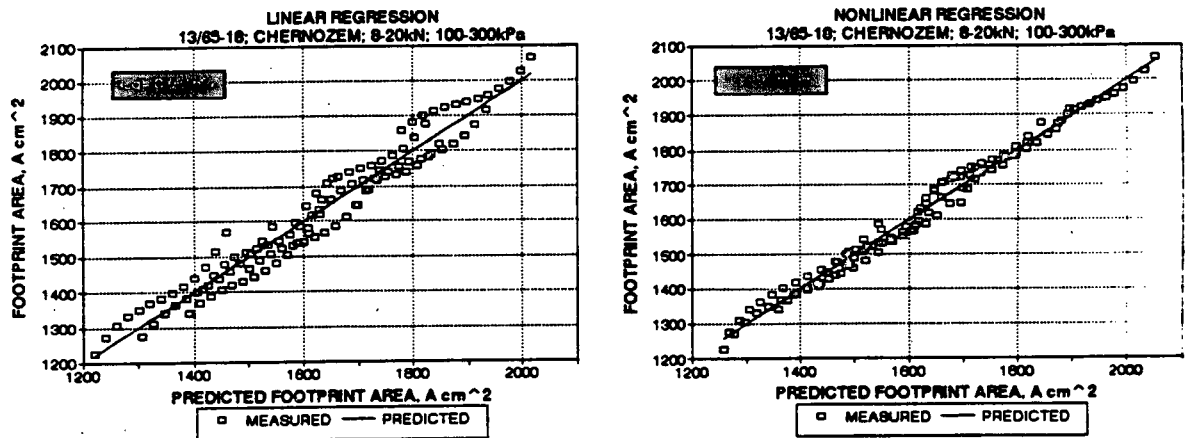


Fig. 12. Comparative analyses of total (nonlinear) and linear regression procedures for footprint area; Conditions are given in the pictures.

Data illustrated in Fig. 11 shows better relation between measured and predicted data for the total regression procedure then for the linear as given in the Fig. 10.

It may also be observed from Fig. 12 that total regression procedure seems to yield more reliable prediction of tire footprint width. Meanwhile, as mentioned before, the prediction equation (8) is valid only within the range of recommended tire loads, inflation pressures and soil moisture content range around the plastic limit.

The comparative analysis of predicted and measured values of footprint area is given in Fig.8 for both, linear and total regression procedure. It may be concluded that measured values for the tire footprint area (A) are more scattered around for linear regression procedure compared to the total regression. This means that both linear and total procedures may be accepted as prediction methods according to their R-square values, but that better prediction can be expected from total regression procedure.

CONCLUSIONS

The presented results show that footprint characteristics of agricultural transport tire in the cohesive types of soil may be successfully predicted within the range of recommended tire load and inflation pressure, and soil moisture around plastic limit.

The analysis of variance of the obtained data shows significant influence of the tire load and inflation pressure, as well as soil moisture content on the tire footprint area, length and sinkage, while the footprint width shows some irregularity. The values of footprint width can be taken as a constant since only small changes of footprint width follow soil moisture content changes.

Although a reasonably good prediction may be achieved using linear regression, the total regression ensures more reliable prediction of footprint parameters and may be recommended for further use.

REFERENCES

- [1] Sohne W., *Die Kraftubertragung zwischen Schleppernreifen und Ackerboden*; Grundlagen der Landtechnik, No3 (1952).
- [2] Ageikin J.S., *Opredelenie deformacii i parametrov kontakta shini s megkhim gruntom*; Avtomobilnaja promjashlenost, No5 (1959).
- [3] Karafiath L.L., Nowatzi E., *Soil Mechanics for Off-Road Vehicle Engineering Series* Rock and Soil Mechanics, Vol 2, No5, Tranch. Tech. Publications Clausthal, Germany (1978).
- [4] Komandy G., *The determination of deflection, contact area, dimensions and load carrying capacity for driven tires operating on concrete pavement*; J. of Terramechanics 13(1), 15-20 (1976).
- [5] Plackett C.V., 1984, *The ground pressure of some agricultural tire at low load and with zero sinkage*; Agr.Eng.Research, 29(2) 159-166, (1984).
- [6] Upadhyaya S.K., Wulfson D., *Relationship between tire deflection characteristics and contact area*; Trans. ASAE, 33(1), 25-30 (1990).
- [7] [7] Kolobov G.G., *Soil pressure measurement beneath tractor tires*; J. Terramechanics 3(1) (1966).
- [8] Fujimoto Y., *Performance of elastic wheel on yielding cohesive soils*; J. Terramechanics, 14(4), 191-210 (1977).

V.2.3. IN-SITU SOIL PROPERTIES MEASURING TECHNIQUE FOR SOIL-TIRE INTERACTION

Soil mechanical properties are the important part for soil-vehicle interaction prediction. The present research describes an experimental and theoretical approach to the measuring method of soil mechanical properties for tire traction and soil compaction purposes.

A special portable, shear-penetration rate device (PSP) was designed, manufactured and tested. The system measured the soil resistance to plate penetration and direct shear resistance by grouser plates.

The PSP is able to perform soil testing either under the laboratory or field conditions, depending on the test's purposes.

Fig. 1 shows the PSP mounted on the front side of the basic tractor, together with the single wheel tester that is located on the rear side.

Specially built connecting frame and two vertical hydraulic cylinders enable vertical movement of the testing unit and location on the desired testing position.



Fig. 1. PSP mounted on the front side of the basic tractor

The scheme of the measuring device (PSP) is given on Fig. 2.

Basically, the measuring system is consisted of main frame (2 and 8), equipped by leading trails (4) and rollers (3) which enables side displacement of the measuring device. The plate penetration part of the measuring device consisted of servo-controlled hydraulic piston (1), leading trails (7), penetration rod (5), penetration plate (6) and load cell (9).

The second part related to shear resistance measuring of the grouser plate, consisted of the basic mechanism (10,11), hydraulic piston for vertical force applying (12), load cell's assembly (13,14) and grouser plate (15).

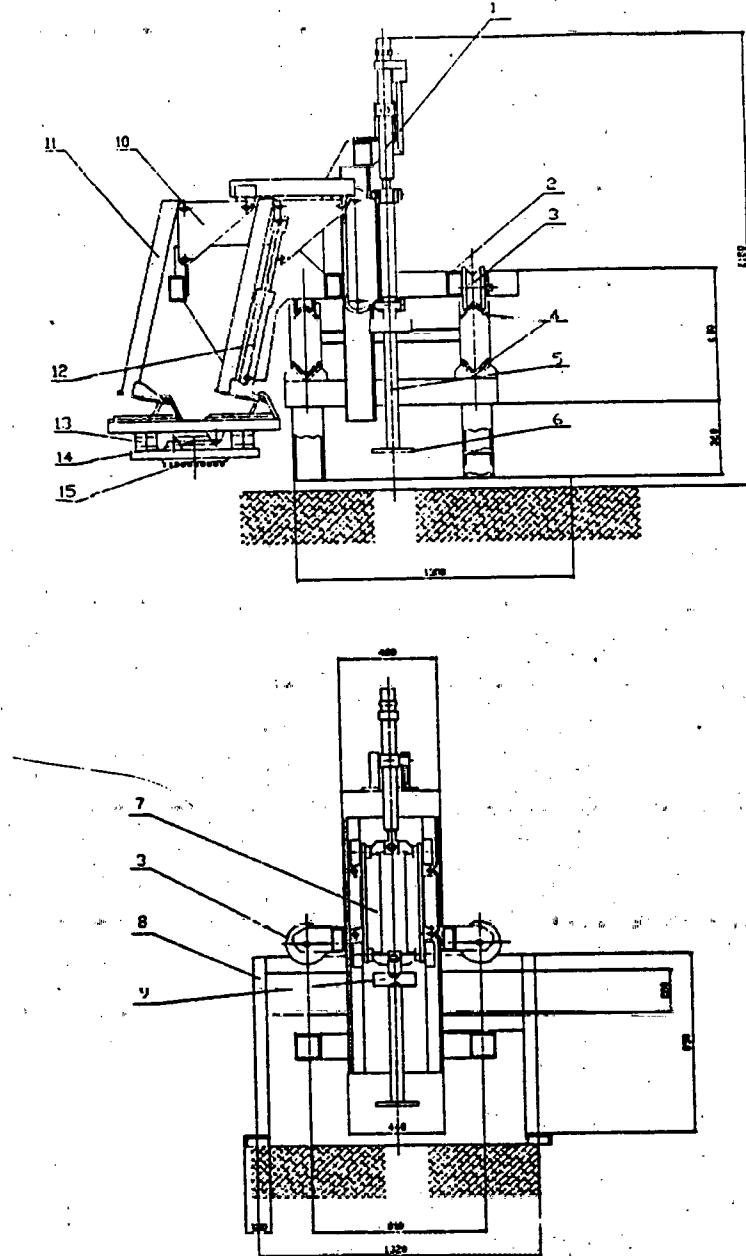


Fig. 2: Scheme of the soil properties measuring device (PSP)

The closer view of the PSP is given on the Fig. 3.

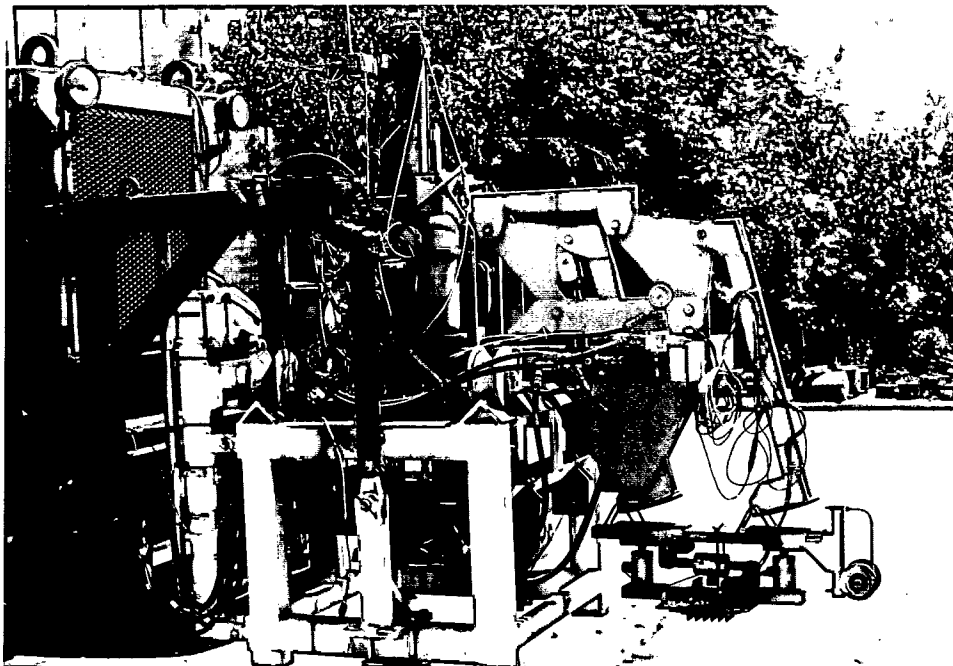
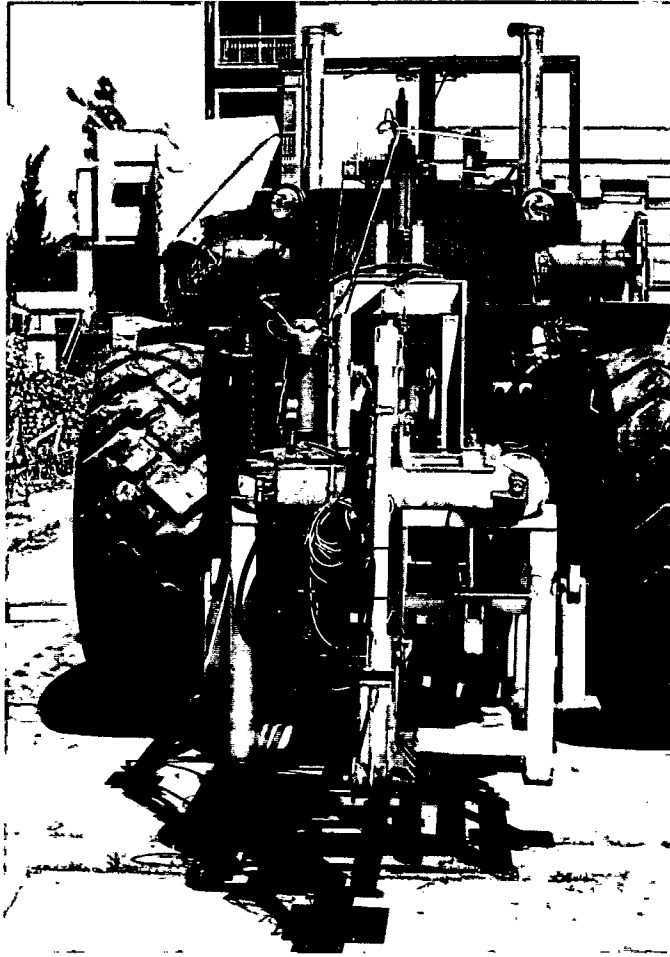


Fig. 3: Closer view of the PSP



Plate penetration part is equipped with servo-controlled piston (Fig. 4) , as it was mentioned before, which allows full control of the penetration rate, applied force and plate sinkage. It means that device enables tests with either constant penetration rate or constant penetration force.

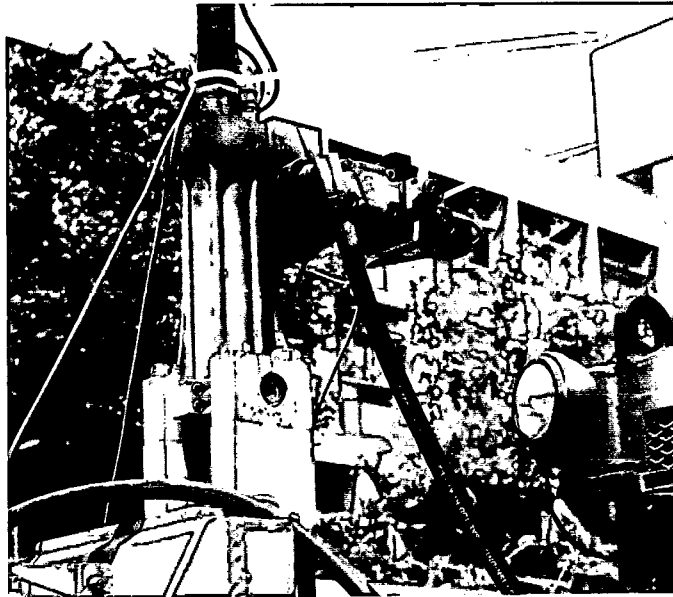


Fig. 4: Servo-controlled piston

The closer view of penetration plate location is given on Fig. 5.

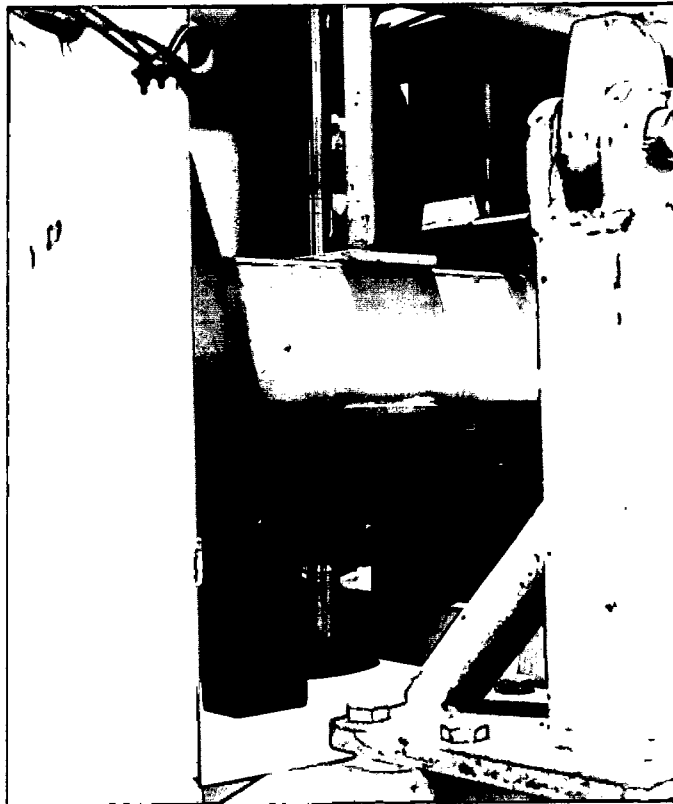


Fig. 5: Penetration plate location

Shearing part of the PSP is given on the Fig. 6. The basic mechanism enables vertical position of the grouser plate, while piston, located inside basic mechanism, applies desired vertical force on the grouser plate.

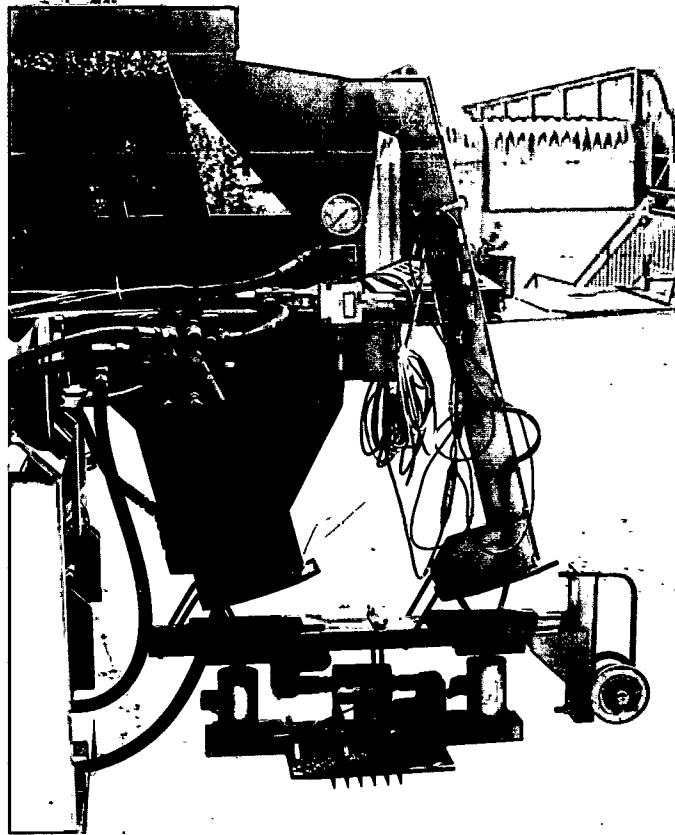


Fig. 6: Shearing part of the PSP

Horizontal movement of already loaded grouser plate is provided by the same servo-controlled piston as it is used for plate penetration. It means, that direct shear test can be performed with controlled rate or horizontal force.

The grouser plate assembly, given on the Fig. 7, consisted of the three load cells. Two of them measure applied vertical load on the grouser plate, and third, horizontal force necessary to shear the soil.

Vertical movement of the whole PSP as well as the vertical force application on the grouser plate is provided by separately regulated hydraulic system, related to the servo control of the main piston. Mentioned control includes constant amount of vertical force applied to the grouser plate during the horizontal movement.



Fig. 7: The grouser plate assembly

The soil properties testing, which are taking place at the present moment, include studying of influence of the soil type, sinkage and shear rate, as well as size and shape of the plate on the observed soil properties.

Taken experimental results will be correlated to the existing theories according to Bekker, Reece and Wong, and by continuum mechanics formulation.

V.2.4. INFLUENCE OF TIRE ACTION ON TOP SOIL COMPACTION.

Analysis of existing data sets was carried out in order to establish some empirical relationships between tire type and mode of operation (tire dimensions, carcass constriction, inflation pressure, axle dynamic load and slip) and soil compaction parameters (tire sinkage, soil bulk density, cone index) for three soils.

Empirical relationships in the form of linear or non linear regressions were established between the tire characteristics and the soil compaction indices.

PART B
ACTIVITIES IN THE UNITED STATES

V.5: DETERMINATION OF ENGINEERING PROPERTIES OF SOIL IN-SITU USING A RESPONSE SURFACE METHODOLOGY:

Developing a response surface methodology to determine engineering properties of soil in-situ was a major achievement of this study. Although we were supposed to address this task during the second year of this study, we started on this objective during the first year of this project and continued to work on various aspects of this objective during the whole project duration. At first, a widely used soil constitutive model - the Drucker Prager model, was selected for this study. Later a critical state model known as modified cam-clay model was investigated. The work involved the development of the methodology, checking its robustness, improving the methodology using higher order corrections to the response surface, conducting some field tests, and providing experimental verification to the methodology. Our results at various stages of this project were shared with scientific community at the national and international meetings. These are listed below:

1. Upadhyaya, S. K., D. Rubinstein, and M. Sime. 1993. An inverse solution technique to determine engineering properties of materials. ASAE Paper 93-1084. ASAE St. Joseph, MI 49085.

This paper outlines the methodology using the example of a two parameter hypoelastic case.

2. Rubinstein, D. S. K. Upadhyaya, and M. Sime. 1993. Determination of in-situ engineering properties of soil using response surface methodology. Proceedings of the 11th International Conference of ISTVS, Vol II, page 634-646.

This paper is similar to the one above but presented to a different audience - primarily interested in off-road mobility and traction.

3. Rubinstein, D., S. K. Upadhyaya, and M. Sime. 1993. A response surface methodology for determination of engineering properties of soil in-situ. 5th ICCPAM International Conference, Sept. 6-8, 1993, Bonn, Germany.

This paper looks at the application of the methodology to the Drucker Prager soil constitutive model. It includes a third order correction to the response surface to provide a better fit to the real surface.

4. Rubinstein, D., S. K. Upadhyaya, and M. Sime. 1994. Determination of in-situ engineering properties of soil using a response surface methodology. J. Terramechanics. Vol 31. p67-92.

This paper is peer reviewed version of (1) and (2) except it extends the methodology to a five parameter Drucker Prager soil constitutive model. This paper contains a second order correction to the response surface.

5. Rubinstein, D., S. K. Upadhyaya, 1994. A response surface methodology for determination of engineering properties of soil in-situ. J. Agrophysics. 8:113-130.

This paper is a peer reviewed version of #3 above. The second order correction to the response presented in #1, #2 and #4 were found to be insufficient in some cases and a third order correction to the surface was added to increase the robustness of the response surface.

6. Upadhyaya, S. K. 1994. Determination of engineering properties of soil in-situ. Proceedings of the workshop on "modeling the mechanics of off-road mobility" held at the Waterways Experiment Station, Vicksburg, Mississippi, April 5-6, 1994.

This was an invited keynote speech delivered by Dr. Upadhyaya and is the most comprehensive paper on the subject. This paper includes some field test results. This paper is included in the body of the report. Note that we did receive some additional funding from the Goodyear Tire and Rubber Co. to conduct this part of the research.

7. Sime, M, S. K. Upadhyaya, 1994. Experimental verification of an inverse solution technique developed for parameter estimation. ASAE Paper. 94-1565. ASAE St. Joseph, 49085.

This paper provides some preliminary results on the experimental verification of the response surface methodology using a modified Cam clay critical state model.

8. Sime, M. and S. K. Upadhyaya. 1995. Development and evaluation of parameter estimation technique using response surface method. Proceedings of the 5th North American ISTVS Conference, May10-12, Saskatoon, SK, Canada. p 249-258.

This is the most comprehensive paper on the verification of the response surface methodology. This has been a part of PhD thesis investigation which is currently in the final phase of completion. This is included in the body this report.

Three copies of all the eight papers are included with the report.

V.5.1 DETERMINATION OF ENGINEERING PROPERTIES OF SOIL IN-SITU

Shrini. K. Upadhyaya
Professor

Department of Biological and Agricultural Engineering
 University of California, Davis CA 95616

SUMMARY:

Soil-tire/Soil-track interaction is of particular interest to researchers involved in off-road mobility and traction research. This includes scientists and engineers involved in research in the field of agriculture, construction, forestry, military, and mining. In agriculture and forestry soil compaction caused by traction devices is also a serious concern. A sound mathematical model is a pre-requisite to obtain a clear understanding of the soil-tire/soil-track interaction process. A key ingredient for any such model is a constitutive relationship which describes the stress-strain behavior of soil. Any suitable constitutive model requires soil physical properties which describe the elastic behavior of soil, onset of yield and subsequent plastic flow, material hardening or softening rules etc. Since in-situ soils seldom behave like remolded laboratory soils or disturbed field samples, it is important to "identify" or "calibrate" the engineering properties of field soil by means of in-situ tests. The technique of obtaining material parameters based on actual system response is known as "back analysis", "inverse solution", "identification", or "calibration procedure". For complex problems such as soil-traction device interaction where closed form analytical solutions do not exist a numerical technique such as a finite element technique is commonly used to solve underlying system differential equation. For such cases the back analysis procedure can take one of the two forms: (1) inverse method, and (2) direct method. This paper addresses the advantages and disadvantages of such techniques, and discusses a new technique which overcomes some of their limitations. This new technique consists of developing a so called "response surface" in the parameter space and then using

this pre-determined surface to "identify" engineering properties of the material based on in-situ tests. Two case studies - (1) a two parameter hypo-elastic model for soil, and (2) a complex five parameter model for soil which includes nonlinear material behavior in elastic range, yield based on Drucker-Prager yield criteria and associated plastic flow upon yield are presented to illustrate the methodology.

INTRODUCTION AND REVIEW OF LITERATURE:

One of the challenges in the design of an off-road vehicle is to equip it with a traction device(tire or track) which can develop high traction efficiently(i.e. optimum tractive efficiency) while deterring soil compaction. Even an increase of one percentage point in the tractive efficiency leads to an annual savings of over 100 million liters(about 25 million gallons) of fuel in U. S. alone[1]. On the other hand, soil compaction has been recognized as a worldwide problem with serious implications on agricultural sustainability[2]. Although, certain amount of soil compaction may even be desirable for some crops under certain environmental conditions (optimum soil compaction), excessive soil compaction can lead to diminished soil porosity, reduced water infiltration, increased resistance to root penetration, increased tillage energy requirements, decreased biological activity, and a reduction in crop yield[3 - 14]. A necessary pre-requisite for the successful design of a traction device is a sound mathematical model for the soil-traction interaction process. This interaction is an extremely complex, dynamic process. A key ingredient of such a model is a constitutive relationship which describes the stress-strain behavior for soil. Schafer et al. [15] stated that an accurate description of soil constitutive relationship is necessary for the integrity and robustness of the model. Soil is perhaps one of the most complex material from engineering point of view[16].

Numerous constitutive models are currently available for soils. Among these are the elasticity models, higher order nonlinear elasticity models, hypo-elasticity models, plasticity models and visco-plasticity models. Desai [16], Desai and Siriwardane [17] and Chen and Baladi[18] have discussed these models and their applicability to a specific loading situation in detail. Piece-wise linear elastic models (hyperbola, parabola, splines and Ramberg-Osgood formulas) tend to be good for a specific loading case but are poor to simulate general loading conditions. Higher order nonlinear elasticity models tend to include too many parameters and have limited appeal. Hypo-elasticity models appear to show some promise. Plasticity models which utilize Von Mises, Mohr-Coulomb and Drucker-Prager failure criteria have been widely used. To include volume changes due to shear in geological materials and also to account for strain hardening or softening behavior critical state models have been developed. CAM and CAP models account for growth of the yield surface and have become increasingly popular in civil engineering. Applicability of critical state models to unsaturated agricultural soils has been a much debated issue. Hettiaratchi and O' Callaghan[19], Hettiaratchi[20] and Kirby[21] have found that critical state concept is applicable to unsaturated soils both qualitatively and quantitatively except that the critical state parameters depend on the soil moisture content. They found that it is reasonable to use total stress in the model(i.e. soil moisture tension can be ignored). Bailey et al.[22] and Bailey and Johnson[23] developed a constitutive model for agricultural soil that relates volumetric strain to octahedral normal and shear stress. This model predicts volumetric strain of soil samples accurately at limiting values of stresses(i.e. zero and very large applied stress). Raper and Erbach[24] and Raper et al.[25] have used this constitutive equation to compute tangent moduli in a finite element program to predict soil compaction.

All the aforementioned constitutive models require material parameters. These material properties describe the elastic behavior of soil, onset of yield and subsequent plastic flow, material hardening or softening rules etc. Typically these parameters are determined using

laboratory tests. Sometimes remolded soils are employed in the laboratory tests which may not behave like field soil. Use of soil properties obtained from remolded samples can often lead to predictions which are unrealistic and of little value to engineers interested in improving tire design. Even if field samples are obtained, one of the main problem with the soil material is that these samples undergo disturbances during excavation and testing, and may not behave like in-situ soil under actual loading conditions in the field. Use of cone penetrometer, grouser plate, and sinkage plate often yield some composite soil parameters which depend on the geometry of the test device and loading conditions. These composite soil parameters are of little use in subsequent model studies based on constitutive relationship. It is preferable to determine the soil material parameters based on undisturbed in-situ tests. The technique of obtaining material parameters based on actual system response is called "back analysis", "inverse solution", "identification", or "calibration procedure". The process of "calibrating" actual field response to model behavior is expected to "identify" the material parameters which can accurately predict system response in subsequent analysis which utilize the same constitutive model.

The back analysis technique has been successfully used in Geomechanics in studying tunneling problems in rocks and in investigating settlement problems[26-43]. If a closed form solution exists for the underlying differential equation describing the physical problem, then back analysis to obtain the material parameters involves optimizing the difference between the analytical and experimental responses. However, most real life problems in geomechanics are geometrically and/or materially nonlinear, and an analytical solution may not exist. In such cases a numerical procedure such as a finite element method[FEM] may be used to obtain solutions to the governing differential equation. When finite element analysis is used, back analysis may take one of the two forms - 1) inverse method, and 2) direct method.

In the inverse method nodal values of displacements and stresses obtained by a FEM technique are used as known boundary conditions and the unknown displacements and stresses are eliminated from the global matrix equation by reduction[41]. A brief discussion of the method is as follows:

Let the FEM result in the following matrix equation:

$$[K]\{u\} = \{F\} \quad (1)$$

where K is the global stiffness matrix, u is the nodal displacement vector and F is the global forcing vector. Let us partition the global stiffness matrix by collecting all nodes at which nodal values are measured in the field as follows:

$$\begin{bmatrix} K_{11} & K_{12} \\ K_{21} & K_{22} \end{bmatrix} \begin{Bmatrix} u_1^* \\ u_2 \end{Bmatrix} = \begin{Bmatrix} F_1 \\ F_2 \end{Bmatrix} \quad (2)$$

where u_1^* is a vector containing measured nodal values and u_2 is a vector containing unknown nodal values. F_1 and F_2 are known nodal force vectors, and K_{ij} 's [$i=1,2; j=1,2$] are partitioned global stiffness matrix elements. Note K_{ij} 's are functions of unknown material parameter vector, p' . Eliminating u_2 out through reduction, we get

$$[K^*]\{u^*\} = \{F^*\} \quad (3)$$

where

$$\begin{aligned} [K^*] &= [K_{11} + K_{12}K_{22}^{-1}K_{21}] \\ \{u^*\} &= \{u_1^*\} \\ \{F^*\} &= \{F_1 - K_{12}K_{22}^{-1}F_2\} \end{aligned}$$

In equation (3) only unknowns are p_i s contained in the elements of matrix $[K^*]$. An iterative scheme or a least square optimization scheme can be used to solve equation for unknown material parameters. This inverse technique is quite sensitive to experimental error and may not converge at all in some cases[35,40,42]. The direct approach results in more accurate parameter values. In the direct method, nodal values of the response are computed using a finite element method for a set of assumed parameter values. These responses are a function of assumed parameter vector (\underline{p}), say $u(\underline{p})$. The actual values of response at the same nodes can be obtained by field or in-situ tests. If u^* is corresponding observed response to $u(\underline{p})$ then $e_i = (u^*_i - u(\underline{p})_i)$ is a measure of error in the i^{th} value. A suitable objective function such as $\phi = \sum e_i^2$ can be optimized using a nonlinear optimization technique[35,40,42]. The direct search methods such as simplex method or its modification such as Rosenbrock's version or gradient based methods such as conjugate gradient method or quasi-Newton method can be successfully used depending on the application[26,32,43]. Nodal displacement values are usually better than stress values in parameter identification[32,35,36]. Moreover, it is preferable to map all the parameters to same range through scaling[32]. Even in the case of simple linear elastic constitutive model, the objective function, ϕ will be a nonlinear function of material parameter vector, \underline{p} . Because of this situation, the objective function, ϕ may have several local minimas[43]. Therefore, the optimal solution may be sensitive to initial guess values. Sometimes different combination of two or more parameters may lead to same response[non-unique solution][43]. More than one type of test or tests using different geometry and/ or loads may be helpful in such cases. Bayesian approach and Kalman filtering have been found to be helpful in improving the accuracy of results in the presence of experimental errors[27,33,40]. The direct method can be computationally very expensive since at each iteration a new FEM analysis with updated parameter vector(\underline{p}) needs to be carried out[42].

Rubinstein, Upadhyaya, and Sime[44] proposed a new methodology which utilized orthogonal regression technique to develop a response surface in the parameter space based on an analytical or numerical (such as a finite element analysis) solution to the system differential equation. This response surface was used in the optimization step. Their methodology consists of following steps:

1. A response surface is built using an orthogonal regression technique based on an analytical or numerical solution to the governing differential equation of the system. The response surface will be a function of unknown material parameters.
2. This response surface is updated using higher order corrections so that the response surface behavior is close to the real surface behavior everywhere in the parameter space. This response surface will be used to predict the response corresponding to the experimental values(i.e. at the same load and nodal point).
3. Experimental results are transformed such that the real surface and the response surface will have one-to-one correspondence everywhere in the region.
4. Experimental results are optimized against the response surface predictions to obtain material properties of the test material.

The proposed technique is particularly useful in dealing with complex problems which require numerical solution such as a FEM solution to the underlying system differential equation. The main advantage of this technique is that once the response surface is created using an FEM analysis, there is no need to go back to the FEM analysis. In the classical direct or indirect approach, hundreds or even thousands of time consuming and expensive FEM evaluations are necessary to determine material parameters through

optimization technique. In this methodology during the optimization technique only the response surface is used to estimate $u(p)$. This approach is expected to make this technique computationally very efficient. These in-situ soil properties can be used in subsequent model studies based on constitutive relationships which utilize these soil parameters. In fact, the methodology is quite general and can be used in other fields to estimate constitutive equation parameters based on in-situ measurements.

MATHEMATICAL MODELING

Response Surface Development:

Let us consider a general material constitutive model for soil (or any other material) consisting of m parameters: $p_1, p_2, p_3, \dots, p_m$. For example, if we select a nonlinear constitutive model with extended Drucker-Prager yield criteria and associated flow rule, then six parameters will be involved[45,46]. These parameters are p_1 =logarithmic bulk modulus, κ ; p_2 =Poisson's ratio, ν ; p_3 =yield surface shape factor(i.e. related to the third invariant of stress), K ; p_4 =cohesion, c ; p_5 = internal angle of friction, ϕ ; p_6 =initial void ratio, e . The last parameter, e is really related to initial stress condition. The response of a system to applied load depends on its geometry, material properties and the load itself. If the applied load and the geometry are fixed(i.e. for a given geometry and loading), the system response is a function of material constants used in the constitutive equation. There is a function $\Phi = \Phi(p_1, p_2, p_3, \dots, p_m)$ which represents the system response as the material properties used in the constitutive equation are changed. In most real situations the differential equation describing the response is nonlinear, this function is seldom known explicitly. One of the goals of this study is to find an approximate representation for this real response, Φ . This approximation to the real response is termed the response surface, F in this study. One convenient way of determining the response surface F is to determine the variation of F as one of the material parameter, p_i is changed while all other parameters are held constant. Let this response function for the single variable p_i be $f_i(p_i)$. If we repeat this process for each of the m material parameters(i.e. for $i=1, 2, \dots, m$), then one easy way of obtaining the response surface is simply to multiply these component equations, $f(p_i)$, i.e.

$$\Phi \equiv F = C f_1(p_1) f_2(p_2) f_3(p_3) \dots f_m(p_m) \quad (4)$$

where

F = response surface

f_i = a component equation which is a function of parameter p_i only.

C = constant.

Note that this type of solution is often sought in the solution of linear partial differential equations and is known as separation of variables. For example, in the case of a circular plate placed on a linear elastic medium and subjected to a uniformly distributed load, the real response, Φ is given on page 350 of Das[47] as

$$\Phi = 1.58 qb \frac{1 - \nu^2}{E} \quad (5)$$

where

Φ = the plate sinkage.

E = Young's Modulus, $E=p_1$.

ν = Poisson's ratio, $\nu=p_2$.

q, b = constants (respectively, uniformly distributed load and plate radius).

Equation (5) is a multiplication of two functions of the parameters, $p_1=E$ and $p_2=\nu$, i.e., $f_1=1/E$ and $f_2=(1-\nu^2)$. Therefore, in this case the response surface, F can be represented by a multiplication of the component equations as we assumed in equation (4). However, in general such a representation is accurate only in a small region due to geometric and/or material nonlinearities in the system. The error is expected to be small if the range of p_i is small for each of the m parameters.

Thus the process of building the response surface requires holding all relevant factors except parameter p_i constant (i.e. geometry, loading, all other material properties $p_j, j=1,2, \dots, m$ but $j \neq i$) and determining the component equation $f(p_i)$. Once all the component equations are determined, equation (4) can be used to build the response surface. It should be recognized that for each given geometry and loading there will be one response surface.

In the case of plate sinkage tests, for a given plate size and load level there will be a response surface. Since there are m unknown parameters, at least m field measurements are needed to solve for these m parameters. In practice, it is preferable to have more than m points(i.e. $n > m$) so that the m parameters can be determined with the help of an optimization algorithm. Since each unreplicated in-situ measurement corresponds to a given geometry and loading, each of these experimental values correspond to a point(or contour) on one response surface. Thus each of the n unreplicated measurements will correspond to a point(or contour) on one of the n distinct response surfaces. Note that more than one observations at a given geometry and loading refer to the same point (or contour) on a response surface that corresponds to that geometry and loading. Thus replicates do not provide additional equations to solve for the parameters, but help in controlling experimental error. Upadhyaya et al.[48] suggested that at least eight replicates to adequately deal with the spatial variability in the case of in-situ plate tests. Suppose we have n distinct combination of geometry and load level there will be n response surfaces, F_i , $i=1,2, \dots, n$. From equation (4) we get

$$\begin{aligned} F_1 &= C_1 f_{11} f_{12} \dots f_{1m} \\ F_2 &= C_2 f_{21} f_{22} \dots f_{2m} \\ &\vdots \\ F_n &= C_n f_{n1} f_{n2} \dots f_{nm} \end{aligned} \quad (6)$$

where f_{ij} is the component equation corresponding to response i and parameter p_j and C_i is the constant corresponding to the same response surface i .

Since each of the material parameter has its own range, some properties such as Poisson's ratio, ν vary in a very narrow range (0.0 to 0.5) whereas others such as Young's modulus, E may vary over a very large range (thousands of kPa). From the point of optimization as well as orthogonal regression, it is preferable to map each of the parameter to the same range through scaling [32,49]. Each of the unknown parameter was nondimensionalized and mapped to vary from -1 to +1 by the following transformation:

$$p'_i = \frac{2(p_i - \bar{p}_i)}{p_{i \max} - p_{i \min}} \quad (7)$$

where:

p'_i = nondimensional value of parameter i .

\bar{p}_i = mid point value of parameter i .

$p_{i \max}$ = upper bound value of parameter i .

$p_{i \min}$ = lower bound value of parameter i .

The value of the mid point is zero, upper bound is 1 and the lower bound is -1 for each of the nondimensionalized parameter.

Let f'_{ij} be the nondimensionalized component equation corresponding to the nondimensionalized parameter p'_j and test condition i . The relationship between f'_{ij} and f_{ij} is given by

$$f'_{ij} = \frac{f_{ij}}{\bar{F}_i} \quad (8)$$

where

\bar{F}_i = computed value of the response surface F_i for test i when all the parameters are set equal to the mid point value of zero.

Moreover, it is convenient if we nondimensionalize the system response to avoid numerical problems in the analysis. The nondimensionalized response surface is given by:

$$F'_i = C'_i f_{i1} f_{i2} \dots f_{im} \quad i=1,2,3,\dots,n \quad (9)$$

Where

F'_i = nondimensionalized response surface values corresponding to the i^{th} test condition,

C'_i = correction constant, approximately equal to 1.

The data for the creation of response surfaces can be obtained from any analytical or numerical models. We propose to use an orthogonal regression technique to determine the component equation f_{ij} . The use of an orthogonal regression technique not only provides an equation to accurately predict the overall system response, but also provides an accurate estimate of regression parameters[49,50,51]. An accurate estimation of regression parameters is essential in order to identify the unknown material parameters by optimization. The function f_{ij} is an orthogonal polynomial of parameter p'_j and is given by:

$$f_{ij} = \sum_{r=0}^k a_{ir} p'^r_j \quad (10)$$

The values of a_{ir} , $r=1,2,\dots,k$ are determined by using model response (analytical or numerical such as FEM) and orthogonal regression techniques. Only requirement for the use of orthogonal regression in curve fitting is that p'_j be equally spaced during model evaluation while all other material parameters be held at the mid point values. The theoretical value of the correction constant, C'_i in equation(9) is one. However, when curve fitting is employed to determine the regression coefficients, a_{ir} , the value of this correction constant may be slightly different than one. The actual value of C'_i can be found

by a employing linear regression technique between F'_i and $(f_{i1}f_{i2}...f_{im})$. To accomplish this linear regression, model response at orthogonal points used in building the response surface and some additional random points may be used.

Higher Order Correction:

As stated previously, in general the orthogonal response surface is expected to be close to the true model response only near the mid point and the parameter axes(p'_i axis). As we start moving away from the origin or the parameter axes, the two surfaces will depart from each other. At large distances from the origin and the parameter axes this error can be significant. The relation between the nondimensionalized true response, Φ'_i and the response surface, F'_i is given by:

$$\Phi'_i = F'_i + \varepsilon_i \quad (11)$$

where ε_i is the error in our approximation, $\Phi'_i \cong F'_i$.

By assuming that the function Φ'_i is "well behaved"(i.e. analytic everywhere in the parameter space),this function can be represented in a Taylor series as follows:

$$\begin{aligned} \Phi'_i = & 1 + b_1p'_1 + b_2p'_2 + \dots + b_mp'_m + b_{11}p'^1_1 + b_{12}p'_1p'_2 + \dots + b_{1m}p'_1p'_m + b_{111}p'^3_1 \\ & + b_{112}p'^2_1p'_2 + \dots + b'_{11m}p'^2_1p'_m + b_{123}p'_1p'_2p'_3 + \dots + b_{12m}p'_1p'_2p'_m + \dots \end{aligned} \quad (12)$$

where coefficients, b_i , b_{ij} , b_{ijk} , etc. for $i=1,2, \dots m$; $j=1,2 \dots m$; $k=1,2,\dots m$ are respectively related to the partial derivatives of the function, Φ'_i with respect to p'_i , $p'_ip'_j$, $p'_ip'_jp'_k$ etc. at the origin(mid point). Equation (12) reduces to f'_{ij} along p'_j axis. i.e.

$$f'_{ij} = 1 + b_jp'_j + b_{jj}p'^2_j + b_{jjj}p'^3_j + \dots \quad (13)$$

Using equations (9), (11), (12) and (13) we get,

$$\begin{aligned} \epsilon_i = & d_{12}p'_1p'_2 + \dots + d_{1m}p'_1p'_m + d_{23}p'_2p'_3 + \dots + d_{2m}p'_2p'_m + \dots \\ & + d_{112}p'^2_1p'_2 + \dots + d_{11m}p'^2_1p'_m + d_{123}p'_1p'_2p'_3 + \dots \end{aligned} \quad (14)$$

where "d" s are constant coefficients related to the cross derivatives of Φ'_i at the origin. It should be noted that strictly from a theoretical point of view, an orthogonal response surface can be created based on equation (12) rather than equation (9) which relies on the product of component equations. In such a case, very little difference is expected between the real surface and orthogonal response surface. If nine equidistant values of each of the parameter p'_i , $i=1,2, \dots, m$ are used in evaluating real surface, 9^m model evaluations will be needed. If $m=2$ then 81 model evaluations are needed. On the other hand, if $m=6$, then an astronomical 531441 model evaluations are necessary. In most real problems, where FEM evaluation of a complex model is necessary, using equation (12) as a basis for the response surface is infeasible except for the case of a two parameter model. The response surface represented by equation (9) requires only $[8*m+1]$ model evaluations (i.e. for $m=2$, 17 model evaluations are necessary whereas for $m=6$, 49 model evaluations are necessary).

Second Order Correction:

In practice, equation (14) will be truncated at some convenient point. The truncated function is an approximation to ϵ_i and is called the correction function, E_i . If we limit ourselves to only the product of the type $p'_ip'_j$ for $i=1,2, \dots, m$ and $j=1,2, \dots, m$, but $i \neq j$, then E_i will be a second order function. This second order function, E_i contains $n_{c \min}$ unknowns given by :

$$n_{c \min} = \frac{m(m-1)}{2} \quad (15)$$

In order to determine the second order correction function, E_i model responses are obtained at n_c additional check points, where n_c is greater or equal to $n_{c \min}$. The additional check points can be selected randomly or in a deterministic way. It can be shown that the form of the second order correction is:

$$E_i = \sum_{j=1}^{m-1} \sum_{k=j+1}^m e_{i, \frac{(j-1)(2m-j)}{2} + k - j} p'_j p'_k \quad (16)$$

The "e" coefficients can be derived from a set of n_c linear equations with $n_{c \min}$ unknowns. A multiple linear regression technique based on equation(16) can be used to estimate the "e" coefficients. Modification to the response surfaces can be accomplished by adding equation (16) to equation (9). The resulting improved response surface is given by:

$$F_i = C_i f_{i1} f_{i2} \dots f_{im} + E_i \quad i=1,2,3,\dots,n \quad (17)$$

It is important to emphasize that the second order correction neglects all higher orders of ϵ_i . There may be some situations where these higher order corrections are necessary. In such cases, it is possible that the second order correction may even give poorer results than not including any corrections. In situations like these, use of equation (9) may give more accurate results than equation (17). More discussion on this important issue will follow when we consider examples.

Third Order Correction:

In order to get more accurate results to the function E_i , we should consider the higher order corrections. In this study we will limit ourselves to a third order correction. The third

order correction consists of all cross product terms of the parameters upto and including the third order terms. The third order function E_i is the summation of n_{cmin} combination of cross products, therefore we have n_{cmin} unknown coefficients. It can be shown that the number of combinations, n_{cmin} is given by:

$$n_{cmin} = \frac{3m(m-1)}{2} + \frac{1}{2} \left[\frac{(m-1)(m-2)}{2} + \sum_{j=1}^{m-2} j^2 \right] \quad (18)$$

The function E_i for the third order correction is:

$$E_i = \sum_{j=1}^{m-1} \sum_{k=j+1}^m e_{i,\alpha(m,j,k)} p_j' p_k' + \sum_{j=1}^{m-2} \sum_{k=j+1}^{m-1} \sum_{l=k+1}^m e_{i,\beta(m,j,k,l)} p_j' p_k' p_l' + \sum_{j=1}^m \sum_{k=1}^m e_{i,\gamma(m,j,k)} p_j'^2 p_k' (1 - \delta_{jk}) \quad (19)$$

Where:

$$\delta_{jk} = \begin{cases} 1 & j = k \\ 0 & j \neq k \end{cases} \quad (20)$$

$$\alpha(m,j,k) = \frac{(j-1)(2m-j)}{2} + k - j \quad (21)$$

$$\beta(m,j,k,l) = \frac{m(m-1)}{2} + \frac{1}{2} \left\{ \frac{j-1}{2} [2m(m-j-1) + j] + \sum_{r=1}^{j-1} r^2 \right\} + \frac{k-j+1}{2} (2m-k+j-2) + 1 - k \quad (22)$$

$$\gamma(m,j,k) = \frac{m(m-1)}{2} + \frac{1}{2} \left[\frac{(m-1)(m-2)}{2} + \sum_{r=1}^{m-2} r^2 \right] + (m-1)(j-1) + \delta \quad (23)$$

$$\delta = \begin{cases} k & k < j \\ k-1 & k > j \end{cases} \quad (24)$$

Once again, "e" coefficients can be derived from a set of n_c ($n_c \geq n_{c \min}$) linear equations with $n_{c \min}$ unknowns. A multiple linear regression technique based on equation (19) can be used to estimate the "e" coefficients. The modified response surface is given by equation (17).

Estimation of Material Parameters:

Let U_i be one of the n independent experimental observations. In order to make U_i consistent with F'_i , we transform it into a nondimensional value, U'_i . The relation between U_i and U'_i is given by:

$$U'_i = \frac{U_i}{\bar{F}_i} \quad (25)$$

The subtraction of equation (25) from equation (17) yields a set of n nonlinear equations in m unknowns.

$$\begin{aligned} F'_1 - U'_1 &= 0 \\ F'_2 - U'_2 &= 0 \\ &\vdots \\ F'_n - U'_n &= 0 \end{aligned} \quad (26)$$

In general equation (26) is seldom an equality due to the presence of approximation as well as experimental errors. One method of determining engineering properties of the material involves optimizing sum of squares of residuals, SSR defined by:

$$SSR = \min \left\{ \sum_{i=1}^n (F'_i - U'_i)^2 \right\} \quad (27)$$

The expression for the SSR in equation(27) is used as an objective function and a nonlinear optimization technique is used to solve for material parameters. Since F'_i is an approximation to Φ'_i , and F'_i can be obtained from equation (9) which corresponds to the original orthogonal response surface or equation (17) which includes higher order correction, we can get different solutions in the vicinity of the real solution depending on which expression for F'_i is used. The SSR of these solutions is of the same order, thus the minimum value of the SSR does not necessarily indicate the best solution. Of course, the best solution can be obtained from the sum squares of the residuals which uses Φ'_i in equation (27), i.e.

$$SSR^* = \min \left\{ \sum_{i=1}^n (\Phi'_i - U'_i)^2 \right\} \quad (28)$$

Where SSR^* is the minimum residuals of the real response surfaces and the test results. It is recommended to use equation (28) at these different optimum solutions suggested by different versions of F'_i to obtain the best results. We will return to this question when we consider example problems.

Transformation of Experimental Results:

As explained previously, the accuracy of function F'_i may be high in some region on the response surface and low in another region. This implies that the estimated parameters will be high in accuracy sometimes and poor in accuracy some other times. Generally speaking, the inaccuracy increases as we move away from the origin and parameter axes. At the origin, the nondimensionalized F'_i has a value of unity[cf. eq. (9)]. In some sense, as the values of F'_i change from unity the difference between the real and the response

surface values(both corrected and uncorrected) tend to increase. Thus the values of F'_i can be used as a measure of this departure. This argument suggests that there exists a function $\Phi'_i = \Phi'_i(F'_i)$. Inverse of this transformation, $F'_i = F'_i(\Phi'_i)$ is of particular interest in our case. This relationship can be used as a transformation rule for experimental values by replacing the real response, Φ'_i by experimental value, U'_i . If we denote the transformed experimental value which corresponds to F'_i by U^*_i , then we have $U^*_i = U^*_i(U'_i)$. The transformation function can be obtained by conducting a polynomial regression between F'_i and Φ'_i in some acceptable range, $\Phi_{i \min}$ and $\Phi_{i \max}$, thus:

$$F'_i = \sum_j g_j \Phi_i^j \quad (29)$$

where " g_j " s are regression coefficients. The corresponding transformation rule for the experimental values is given by:

$$U_i^* = \sum_{j=0}^k g_j U_i^j \quad (30)$$

The value of U^*_i calculated from equation (30) can be used for replacing U_i in equation (26) and (27). This modification may significantly improve the accuracy of the parameters obtained through optimization. We will explore this aspect in more detail when we consider the example problems.

COMPUTER IMPLEMENTATION OF THE MODEL:

A FORTRAN program was developed to implement this inverse solution technique to estimate material parameter values. This task involves several steps as shown in figure 1. An interface program is used to transform the analytical or numerical results to a format

acceptable to our inverse solution program. The inverse solution program uses model response (either analytical or numerical such as FEM analysis) for the creation of the orthogonal response surface. Higher order correction are implemented on to this orthogonal response surface in the next step. Following this experimental data are input and a transformation is performed on these data to relate them to response surface points. In the last step, an optimization procedure is carried out to obtain the best estimates of the values of material parameters. This program allows for selection of any one of the following optimization subroutines called from IMSL library:

1. Nonlinear least squares techniques,
2. Complex algorithm,
3. Quasi-Newton method,
4. Modified Newton Method,
5. Conjugate Gradient Method.

CASE STUDIES:

Two Parameter Model:

A simple two parameter material model is selected to illustrate the main features of this technique. A cylindrical bar or soil column under uniaxial compression is considered. The bar is made of a hypoelastic material with an incremental constitutive law given by (p 139, Desai and Siriwardane [17]):

$$d\sigma = (E_0 + E_1\sigma)d\varepsilon \quad (31)$$

where E_0 and E_1 are the material parameters of interest in this model, σ is axial stress(positive in compression), and ϵ is axial strain. Integration of equation (31) yields:

$$u = \frac{L}{E_1} \ln\left(\frac{E_0 + E_1\sigma}{E_0}\right) \quad (32)$$

where:

u = deformation of the bar (the contraction).

L = length of the undeformed bar.

Equation (32) will be used as a basis to build the response surface, F_i . The response surface will be developed in the following range of parameters E_0 and E_1 :

$$\begin{aligned} E_{0 \min} &= 689.5 \text{ kPa (100 psi)} & E_{0 \max} &= 6894.8 \text{ kPa (1000 psi)} \\ E_{1 \min} &= 10.0 & E_{1 \max} &= 100.0 \\ E_{0 \text{ mid point}} &= 3792.1 \text{ kPa (550 psi)} & E_{1 \text{ mid point}} &= 55.0 \end{aligned}$$

The nondimensional parameters (equation 7) for this case are:

$$E_0' = \frac{2(E_0 - E_{0 \text{ mid point}})}{E_{0 \max} - E_{0 \min}} \quad \text{and} \quad E_1' = \frac{2(E_1 - E_{1 \text{ mid point}})}{E_{1 \max} - E_{1 \min}} \quad (33)$$

The response at the mid point of the parameters is(i.e. origin):

$$\bar{F}_i = \frac{L}{E_{1 \text{ mid point}}} \ln\left(\frac{E_{0 \text{ mid point}} + E_{1 \text{ mid point}}\sigma_i}{E_{0 \text{ mid point}}}\right) \quad (34)$$

The nondimensional representation of the real surface is obtained by dividing equation (32) by equation (34). The plot of the nondimensionalized real surface obtained by using an applied stress of $\sigma = 689.5$ kPa(100 psi), is given in Fig. 2. The approximation of the surface without any higher order correction is shown in Fig. 3, and the error of this approximation is shown in Fig. 4. The response surface describes the real function with reasonable accuracy except at the corners. The error is particularly high as both parameters (E_0 and E_1) approach their minimum values. The response surface for this case which includes second order correction is:

$$F'_i = f'_1(E'_0)f'_2(E'_1) + e_i E'_0 E'_1 \quad (35)$$

where f'_1 and f'_2 are orthogonal polynomial functions of E'_0 and E'_1 respectively and e_i is second order correction coefficient. The function f'_1 , f'_2 and the coefficient e_i were found as described previously.

The second order correction for this case was obtained by using the edge points, the mid points of the lower and upper range for each parameter - a total of 16 combinations. The response surface with second order correction is shown in Fig. 5, and the difference between the real values and the response surface values is plotted in Fig. 6. The second order correction decreases the error in the zones of high error (e.g. in the region near the minimum values of E_0 and E_1). However, this correction to the response surface increased the error in some other regions where the error was negligible previously. The basic assumption of the second order correction is that all higher order(third order and higher) cross products are negligible. In this particular example, the plot of the error shown in Fig. 4 indicates a high curvature in a small region [in fact only about 3% region] where both

parameters approach their minimum values. Thus, second order correction does not represent the error properly everywhere in the region.

Effect of including the third order correction (TOC) was also examined for this two parameter case. The form of the third order correction is:

$$E_i = e_{i1}E_0E_1 + e_{i2}E_0^2E_1 + e_{i3}E_0E_1^2 \quad (36)$$

Figure 7 shows the effect of including third order correction on the response surface. Inclusion of third order correction further reduces the error in the zone of high error (i.e. in the 3% region where E_0 and E_1 values are near or at their minimum). Figure 8 is a plot of error when the third order correction is included. Comparison of this figure with figures 4 and 6 shows that although the response surface which includes third order correction reduces the error in the zone of high error, the error in other regions does not necessarily decrease. In fact, the error increases slightly in some areas.

In order to determine the material parameters(E_0 and E_1), seven different response surfaces were created using seven different applied stresses. The stress values used were 344.7 kPa (50 psi), 517.1 kPa (75 psi), 689.5 kPa (100 psi), 861.8 kPa (125 psi), 1034.2 kPa (150 psi), 11206.6 kPa (175 psi) and 1379.0 kPa (200 psi). The adequacy of the method is illustrated by 12 examples. Table 1 lists the parameter values selected for the simulation purpose. The first set of parameter values are randomly selected. The other eleven examples are based on parameter values along the diagonal, $E'_0=E'_1$. The equation (32) was used to calculate the real response. These values were used instead of the experimental values in the optimization step. Since there is no experimental error in this case, we should, in principle, get exact values of the assumed parameters back. Inaccuracy

in the results is solely due to the inadequacy of the response surface. Five different initial guess values of the parameters were considered in the nonlinear optimization process for each one of these examples. The first initial guess values were the mid point values of the parameters, three others were selected randomly and the fifth one was the exact solution.

The transformation equation was estimated using 50 random points of the real surface using equation (29) as a basis for regression.

Example 1: E_0 and E_1 were selected randomly:

The values of the simulated parameters were : $E_0 = 5666.1$ kPa (821.8 psi) and $E_1 = 61.8$. The nondimensionalized real function value at an applied pressure of 689.5 kPa (100 psi) is 0.80. The results of optimization are listed in Table 2.

Note that both uncorrected response surface and response surface with third order correction resulted very good solutions with negligible errors. However, the second order correction yielded relatively poorer results. When the transformation based on equation(30) was employed, all three correction methods yielded reasonably good results (Table 3). Transformation technique significantly improved the parameter estimation for the case in which no correction was employed. This transformation was beneficial in reducing error for the second order correction technique also, particularly at low parameter values. However, the transformation technique was not quite as beneficial in the case of the third order correction method. Even in this case the error in estimation of the parameters were reduced slightly. Thus, in general transformation technique leads to more accurate parameter estimation.

It should be noted that this particular soil model shows large increases in response when E_0 and E_1 values are very small compared to all other values of E_0 and E_1 . This portion of the graph corresponds to only 3% of the parameter range (low values of the parameters). This makes it difficult to generate a response surface which is good everywhere in the region. Higher order corrections tend to predict the response better in this region. In so doing, they become less accurate in other regions - especially at large values of the parameters (see Figs. 3 through 8). This is an unusual situation which resulted in the uncorrected surface to generally estimate parameter values more accurately than when the third order correction was employed along with the transformation technique. In a well behaved system (i.e. no singularities or large increases in responses for small changes in parameter values) the method which employs third order correction is expected to yield more accurate parameter values. In fact, even very complicated models do not show such singularities or large changes in a small region as we will see with a five parameter Drucker-Prager model described below.

A Five Parameter Nonlinear Elastic Soil Model with Extended Drucker Prager Yield Criteria:

The elasto-plastic constitutive material model with Drucker-Prager yield criteria is widely used in geomechanics[45,46]. We assume that in-situ tests consist of plate penetration tests using circular plates. Here we will not consider the actual field data. Analysis of the field data to identify material parameters will be dealt later. We explore the feasibility of the proposed methodology in this example for this fairly complex material model. A commercial finite element program, ABAQUS was used in this study to obtain model response. The orthogonal response surfaces were built using six parameters κ, ν, K, C, ϕ and e .

Two plates of diameters 50 mm(2 in.) and 100 mm (4 in.) were simulated, with applied load ranging from 137.9 kPa(20 psi) to 1034.2 kPa (150 psi) in increments of 68.9 kPa(10 psi), a total of 14 tests for each plate. A response surface was built for each of those tests in the following parameter range:

$\kappa_{\min}= 0.01$	$\kappa_{\max}= 0.10$	$\kappa_{\text{mid point}}= 0.19$	No. of points= 9
$\nu_{\min}= 0.05$	$\nu_{\max}= 0.37$	$\nu_{\text{mid point}}= 0.21$	No. of points= 9
$K_{\min}= 0.60$	$K_{\max}= 1.0$	$K_{\text{mid point}}= 0.8$	No. of points= 11
$C_{\min}= 9.0$	$C_{\max}= 21.0$	$C_{\text{mid point}}= 15.0$	No. of points= 9
$\phi_{\min}= 22.5$	$\phi_{\max}= 47.5$	$\phi_{\text{mid point}}= 35.0$	No. of points= 11
$e_{\min}= 0.6$	$e_{\max}= 1.6$	$e_{\text{mid point}}= 1.1$	No. of points= 11

A typical plot of the non-dimensional sinkage as a function of non-dimensional values of parameter κ for a 100 mm (4 in) plate subjected to 551.6 kPa pressure (80 psi) is shown in Fig. 9. Note that all other parameters are held constant at their corresponding midpoint values. Figures 10 through 14 are similar plots except that the dependent variable has been changed to ν , K , C , ϕ , and e respectively. These curves show an extremely good fit between the real response curve and the response curve obtained by the orthogonal regression ($R^2 > 0.997$ for all cases).

The graph of the real surface versus the orthogonal response surface without any correction for a 100 mm (4 in.) plate subjected to an applied load of 103.4 kPa (15 psi) is shown in Fig. 15. This graph consists of 55 orthogonal points and an additional 60 random points. Figure 16 is similar to Fig. 15 except that the applied load is 551.6 kPa (80 psi) in this case. When the applied pressure is low, soil deformation is small and the soil medium behaves similar to elastic material (in fact, in our case soil is modeled as nonlinear elastic but if displacements are small even nonlinear behavior can be approximated by linear behavior). In this case the real surface and orthogonal surface are

almost identical (Fig. 15). As the load is increased, soil will yield and subsequent plastic flow will take place as per the assumed model. Figure 16 reveals that under high load the orthogonal response surface begins to depart from the real surface when non-dimensionalized displacements are below 0.5 or exceed 1.5. Figures 17 and 18 are similar to figures 15 and 16 except that a second order correction has been added to the orthogonal response surface. These figures indicate that there has been only marginal improvements in these curves (especially Fig. 18). Perhaps a higher order correction is beneficial especially at high plate loads. Figures 19 and 20 are similar to figures 15 and 16 (also 17 and 18) respectively, except that a third order correction has also been added to the orthogonal response surface. Inclusion of third order correction has resulted in an orthogonal response surface which is almost identical to the real surface even at high loads. This indicates that an orthogonal response surface with third order correction can be used reliably to predict the real response without having to resort to FEM analysis.

Parameter Estimation:

Since we are dealing with a nonlinear problem the solution is not necessarily unique. Following recommendations may be used as a guide for selecting the best solution from several optimum solutions resulting from the presence of "local minimums":

1. Discard all solutions that have a significantly high SSR (cf. equation 27).
2. Use more than one geometry (i.e. 50 mm and 100 mm diameter plates) and look for optimum for each of the geometries and also the combination of all the geometries. Accept those solutions which are approximately same in all cases. From a practical point of view two plates will be sufficient.

3. Reject any solution in which more than one parameters hit the bounds of the search domain. The probability of more than one parameter hitting the bounds simultaneously is low. If in fact, if this really is the case for several initial guesses, and the above two criteria will be met.

4. In spite of these steps, if more than one optimal solutions are obtained, we recommend the use of equation (27) to compute SSR. If the response surface with higher order corrections has been properly verified as good (i.e. using figures such as 19 and 20 described earlier), then the solution which yields the minimum SSR should be accepted as the best solution. If possible one could use equation (28) to compute SSR* to provide additional verification. Although, such an approach is preferable, evaluation of equation (28) requires some limited FEM analysis (i.e. one for each plate for each competing solution).

To explore the suitability of this method to identify the material parameters of this complex constitutive equation for soil, we selected five different random sets of parameters and conducted simulation studies to obtain true response. Subsequently, these true responses were used as inputs into the response surface methodology to re-predict those parameters. Since third order correction (TOC) to the orthogonal response surface appears to be necessary to obtain reasonable results, we will only explore the situation in which TOC is added to the orthogonal response surface. We chose five different random sets of parameter values to be re-predicted using the optimization technique. These random sets of points are as follows:

Point #1:	$\kappa=0.127$	$\nu=0.132$	$K=0.938$	$C=19.406$	$\phi=26.984$	$e=0.630$
Point #2:	$\kappa=0.011$	$\nu=0.343$	$K=0.611$	$C=16.813$	$\phi=31.305$	$e=0.755$
Point #3:	$\kappa=0.056$	$\nu=0.146$	$K=0.946$	$C=16.512$	$\phi=28.985$	$e=1.095$

Point #4:	$\kappa=0.022$	$\nu=0.093$	$K=0.776$	$C=13.893$	$\phi=41.297$	$e=1.049$
Point #5:	$\kappa=0.083$	$\nu=0.233$	$K=0.884$	$C=16.867$	$\phi=34.856$	$e=1.123$

The initial guess values selected were the "exact solution", "mid point values" and a set of five randomly selected parameter values listed below:

Point #6:	$\kappa=0.356$	$\nu=0.238$	$K=0.889$	$C=10.791$	$\phi=34.579$
Point #7:	$\kappa=0.131$	$\nu=0.297$	$K=0.996$	$C=45.693$	$\phi=23.932$
Point #8:	$\kappa=0.039$	$\nu=0.116$	$K=0.889$	$C=16.271$	$\phi=30.728$
Point #9:	$\kappa=0.110$	$\nu=0.088$	$K=0.610$	$C=20.472$	$\phi=23.566$
Point #10:	$\kappa=0.014$	$\nu=0.360$	$K=0.907$	$C=16.979$	$\phi=23.778$

The re-prediction process was carried out using 50 mm (2 in.) plate, 100 mm (4 in.) plate and a combination of 50 mm (2 in.) and 100 mm (4 in.) plates. For each case we used the exact solution and the mid point as initial guesses. The five randomly selected guess points were used only for point # 1 for both plates and also the combination of plates. However, for the 100 mm (4 in.) plate all seven initial guess values were use to seek the optimum solution for each of the five random set of parameter values.

The results of this analysis are listed in Table 4. An examination of the results indicates that the reasonable solution with minimum SSE usually leads to good solution except for point #4. Point #4 results in very large errors for both parameters κ and ν . However, an examination of SSE indicates that none of the solutions is reasonable. Our suspicion is that for this values of κ and ν , the soil is extremely hard and deforms very little. Under these circumstances, the nonlinear elastic model for soil with Drucker-Prager yield criteria is perhaps inappropriate.

In order to explore the effect of random noise on the optimization procedure, a random noise derived from a normal distribution with mean zero and variance 0.01 was added to the numerical displacement values (non-dimensionalized) derived from the FEM analysis. This technique of adding a random, normal noise was thought to simulate the experimental noise in real data. Rubinstein et al. (1994) found that the presence of noise did not have an adverse effect on the accuracy of parameters identified. Although some of the parameters were less accurate, others were more accurately predicted in the presence of noise. The range of error in the estimated parameters were about the same as in the case where the true model response was used.

DETERMINATION OF IN-SITU SOIL PROPERTIES:

Field tests were conducted during November, 1991 and September, 1992 using our instrumented soil-test device in a Yolo loam soil in the vicinity of the U.C. Davis campus. In November 1991 tests were conducted in an undisturbed soil using 50.8 mm (2 in.), 76.2 mm (3 in.), 101.6 mm (4 in.), 127 mm (5 in.), and 152.4 mm (6 in.) sinkage plates. When we conducted the field tests we were under the impression that more than one geometry (plate sizes) were necessary to obtain the engineering properties of soil by the inverse solution technique. However, later we found that this is not necessarily the case. Even use of one plate size appears to be sufficient. In this study, field test results for 50.8 mm (2") and 101.6 mm (4") plates were only used to determine the engineering properties of soil by the inverse solution technique.

Eight replicates were obtained for each plate. Sinkage test data were analyzed using Reece's approach, i.e.

$$p = k (z/r)^n \quad (37)$$

where

p = applied pressure

k = sinkage constant

z = soil sinkage

r = plate radius

n = empirical constant.

Table 9 lists the mean values of sinkage coefficients for each of the plate tested. The values of k and n for the 50.8 mm (2") and 101.6 mm(4") plate were used in estimating mean field response corresponding to a desired pressure for a given plate during the optimization process to "identify " soil parameters.

Soil shear tests were conducted using two different grouser plates [Plate #1: 203 mm long x 76 mm wide, and Plate #2: 178 mm long x 86 mm wide]. Each plate was tested at two different vertical loads and each test was replicated three times. Grouser plate test results were analyzed using the following equation:

$$\tau = [c + p * \tan(\phi)](1 - e^{-\frac{j}{K}}) \quad (38)$$

where

τ = shear stress, kPa

c = cohesion, kPa

p = pressure on the plate, kPa

ϕ = soil internal friction angle

j = shear deformation, mm

K = shear modulus, mm

A nonlinear regression technique was employed to fit the data to equation (38) and obtain shear parameters. Maximum shear stress, τ_{\max} for each test was calculated using the following equation:

$$\tau_{\max} = c + p * \tan(\phi) \quad (39)$$

The analysis of the experimental data resulted in a mean value of cohesion of 11.5 kPa and soil internal friction angle of 32.9 deg. for these tests.

Cone index, bulk density and moisture content data were also obtained in the test site. Eight replicates of cone index profiles were obtained in the top 152.4 mm (6") layer. The cone index values were averaged over the depth to get a representative cone index value for each location. Subsequently, all eight replicates were averaged to get a mean cone index value for this particular soil condition. Five bulk density and moisture content data were also obtained in the test site. Average cone index value was 816 kPa, dry bulk density was 1510 kg/m³, and moisture content was 8.9% (dry basis). The void ratio was 0.755 based on a particle density of 2650 kg/m³.

During September, 1992 only three sinkage plates were used for sinkage tests. Two distinct soil conditions (undisturbed and tilled/loose) were included in these tests. Once again eight replicates of sinkage tests were obtained for each plate and analyzed using equation (37). Sinkage parameters for the undisturbed and tilled soil conditions of the November 1992 tests are also listed in Table 5. Once again, the mean sinkage parameters corresponding to 50.8 mm (2") plate and 101.6 mm (3") plate were used in estimating field response for identifying Engineering parameters of soil.

Shear test procedure as well as data analysis techniques were similar to the procedure employed in analyzing the November, 1991 shear tests. The mean value of cohesion for the undisturbed soil condition was 32.3 kPa, and the internal angle of friction was 27.2 deg. The corresponding values for the tilled soil was 22.7 kPa and 22.8 deg.

Moreover, soil bulk density, cone index and moisture content data were also obtained as described for the November 1991 tests. The undisturbed (also referred as firm) soil had a mean dry bulk density of 1510 kg/m³, moisture content of 5.14 % (dry basis), and a void ratio of 0.755. The loose or tilled soil had a dry bulk density of 1433 kg/m³, 4.55 % moisture content (dry basis), and a void ratio of 0.851. The cone index data were inconsistent and were ignored for these soil conditions.

Table 6 lists the Engineering parameters of soil estimated from the optimization process which utilized the orthogonal response surface including the third order correction. Both the best results based on SSE and SSR, and reasonable results based on our search criteria are listed in Table 6 for all the three soil conditions. The best estimates of the cohesion and soil internal friction angle values listed in Table 6 do not agree with the corresponding values listed in Table 5, which are grouser shear test results. This agrees with our hypothesis that the grouser shear test provides geometry dependent soil parameters, but not the basic soil constitutive property. Only the 101.6 mm (4 in.) plate was used for "identifying" soil parameters through optimization. Figures 21 and 22 show the experimental and simulated sinkage for a 101.6 mm (4 in.) plate obtained using back-calculated soil parameters for September 1992 tests in an undisturbed soil (firm soil). These results indicate that the estimated soil parameters are very good. However, when these same parameters were used to compare the response of a 50.8 mm (2 in.) plate in the same soil condition poor agreement was found between experimental and simulated sinkage (Figs. 23). This plot indicates that the parameters predicted from 101.6 mm (4 in.) plate

tests are unable (under predict) to predict the behavior of 50.8 mm (2 in.) plate in the field. Similar results were obtained in the other soil conditions tested also. We feel that this is due to the edge effect which is not included in our model. Use of an interface element at the soil-plate interface appears to be necessary. Since 101.6 mm (4 in.) plate is less susceptible to edge effect compared to the 50.8 mm (2 in.) plate, we feel the parameters estimated from a 101.6 mm (4 in.) plate are more reliable. We recommend using a large diameter plates in future tests.

CONCLUSIONS

Based on this study we reached the following conclusions:

- 1) A response surface methodology based on an orthogonal regression in the parameter space has been developed to "identify" , or "calibrate" engineering properties of any material based on in-situ tests. The orthogonal response surface was created from an analytical or numerical(such as FEM) solution to the underlying differential equation of the system which utilizes these engineering properties in a constitutive equation. A transformation technique was developed to map the model response or experimental data on to the response surface.
- 2) The proposed methodology worked very well (i.e. very little error) in the case of a two parameter hypo-elastic model for soil. When the second order correction was included with a transformation of data very small errors resulted in parameter estimation. Inclusion of third order correction to the orthogonal response surface reduced the chance of large error in parameter values.

3) When this technique was used in the presence of random noise, the predicted parameters were found to be insensitive to the noise.

4) When this methodology was applied to a complex five parameter model for soil (nonlinear elastic behavior with Drucker-Prager yield criteria and associated plastic flow upon yield), it appeared to work reasonably well. A third order correction to the orthogonal response surface appears to be necessary to obtain reasonably good solution. When both the logarithmic bulk modulus (κ) and Poisson's ratio (ν) are low, soil becomes very rigid and the methodology will not yield a good solution. Under such circumstances, perhaps the soil model chosen is inappropriate.

5) The response surface methodology was successfully employed to "identify" engineering properties of soil based on field tests for different soil conditions in a Yolo loam soil. We suspect that edge effect makes the parameter prediction using field data corresponding to small plates such as 50.8 mm (2 in.) diameter plate inaccurate. Use of larger plates such as 101.6 mm (4 in.) plate is recommended to reduce this edge effect. Use of Teflon coated plate with beveled edges and slip elements at the plate edge in the model may also increase the accuracy of parameter prediction.

The proposed methodology has not only applications in geomechanics, but also in other areas such as biological engineering(plants and animal tissues, food products etc.) where non-destructive in-situ tests are the only means of obtaining accurate estimate of engineering parameters.

ACKNOWLEDGEMENTS

The financial support received from the Goodyear Tire and Rubber Co. and the Bi-National (United States-Israel) Agricultural Research Development [BARD] agency to conduct this study is gratefully acknowledged.

REFERENCES

- [1] W. R. Gill and G. E. VandenBerg, Soil dynamics in tillage and traction. agriculture Handbook No. 316, U. S. Govt. Printing Office, Washington, D. C. 511p. (1968).
- [2] S. C. Gupta and R. R. Allmaras, Model to assess the susceptibility of soils to excessive compaction. In Adv. Soil Sci., Springer Verlag, NY, p 56-100 (1987).
- [3] S. C. Gupta and W. E. Larson, Modeling soil mechanical behavior during tillage, In P. Unger et al.(eds.), Symposium on predicting tillage effects on soil physical properties and processes. Am. Soc. Agro., Pub. #44, Madison, WI, p 151-178 (1982).
- [4] H. M. Taylor and G. F. Arkin, Root zone modification: Fundamentals and alternatives, In G. F. Arkin and H. M. Taylor(eds.), Modifying the Root Environment to Reduce Crop Stress, ASAE Monograph #34, St. Joseph, MI. p 3-19 (1982).
- [5] R. Q. Cannel and M. B. Jackson Alleviating aeration stresses, In G. F. Arkin and H. M. Taylor(eds.), Modifying the Root Environment to Reduce Crop Stress, ASAE Monograph #34, St. Joseph, MI. p 141-193 (1982).
- [6] W. J. Chancellor , Compaction of soil by agricultural equipment, Div. of Agr. Ser., Univ. Cal., Davis, Bulletin, 53pp (1977).
- [7] LAWR - Cooperative Extension, Water penetration in California soils, Tech. Rep., Joint Infiltration Committee, Dept. of LAWR, Univ. Cal., Davis, Davis, CA (1984).
- [8] A. Hadas, D. Wolf and E. Rawitz, Zoning soil compaction and cotton stand under controlled traffic operations, ASAE Paper 83- 1042, ASAE St. Joseph, MI 49085 (1983).
- [9] A. Hadas, D. Wolf and E. Rawitz, Residual compaction effect on cotton stand and yields, Trans. ASAE 28, 691-696 (1985)
- [10] A. Hadas, W. E. Larson and R. R. Allmaras, Advances in modeling machine-soil-plant interactions. Soil and Tillage Res. 11, 349-372. (1988).
- [11] H. D. Bowen, Alleviating mechanical impedance, In G. F. Arkin and H. M. Taylor(eds.), Modifying the Root Environment to Reduce Crop Stress, ASAE Monograph #34, St. Joseph, MI. p 141-193 (1982).
- [12] A. Hadas and D. Wolf, Soil aggregates and clod strength dependence on clod size cultivation and stress load rates, Soil Sci. Soc. Am. J. 43, 1157-1164 (1984).
- [13] D. Wolf and A. Hadas, Conventional versus controlled traffic and precision system for cotton, ASAE paper 83-1040, ASAE St. Joseph, MI 49085, (1983).

- [14] D. Wolf and A. Hadas, Soil compaction effects on cotton emergence, Trans. ASAE, 27,655-659 (1984).
- [15] R. L. Schafer, A. C. Bailey, C. E. Johnson and R. L. Raper, A rationale for modeling soil compaction behavior: An engineering mechanics approach, Trans. ASAE, 34(4), 1609-1617 (1991).
- [16] C. S. Desai, Some aspects of constitutive models for geologic media. Third Int. Conf. on Numerical Methods in Geomechanics, Aachen, p2-6, (1979).
- [17] C. S. Desai and H. J. Siriwardane, Constitutive laws for engineering materials with emphasis on geologic materials. Prentice Hall Inc., Englewood Cliffs, NJ, 468pp (1984).
- [18] W. F. Chen and G. Y. Baladi, Soil plasticity - Theory and implementation, developments in Geotechnical engineering 38, ELSEVIER, NY, 231pp, (1985).
- [19] D. R. P. Hettiaratchi and J. R. O' Callaghan, Mechanical behavior of agricultural soils. J. Agr. Eng. Res. 25, 239-259 (1980)
- [20] D. R. P. Hettiaratchi, A critical state soil mechanics for agricultural soils. Soil use and Management, 3(3), 94-105 (1987).
- [21] J. M. Kirby, Measurements of the yield surfaces and critical state of some unsaturated agricultural soils, J. Soil Sci. 40, 167-182 (1989).
- [22] A. C. Bailey, C. E. Johnson and R. L. Schafer, Hydrostatic compaction of agricultural soils. Trans. ASAE, 27(4), 952-955 (1984)
- [23] A. C. Bailey and C. E. Johnson, A soil compaction model for cylindrical stress state. Trans. ASAE. 32(3), 822-825 (1989).
- [24] R. L. Raper and D. C. Erbach, Prediction of soil stresses using the finite element method. Trans. ASAE. 33(3):725-730 (1990).
- [25] R. L. Raper, C. E. Johnson and A. C. Bailey, Coupling normal and shearing stresses to use in finite element analysis of soil compaction. ASAE Paper No. 90-1086, ASAE, St. Joseph, MI 49085, (1990).
- [26] G. Gioda, A numerical procedure for defining the values of soil parameters affecting consolidation, In Design Parameters in Geotechnical Engineering, British Geotechnical Society London, Proceedings of the 7th European Conference on Soil Mechanics and Foundation Engineering, Vol. I, p169-172 (1979)
- [27] A. Asaoka and M. Matsuo, Bayesian approach to inverse problem in consolidation and its application to settlement prediction, Third Int. Conference on Numerical Methods in Geomechanics, Aachen, p115-123 (1979)
- [28] A. Asaoka and M. Matsuo, an inverse problem approach to settlement prediction, Soils and Foundations, Japanese Society of Soil Mechanics and Foundation Engineering, 20(4),53-66 1980

- [29] G. Gioda and G. Maier, Direct search solution of an inverse problem in elastoplasticity: Identification of cohesion, friction angle, and in-situ stresses by tunnel tests, *Int. J. for Numerical Methods in Eng.*, 15, 1823-1848 (1980)
- [30] S. Leroueil and F. Tavenas, Pitfalls in back analysis, 10th Conference of Int. Soc. for Soil Mechanics and Foundation Eng., p285-290, (1981).
- [31] G. Maier, F. Giannessi and A. Nappi, Indirect identification of yield limits by mathematical programming, *Engineering Structures*, 4(2), 86-98 (1982)
- [32] K. Arai, H. Ohta and T. Yasui, Simple optimization techniques for evaluating deformation moduli from field observations, *Soils and Foundations*, 23(1), 107-113 (1983).
- [33] A. Cividini, G. Maier and Nappi, Parameter estimation of a static Geotechnical model using Baye's approach, *Int. J. Rock Mechanics*, 20(5), 215-226 (1983)
- [34] P. T. Brown and J. B. Burland, Soil parameter evaluation from large scale loading tests, *Symposium Int.*, Paris, p25-28 (1983)
- [35] S. Sakurai and K. Takeuchi, Back analysis of measured displacement of tunnels, *Rock Mechanics and Rock Engineering*, 16, p173-180 (1983)
- [36] K. Arai, H. Ohta and K. Kojima, Estimation of soil parameters based on monitored movement of subsoil under consolidation, *Soils and Foundations*, 24(4), 95-108 (1984)
- [37] A. Asaoka and M. Matsuo, An inverse problem approach to multi-dimensional consolidation behavior, *Soils and Foundations*, 24(1), 49-62 (1984)
- [38] V. U. Nguyen, Back calculations of slope failures by the secant method. *Special Notes*, 34(3), 423-427 (1984)
- [39] A. Cividini, G. Gioda and G. Barla, Calibration of geological material model on the basis of field measurement, *Fifth Int. Conference on Numerical methods in Geomechanics*, Nagoya, p1621-1627 (1985)
- [40] G. Gioda, Some remarks on back analysis and characterization problems in geomechanics, *Fifth Int. Conference in Geomechanics*, Nagoya, p47-61 (1985)
- [41] G. Gioda, A. Pandolfi, and A. Cividini, A comparative evaluation of some back algorithms and their application to in-situ load tests, *Second Int. Symposium on Field Measurements in Geomechanics*, Sakukai(ed.) p1131-1144 (1988)
- [42] A. Anandarajah and D. Agarwal, Computer-aided calibration of a soil plasticity model, *Int. j. for Numerical and Analytical Methods in Geomechanics*, 15, 835-856 (1991).
- [43] Y. Ichikawa and T. Ohkami, A parameter identification procedure as a dual boundary control problem for linear elastic materials, *Soils and Foundations*, 32(2), 35-44 (1992).

- [44] D. Rubinstein, S. K. Upadhyaya, and M. Sime. 1994. Determination of in-situ properties of soil using response surface methodology. Accepted for publication in J. Terramechanics.
- [45] D. C. Drucker and W. Prager, Soil mechanics and plastic analysis or limit design, Quarterly Appl. Mech., 10, 157-165 (1952).
- [46] ABAQUS, Thoery Manual, Version 4.8, Hibbitt, Karlsson and Sorensen, Inc. (1989)
- [47] B. M. Das, Evaluation of soil settlement, In Advanced soil mechanics, Ch. 6, Hemisphere Publishing Corporation, NY, p339-401 (1983).
- [48] S. K. Upadhyaya, D. Wulfsohn and J. Mehlschau, An instrumented device to obtain traction related parameters, Accepted for publication in J. Terramechanics, (1992).
- [49] G. W. Snedecor and W. G. Cochran, Curvilinear regression, In Statistical Methods, Ch. 15, Sixth ed., p447-471 (1967).
- [50] J. L. Glancey and S. K. Upadhyaya, A testing procedure for agricultural implements, ASAE Paper No. 90-1542, ASAE St. Joseph, MI 49085, (1990).
- [51] J. L. Glancey, S. K. Upadhyaya, W. J. Chancellor and J. W. Rumsey, Prediction of implement draft using an instrumented analog tillage tool, ASAE Paper No. 91-1065, ASAE St. Joseph, MI 49085, (1991).

Table 1. Parameter values used in the simulation studies

Sequence number	True parameters values		Nondimensional parameters values	
	E_0 (kPa)	E_1	E'_0	E'_1
1	5666.1	61.8	0.604	0.151
2	999.7	14.5	-0.9	-0.9
3	1310.0	19.0	-0.8	-0.8
4	1930.5	28.0	-0.6	-0.6
5	2551.0	37.0	-0.4	-0.4
6	3171.6	46.0	-0.2	-0.2
7	3792.1	55.0	0.0	0.0
8	4412.6	64.0	0.2	0.2
9	5033.2	73.0	0.4	0.4
10	5653.7	82.0	0.6	0.6
11	6274.2	91.0	0.8	0.8
12	6894.8	100.0	1.0	1.0

Table 2. Parameter values obtained through optimization for the cases when no correction was included as well as the case for which second order and third order correction were included

No.	Without correction			Second order correction			Third order correction		
	% error of E_0	% error of E_1	SSE $\times 10^{-3}$	% error of E_0	% error of E_1	SSE $\times 10^{-3}$	% error of E_0	% error of E_1	SSE $\times 10^{-3}$
1	1.34	0.07	0.1810	13.88	0.66	19.312	0.95	1.48	0.3104
2	31.03	17.89	124.01	31.03	0.65	96.300	1.88	4.32	2.2190
3	42.65	5.32	184.74	18.62	5.34	37.538	17.13	3.30	30.417
4	17.55	1.84	31.156	1.34	2.56	0.8340	17.02	2.21	29.463
5	5.81	0.53	3.3998	3.83	1.12	1.1594	8.92	1.12	8.0740
6	1.19	0.14	0.1448	1.56	0.36	0.2569	2.38	0.37	0.5784
7	0.03	0.00	0.0001	0.03	0.00	0.0001	0.03	0.00	0.0001
8	0.71	0.03	0.0503	4.55	0.56	2.1033	1.85	0.44	0.3632
9	2.52	0.27	0.6448	14.98	17.23	52.147	1.01	1.74	0.4030
10	4.63	0.43	2.1586	28.31	19.59	185.15	3.06	0.15	0.9370
11	14.06	9.50	28.790	44.41	7.77	203.25	15.69	8.03	31.064
12	8.34	0.00	6.9556	66.85	0.00	446.88	25.21	0.08	63.575

Table 3. Parameter values obtained through optimization when transformation technique was employed

No.	Without correction			Second order correction			Third order correction		
	% error of E_0	% error of E_1	SSE $\times 10^{-3}$	% error of E_0	% error of E_1	SSE $\times 10^{-3}$	% error of E_0	% error of E_1	SSE $\times 10^{-3}$
1	0.86	0.24	0.0798	1.98	0.33	0.4030	1.78	0.55	0.3456
2	4.09	2.83	2.4780	2.81	1.88	1.1470	0.56	0.09	0.0395
3	1.49	3.92	1.7567	2.79	0.09	0.7796	2.06	5.47	3.4132
4	5.48	2.83	3.8048	0.06	1.75	0.3060	9.12	4.33	10.202
5	4.59	2.39	2.6734	2.47	2.62	1.3003	5.98	2.49	4.1949
6	4.14	1.49	1.9347	2.01	0.71	0.4562	3.95	0.78	1.6195
7	0.27	0.14	0.0091	0.89	0.47	0.1014	4.35	0.50	1.9139
8	2.69	1.04	0.8321	2.45	0.69	0.6496	9.73	0.65	9.5151
9	2.30	0.59	0.5612	4.38	10.15	12.225	9.22	0.37	8.5214
10	0.15	1.13	0.1288	14.03	21.95	67.882	1.93	2.44	0.9664
11	3.36	4.98	3.6090	22.54	9.89	60.572	9.50	9.54	18.118
12	0.00	2.47	0.6082	18.51	17.95	66.497	20.26	0.44	41.064

V.5.1 DETERMINATION OF ENGINEERING PROPERTIES OF SOIL IN-SITU

Shrini. K. Upadhyaya
Professor

Department of Biological and Agricultural Engineering
University of California, Davis CA 95616

SUMMARY:

Soil-tire/Soil-track interaction is of particular interest to researchers involved in off-road mobility and traction research. This includes scientists and engineers involved in research in the field of agriculture, construction, forestry, military, and mining. In agriculture and forestry soil compaction caused by traction devices is also a serious concern. A sound mathematical model is a pre-requisite to obtain a clear understanding of the soil-tire/soil-track interaction process. A key ingredient for any such model is a constitutive relationship which describes the stress-strain behavior of soil. Any suitable constitutive model requires soil physical properties which describe the elastic behavior of soil, onset of yield and subsequent plastic flow, material hardening or softening rules etc. Since in-situ soils seldom behave like remolded laboratory soils or disturbed field samples, it is important to "identify" or "calibrate" the engineering properties of field soil by means of in-situ tests. The technique of obtaining material parameters based on actual system response is known as "back analysis", "inverse solution", "identification", or "calibration procedure". For complex problems such as soil-traction device interaction where closed form analytical solutions do not exist a numerical technique such as a finite element technique is commonly used to solve underlying system differential equation. For such cases the back analysis procedure can take one of the two forms: (1) inverse method, and (2) direct method. This paper addresses the advantages and disadvantages of such techniques, and discusses a new technique which overcomes some of their limitations. This new technique consists of developing a so called "response surface" in the parameter space and then using

Table 4. Prediction of soil parameters using the orthogonal response surface developed when a third order correction was employed

Point #	Plate size	Reasonable solution #	% error of κ	% error of ν	% error of K	% error of C	% error of ϕ	SSE $\times 10^{-3}$	SSR $\times 10^{-3}$
1	2 in	1	0.82	3.77	10.07	6.82	1.00	16.390	0.010
		2	3.93	9.01	8.33	6.26	1.38	20.710	0.004
	4 in	1	4.93	14.83	3.28	14.39	3.07	47.140	0.010
		2	3.04	10.70	10.56	10.93	1.00	35.570	0.040
		3	0.72	0.84	8.39	4.79	0.21	9.470	0.040
	2 and 4 in	1	0.11	1.58	5.13	6.43	1.86	7.370	0.110
2		0.09	1.51	5.20	5.11	1.54	5.780	0.110	
2	2 in	1	6.60	6.79	3.42	22.34	6.21	63.900	0.110
	4 in	1	4.96	15.51	0.92	2.17	0.76	27.130	0.030
		2	3.34	15.88	14.55	30.12	16.90	166.810	0.750
	2 and 4 in	1	0.37	0.98	2.04	3.01	0.76	1.490	1.830
		2 in	1	9.09	2.62	1.69	38.73	1.14	159.360
	4 in	1	9.09	5.14	3.63	6.56	2.65	17.220	2.390
3	2 and 4 in	2	9.09	6.32	33.64	4.41	32.12	230.560	0.650
		1	9.09	2.05	3.80	15.13	28.45	113.960	5.700
	2 in	1	30.51	79.76	1.61	0.55	11.84	743.630	0.120
	4 in	1	54.55	121.88	10.00	15.90	13.18	1836.000	0.950
	2 and 4 in	1	43.34	147.46	0.09	2.17	11.84	2376.830	0.120
		2 in	1	4.90	6.10	2.60	3.42	0.24	7.970
4	2 in	1	1.12	1.37	2.24	1.93	0.47	1.120	0.003
		2	15.12	19.22	8.39	4.64	2.43	69.570	0.004
	4 in	3	9.06	11.54	5.26	4.10	0.83	1.490	0.004
		1	5.40	6.78	2.14	3.50	0.06	9.190	0.020

Table 5. Sinkage parameters obtained from filed tests conducted in a Yolo loam soil.

Test Date	Soil* Condition	Plate Size, mm	Sinkage** Constant,k kPa	Sinkage Constant, n	Overall R ²
November, 1991	Undisturbed	50.8	695.6	0.609	0.774
	C=11.5 kPa	76.2	819.6	0.84	0.921
	$\phi=32.9$ deg.	101.6	1091.2	0.828	0.911
	MC=8.9%	127.0	778.3	0.767	0.743
	$\rho=1510$, kg/m ³ e=0.755	152.4	1054.4	0.971	0.942
September, 1992	Undisturbed	50.8	959.5	0.646	0.776
	C=32.3 kPa	76.2	921	0.499	0.715
	$\phi=27.2$ deg.				
	MC = 5.14%	101.6	1839.4	0.992	0.934
	$\rho=1510$, kg/m ³ e=0.755				
	Tilled	50.8	607.6	0.918	0.776
	C=22.7 kPa	76.2	605.6	0.776	0.875
	$\phi=22.8$ deg.				
	MC=4.55%	101.6	796.7	0.958	0.875
	$\rho=1433$, kg/m ³ e=0.85				

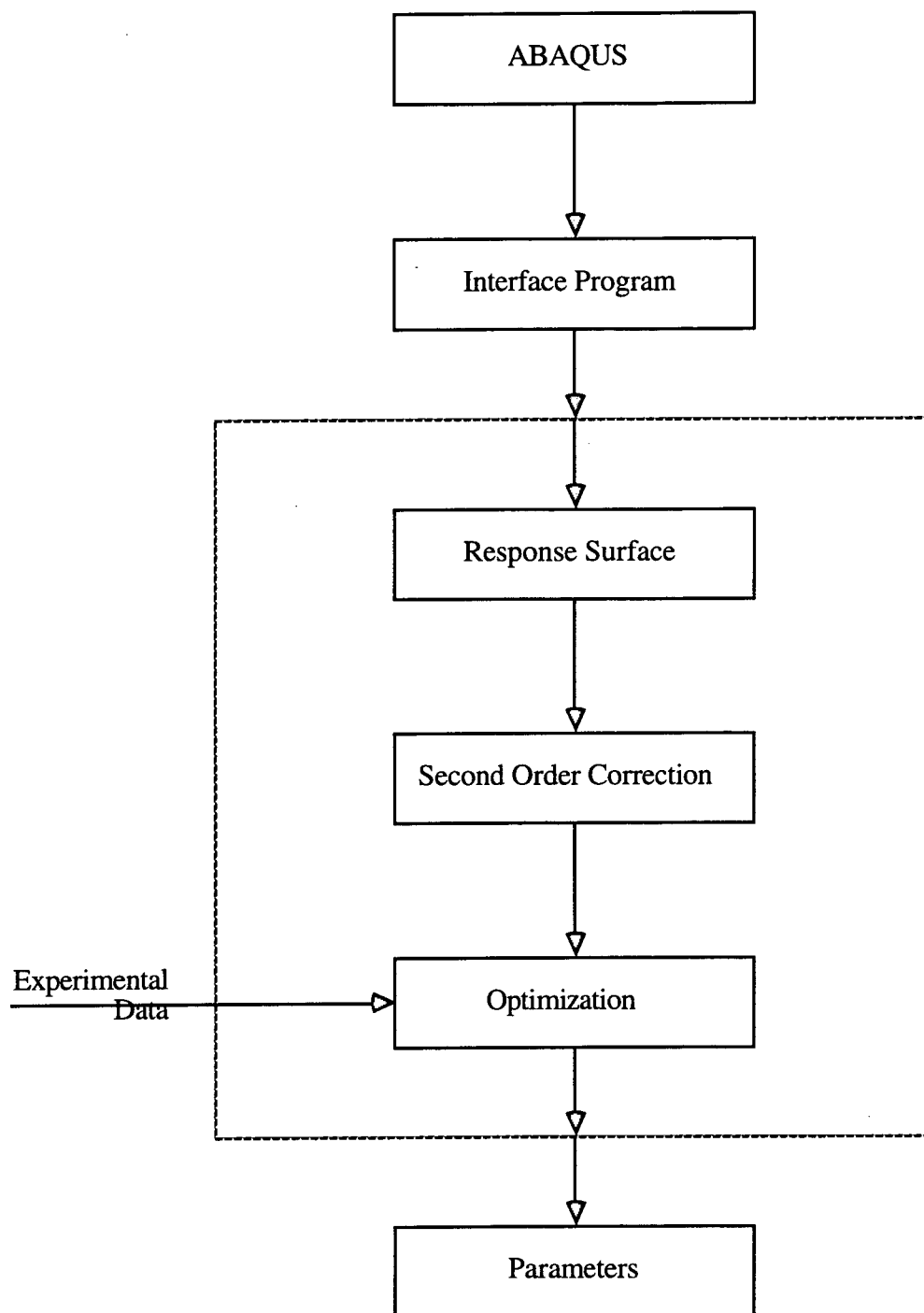
* C = cohesion; ϕ = soil internal angle of friction; MC = moisture content, dry basis; ρ = bulk density;
e = void ratio.

** Logarithmic mean of all eight replicates.

Table 6. The parameter prediction from the soil tests

Test Description	Best Results	Reasonable Results	Reasonable Results
		No. 1	No. 2
Test #1 Undisturbed Soil November, 1991	$\kappa=0.0545$ $\nu=0.1310$ $K=0.7124$ $C=12.348 \text{ kPa}$ $\phi=22.5 \text{ deg.}$ $SSE=0.00380$ $SSR=0.00249$	$\kappa=0.0446$ $\nu=0.2089$ $K=0.8928$ $C=11.371 \text{ kPa}$ $\phi=22.5 \text{ deg.}$ $SSE=0.00490$ $SSR=0.00601$	$\kappa=0.0638$ $\nu=0.0983$ $K=0.7955$ $C=15.344 \text{ kPa}$ $\phi=22.5 \text{ deg.}$ $SSE=0.02146 *$ $SSR=0.01295$
Test #2 Undisturbed Soil September, 1992	$\kappa=0.0513$ $\nu=0.159$ $K=0.7365$ $C=14.321 \text{ kPa}$ $\phi=28.333 \text{ deg.}$ $SSE=0.00665$ $SSR=0.00089$	$\kappa=0.0225$ $\nu=0.370$ $K=0.8950$ $C=15.068 \text{ kPa}$ $\phi=26.050 \text{ deg.}$ $SSE=0.01332 *$ $SSR=0.00345$	
Test #3 Tilled Soil September 1992	$\kappa=0.1037$ $\nu=0.1859$ $K=0.6247$ $C=8.997 \text{ kPa}$ $\phi=31.820 \text{ deg.}$ $SSE=0.00378$ $SSR=0.00016$	$\kappa=0.0505$ $\nu=0.370$ $K=0.8993$ $C=16.516 \text{ kPa}$ $\phi=25.247 \text{ deg.}$ $SSE=0.00444$ $SSR=0.00337$	

* Relatively high SSE indicating an unreasonable solution.



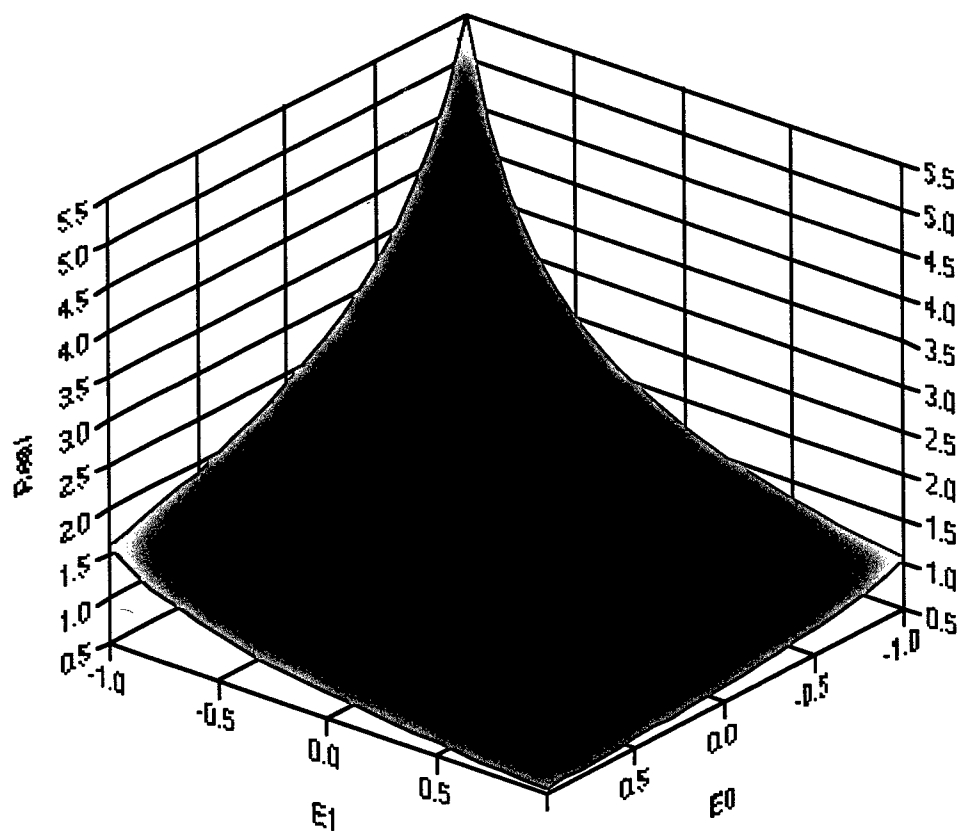


Figure 2. The plot of real function in $E_0 - E_1$ space

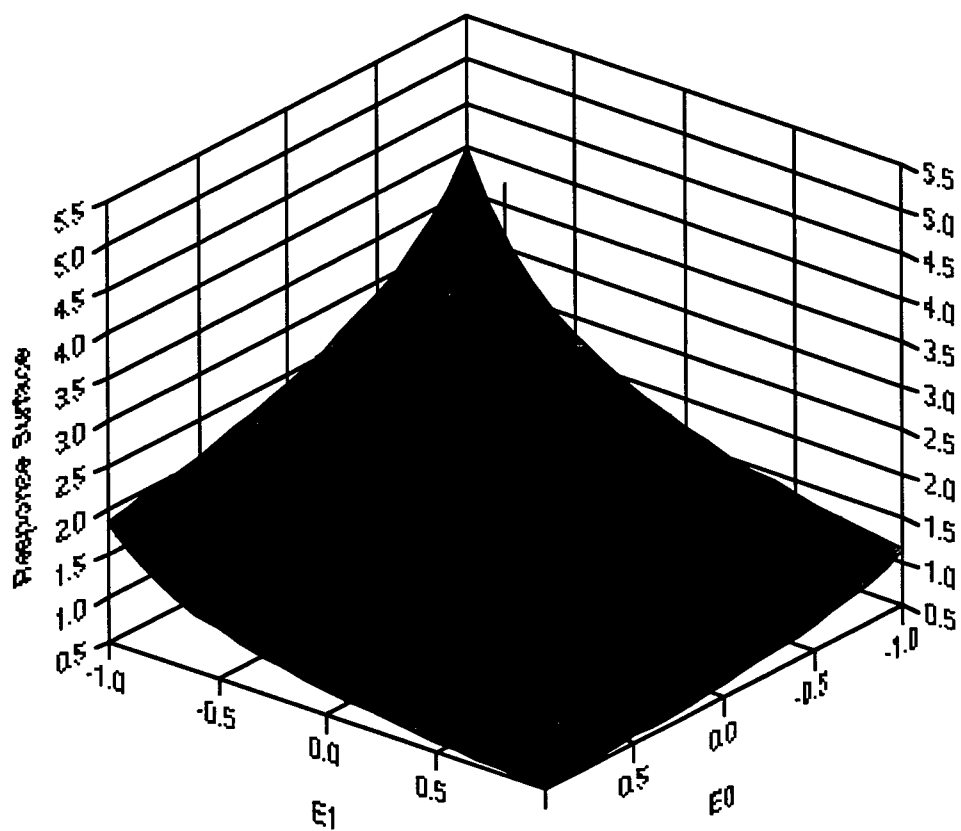


Figure 3. The plot of orthogonal response surface in E_0 - E_1 space

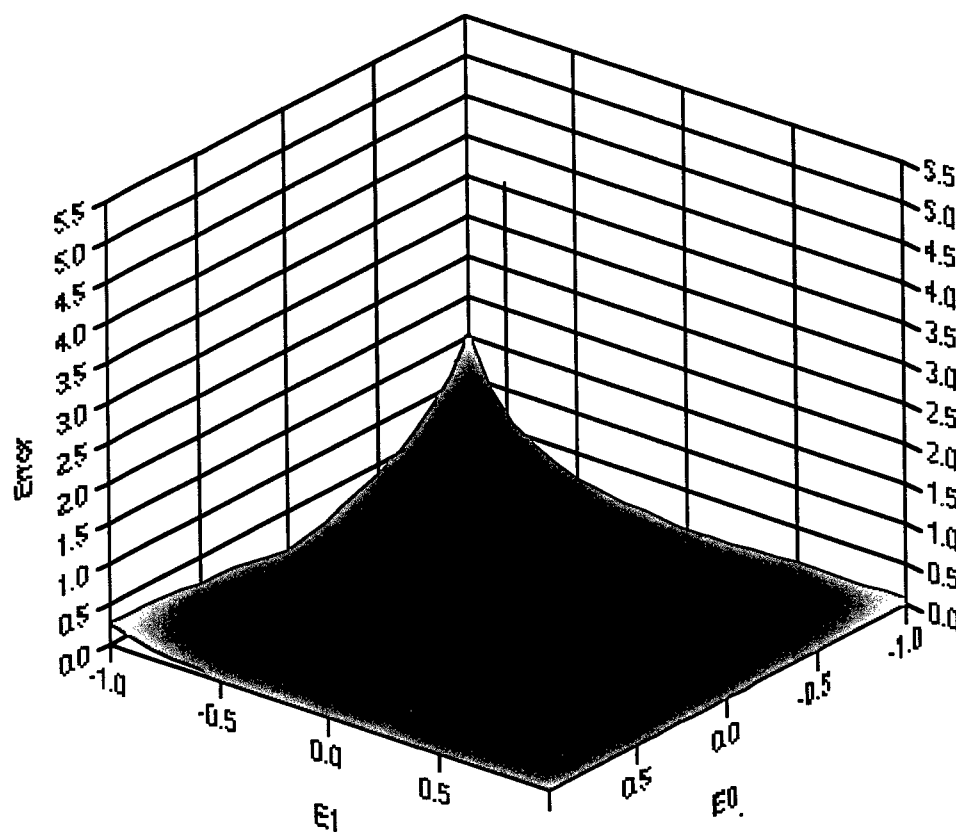


Figure 4. The plot of error without any correction in $E_0 - E_1$ space

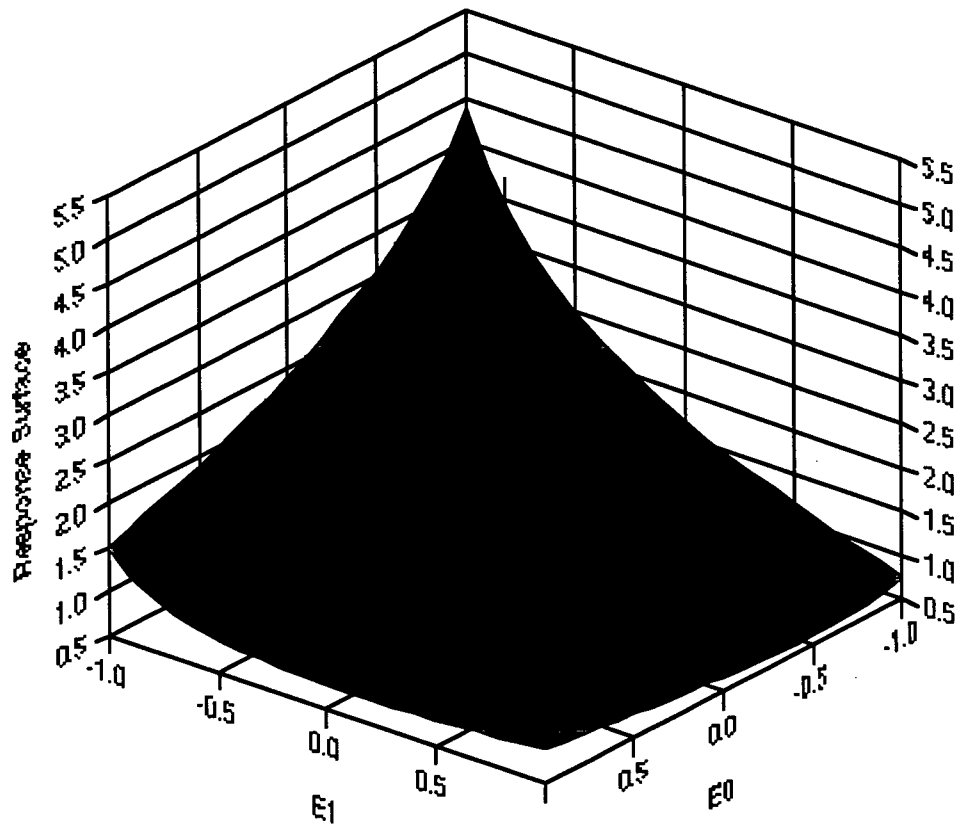


Figure 5. The plot of orthogonal response surface in E_0 - E_1 space when a second order correction was included

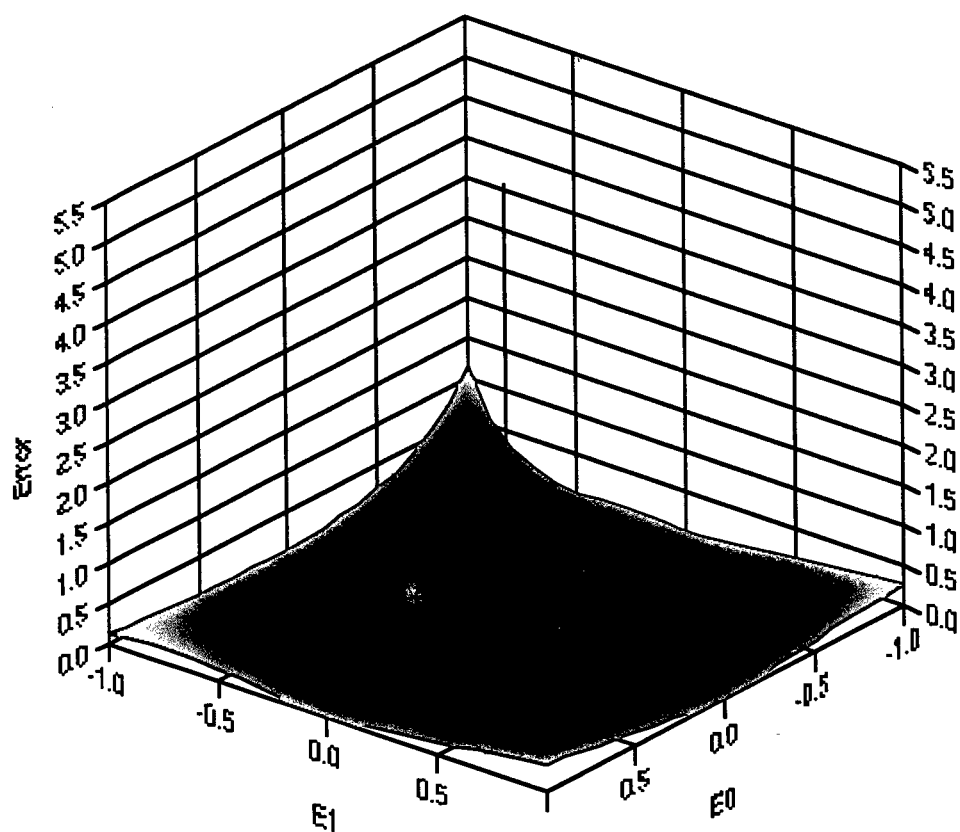


Figure 6. The plot of error in $E_0 - E_1$ space when second order correction is included

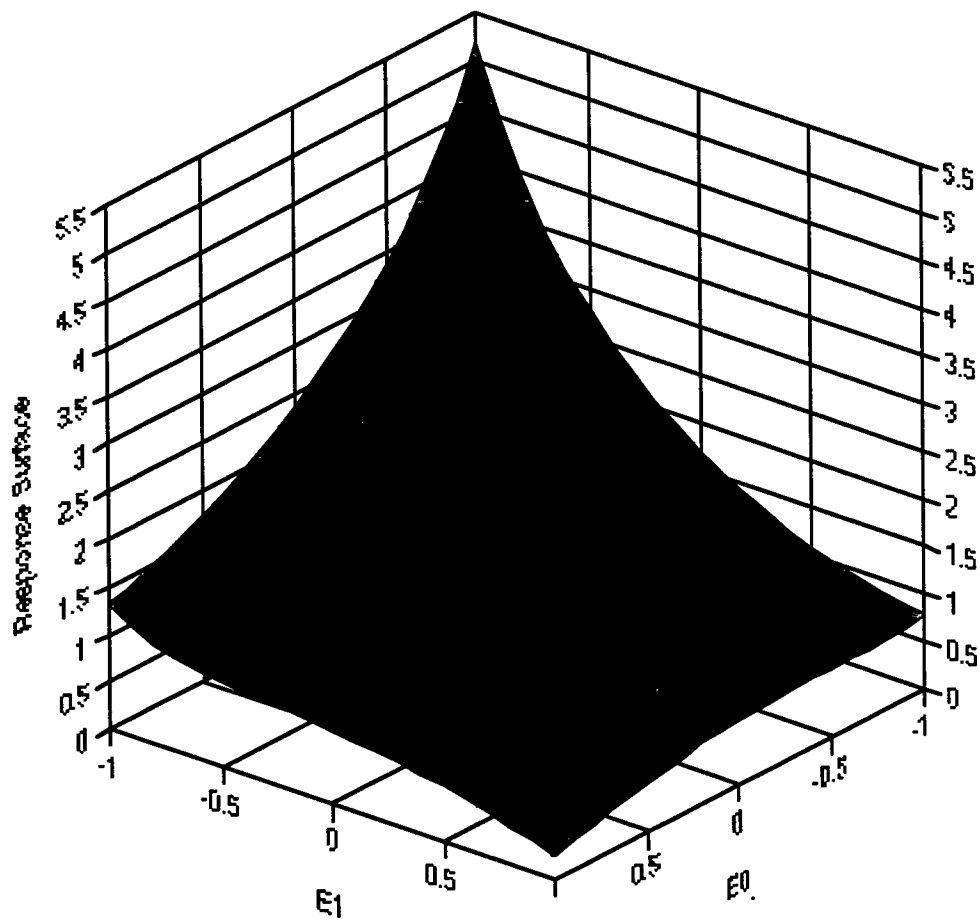


Figure 7. Plot of orthogonal response surface in E_0 - E_1 space when a third order correction was included

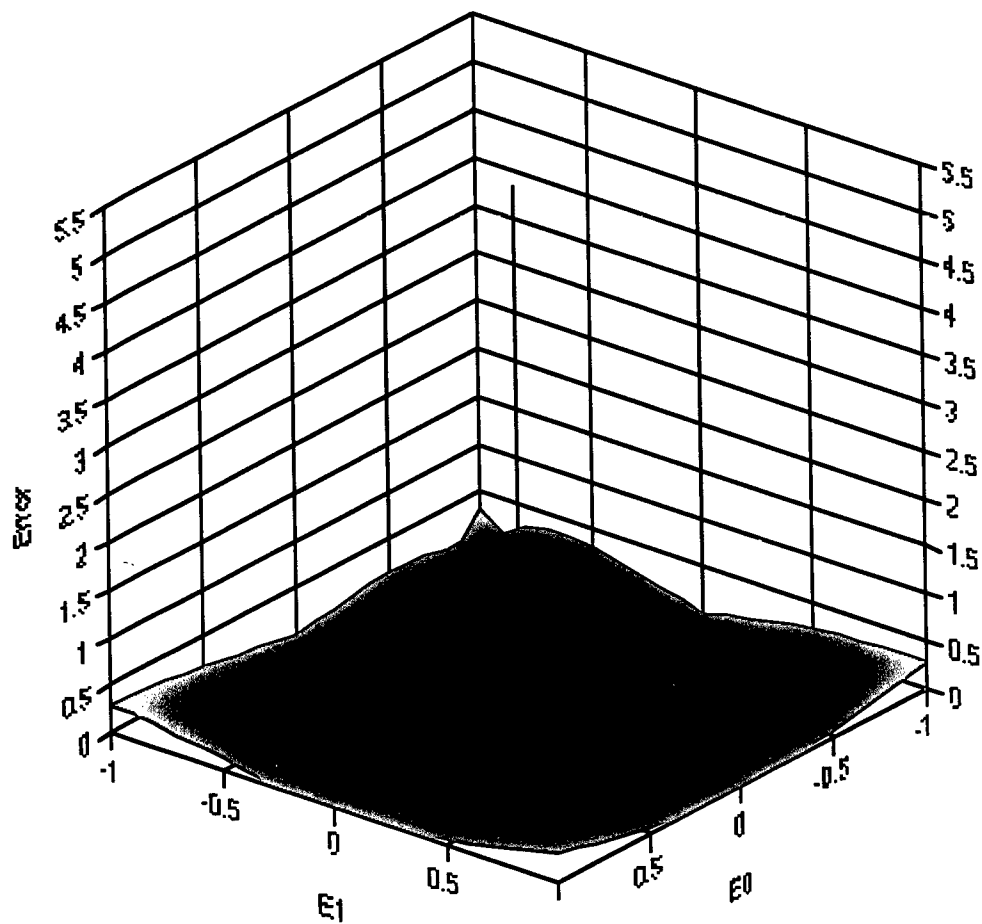


Figure 8. plot of error in $E_0 - E_1$ space when a third order correction was included.

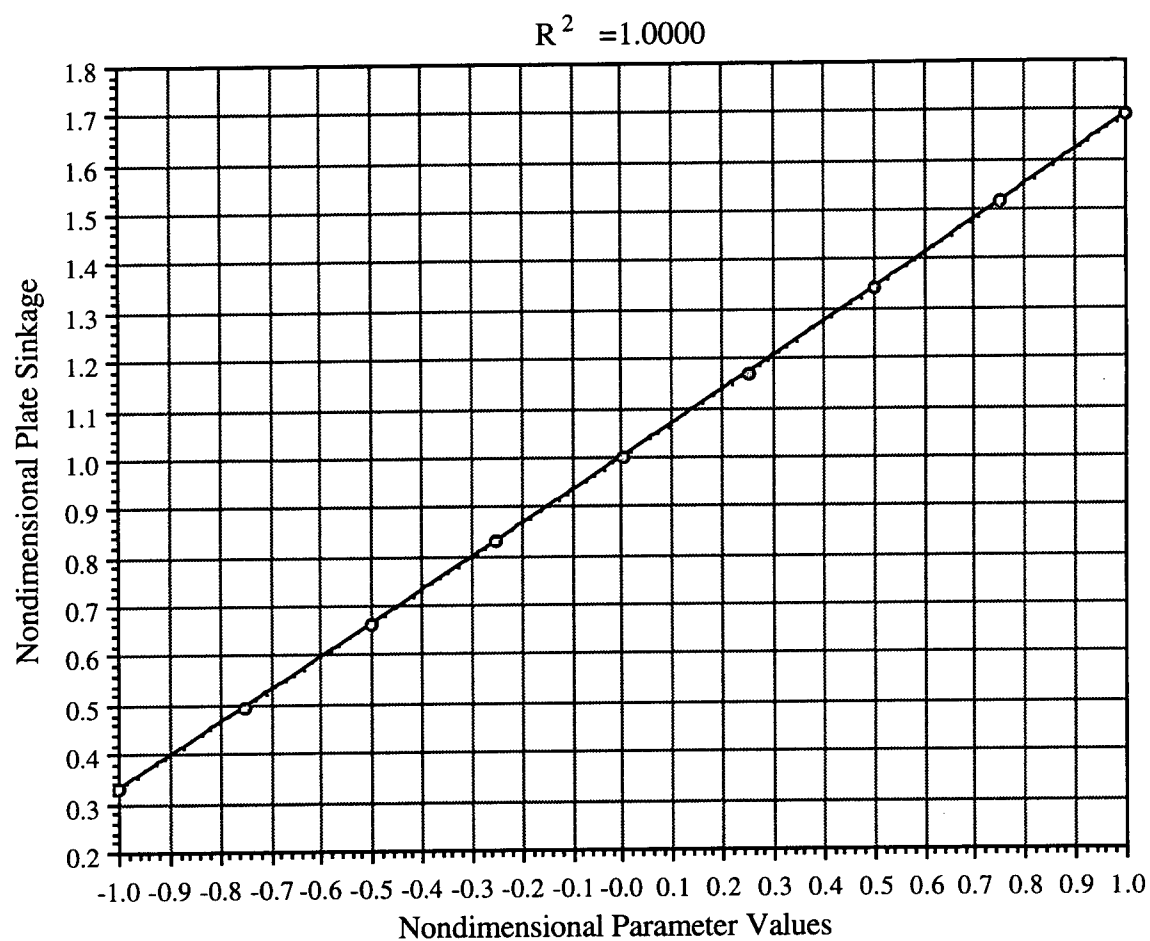


Figure 9. Plate sinkage vs. nondimensional values of parameter κ for a 4 in plate subjected to 80 PSI applied load

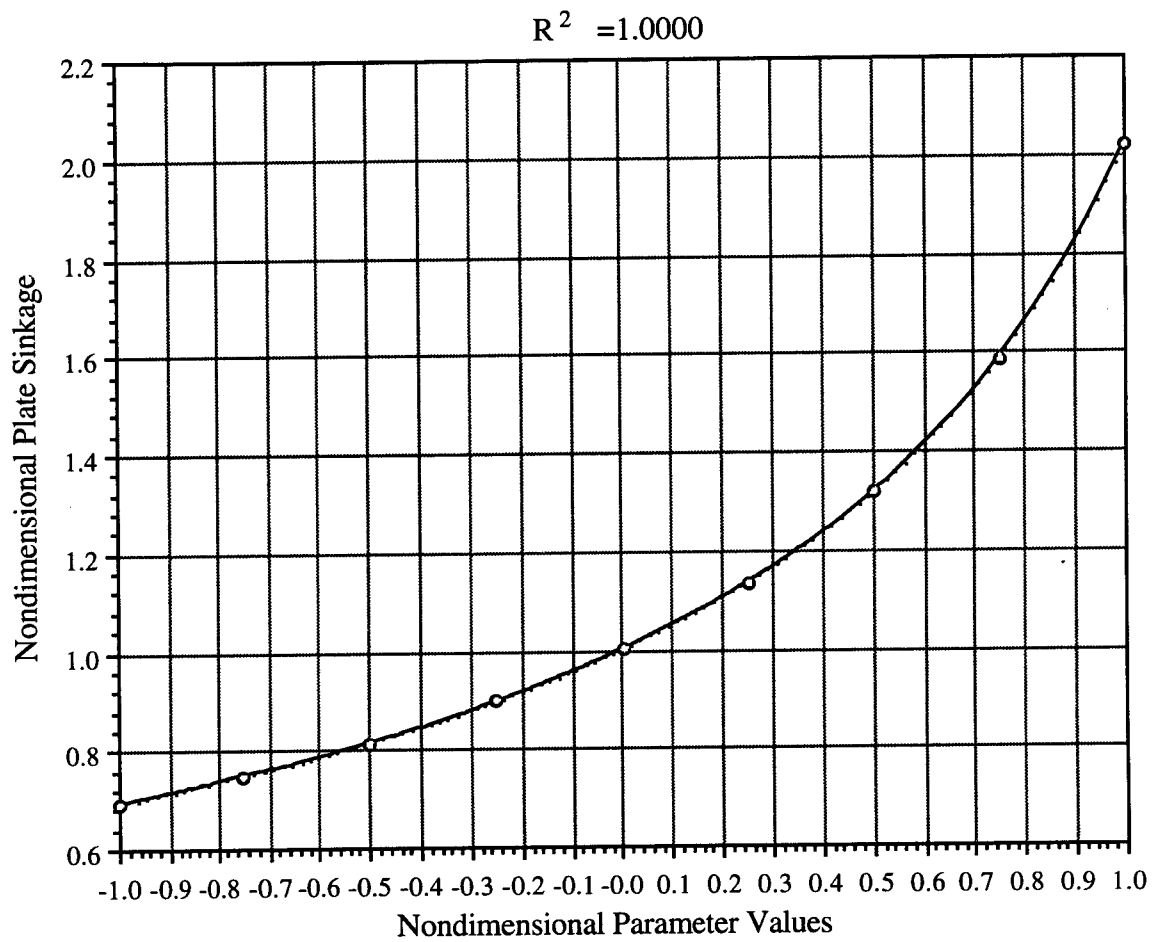


Figure 10. Plate sinking vs. nondimensional values of parameter ν for a 4 in plate subjected to 80 PSI applied load

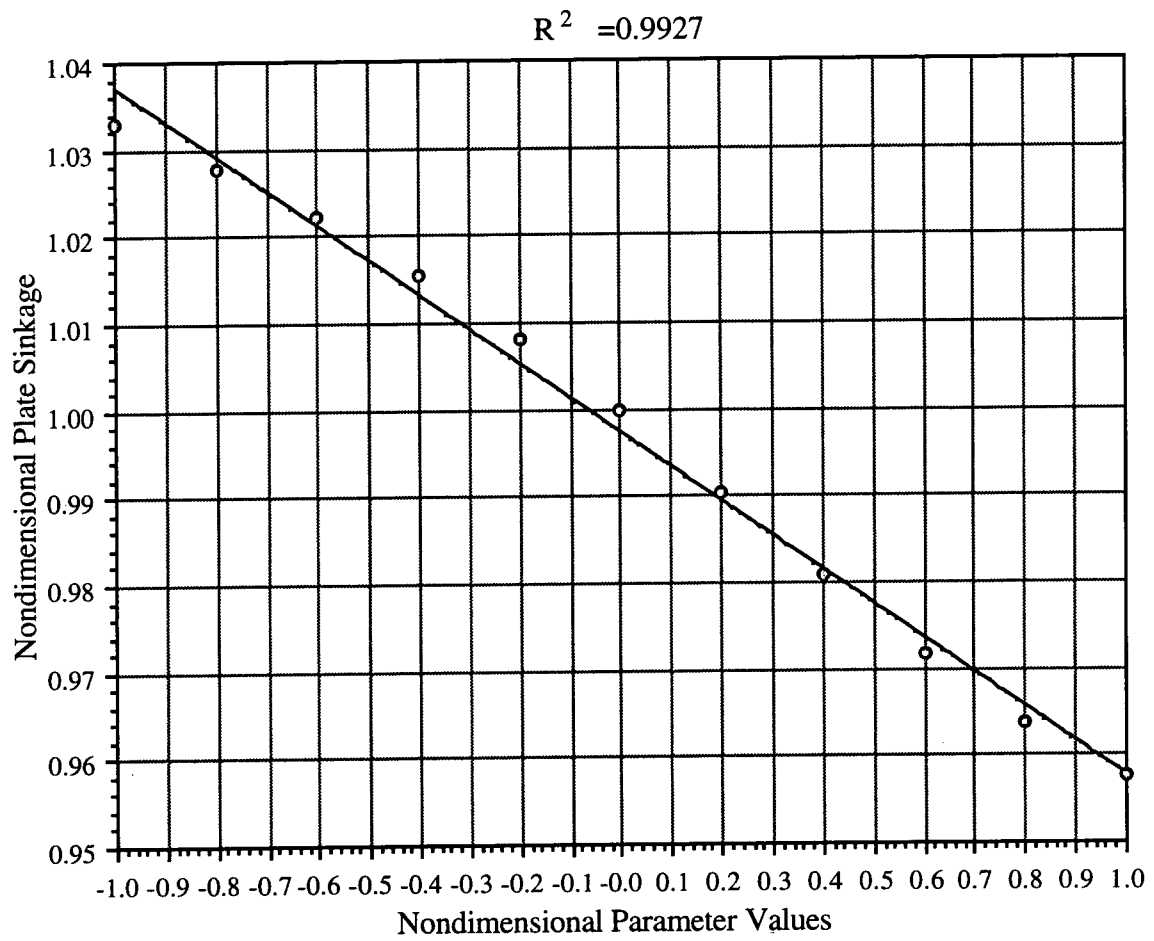


Figure 11. Plate sinkage vs. nondimensional values of parameter K for a 4 in plate subjected to 80 PSI applied load

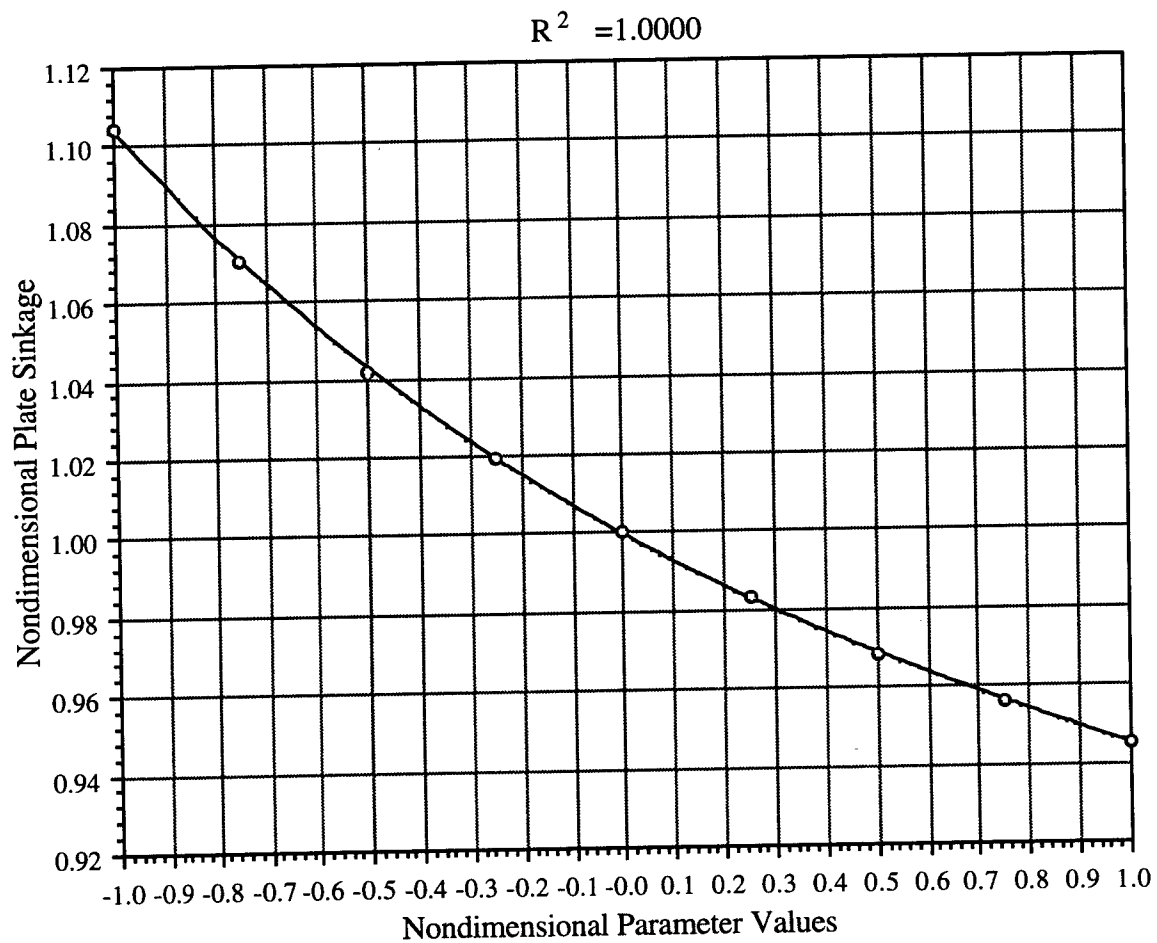


Figure 12. Plate sinkage vs. nondimensional values of parameter C for a 4 in plate subjected to 80 PSI applied load

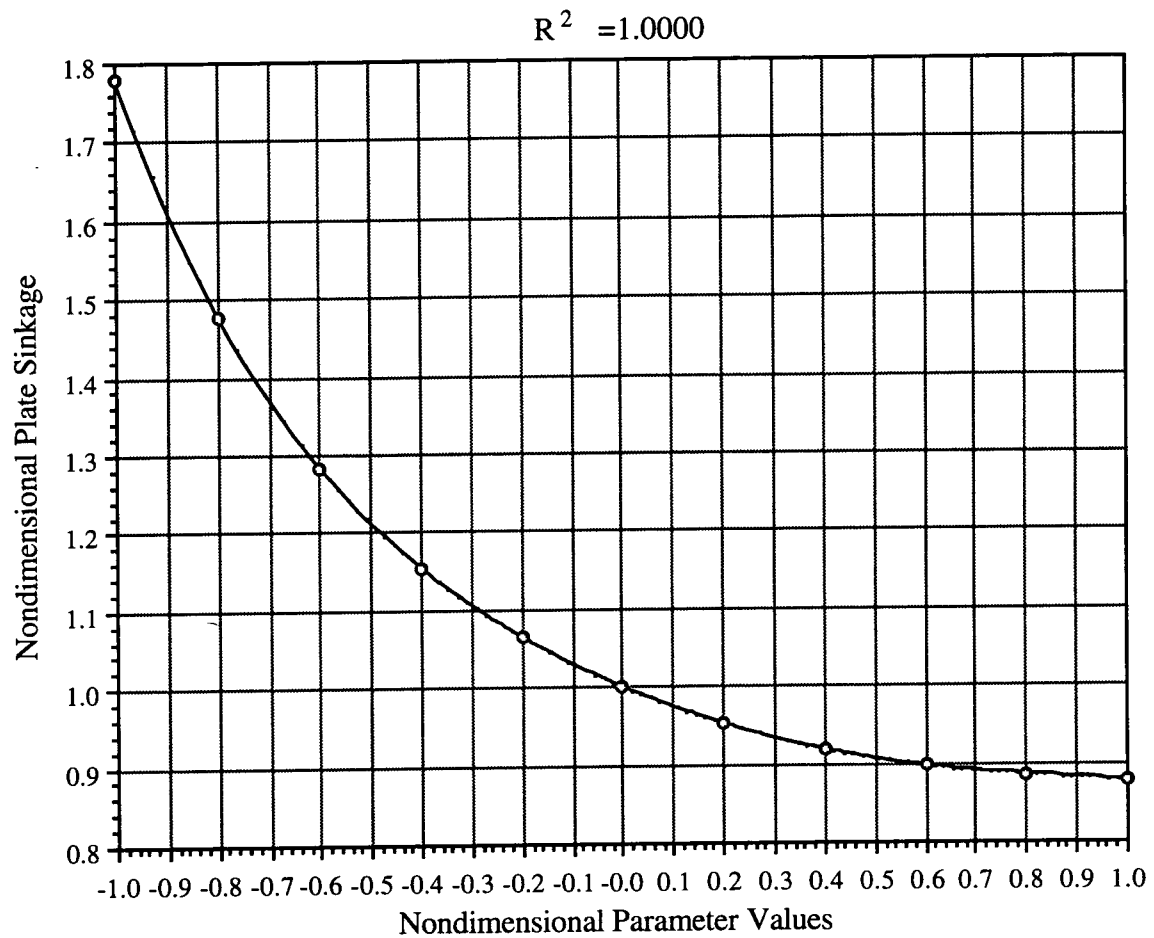


Figure 13. Plate sinkage vs. nondimensional values of parameter ϕ for a 4 in plate subjected to 80 PSI applied load

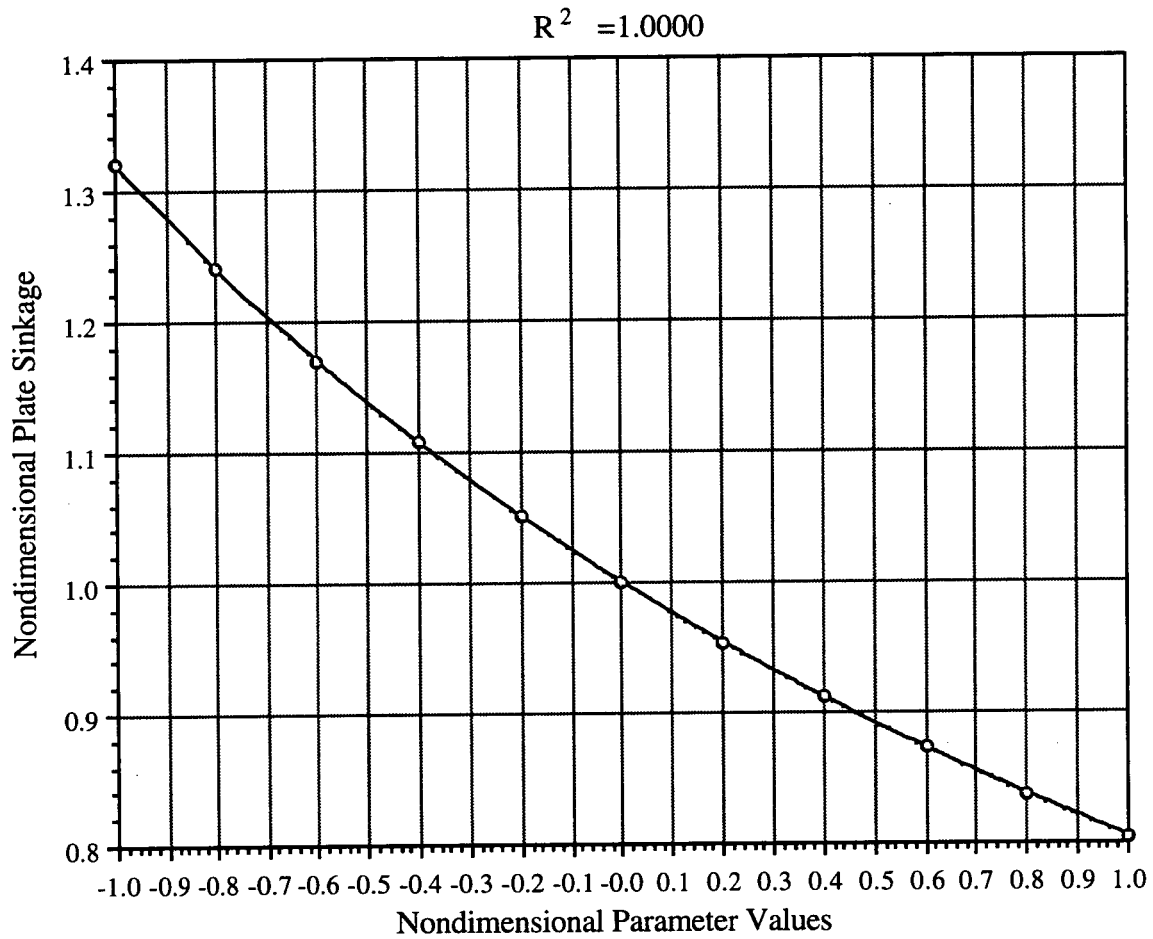


Figure 14. Plate sinkage vs. nondimensional values of parameter e for a 4 in plate subjected to 80 PSI applied load

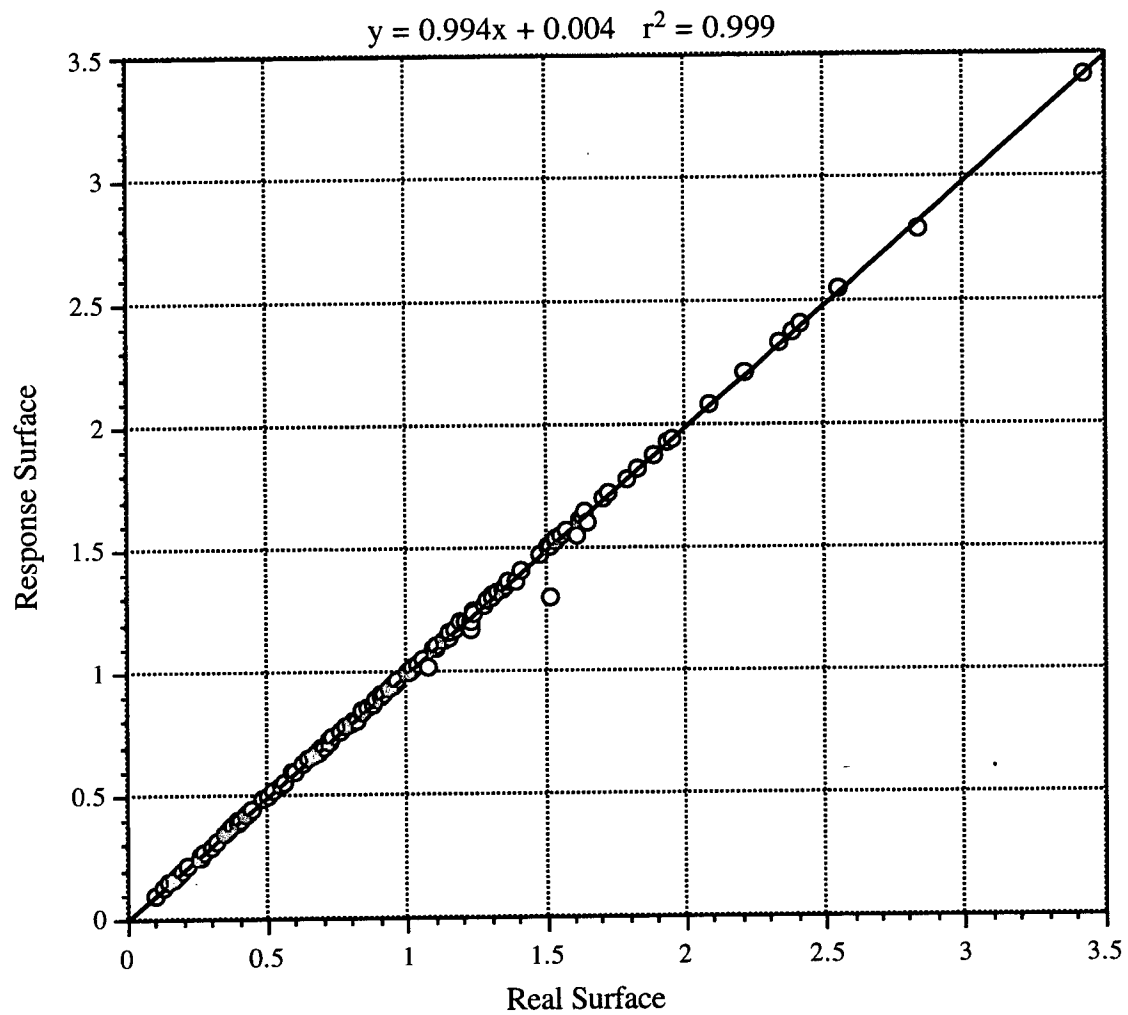


Figure 15. Response surface vs. real surface for a 4 in plate subjected to 15 PSI pressure - without correction

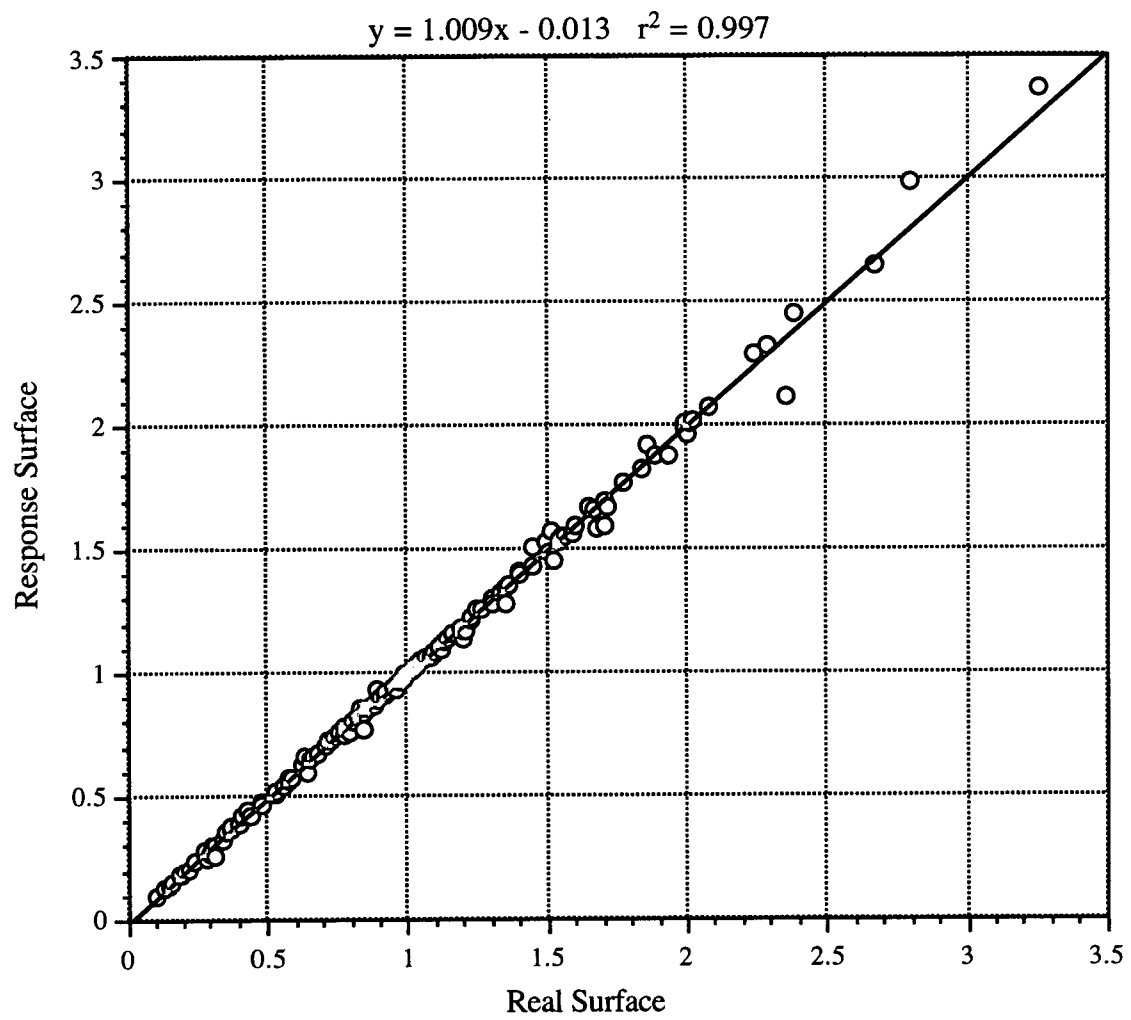


Figure 16. Response surface vs. real surface for a 4 in plate subjected to 80 PSI pressure - without correction

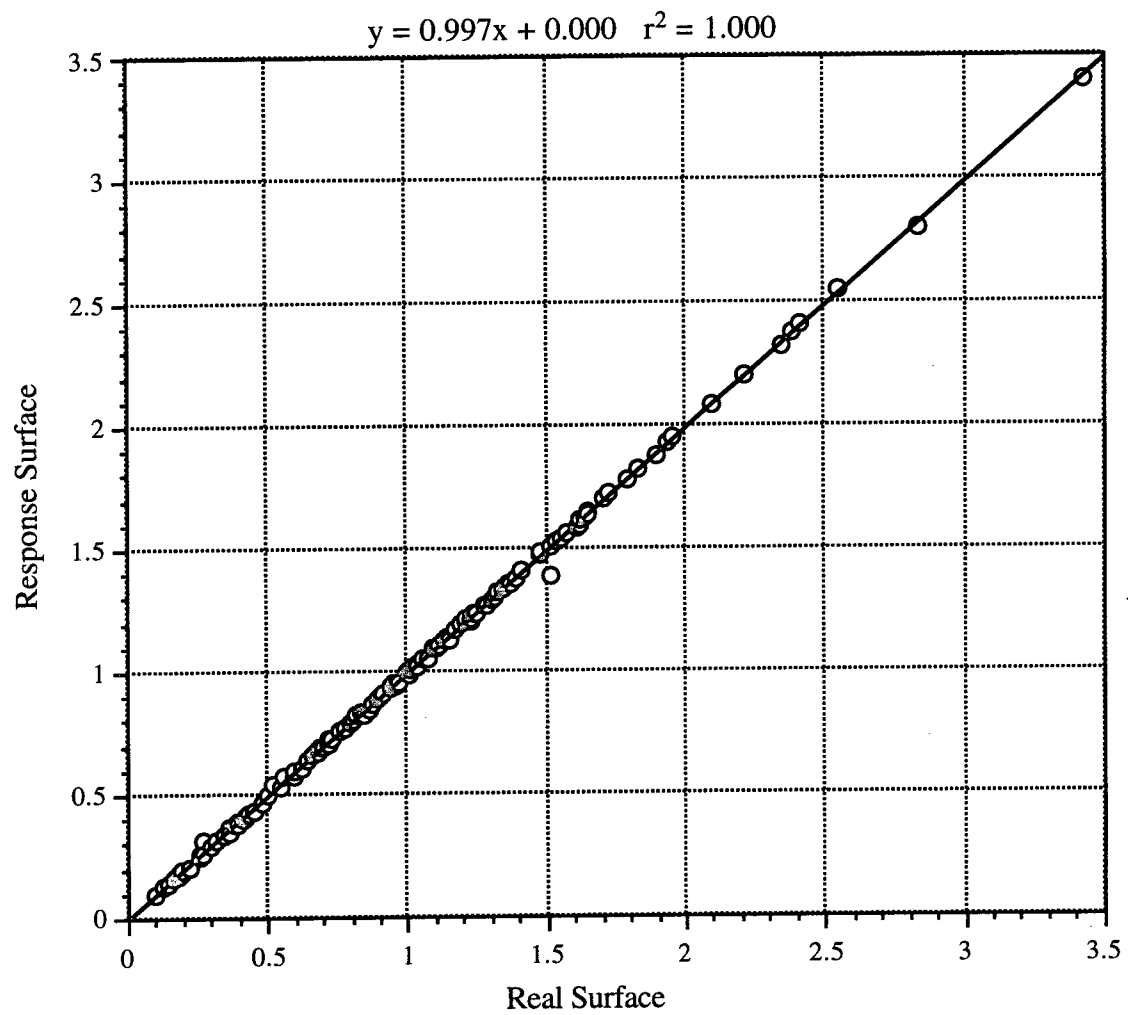


Figure 17. Response surface vs. real surface for a 4 in plate subjected to 15 PSI pressure - using second order correction

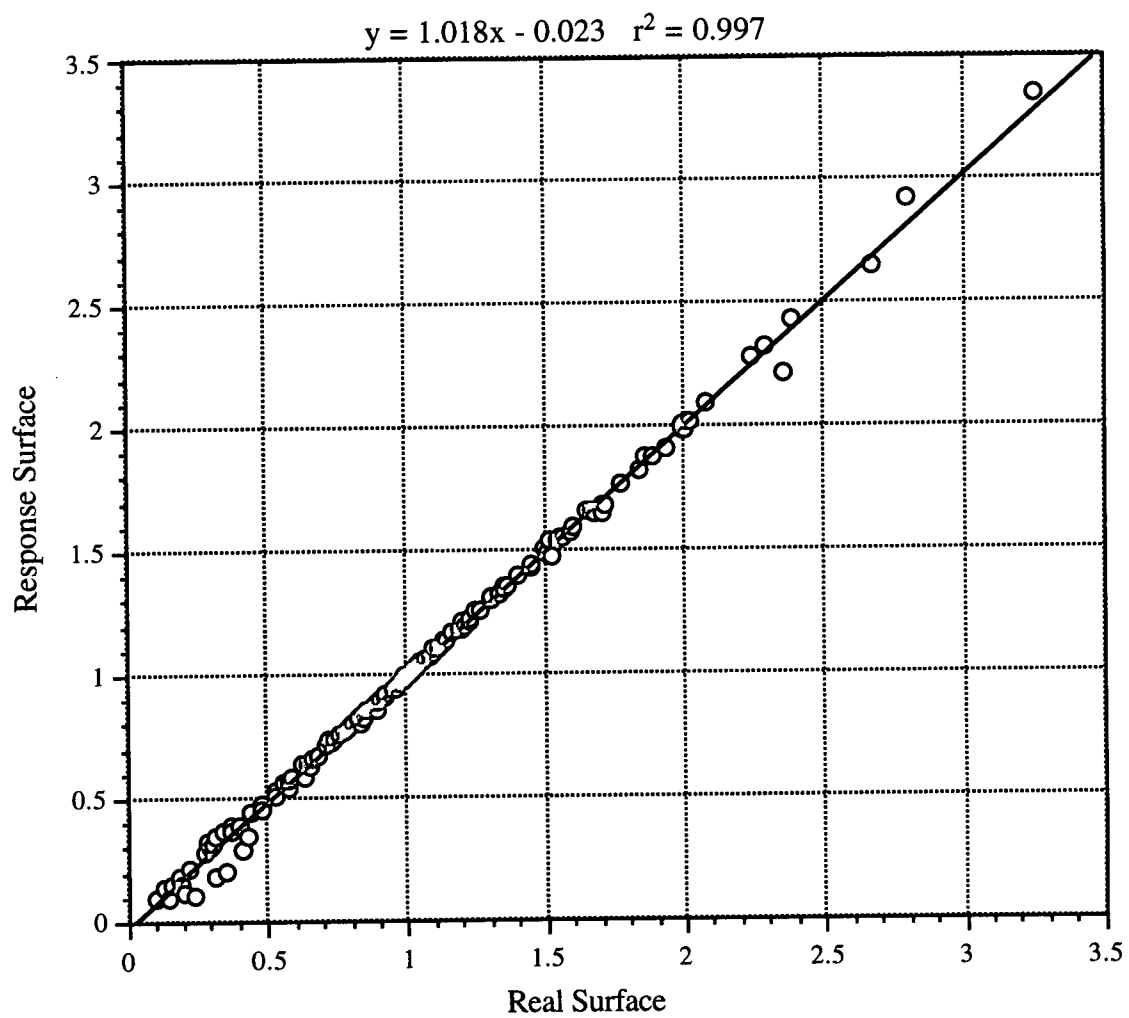


Figure 18. Response surface vs. real surface for a 4 in plate subjected to 80 PSI pressure - using second order correction

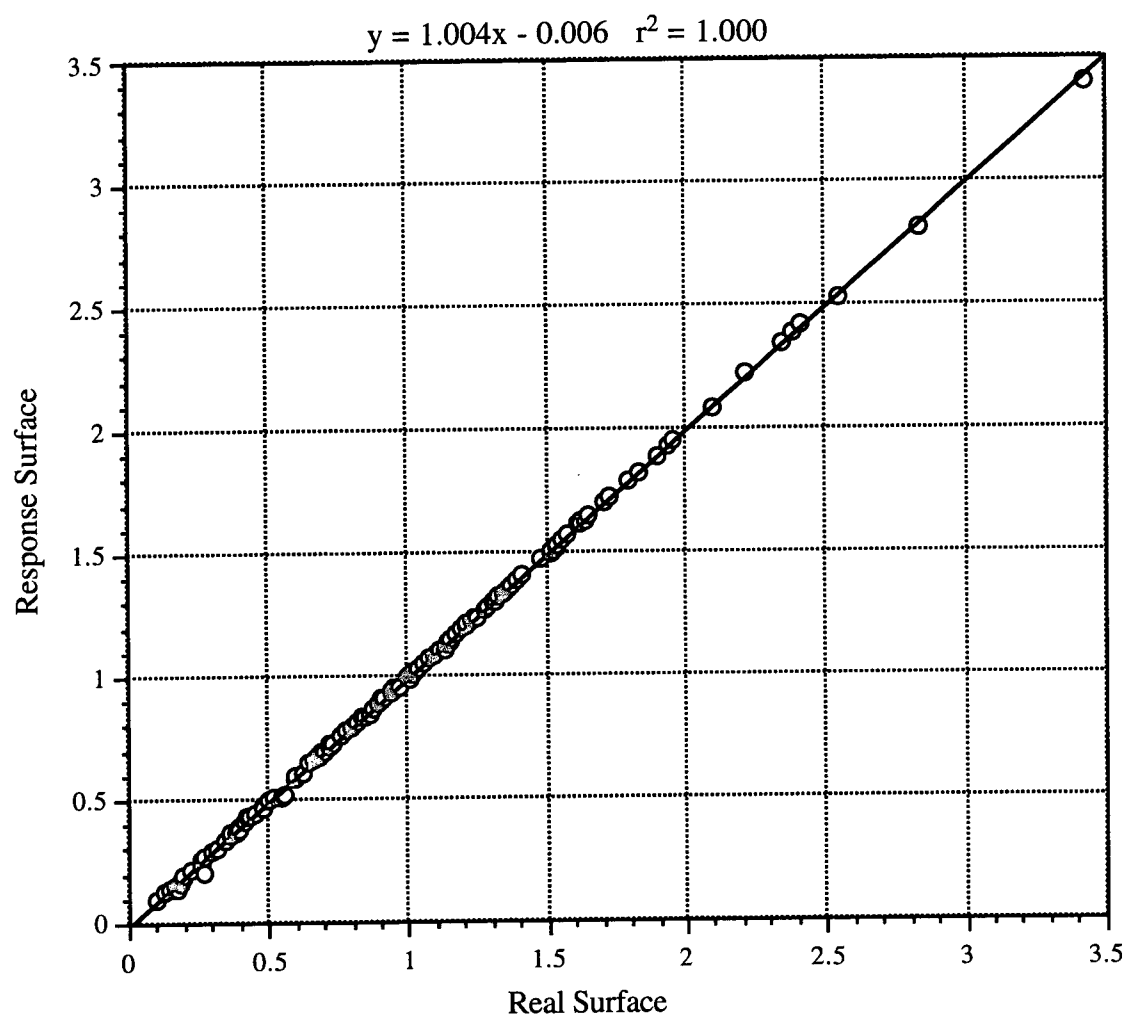


Figure 19. Response surface vs. real surface for a 4 in plate subjected to 15 PSI pressure - using third order correction

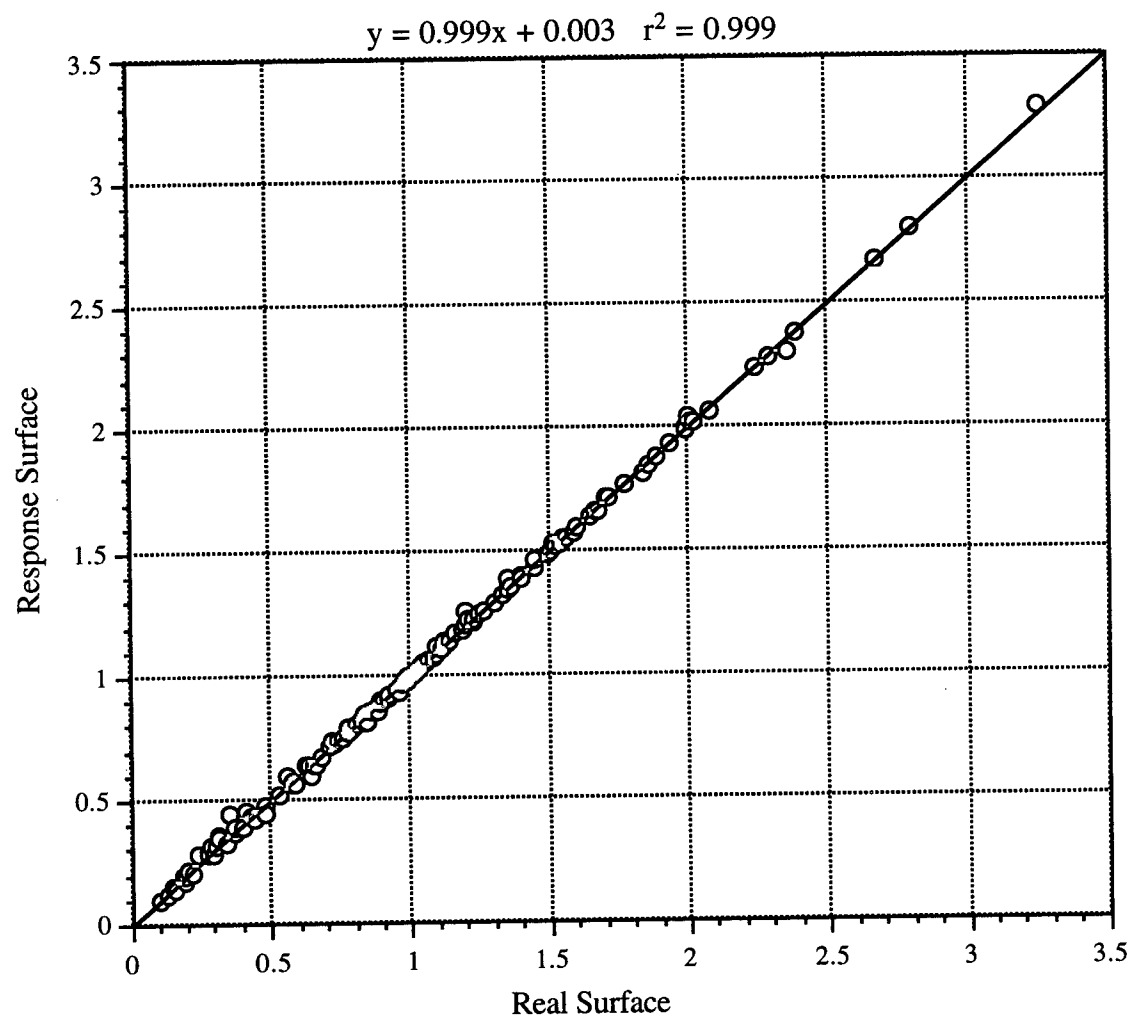


Figure 20. Response surface vs. real surface for a 4 in plate subjected to 80 PSI pressure - using third order correction

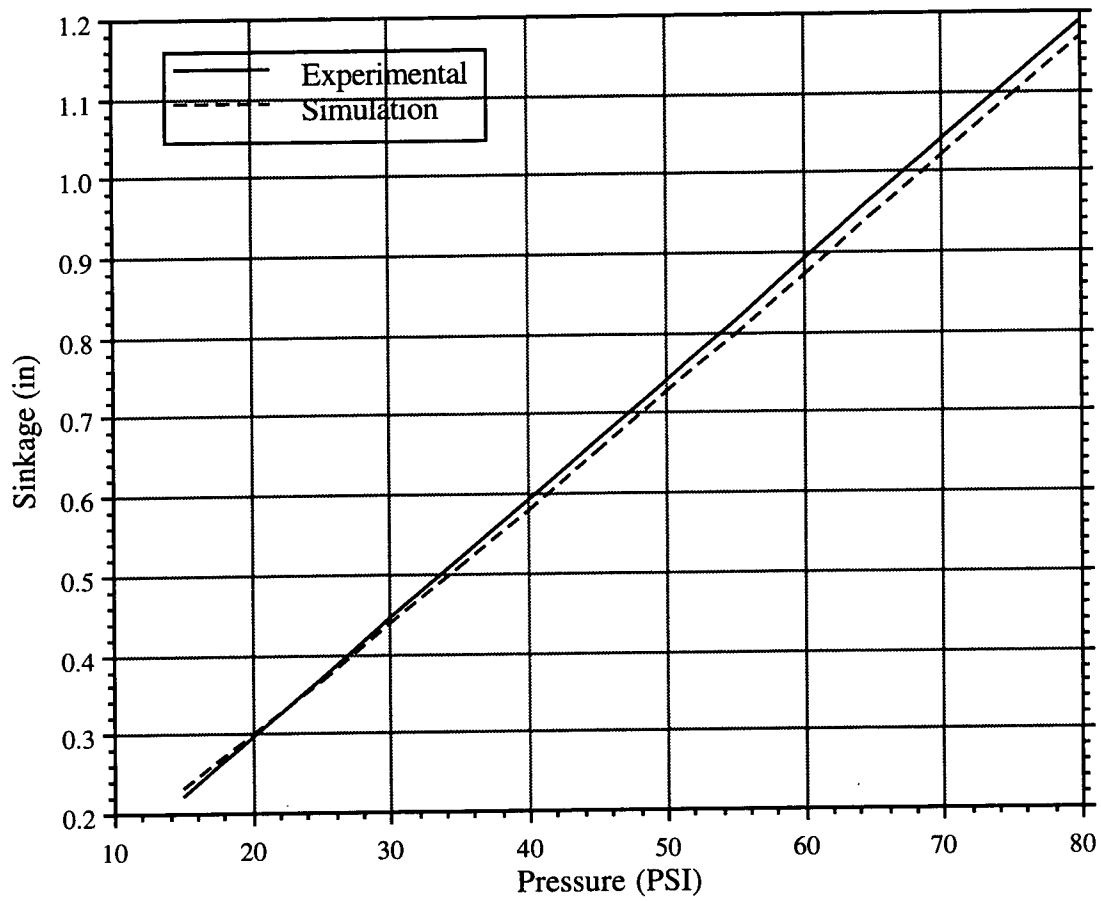


Figure 21. Experimental and simulated sinkage for a 4 in plate in an undisturbed soil. Experimental results correspond to September 1992 tests.

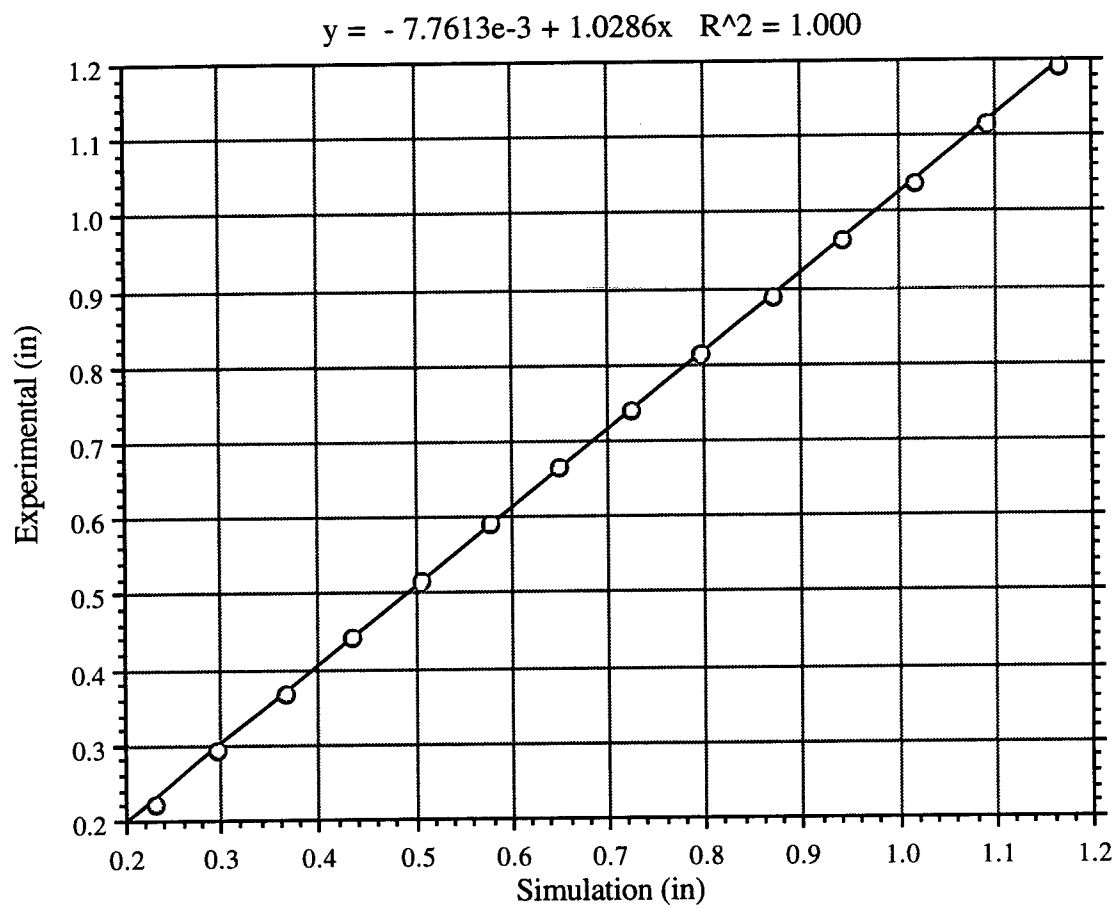


Figure 22. Experimental vs. simulated sinkage for a 4 in plate in an undisturbed soil.
Experimental results correspond to September 1992 tests.

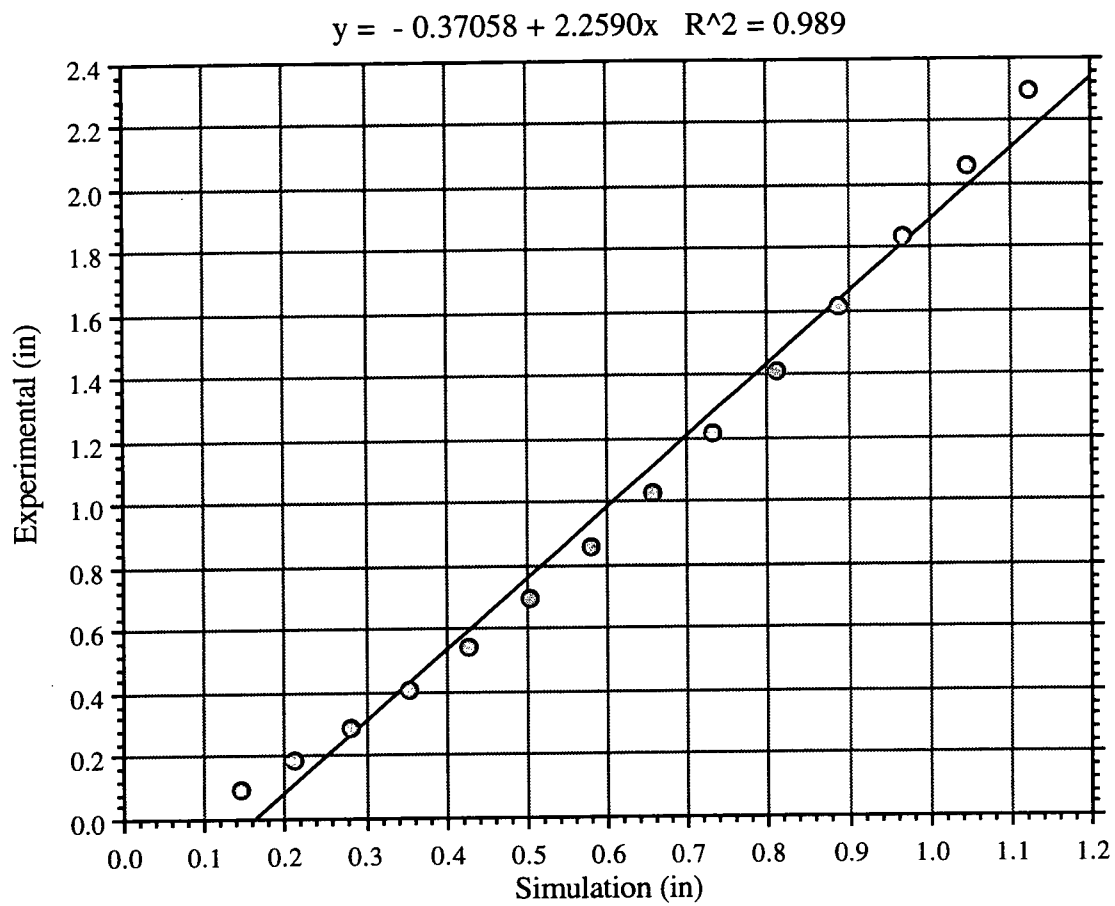


Figure 23. Experimental and simulated sinkage for a 2 in plate in an undisturbed soil when the soil parameters obtained using the inverse solution technique for a 4 in plate test was used to simulate 2 in plate behavior. Experimental results correspond to September 1992 tests.

V.5.2 EXPERIMENTAL VERIFICATION OF THE RESPONSE SURFACE METHODOLOGY.

This project was undertaken by Mr. Sime as a part of his PhD thesis project. Publication # 7 and 8 deal with this subject. A Critical state soil constitutive model known as the modified Cam clay model was considered in this study. As mentioned earlier, publication #8 is a comprehensive treatment of this subject which is included below.

DEVELOPMENT AND EVALUATION OF PARAMETER ESTIMATION TECHNIQUE USING RESPONSE SURFACE METHODOLOGY

Muluneh Sime and S. K. Upadhyaya

Department of Biological and Agricultural Engineering, University of California, Davis CA
95616 USA

Abstract:

An inverse solution technique based on response surface method for estimating three Cam Clay model parameters (λ , M , e_1) was developed. The parameter values obtained using the inverse solution technique were compared to those obtained through conventional tests for four different soil conditions. The method identified the parameters reasonably well in all four cases.

INTRODUCTION AND REVIEW OF LITERATURE

Soil-tire/track interaction of off-road vehicles is of considerable interest because of its implication on traction and soil compaction. An increase of one percentage point in the tractive efficiency leads to an annual savings of over 100 million liters of fuel in the U.S. alone [1]. Compaction changes bulk density, soil strength and pore size distribution.

Changes in these factors can adversely affect yield due to restricted root growth, seedling emergence and reduced movement of gases, water and nutrients [2]. Accurate evaluation of engineering properties of terrain plays an important role in predicting the performance of off-road vehicles. Rubinstein et al., [5] developed an inverse solution technique for determining properties of soil *in-situ* using a response surface methodology. A Drucker Prager soil constitutive model was used in their study. However, they did not provide any experimental verification. Sime and Upadhyaya [6] evaluated the performance of the inverse solution technique using a modified Cam Clay model. They found that for the type of loading they investigated the variations in the elastic parameters were not important in the load-deformation relationship.

The objectives of this study are (i) to determine engineering properties of soil based on the modified Cam Clay constitutive relations using an inverse solution or back analysis technique; (ii) to verify this back analysis technique based on data obtained by conducting triaxial tests as well as one dimensional compression tests on remolded soil. A response surface was built based on load-deformation results obtained using a one dimensional Cam Clay compaction model and an orthogonal regression technique. The main advantage of the proposed Response Surface Method (RSM) is once the response surface is created using numerical or analytical methods the subsequent estimation of deformations can be accomplished using this response surface. Here it is worth noting that, although our attention is focused on a particular soil model the response surface methodology as proposed is applicable in other fields of study as well.

Critical State Concept and Cam Clay model: The variation of soil critical state parameters with water content has been investigated by several researchers. Leeson and Campbell [7] reported that the effect of moisture content on critical state parameters based on laboratory compression test results on a loam and a sandy loam soil. As the water content and degree of saturation of a soil increased, the gradient of the virgin compression

line, expressed in terms of specific volume and log of mean effective pressure, increased and its intercept decreased. Moreover, they indicated that the position of the critical state line also varied with soil water content and that the critical state theory can be extended to unsaturated soils. One of the models based on the critical state concept that can be applied to unsaturated soils is the modified Cam Clay model and its yield surface is defined, in terms of total stress as follows:

$$f(p, q) = \left(\frac{p}{a} - 1 \right)^2 + \left(\frac{q}{Ma} \right)^2 - 1 = 0 \quad (1)$$

$$a = a_0 \exp \left((1 + e_0) \frac{1 - J^{pl}}{\lambda - \kappa J^{pl}} \right)$$

$$a_0 = \frac{1}{2} \exp \left(\frac{e_1 - e_0 - \kappa \ln p_0}{\lambda - \kappa} \right)$$

where p_0 is the initial value of the equivalent pressure, J^{pl} is the plastic part of the ratio of current to initial volume of the soil, e_0 is the initial void ratio, κ and λ are the logarithmic bulk modulus and the slope of the virgin compression line in the void ratio vs. $\ln p$ space respectively and e_1 is the intercept of the virgin consolidation line in the same space. Moreover, "a" defines the size of the yield surface, a_0 defines the position of "a" at the beginning of the analysis, M is the slope of the critical state line in the p - q plane.

Inverse Solution Technique: A mathematical model for the analysis of geotechnical system rests on the knowledge of a the system and suitable idealization of its geometrical and physical properties. When the external inputs in a system of interest are simulated the model provides the response of the system. In general, however, the model prediction will not coincide with the real geotechnical response. Cividini et al., [8] pointed out two sources of prediction inaccuracies: (i) approximations in modeling and numerical solution procedures and (ii) inadequate knowledge of some aspects of the geotechnical system, the latter source of inaccuracy generally being much more significant. As a result, there has been much emphasis on the back analysis technique, also known as system identification

methods, which, by analyzing system experimental behavior, might lead to a reduction of model uncertainties [8,9,10].

THEORETICAL DEVELOPMENT

Model Development: Consider a soil body confined in a cylinder subjected to an axial stress σ_z . An elemental free body diagram is shown in Fig. 1. Friction along the wall of the cylinder can be neglected because (i) relatively large diameter was used; (ii) oil was used as a lubricant to reduce friction. Summing forces in the z direction gives:

$$-\sigma_z dA + \left(\sigma_z + \frac{\partial \sigma_z}{\partial z} dz \right) dA = 0$$

$$\frac{\partial \sigma_z}{\partial z} = 0 \quad (2)$$

$$\sigma_z = \text{constant} \quad (3)$$

where dA is the infinitesimal area.

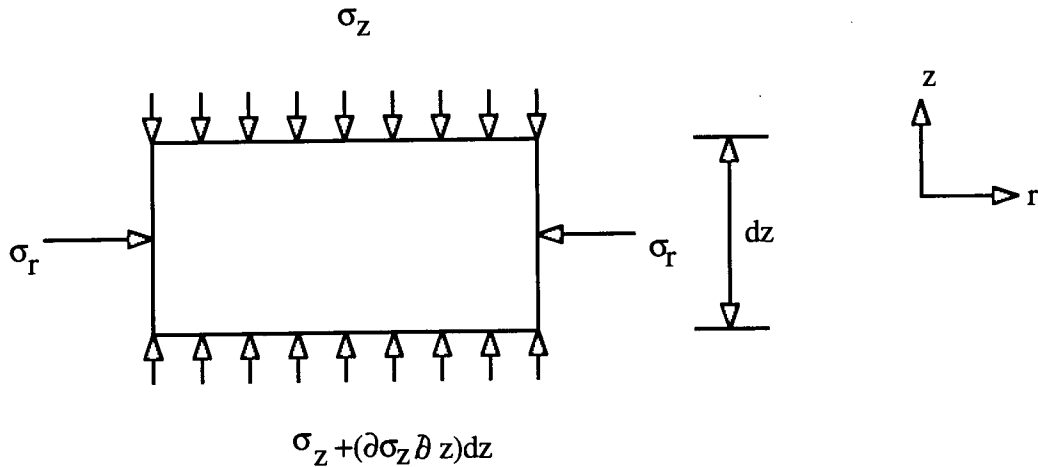


Fig. 1. Elemental analysis of the one dimensional model

Equation (2) is the equilibrium equation for the one dimensional system under consideration. If we propose that behavior of soil can be represented by a modified Cam Clay model one can show that the total strain in the axial (Z) direction may be given as

$$d\epsilon_z = \frac{1}{3K(1-2\nu)} (d\sigma_z - 2\nu d\sigma_r) + L \frac{\partial F}{\partial \sigma_z} \quad (4)$$

$$L = \frac{dp_v}{M^2(2p-p_v) \left(\frac{p_v(1+e)}{\lambda-\kappa} \right)} \quad (5)$$

where

$d\epsilon_z$ = incremental total strain in the axial direction

K = elastic bulk modulus

$d\sigma_r$ = incremental radial stress

L = hardening parameter representing the material parameters

as shown in equation (5).

dp_v = yield size increment.

F = yield function assuming associated flow rule

P_v = point at which the yield surface crosses the p axis to the right of the origin

P^\dagger = total equivalent stress

If the axial deformation in the z direction is denoted by w , we can represent $\sum d\epsilon_z = \epsilon_z$ by $\frac{dw}{dz}$. Solving for w , we can obtain give the response of the soil body (for a given set of material parameter values assumed to be known) under the applied load. Thus w is a function of assumed material and state parameter vector (\mathbf{x}) , {i.e. $w = w(\mathbf{x})$ }. The actual values of the response under the same loading conditions and similar geometry can be obtained by conducting laboratory experiments or *in-situ* tests. If w^* is a corresponding observed response to $w(\mathbf{x})$, then $e_i = [w_i^* - w_i]$ is a measure of error in the i^{th} observation. An objective function such as $\phi = \sum_i e_i^2$ (i.e. summation over all

[†]In all our discussions we will be dealing with total stress space unless specified otherwise.

observations) can be optimized using a nonlinear optimization technique ([9,11]. The objective function, ϕ , will be a nonlinear function of material parameter vector, \mathbf{x} . Our intention here is to develop a method to determine modified Cam Clay parameters for soil on the basis of *in-situ* tests. This will essentially calibrate the model parameters to field values. However, there is no known way to verify the method using *in-situ* soil. Therefore, remolded soil will be used to verify the methodology. Modified Cam clay parameters of the remolded soil will be determined using our inverse solution technique and conventional laboratory tests.

Response Surface Development: We refer the reader of this article to two recent papers [5,6] for a detailed description of the procedure followed in the creation of the response surface. The process can be summarized as follows:

1. Develop a response surface based on numerical or analytical solution to the governing differential equation of the system using an orthogonal regression technique.
2. Incorporate a third order correction to this surface to make the response surface as close to the
real surface as possible everywhere in the region.
3. Map the experimental results on to the response surface using a transformation technique.
4. Optimize the mapped experimental results against the response surface prediction to obtain engineering parameters.

EXPERIMENTAL TECHNIQUE

The intent of the laboratory experiments was to determine the Cam Clay parameters and evaluate the inverse solution procedure by comparing the values predicted by this method with those obtained through experiments. Two soil types, Yolo Loam and Capay Clay, were investigated in this study. The moisture levels of the soils were chosen as 5% and 10%. Once the sample was prepared vacuum triaxial compression tests and one dimensional compression tests were conducted to estimate the Cam Clay parameters. The particle density was assumed to be 2650 kg/m³.

Table 1. Description of soil conditions for the soil sample used in vacuum triaxial compression tests.

soil type	average moisture content %	average dry bulk density (kg/m ³)	average degree of saturation (%)
Moist Capay Clay	9.4	1258.5	22.6
Dry Capay Clay	5.2	1315.8	13.6
Moist Yolo loam	9.0	1193.6	17.0
Dry Yolo loam	4.3	1188.8	9.2

Determination of Cam Clay Parameters

Parameter M: To estimate the values of the slope of the critical state line, M and the intercept of the normal consolidation line, e_1 , in $e \log p$ space, a vacuum triaxial test was conducted on the soil samples. The values of total mean stress, p and the deviatoric stress, q at ultimate (failure) conditions at five different confining stresses (6.6, 10.0, 13.4, 16.8, 20.2 kPa) were determined. Also, to determine the void ratio at failure the diameter of the

loaded specimen was measured at five locations along the height of the specimen at failure. These diameters were then averaged to estimate the lateral strain in the specimen. With the knowledge of the axial strain (i.e. axial strain at the end of the test), the volumetric strain was estimated from which the void ratio at failure was calculated. When no confining stress was applied to the specimen the strength of the soil was found to be zero or very close to zero. The deviatoric shear stress, q , which is the same as the applied load for this case was plotted against axial strain/deformation and curve fitted through a polynomial regression to describe the behavior of the soil under this loading condition. The peak values of q associated with each level of confining stress were then picked from the fitted data and the corresponding value of total mean stress, p were calculated as shown in equation (11).

$$p_f = \frac{q_f + 3\sigma_3}{3} \quad (11)$$

where p_f is mean total stress at failure and q_f is the peak deviatoric stress at failure. q_f and p_f were then curve fitted using a simple linear regression analysis. The slope of this fitted line is assumed to be the value for M , the slope of the critical state line in p vs. q plane. Since vacuum triaxial tests were recommended for fine, very dry soils (sand) it was necessary to investigate the effect of applying vacuum on the moisture content of the specimen. This was accomplished by measuring the moisture content of the soil before and immediately after each test. It was found that for the levels of vacuum applied and the moisture levels under consideration the change in moisture content was insignificant. The loading rate of the specimen was maintained at 0.508 mm per minute (0.02 in per minute).

Parameter ϵ_1 : In modified Cam Clay model if mean effective pressure, p'_f , at failure is known, the fixed ratio of p'_v to p'_f can be used to determine the size of the yield surface. As described earlier the void ratio at failure can be determined by measuring the changes in the dimensions of the specimen at the end of the test. The following relations can be used to calculate the intercept in e - $\ln p'$ space (Fig. 2).

$$e_f = e_1 - \lambda \ln p'_v + \kappa \ln \left(\frac{p'_v}{p'_f} \right)$$

Replacing the mean effective stress by their respective total mean stress and solving for e_1

we get

$$e_1 = e_f + \lambda \ln p_v + \kappa \ln \left(\frac{p_v}{p_f} \right) \quad (12)$$

CSL = critical state line

e_1 = void ratio -intercept in e - $\ln p'$ space

e_f = void ratio at failure

p'_f = effective stress at failure

p'_v = size of yield surface (hydrostatic pressure) when failure occurred, computed using equation (3).

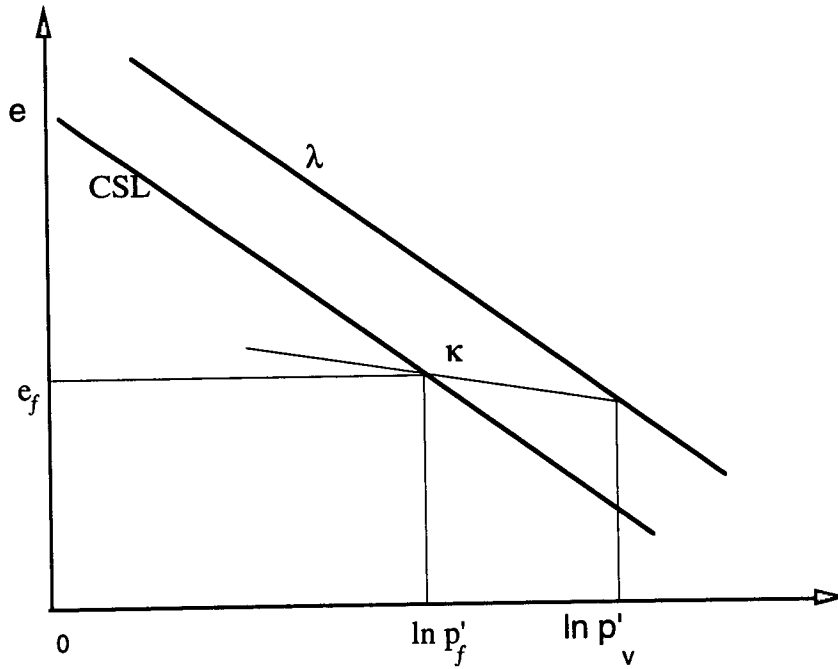


Fig. 2. e - $\ln p'$ plot

Parameter λ : One dimensional (1-D) compression tests were conducted to determine the slope of NCL. A remolded soil with known moisture content and density was prepared

in a cylinder of 190.5 mm (7.5 inches) diameter and 198.4 mm (~8.0 inches) height. The soil was subjected to compressive loading with a circular plate of ~7.5 inches diameter (clearance provided). The applied loads and the responses were recorded using a digital data recorder. The loading rate was always maintained below 1829 mm (72 inches) per minute. This is based on the recommendation of the American Society of Agricultural Engineers (ASAE) standards for cone index determination. Three replicates of one dimensional compression tests were conducted on Yolo Loam and Capay Clay soils at two levels of moisture contents as described earlier. Later it was found that the tests conducted were well reproducible. Hence, we decided to use two of the three replicates to establish a load deformation relationship via polynomial curve fitting for use in the optimization process. The equations obtained were used to estimate the mean response to applied pressure which was used in the optimization process to estimate the soil parameters. The other remaining observation was used for the estimation of the slope of the NCL (λ) by plotting the void ratio against the log of the total axial stress. The experimental results are listed in Table 2.

Table 2. Experimentally obtained parameter values

soil	λ	M	OCR	e_1	e_0
Moist Capay Clay	0.077	2.50	6.44	1.431	1.092
Dry Capay Clay	0.037	2.47	2.90	1.268	1.135
Moist Yolo loam	0.15	2.14	4.56	1.748	1.135
Dry Yolo loam	0.11	2.36	6.35	1.659	1.175

Inverse Solution: In order to estimate the three soil parameters (λ , M , e_1), sixteen different response surfaces were created using sixteen different pressure levels starting from 200 kPa upto 650 kPa with an increment of 30 kPa. A response surface was built for each pressure level in the parameter space shown in Table 3. The over consolidation ratio (OCR) was used as a substitute for e_1 for the creation of the response surface. The difficulty associated with the use of e_1 is that its value is affected by a change in any one of the other parameters for a given initial yield surface. Therefore e_1 is calculated after an acceptable OCR is obtained as a solution using the following expression.

$$e_1 = e_0 + \lambda \ln p_0 + (\lambda - \kappa) \ln(\text{OCR}) \quad (13)$$

where p_0 is the initial total volumetric stress.

Table. 3. Parameter ranges used in the creating response surfaces.

	λ	M	OCR	e_0
minimum	0.02	1.0	1.0	0.6
maximum	0.16	4.0	11.0	1.6
mid point	0.09	2.50	6.0	1.1

Each range was divided into eleven equally spaced values. Each parameter was normalized to the same range $[-1,1]$. We recall that during the response surface creation all but one parameters were held constant at the mid point values of their respective ranges.

Fig. 3 shows a typical plot of the response surface and real surface at a given load. All such plots for the sixteen load levels have shown extremely good fit between the real surface and the response surface. These results imply that the response surface can be used to estimate real surface with a very high degree of accuracy. The sets of points shown in Table 4 hereafter referred to as "set #i" were randomly selected to study the robustness of this methodology. The deformation obtained using these values are treated as "check

values" to see if the response surface methodology described could predict the same parameter set back. The objective of parameter identification procedure was to choose a set of parameter values in an admissible parameter set such that the solution corresponding to the chosen set of parameter values agrees with the measured value. We used the preselected four parameter sets to be able to compute the actual sum of square of error and SSE (Tables 5(a) and (b)). However, since in a real situation the true solution is not known apriori, our decision would be based solely on the minimum sum of squares of the residuals. Several reasonable solutions result in the same amount of deformation. We shall consider set #1 as an example. There are six reasonable solutions with initial guesses different from the "exact" set of parameters in set #1 (Table 5 (a)). Among the six sets of the reasonable solutions, solutions #3 appears to be the "best". (i.e. low percent error and hence low SSE). Nevertheless, the SSR associated with this particular solution set is not the least among the six reasonable solutions in set #1. Since in a general situation we have no knowledge of the SSE one is opt to pick solution #1 as the "best" since it has the minimum SSR.

The parameter values obtained from the optimization were used in a one dimensional modified Cam Clay model, (i.e. model used to create the original response surfaces) to evaluate the deformations that occur for the various possible solutions. All the possible solutions for a given set of parameters shown in Table 4 have resulted in the same amount of compression. Fig. 4 shows the plots of predicted compression using the reasonable parameter sets associated with set #1 (Table 5(a)) versus the compression obtained using the exact value of set #1 in Table 4. Thus, there exist several set of parameter combinations that result in the same amount of deformation for different soil conditions. For strictly sinkage oriented studies, therefore, the error introduced by picking one of the possible solutions as the "best" solution may not affect the resulting compression under a uniaxial load. Table 5 shows that the lowest sum of squares of the residual (SSR) does not necessarily correspond to the lowest SSE. This is because there is a slight

deviation between the real surface and the response surface as illustrated in Fig. 3. However, the best solution selected based on the lowest SSR was close to the solution with the minimum SSE.

Table 4. Randomly selected parameter values for the robustness of the methodology.

λ	M	OCR	e_0	
0.07972	2.92843	2.99079	0.75734	set #1
0.13824	1.43470	2.96097	0.81446	set #2
0.08937	3.8194	2.7284	1.57683	set #3
0.10434	1.32790	3.95823	0.77411	set #4

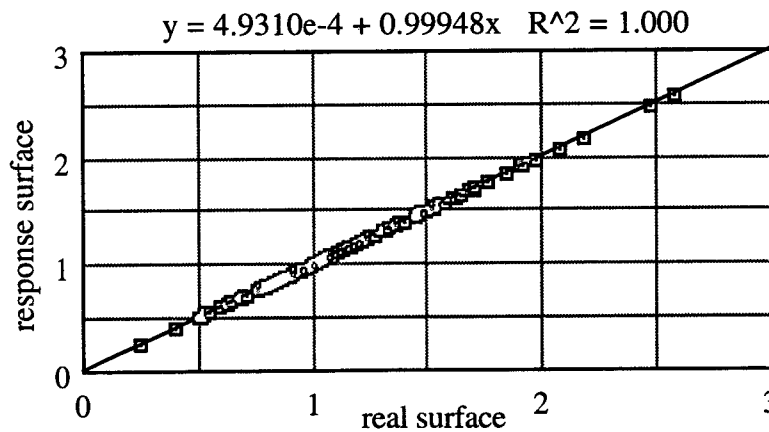


Fig. 3. Response surface vs. real surface for axial load of 410 kPa

The parameter values listed in Table 2 were used in the 1-D model to estimate the deformation. This model deformation mapped with the experimental deformation was used during optimization to evaluate how well the inverse solution technique can predict the experimental parameter values. Table 5(b) shows the percent error associated with

admissible solutions obtained during this process. Except in the case of moist Yolo loam soil, which has a relatively higher percent error, the other three soil conditions have given a "unique" solution with significantly low percent error. It is also worth noting the closeness of the order of magnitudes of associated SSR.

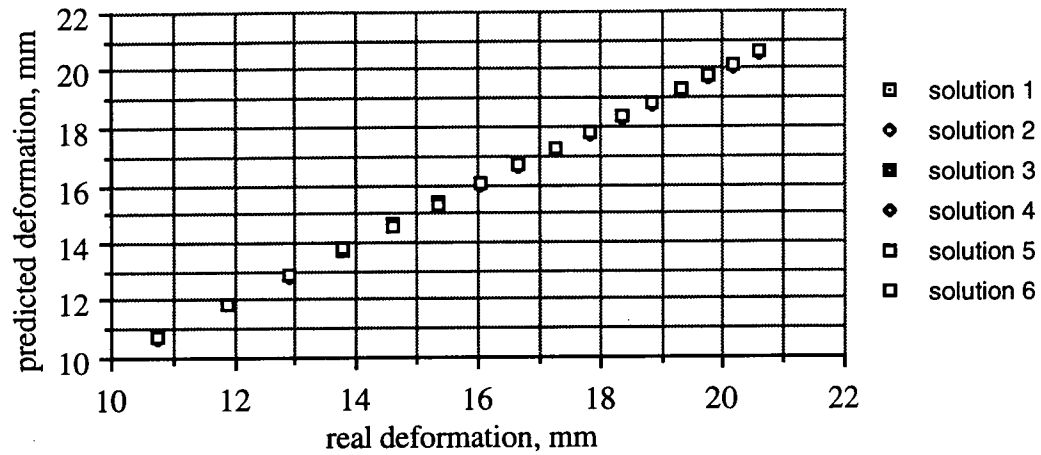


Fig. 4. Predicted deformation using reasonable solution vs. deformation obtained using parameter set #1

CONCLUSIONS

On the basis of this study we reached the following conclusions:

1. The proposed response surface method and inverse solution technique was used to predict the Cam Clay parameters reasonably well.
2. The Cam Clay parameters for two soils at two different moisture contents were determined by conducting vacuum triaxial and one dimensional compression tests.
3. For sinkage oriented studies where plastic deformation is predominant the Cam Clay parameters λ , M , and e_1 play a major role in controlling deformation. Elastic parameters have very small or negligible effect.

Table 5a . Percent errors, SSE and SSR associated with reasonable solutions to estimate the preselected set of points (set #1).

Set #	Reasonable solution #	% error λ	% error M	% error OCR	SSE	SSR
1	1	0.17	7.15	5.09	0.0077076	0.0000175
	2	0.43	57.93	41.12	0.504757	0.0000448
	3	0.11	1.04	0.00	0.0001103	0.0000545
	4	0.23	10.65	6.12	0.0150950	0.0000883
	5	0.19	18.33	11.14	0.0459988	0.0000968
	6-mid point ig.	0.12	2.45	0.85	0.0006747	0.0000607
	7-exact ig	0.09	0.05	0.62	0.0000389	0.0000499

Table 5b. Percent errors, SSE and SSR associated with reasonable solutions to estimate experimental values.

Soil	Reasonable solution #	% λ	% M	% OCR	SSE	SSR
Moist clay	1(5)*	3.57	5.89	1.32	0.0049128	0.0007929
	2-exact ig	3.57	5.89	1.32	0.0049128	0.0007929
Dry Capay Clay	1	1.12	13.47	4.85	0.0206106	0.0000942
	2	1.00	11.59	3.80	0.0149773	0.0000950
	3	0.90	10.92	3.24	0.0130588	0.0000956
	4	0.91	10.28	3.00	0.0115521	0.0000959
	5	1.25	2.19	0.43	0.0006535	0.0001003
	6	1.46	5.97	4.42	0.0057380	0.0001193
	7-exact ig	1.24	0.15	1.55	0.0003971	0.0001044
Moist Yolo Loam	1	10.13	15.56	21.87	0.0823113	0.0831645
	2	10.42	15.47	22.35	0.0847488	0.0831824
	3	10.15	20.36	23.32	0.1061630	0.0832123
	4	10.06	21.17	23.49	0.1101030	0.0832171
	5	10.39	11.65	20.65	0.0681899	0.0832592
	6	10.07	16.35	21.91	0.0848697	0.0832741
	7-exact ig	10.48	17.72	23.11	0.0957901	0.0832197
Dry Yolo Loam	1 (4)	4.37	6.07	3.24	0.0066500	0.0012020
	2-exact ig	4.38	6.39	3.38	0.0071444	0.0012019

ig = initial guess

* = number of solutions with the similar results

REFERENCES

1. Gill W. R., and G. E. Vanderberg (1968). Soil dynamics in tillage and traction. Agriculture handbook NO. 316, U. S. Gvt. printing office, Washington, D. C. 511p.
2. Chancellor W. J. (1977). Compaction of soil by agricultural equipment. Division of agricultural sciences, University of California. Bulletin 1881.
3. Musick J. T., F. B. Pringle, P. N. Johnson, (1985). Furrow compaction for controlling excessive irrigation water intake. Trans. of the ASAE vol. 28(2), pp. 502-506.
4. Fornstrom K. J., J. A. Michel, Jr., J. Borelli, G. D. Jackson, (1985). Furrow firming for control of irrigation advance rates. Trans. of the ASAE, Vol. 28(2) pp. 529-531.
5. Rubinstein D., S. K. Upadhyaya, M. Sime (1994). Determination of in-situ engineering properties of soil using response surface methodology. Journal of Terramechanics, vol. 31, No. 2. Elsevier Science Ltd. pp.
6. Sime M. and S. K. Upadhyaya. Experimental verification of an inverse solution technique developed for parameter estimation. Presented at the 1994 ASAE Winter meeting, Paper No. 94-1565. ASAE, 2950 Niles Rd., St. Joseph, MI 49085-9659 USA
7. Leeson J. J., and D. J. Campbell (1983). The variation of soil critical state parameters with water content and its relevance to the compaction of two agricultural soils. Journal of Soil Science. Blackwell Scientific Publications. Oxford. vol. 34. No. 1 pp. 33-44.
8. Cividini A., G. Maier, A. Nappi (1983). Parameter Estimation of a static geotechnical model using a Bayes' approach. Int. journal of rock mechanics, mining science and geomechanical abstracts. vol. 20. No. 5, pp 215-226.
9. Sakurai s. and K. Takeuchi (1983). Back analysis of measured Displacements of tunnels. Rock mechanics and Rock Engineering 16, pp. 173-180
10. Gioda G., A. Pandolfi, A. Cividini (1988) Comparative evaluation of some back analysis algorithms and their application to in situ load tests (2nd international symposium on field measurements in geomechanics, Sakurai (ed.) Balkema, Rotterdam
11. Gioda G. (1985). Some remarks on back analysis and characterization problems in geomechanics. Fifth Int. Conf. in Geomechanics, Nagya, pp. 47-61.
12. Arai K., H. Ohita and T. Yasui (1983). Simple optimization techniques for evaluating deformation moduli from field observations. Soils Foundations **23** (1) 107-113.

V.5.3 MEASUREMENT OF SOIL PARAMETERS RELEVANT TO TRACTION AND TRACTION TESTS:

These tests were originally planned as tasks to be performed during the first year of study but later postponed to the second year because of the enormous effort that was necessary to address the estimation of soil parameters in-situ using the response surface methodology. Extensive field tests were conducted using four different radial ply tires, in two different soil types and four soil conditions in each soil type. Within each soil condition, each tire was tested using three axle loads and three inflation pressures. Soil parameters such as sinkage constant and exponent, soil cohesion, internal angle of friction, shear modulus, soil cone index, bulk density, and moisture content were obtained. Semi-empirical traction prediction equation based on traction mechanics, dimensional analysis, and conservation of energy principle were developed using the procedure outlined by Upadhyaya and Wulfsohn (1993).

DEVELOPMENT OF SEMI-EMPIRICAL TRACTION PREDICTION EQUATIONS BASED ON EXTENSIVE FIELD TESTS AND RELEVANT SOIL PARAMETERS:

S. K. Upadhyaya
Professor

M. Sime
Graduate
Assistant

N. Raghuwanshi
Graduate
Assistant

B. Adler
Undergraduate
Assistant

Biological and Agricultural Engineering Department, Univ. Cal., Davis, CA 95616

Introduction and Review of Literature:

Upadhyaya and Wulfsohn (1989) conducted extensive field tests using the UC Davis single wheel tire tester (3 tires x 2 soils x 5 soil conditions x 3 axle loads x 2 inflation pressures). Using a nonlinear regression technique, they found that the traction test results always

fitted equations of the following type with very high coefficients of multiple determination (R^2):

$$\begin{aligned}\mu_{nt} &= NT / W = a(1 - e^{-cS}) \\ \mu_{gt} &= T / (rW) = a'(1 - be^{c'S})\end{aligned}\quad (1)$$

where a , c , a' , b , and c' are soil, tire, and loading (inflation pressure and axle load) related empirical coefficients. They found that c was approximately equal to c' in all cases. They used traction mechanics, conservation of energy principle, and dimensional analysis to relate these empirical coefficients to soil, tire, and loading parameters. They had limited success in relating these coefficients to soil parameters when only soil cone index and moisture content values were used to represent soil type and conditions. They obtained the following empirical equations:

$$\begin{aligned}a &= 0.311 + 0.067 (b/l) + 0.001 (C_i/p) + 1.089 (\theta) - 0.933 (C_i/p) (W/C_i b l)^2 \\ 1/c &= -5.376 - 0.764 (aW/l) + 4.923 (b/l) - 211.152 \{W/(C_i b l)\} (\theta) \\ &\quad + 101 (a/l) \{W/(C_i b l)\} + 32.646 (\theta) + 30.913 a \\ a' &= 0.245 + 0.411 (\theta) + 0.474 a + 0.251(a/l) - 0.001 a (aW/l)^2 \\ b &= 0.2993 + 0.5343 (a/a') + 0.1336 \{a/(a'l)\} - 0.0002 (a/a')(aW/l)^2\end{aligned}\quad (2)$$

where l = contact length, m
 p = inflation pressure, kPa
 θ = moisture content in dry basis, fraction

All quantities in equation (2) are expressed in SI units (i.e. length units are in m, forces are in kN, pressures are in kPa). The coefficients of multiple determination for parameters a , c , a' , and b are respectively 0.61, 0.73, 0.71, and 0.76.

Realizing the inadequacy of using only soil cone index values to represent soil characteristics (as in equation 1 above), Upadhyaya et al. (1993) developed an instrumented soil test device to measure soil sinkage (sinkage constant, k , and exponent, n), and shear (cohesion, C , internal angle of friction, ϕ , and shear modulus, K) parameters. Using these soil parameters, traction mechanics, and conservation of energy principle, Upadhyaya and Wulfsohn (1993) developed empirical equations to predict traction parameters a , c , a' , and b . In deriving the theoretical basis for these equations they assumed the soil-tire contact area to be elliptical in a 2-D space. These prediction equations are of the following form* :

$$a = 6.675 + 0.952 A_c \tau_{\max} - 19.208 \tau_{\max} K l_w$$

$$1/c = -4.682 + 413.067 [a (\bar{p} / \tau_{\max})(K/l_c)] + 41.377 [aW/(K_t l_c)] \quad (3)$$

$$a' W = 8.527 - 15.793 (aWK/l_c) + 10.943 [(aW)^2/(K_t l_c)]$$

$$a'(1-b) = 0.921 - 13.269 x_1 + 4.681 x_2 + 48.846 x_1^2 - 19.878 x_2^2 \\ - 23.078 x_1 x_2$$

where

$$A_c = \text{2-D contact area, m}^2$$

$$\tau_{\max} = C + \bar{p} \tan (\phi), \text{ kPa}$$

* Unfortunately the equations for a' and b' contained a typographical error in the article published in the J. Terramechanics.

l_w = contact width, m

K = shear modulus, m

K_t = tire stiffness in the tangential direction, kN/m

\bar{p} = average contact pressure, W/A_c , kPa

l_c = contact length, m

$x_1 = \delta_t / l_c$

$x_2 = [\delta_s / (n + 1)] / l_c$

d_s = soil deformation, m

d_t = tire deformation in the vertical direction, m

The coefficients of multiple determination for a , c , a' , and b were respectively 0.82, 0.79, 0.92, and 0.84. However, these equations were based on limited tests. Only one tire (18.4R38 tire) was tested in a tilled and untilled Yolo loam soil. Two levels of inflation pressure (83 and 124 kPa) and three levels of vertical load (15, 21, and 27 kN) were included in this study. *The objective of this study was to extend this methodology to several tires and soil type and conditions in order to obtain more general semi-empirical prediction equations.*

Experimental Techniques:

During the summer of 1993 extensive field tests were conducted using the UCD single wheel tester. Four radial ply tires** [13.6R28, 16.9R38, 18.4R38, and 24.5R32] were used in this study. The tests were conducted in a Capay clay and a Yolo loam soil on the UCD campus. In each of these two soils four soil conditions were created. A 240 m x 240 m plot was marked off in each field. This plot was divided into two subplots, one of which was irrigated and the other was left dry. Both the irrigated (wet) and dry subplots were further subdivided into two sub-subplots. One each of these sub-subplots was tilled

** We are grateful to the Goodyear Tire and Rubber Co., Akron, Ohio for providing these tires.

and the other was left undisturbed. Each tire was tested in each of these soil conditions at three levels of vertical loads (approximately 26, 20, and 14 kN) and three levels of inflation pressures (64, 85, and 106 kPa). This test plan resulted in 288 traction tests. Each traction test consisted of eight to ten runs using the UCD single wheel tester. During each run the traction tester was parked in a given location and both the vertical load and slip were selected according to the test plan. The tire moved from the rear of the tester to the front during a given run. A data logger was used to record vertical load on the axle, draft load generated, input torque, wheel speed, and true forward speed. In a given test, the first run usually corresponded to the zero slip run (Note that this may not be the true no slip run. Our data analysis determined the true no-load radius and zero slip conditions as described by Upadhyaya et al., 1988). Subsequent runs were conducted at increasingly higher level of slip until the tire begins to slip excessively. The complete test plan consists of over 2500 traction runs! Each run was conducted on a new strip of land. Moreover, in each of these soil condition plate sinkage tests, grouser shear tests, cone penetrometer tests were conducted to obtain soil parameters related to traction. Furthermore, soil density and moisture content data were obtained to quantify soil conditions.

In each sub-sub-plots eight replicates each of plate sinkage tests were conducted with a 100 mm and a 50 mm plate using our in-situ soil test device. Moreover, three replicates each of grouser tests were conducted at two different vertical loads. Furthermore, eight replicates of cone index values were obtained in each of these sub-sub plots. In addition, six replicates of soil moisture content and bulk density data were obtained in each sub-sub-plot at two different depths (37.5 mm and 112.5 mm from the surface) using core samples.

Results and Discussion:

Measurement of soil properties: Figure 1 is a typical plot of pressure versus plate sinkage. This particular test was conducted in a tilled, wet Capay clay soil using a 100 mm

plate. All eight replicates are plotted on the same graph. There is considerable variability between replicates. Each replicate was analyzed using Reece's sinkage formula as follows:

$$p = k_r (z/b)^n \quad (4)$$

where
 p = pressure
 k_r = Reece's sinkage constant
 z = sinkage
 b = minimum plate width.

Note Reece's approach makes the units of k_r same as that of applied pressure, p . This analysis gave us 32 values of k_r and n in each soil conditions (eight replicates and four subplots in each subplot which was subjected to similar soil treatment). Since equation (4) is linear in a log-log plane[i.e. $\log(p) = \log(k_r) + n \log(z/b)$], a geometrical mean of k_r was evaluated using these 32 values and used in the later analysis. Values of k_r obtained using 50 mm and 100 mm plates were used to scale up the values of k_r to actual tire conditions assuming the following relationship between k_r and plate width (Upadhyaya and Wulfsohn, 1993):

$$k_r = k_1 + k_2 b \quad (5)$$

If k_2 was less than zero it was ignored. This happened only in one soil condition (untilled, wet Yolo loam) where k_r large and highly variable. In this particular situation, it was a small negative value but was treated as zero in our analysis. Simple arithmetic mean of the sinkage exponent, n was evaluated since that is the representative value for this parameter. Mean values as well as standard deviations of sinkage constants for all eight soil conditions and both plates are presented in Table 1.

Figure 2 is a typical plot of grouser test results. This particular test was conducted in a Tilled, wet, Capay clay soil using a vertical load of about 60 kPa. The plot contains three replicates each of vertical load, shear stress, and slip sinkage as a function of shear deformation. Each shear stress curve was analyzed using the following equation:

$$\tau = \tau_{\max} (1 - e^{-j/K}) \quad (6)$$

A nonlinear regression routine was used to obtain maximum shear stress, τ_{\max} and shear modulus, K for each replicate. In each sub-sub-plot, grouser shear tests were conducted at two different vertical loads. In a given subplot, there were 12 shear tests (four sub-sub-plots x three replicates in each sub-sub-plot) at high vertical load and 12 at low vertical load. Harmonic mean of the 24 values of the shear modulus, K was evaluated to obtain a representative value for this parameter because of the nature of equation (6). The 24 values of τ_{\max} , 12 at low vertical load and 12 at high vertical load, were analyzed using the following equation to obtain soil cohesion and internal angle of friction:

$$\tau_{\max} = C + p \tan (\phi) \quad (7)$$

Values of cohesion, internal angle of friction, and shear modulus along with its standard deviation are listed in Table 1.

Soil cone index data were analyzed to obtain average cone index values in each soil condition in the top 150 mm layer of soil. Each mean value of soil cone index is an average of 32 values (eight per sub-sub-plot x four sub-sub-plots in each sub-plot). Means and standard deviations of cone index values are also listed in Table 1. This table also contains the average moisture content and bulk density data in the top 150 mm of soil. Note that each reading is an average of 48 individual observations (six at each depth x two depth in each sub-sub-plot x four sub-sub-plot). We have also included the standard deviations of

soil bulk density and moisture content in Table 1 to provide some idea of variability in these values.

Traction tests: Figure 3 is a graph of a typical traction test. This plot corresponds to a test conducted in an untilled, wet, Capay clay soil using a 18.4R 38 tire at 62 kPa inflation pressure and 14 kN axle load. It is a plot of NT/W, T/rW, and TE as a function of slip. Using a nonlinear regression technique, NT/W and T/rW were fitted to the expression of the type shown in equation (1). The expression for TE is given by:

$$TE = \frac{\frac{NT}{W}}{\frac{T}{rW}} (1 - s) \quad (8)$$

In all 288 cases the experimental data fitted equation (1) with a very high coefficient of multiple determination. 0.90 or higher (mostly above 0.97). We have obtained similar results in our previous studies. Table 2 lists the empirical coefficients (a, c, a', and b') obtained through non linear regression for all 288 cases tested. Upadhyaya and Wulfsohn (1993) have outlined a procedure to relate these empirical coefficients to tire and soil characteristics using traction mechanics, dimensional analysis, and principle of energy conservation. Using this procedure and utilizing multiple linear regression following expressions were obtained for the empirical coefficients.

$$aW = 1.73 + 0.572 * \tau_{\max} * A_c + 3.589 * \tau_{\max} K * l_w + 5.672 * \left(\frac{p}{K_r} \right) \quad (9)$$

$$acW = 0.881 * \left[\frac{\delta_t - \delta_s}{l_c} \right]^{0.183} \left[\frac{\delta_t}{l_c} \right]^{1.346} \left[\frac{l_w}{K} \right]^{-1.717} \left[\frac{l_c}{K} \right]^{1.743} \left[\frac{l_c l_w}{A_c} \right]^{4.198} [\tau_{\max} A_c]^{0.685} \quad (10)$$

$$a'W = 5.843 - 3.697 \left[\frac{aWK}{l_c} \right] + 11.778 \left[\frac{(aW)^2}{294.1 * l_c} \right] \quad (11)$$

$$a'b = 0.053 + 0.865 a' - 1.488 x_1 + 13.496 x_1^2 \quad (12)$$

where K_r is the Reece's sinkage constant, δ_t (m) is the total deformation (soil+tire), and δ_s (m) is the maximum soil deformation.

Figs. 4 through 7 are plots of experimental values versus predicted values for coefficient a , c , a' and b' . The coefficients of multiple determination for a , c , a' , and b were respectively 0.79, 0.71, 0.88, and 0.91. It was further found that a' and b' may be determined using following simpler equations with out sacrificing much on accuracy. i.e.

$$a' = 0.878 a + 0.187 \quad (13)$$

$$b' = 0.91 \quad (14)$$

The coefficient of determination for a' in equation 13 was 0.82.

From equations 3, 11, and 12 it is clear that equations for coefficients a' and b' are similar for the more general case compared to the one obtained earlier. Equation for coefficient " a " has an additional term which is related to soil sinkage and was found to be necessary to account for different soil types and conditions included in this study. The coefficient c was the hardest to predict and needed several terms to account for various soil types and conditions and tire sizes.

Simulation studies were conducted using 15 randomly selected test conditions. Table 3 lists the soil and tire parameters used in simulations. Table 4 lists the simulation results. Predictions are usually within 25% of the experimental values. Predicting a' using the

simple equation (14) appears to be acceptable. When coefficient c was very large, errors upto 40% were found in predicting " c ". The large values of " c " are usually found in very hard soil where tractive ability is not a concern.

Conclusions: Based on our extensive field tests which included four tires, two soil types, four soil conditions within each soil type, three levels of vertical loads, and three levels of inflation pressures (altogether 288 tests), we obtained following semi-empirical prediction equations for traction coefficients using traction mechanics, dimensional analysis, and principle of energy conservation:

$$aW = 1.73 + 0.572 * \tau_{\max} * A_c + 3.589 * \tau_{\max} K * l_w + 5.672 * \left(\frac{p}{K_r} \right) \quad (9)$$

$$acW = 0.881 * \left[\frac{\delta_t - \delta_s}{l_c} \right]^{0.183} \left[\frac{\delta_t}{l_c} \right]^{1.346} \left[\frac{l_w}{K} \right]^{-1.717} \left[\frac{l_c}{K} \right]^{1.743} \left[\frac{l_c l_w}{A_c} \right]^{4.198} [\tau_{\max} A_c]^{0.685} \quad (10)$$

$$a'W = 5.843 - 3.697 \left[\frac{aWK}{l_c} \right] + 11.778 \left[\frac{(aW)^2}{294.1 * l_c} \right] \quad (11)$$

$$a'b = 0.053 + 0.865 a' - 1.488 x_1 + 13.496 x_1^2 \quad (12)$$

The coefficients of multiple determination for a , c , a' , and b in equations (9) through (12) were respectively 0.79, 0.71, 0.88, and 0.91. Moreover, we found that simpler expressions for a' and b' can be used without sacrificing on the accuracy much. The simpler expressions for a' and b' are:

$$a' = 0.878 a + 0.187 \quad (13)$$

$$b' = 0.91$$

(14)

The coefficient of determination for a' in equation (14) was 0.82.

Once the traction parameters are determined, net traction coef., gross traction coef., and TE as a function of slip can be determined by:

$$\mu_{nt} = NT / W = a(1 - e^{-cS}) \quad (1)$$

$$\mu_{gt} = T / (rW) = a'(1 - be^{c'S})$$

and

$$TE = \left[\frac{\frac{NT}{W}}{\frac{T}{rW}} \right] (1 - s) \quad (8)$$

Acknowledgment: This research was supported by Bi-national (United States and Israel) Agricultural Research Development Agency, BARD.

References:

- Upadhyaya, S. K., W. J. Chancellor, D. Wulfsohn, and J. L. Glancey. 1988. Sources of variability in traction data. *J. Terramechanics*. 25(4): 249-272.
- Upadhyaya, S. K., D. Wulfsohn, and G. Jubbal. 1989. Traction prediction equations for radial ply tires. *J. Terramechanics*. 26(2):149-175.
- Upadhyaya, S.K. and D. Wulfsohn, 1993. Traction prediction using soil parameters obtained with an instrumented analog device. *J. Terramech*. 30(2):85-100.
- Upadhyaya, S. K., D. Wulfsohn, and J. Mehlschau. 1993. An instrumented device to obtain traction related parameters. *J. Terramech*. 30(1):1-20.

Table 1. Means and standard deviations of soil properties and parameters measured in test plots.

Soil	Condition	Statistics	Soil Density (kg/m ³)	Moisture Content (%)	Cone Index (kPa)	Shear			Sinkage		
						tan ϕ	K * (mm)	C (kPa)	50 mm Plate k **	100 mm Plate k **	n
Yolo Loam	T-DRY	Mean	1320	5.82	164.26	0.66	3.12	3.53	163.80	304.50	1.00
		Std. Dev.	60	0.95	39.84		2.69		19.60	115.70	0.20
	NT-DRY	Mean	1320	7.13	865.12	0.79	2.27	0.86	2147.40	4011.90	1.20
		Std. Dev.	60	1.19	198.15		4.17		622.40	1609.70	0.30
	T-WET	Mean	1230	8.60	122.29	0.60	2.60	11.93	113.10	177.60	1.00
		Std. Dev.	70	0.85	25.82		1.95		18.20	25.20	0.10
	NT-WET	Mean	1440	16.77	1146.80	0.71	6.62	5.22	3790.20	3029.30	0.90
		Std. Dev.	100	1.70	831.92		3.15		1936.60	1490.50	0.10
Capay Clay	T-DRY	Mean	1170	7.82	283.08	0.20	8.41	22.79	216.80	295.90	1.00
		Std. Dev.	20	1.08	136.25		4.22		39.30	7.90	0.10
	NT-DRY	Mean	1150	9.41	380.27	0.65	9.66	1.54	362.00	494.60	0.90
		Std. Dev.	30	1.14	73.07		4.71		156.20	184.60	0.04
	T-WET	Mean	1140	11.50	194.68	0.39	8.81	13.93	113.10	256.40	1.00
		Std. Dev.	30	2.04	42.37		3.25		18.70	27.30	0.20
	NT-WET	Mean	1180	16.29	347.72	0.75	16.70	2.41	493.30	679.60	0.90
		Std. Dev.	50	1.54	115.38		3.27		219.40	350.60	0.10

* K Harmonic mean, and simple standard deviation

** k Geometric mean and simple Standard Deviation

Table 2. Traction parameters estimated using a nonlinear regression technique for all 288 tests.

Soil	Tire	Condition	Inflation Pressure kPa	Axle Load KN	Draft Equation			Torque Equation		
					a	c	R ²	a'	b'	R ²
Clay	13.6R28	NT-Dry	62.05	13.33	0.551	0.152	0.98	0.678	0.920	0.99
Clay	13.6R28	NT-Dry	62.05	19.38	0.562	0.171	0.99	0.688	0.915	0.99
Clay	13.6R28	NT-Dry	62.05	25.46	0.540	0.163	0.99	0.672	0.906	0.99
Clay	13.6R28	NT-Dry	82.73	13.58	0.544	0.101	0.96	0.664	0.975	0.98
Clay	13.6R28	NT-Dry	82.73	19.43	0.560	0.140	0.99	0.668	0.963	0.99
Clay	13.6R28	NT-Dry	82.73	25.56	0.546	0.160	0.99	0.647	0.947	0.99
Clay	13.6R28	NT-Dry	103.42	13.62	0.506	0.137	0.98	0.619	0.947	0.98
Clay	13.6R28	NT-Dry	103.42	19.60	0.543	0.135	0.99	0.652	0.959	0.99
Clay	13.6R28	NT-Dry	103.42	25.57	0.537	0.161	0.99	0.643	0.956	0.99
Clay	13.6R28	T-Dry	62.05	13.39	0.458	0.160	0.98	0.601	0.878	0.98
Clay	13.6R28	T-Dry	62.05	19.34	0.512	0.135	0.96	0.627	0.891	0.96
Clay	13.6R28	T-Dry	62.05	25.39	0.452	0.180	0.99	0.590	0.884	0.99
Clay	13.6R28	T-Dry	82.73	13.34	0.440	0.138	0.98	0.600	0.876	0.98
Clay	13.6R28	T-Dry	82.73	19.46	0.462	0.168	0.98	0.603	0.875	0.98
Clay	13.6R28	T-Dry	82.73	25.57	0.473	0.155	0.98	0.618	0.882	0.98
Clay	13.6R28	T-Dry	103.42	13.51	0.435	0.117	0.98	0.590	0.900	0.98
Clay	13.6R28	T-Dry	103.42	19.38	0.470	0.141	0.98	0.600	0.904	0.98
Clay	13.6R28	T-Dry	103.42	25.82	0.477	0.128	0.99	0.599	0.912	0.98
Clay	13.6R28	T-Wet	62.05	13.63	0.519	0.134	0.99	0.643	0.892	0.99
Clay	13.6R28	T-Wet	62.05	19.39	0.557	0.105	0.97	0.662	0.891	0.97
Clay	13.6R28	T-Wet	62.05	25.36	0.512	0.160	0.99	0.635	0.884	0.99
Clay	13.6R28	T-Wet	82.73	13.60	0.505	0.123	0.98	0.652	0.880	0.98
Clay	13.6R28	T-Wet	82.73	19.37	0.548	0.129	0.98	0.672	0.886	0.98
Clay	13.6R28	T-Wet	82.73	25.50	0.529	0.134	0.98	0.640	0.874	0.98
Clay	13.6R28	T-Wet	103.42	13.50	0.485	0.111	0.98	0.651	0.858	0.98
Clay	13.6R28	T-Wet	103.42	19.54	0.517	0.122	0.98	0.660	0.858	0.98

Table 2 - Continued

Soil	Tire	Condition	Inflation Pressure kPa	Axle Load KN	Draft Equation			Torque Equation		
					a	c	R ²	a'	b'	R ²
Clay	13.6R28	T-Wet	103.42	25.47	0.535	0.141	0.99	0.663	0.895	0.99
Clay	13.6R28	NT-Wet	62.05	13.48	0.640	0.097	0.98	0.792	0.901	0.98
Clay	13.6R28	NT-Wet	62.05	19.32	0.695	0.100	0.97	0.819	0.902	0.97
Clay	13.6R28	NT-Wet	62.05	25.50	0.554	0.141	0.98	0.684	0.891	0.99
Clay	13.6R28	NT-Wet	82.73	13.60	0.612	0.098	0.98	0.731	0.960	0.99
Clay	13.6R28	NT-Wet	82.73	19.17	0.632	0.103	0.99	0.724	0.937	0.99
Clay	13.6R28	NT-Wet	82.73	25.11	0.586	0.136	0.99	0.665	0.936	0.99
Clay	13.6R28	NT-Wet	103.42	13.33	0.649	0.067	0.98	0.777	0.920	0.99
Clay	13.6R28	NT-Wet	103.42	19.40	0.653	0.080	0.99	0.762	0.917	0.99
Clay	13.6R28	NT-Wet	103.42	25.68	0.581	0.120	0.99	0.698	0.916	0.99
Clay	16.9R38	NT-Wet	62.05	14.48	0.646	0.092	0.98	0.748	0.938	0.99
Clay	16.9R38	NT-Wet	62.05	20.35	0.631	0.122	0.99	0.733	0.941	0.99
Clay	16.9R38	NT-Wet	62.05	26.59	0.601	0.147	0.99	0.702	0.925	0.99
Clay	16.9R38	NT-Wet	82.73	14.60	0.592	0.134	0.99	0.710	0.928	0.99
Clay	16.9R38	NT-Wet	82.73	20.29	0.631	0.111	0.99	0.724	0.937	0.99
Clay	16.9R38	NT-Wet	82.73	26.39	0.588	0.161	0.98	0.675	0.939	0.98
Clay	16.9R38	NT-Wet	103.42	14.42	0.615	0.090	0.99	0.727	0.951	0.99
Clay	16.9R38	NT-Wet	103.42	20.29	0.617	0.106	0.99	0.730	0.938	0.99
Clay	16.9R38	NT-Wet	103.42	26.65	0.603	0.109	0.99	0.708	0.930	0.99
Clay	16.9R38	T-Wet	62.05	14.38	0.557	0.103	0.97	0.657	0.886	0.97
Clay	16.9R38	T-Wet	62.05	20.31	0.573	0.114	0.96	0.666	0.904	0.96
Clay	16.9R38	T-Wet	62.05	26.57	0.532	0.197	0.99	0.626	0.897	0.99
Clay	16.9R38	T-Wet	82.73	14.56	0.511	0.135	0.99	0.658	0.826	0.99
Clay	16.9R38	T-Wet	82.73	20.40	0.531	0.144	0.99	0.656	0.848	0.99
Clay	16.9R38	T-Wet	82.73	26.55	0.650	0.060	0.86	0.744	0.893	0.87
Clay	16.9R38	T-Wet	103.42	14.64	0.498	0.118	0.98	0.637	0.878	0.99
Clay	16.9R38	T-Wet	103.42	20.52	0.546	0.103	0.97	0.663	0.892	0.98

Table 2 - Continued

Soil	Tire	Condition	Inflation Pressure kPa	Axle Load KN	Draft Equation			Torque Equation		
					a	c	R ²	a'	b'	R ²
Clay	16.9R38	T-Wet	103.42	26.64	0.507	0.179	0.96	0.622	0.897	0.96
Clay	16.9R38	T-Dry	62.05	14.57	0.486	0.115	0.96	0.628	0.868	0.96
Clay	16.9R38	T-Dry	62.05	20.56	0.519	0.149	0.96	0.653	0.900	0.97
Clay	16.9R38	T-Dry	62.05	26.99	0.522	0.210	0.98	0.632	0.886	0.98
Clay	16.9R38	T-Dry	82.73	14.62	0.485	0.085	0.97	0.570	0.907	0.97
Clay	16.9R38	T-Dry	82.73	20.70	0.457	0.151	0.98	0.553	0.923	0.98
Clay	16.9R38	T-Dry	82.73	26.69	0.508	0.189	0.98	0.577	0.924	0.98
Clay	16.9R38	T-Dry	103.42	14.71	0.450	0.098	0.98	0.558	0.894	0.98
Clay	16.9R38	T-Dry	103.42	20.64	0.492	0.111	0.97	0.586	0.914	0.97
Clay	16.9R38	T-Dry	103.42	26.60	0.526	0.106	0.96	0.607	0.925	0.97
Clay	16.9R38	NT-Dry	62.05	14.73	0.544	0.132	0.99	0.670	0.907	0.98
Clay	16.9R38	NT-Dry	62.05	20.61	0.549	0.188	0.99	0.655	0.920	0.99
Clay	16.9R38	NT-Dry	62.05	26.75	0.534	0.196	0.99	0.632	0.920	0.99
Clay	16.9R38	NT-Dry	82.73	14.71	0.537	0.147	0.98	0.680	0.908	0.98
Clay	16.9R38	NT-Dry	82.73	20.42	0.549	0.138	0.99	0.672	0.916	0.99
Clay	16.9R38	NT-Dry	82.73	26.74	0.535	0.194	0.99	0.639	0.907	0.99
Clay	16.9R38	NT-Dry	103.42	14.68	0.518	0.101	0.98	0.626	0.935	0.98
Clay	16.9R38	NT-Dry	103.42	20.46	0.529	0.142	0.99	0.620	0.938	0.99
Clay	16.9R38	NT-Dry	103.42	26.59	0.520	0.197	0.99	0.587	0.943	0.99
Clay	24.5R32	NT-Wet	62.05	15.09	0.630	0.081	0.99	0.796	0.865	0.98
Clay	24.5R32	NT-Wet	62.05	20.90	0.632	0.114	0.99	0.782	0.878	0.99
Clay	24.5R32	NT-Wet	62.05	26.95	0.604	0.135	0.98	0.744	0.883	0.98
Clay	24.5R32	NT-Wet	82.73	15.02	0.545	0.110	0.99	0.709	0.886	0.98
Clay	24.5R32	NT-Wet	82.73	20.76	0.559	0.118	0.99	0.686	0.800	0.9
Clay	24.5R32	NT-Wet	82.73	27.02	0.612	0.098	0.98	0.737	0.874	0.97
Clay	24.5R32	NT-Wet	103.42	15.11	0.615	0.064	0.98	0.792	0.880	0.98
Clay	24.5R32	NT-Wet	103.42	20.91	0.568	0.102	0.99	0.710	0.888	0.99

Table 2 - Continued

Soil	Tire	Condition	Inflation Pressure kPa	Axle Load KN	Draft Equation			Torque Equation		
					a	c	R ²	a'	b'	R ²
Clay	24.5R32	NT-Wet	103.42	27.03	0.540	0.126	0.99	0.674	0.881	0.99
Clay	24.5R32	T-Wet	62.05	15.05	0.508	0.098	0.97	0.643	0.863	0.98
Clay	24.5R32	T-Wet	62.05	20.84	0.518	0.116	0.97	0.655	0.875	0.97
Clay	24.5R32	T-Wet	62.05	26.85	0.502	0.207	0.99	0.632	0.885	0.99
Clay	24.5R32	T-Wet	82.73	14.91	0.455	0.118	0.98	0.607	0.856	0.98
Clay	24.5R32	T-Wet	82.73	21.05	0.530	0.102	0.98	0.661	0.864	0.98
Clay	24.5R32	T-Wet	82.73	26.92	0.496	0.173	0.99	0.627	0.871	0.99
Clay	24.5R32	T-Wet	103.42	14.90	0.509	0.079	0.98	0.645	0.881	0.98
Clay	24.5R32	T-Wet	103.42	20.94	0.536	0.094	0.98	0.655	0.881	0.98
Clay	24.5R32	T-Wet	103.42	26.95	0.559	0.089	0.96	0.673	0.899	0.97
Clay	24.5R32	T-Dry	62.05	14.97	0.449	0.110	0.98	0.611	0.857	0.98
Clay	24.5R32	T-Dry	62.05	20.79	0.469	0.176	0.99	0.600	0.880	0.99
Clay	24.5R32	T-Dry	62.05	27.02	0.519	0.183	0.98	0.652	0.887	0.98
Clay	24.5R32	T-Dry	82.73	15.05	0.452	0.095	0.98	0.559	0.863	0.97
Clay	24.5R32	T-Dry	82.73	20.76	0.468	0.111	0.98	0.593	0.906	0.98
Clay	24.5R32	T-Dry	82.73	26.93	0.477	0.133	0.99	0.582	0.894	0.99
Clay	24.5R32	T-Dry	103.42	15.14	0.422	0.089	0.98	0.565	0.863	0.98
Clay	24.5R32	T-Dry	103.42	21.00	0.440	0.092	0.98	0.575	0.883	0.98
Clay	24.5R32	T-Dry	103.42	27.23	0.514	0.112	0.99	0.646	0.894	0.98
Clay	24.5R32	NT-Dry	62.05	15.02	0.552	0.105	0.99	0.698	0.886	0.99
Clay	24.5R32	NT-Dry	62.05	21.14	0.558	0.116	0.98	0.703	0.883	0.98
Clay	24.5R32	NT-Dry	62.05	27.25	0.529	0.220	0.99	0.662	0.887	0.99
Clay	24.5R32	NT-Dry	82.73	15.05	0.536	0.084	0.95	0.658	0.903	0.95
Clay	24.5R32	NT-Dry	82.73	21.15	0.531	0.130	0.99	0.669	0.909	0.99
Clay	24.5R32	NT-Dry	82.73	27.20	0.529	0.139	0.99	0.652	0.904	0.99
Clay	24.5R32	NT-Dry	103.42	15.28	0.511	0.090	0.98	0.650	0.876	0.99
Clay	24.5R32	NT-Dry	103.42	21.10	0.504	0.121	0.99	0.641	0.900	0.99

Table 2 - Continued

Soil	Tire	Condition	Inflation Pressure kPa	Axle Load KN	Draft Equation			Torque Equation		
					a	c	R ²	a'	b'	R ²
Clay	24.5R32	NT-Dry	103.42	27.28	0.572	0.100	0.98	0.693	0.906	0.98
Clay	18.4R38	NT-Wet	62.05	13.61	0.649	0.119	0.98	0.787	0.905	0.98
Clay	18.4R38	NT-Wet	62.05	19.79	0.613	0.183	0.99	0.744	0.899	0.99
Clay	18.4R38	NT-Wet	62.05	26.43	0.626	0.179	0.99	0.763	0.896	0.99
Clay	18.4R38	NT-Wet	82.73	13.93	0.602	0.112	0.99	0.721	0.935	0.99
Clay	18.4R38	NT-Wet	82.73	19.80	0.650	0.108	0.96	0.764	0.937	0.96
Clay	18.4R38	NT-Wet	82.73	26.01	0.582	0.171	0.99	0.698	0.928	0.99
Clay	18.4R38	NT-Wet	103.42	13.89	0.596	0.123	0.99	0.731	0.929	0.99
Clay	18.4R38	NT-Wet	103.42	19.73	0.631	0.122	0.99	0.739	0.919	0.99
Clay	18.4R38	NT-Wet	103.42	26.09	0.623	0.113	0.95	0.734	0.926	0.96
Clay	18.4R38	T-Wet	62.05	13.81	0.522	0.144	0.99	0.675	0.877	0.99
Clay	18.4R38	T-Wet	62.05	19.87	0.545	0.204	0.99	0.682	0.892	0.99
Clay	18.4R38	T-Wet	62.05	26.12	0.527	0.252	0.99	0.656	0.890	0.99
Clay	18.4R38	T-Wet	82.73	14.01	0.531	0.109	0.97	0.651	0.908	0.98
Clay	18.4R38	T-Wet	82.73	19.81	0.537	0.125	0.98	0.647	0.920	0.98
Clay	18.4R38	T-Wet	82.73	25.96	0.559	0.125	0.98	0.663	0.911	0.98
Clay	18.4R38	T-Wet	103.42	14.08	0.535	0.086	0.98	0.664	0.877	0.98
Clay	18.4R38	T-Wet	103.42	19.84	0.518	0.111	0.98	0.641	0.904	0.98
Clay	18.4R38	T-Wet	103.42	26.10	0.552	0.112	0.97	0.662	0.907	0.98
Clay	18.4R38	NT-Dry	62.05	14.16	0.550	0.158	0.99	0.714	0.885	0.99
Clay	18.4R38	NT-Dry	62.05	20.28	0.556	0.192	0.99	0.704	0.888	0.99
Clay	18.4R38	NT-Dry	62.05	26.55	0.569	0.220	0.99	0.702	0.888	0.99
Clay	18.4R38	NT-Dry	82.73	14.07	0.576	0.100	0.98	0.697	0.925	0.98
Clay	18.4R38	NT-Dry	82.73	20.10	0.537	0.140	0.99	0.658	0.921	0.99
Clay	18.4R38	NT-Dry	82.73	26.34	0.583	0.138	0.99	0.697	0.928	0.99
Clay	18.4R38	NT-Dry	103.42	14.14	0.562	0.126	0.99	0.702	0.917	0.99
Clay	18.4R38	NT-Dry	103.42	20.10	0.518	0.111	0.98	0.641	0.904	0.98

Table 2 - Continued

Soil	Tire	Condition	Inflation Pressure kPa	Axle Load KN	Draft Equation			Torque Equation		
					a	c	R ²	a'	b'	R ²
Clay	18.4R38	NT-Dry	103.42	26.54	0.559	0.158	0.99	0.670	0.915	0.99
Clay	18.4R38	T-Dry	62.05	14.32	0.475	0.111	0.97	0.632	0.846	0.97
Clay	18.4R38	T-Dry	62.05	20.19	0.491	0.150	0.98	0.628	0.868	0.98
Clay	18.4R38	T-Dry	62.05	26.51	0.543	0.156	0.96	0.679	0.882	0.96
Clay	18.4R38	T-Dry	82.73	14.28	0.456	0.160	0.99	0.626	0.863	0.98
Clay	18.4R38	T-Dry	82.73	20.39	0.499	0.126	0.98	0.644	0.860	0.99
Clay	18.4R38	T-Dry	82.73	26.33	0.515	0.151	0.97	0.649	0.889	0.97
Clay	18.4R38	T-Dry	103.42	14.32	0.479	0.087	0.97	0.638	0.861	0.97
Clay	18.4R38	T-Dry	103.42	20.28	0.495	0.111	0.98	0.624	0.876	0.98
Clay	18.4R38	T-Dry	103.42	26.39	0.514	0.129	0.98	0.633	0.896	0.98
Yolo	16.9R38	NT-Dry	62.05	14.60	0.601	0.138	0.96	0.698	0.981	0.96
Yolo	16.9R38	NT-Dry	62.05	20.81	0.557	0.238	0.99	0.650	0.961	0.99
Yolo	16.9R38	NT-Dry	62.05	27.04	0.487	0.280	0.99	0.569	0.943	0.99
Yolo	16.9R38	NT-Dry	82.73	14.70	0.514	0.176	0.99	0.621	0.949	0.98
Yolo	16.9R38	NT-Dry	82.73	20.91	0.532	0.198	0.98	0.608	0.956	0.98
Yolo	16.9R38	NT-Dry	82.73	26.72	0.445	0.293	0.98	0.499	0.957	0.98
Yolo	16.9R38	NT-Dry	103.42	14.68	0.572	0.156	0.99	0.669	0.925	0.99
Yolo	16.9R38	NT-Dry	103.42	20.58	0.506	0.212	0.99	0.585	0.943	0.99
Yolo	16.9R38	NT-Dry	103.42	26.76	0.513	0.226	0.97	0.578	0.954	0.97
Yolo	16.9R38	T-Dry	62.05	14.47	0.487	0.120	0.97	0.631	0.881	0.97
Yolo	16.9R38	T-Dry	62.05	20.22	0.543	0.132	0.98	0.663	0.901	0.98
Yolo	16.9R38	T-Dry	62.05	26.47	0.587	0.128	0.96	0.684	0.913	0.96
Yolo	16.9R38	T-Dry	82.73	14.69	0.407	0.093	0.97	0.541	0.865	0.97
Yolo	16.9R38	T-Dry	82.73	20.51	0.460	0.151	0.98	0.597	0.907	0.97
Yolo	16.9R38	T-Dry	82.73	26.68	0.467	0.191	0.97	0.586	0.914	0.97
Yolo	16.9R38	T-Dry	103.42	14.66	0.444	0.079	0.98	0.592	0.878	0.98
Yolo	16.9R38	T-Dry	103.42	20.55	0.475	0.090	0.98	0.598	0.878	0.98

Table 2 - Continued

Soil	Tire	Condition	Inflation Pressure kPa	Axle Load KN	Draft Equation			Torque Equation		
					a	c	R ²	a'	b'	R ²
Yolo	16.9R38	T-Dry	103.42	26.59	0.476	0.150	0.99	0.580	0.918	0.99
Yolo	16.9R38	T-Wet	62.05	14.47	0.536	0.080	0.97	0.687	0.869	0.98
Yolo	16.9R38	T-Wet	62.05	20.12	0.545	0.106	0.98	0.666	0.880	0.98
Yolo	16.9R38	T-Wet	62.05	26.47	0.712	0.089	0.91	0.802	0.916	0.92
Yolo	16.9R38	T-Wet	82.73	14.32	0.551	0.083	0.98	0.688	0.870	0.98
Yolo	16.9R38	T-Wet	82.73	20.24	0.559	0.109	0.97	0.676	0.886	0.97
Yolo	16.9R38	T-Wet	82.73	26.44	0.533	0.148	0.99	0.656	0.884	0.99
Yolo	16.9R38	T-Wet	103.42	14.53	0.561	0.069	0.97	0.694	0.857	0.98
Yolo	16.9R38	T-Wet	103.42	•	•	•	•	•	•	•
Yolo	16.9R38	T-Wet	103.42	26.39	0.525	0.122	0.98	0.637	0.891	0.98
Yolo	16.9R38	NT-Wet	62.05	14.49	0.607	0.148	0.98	0.722	0.929	0.98
Yolo	16.9R38	NT-Wet	62.05	20.31	0.554	0.182	0.99	0.643	0.928	0.99
Yolo	16.9R38	NT-Wet	62.05	26.53	0.560	0.178	0.99	0.637	0.925	0.98
Yolo	16.9R38	NT-Wet	82.73	14.90	0.556	0.144	0.99	0.671	0.935	0.99
Yolo	16.9R38	NT-Wet	82.73	14.78	0.536	0.170	0.98	0.624	0.947	0.98
Yolo	16.9R38	NT-Wet	82.73	26.32	0.500	0.248	0.99	0.564	0.958	0.99
Yolo	16.9R38	NT-Wet	103.42	14.58	0.584	0.109	0.98	0.686	0.937	0.98
Yolo	16.9R38	NT-Wet	103.42	20.50	0.575	0.156	0.99	0.675	0.955	0.99
Yolo	16.9R38	NT-Wet	103.42	26.77	0.500	0.196	0.98	0.586	0.947	0.98
Yolo	18.4R38	NT-Wet	62.05	15.15	0.588	0.168	0.99	0.727	0.926	0.98
Yolo	18.4R38	NT-Wet	62.05	20.82	0.511	0.281	0.88	0.624	0.928	0.87
Yolo	18.4R38	NT-Wet	62.05	26.77	0.499	0.313	0.99	0.597	0.931	0.99
Yolo	18.4R38	NT-Wet	82.73	15.01	0.553	0.159	0.98	0.685	0.932	0.97
Yolo	18.4R38	NT-Wet	82.73	20.68	0.577	0.171	0.98	0.681	0.935	0.98
Yolo	18.4R38	NT-Wet	82.73	26.86	0.502	0.303	0.98	0.592	0.931	0.98
Yolo	18.4R38	NT-Wet	103.42	14.83	0.530	0.121	0.98	0.659	0.924	0.99
Yolo	18.4R38	NT-Wet	103.42	20.57	0.577	0.137	0.99	0.674	0.931	0.99

Table 2 - Continued

Soil	Tire	Condition	Inflation Pressure kPa	Axle Load KN	Draft Equation			Torque Equation		
					a	c	R ²	a'	b'	R ²
Yolo	18.4R38	NT-Wet	103.42	27.11	0.490	0.246	0.99	0.584	0.926	0.99
Yolo	18.4R38	T-Wet	62.05	14.97	0.534	0.154	0.98	0.698	0.868	0.98
Yolo	18.4R38	T-Wet	62.05	20.92	0.540	0.217	0.99	0.668	0.871	0.99
Yolo	18.4R38	T-Wet	62.05	26.98	0.569	0.196	0.97	0.677	0.874	0.98
Yolo	18.4R38	T-Wet	82.73	14.86	0.509	0.129	0.98	0.649	0.889	0.99
Yolo	18.4R38	T-Wet	82.73	20.73	0.541	0.134	0.99	0.663	0.900	0.99
Yolo	18.4R38	T-Wet	82.73	26.79	0.512	0.174	0.99	0.630	0.907	0.99
Yolo	18.4R38	T-Wet	103.42	14.91	0.546	0.067	0.98	0.690	0.862	0.98
Yolo	18.4R38	T-Wet	103.42	20.77	0.505	0.121	0.99	0.625	0.881	0.99
Yolo	18.4R38	T-Wet	103.42	26.85	0.620	0.075	0.96	0.716	0.900	0.96
Yolo	18.4R38	T-Dry	62.05	14.94	0.511	0.095	0.96	0.628	0.906	0.97
Yolo	18.4R38	T-Dry	62.05	20.50	0.513	0.182	0.98	0.603	0.921	0.98
Yolo	18.4R38	T-Dry	62.05	26.60	0.569	0.123	0.96	0.677	0.921	0.964
Yolo	18.4R38	T-Dry	82.73	14.98	0.495	0.131	0.98	0.638	0.890	0.98
Yolo	18.4R38	T-Dry	82.73	20.79	0.510	0.193	0.99	0.624	0.900	0.99
Yolo	18.4R38	T-Dry	82.73	26.94	0.482	0.175	0.99	0.593	0.907	0.98
Yolo	18.4R38	T-Dry	103.42	15.34	0.491	0.093	0.95	0.609	0.919	0.96
Yolo	18.4R38	T-Dry	103.42	20.91	0.493	0.133	0.98	0.589	0.912	0.98
Yolo	18.4R38	T-Dry	103.42	26.95	0.503	0.174	0.99	0.590	0.915	0.99
Yolo	18.4R38	NT-Dry	62.05	14.91	0.547	0.196	0.99	0.651	0.945	0.99
Yolo	18.4R38	NT-Dry	62.05	21.17	0.540	0.266	0.98	0.656	0.944	0.98
Yolo	18.4R38	NT-Dry	62.05	26.38	0.565	0.185	0.98	0.626	0.952	0.98
Yolo	18.4R38	NT-Dry	82.73	15.67	0.563	0.155	0.97	0.659	0.951	0.97
Yolo	18.4R38	NT-Dry	82.73	20.74	0.603	0.207	0.99	0.695	0.963	0.99
Yolo	18.4R38	NT-Dry	82.73	26.86	0.489	0.276	0.99	0.578	0.955	0.99
Yolo	18.4R38	NT-Dry	103.42	15.57	0.560	0.132	0.97	0.660	0.918	0.98
Yolo	18.4R38	NT-Dry	103.42	20.58	0.952	0.099	0.76	0.588	0.754	0.64

Table 2 - Continued

Soil	Tire	Condition	Inflation Pressure kPa	Axle Load KN	Draft Equation			Torque Equation		
					a	c	R ²	a'	b'	R ²
Yolo	18.4R38	NT-Dry	103.42	27.22	0.535	0.165	0.97	0.635	0.942	0.97
Yolo	24.5R32	NT-Wet	62.05	15.99	0.590	0.150	0.98	0.691	0.944	0.98
Yolo	24.5R32	NT-Wet	62.05	21.69	0.598	0.147	0.97	0.674	0.942	0.98
Yolo	24.5R32	NT-Wet	62.05	27.47	0.516	0.196	0.99	0.590	0.947	0.99
Yolo	24.5R32	NT-Wet	82.73	15.87	0.686	0.057	0.92	0.790	0.944	0.92
Yolo	24.5R32	NT-Wet	82.73	21.67	0.605	0.148	0.98	0.704	0.936	0.98
Yolo	24.5R32	NT-Wet	82.73	27.85	0.510	0.232	0.98	0.593	0.935	0.98
Yolo	24.5R32	NT-Wet	103.42	15.86	0.517	0.114	0.96	0.633	0.907	0.97
Yolo	24.5R32	NT-Wet	103.42	21.81	0.555	0.155	0.99	0.653	0.923	0.99
Yolo	24.5R32	NT-Wet	103.42	27.93	0.530	0.159	0.98	0.620	0.927	0.98
Yolo	24.5R32	T-Wet	62.05	15.86	0.517	0.114	0.96	0.633	0.907	0.97
Yolo	24.5R32	T-Wet	62.05	21.74	0.523	0.139	0.99	0.646	0.867	0.99
Yolo	24.5R32	T-Wet	62.05	27.74	0.538	0.168	0.96	0.642	0.893	0.97
Yolo	24.5R32	T-Wet	82.73	15.76	0.518	0.082	0.97	0.644	0.934	0.95
Yolo	24.5R32	T-Wet	82.73	21.72	0.527	0.118	0.99	0.653	0.921	0.99
Yolo	24.5R32	T-Wet	82.73	27.70	0.527	0.121	0.99	0.632	0.910	0.99
Yolo	24.5R32	T-Wet	103.42	15.83	0.491	0.079	0.97	0.649	0.902	0.98
Yolo	24.5R32	T-Wet	103.42	21.85	0.555	0.079	0.98	0.701	0.883	0.98
Yolo	24.5R32	T-Wet	103.42	28.15	0.518	0.108	0.99	0.637	0.880	0.99
Yolo	24.5R32	T-Dry	62.05	15.65	0.479	0.107	0.97	0.648	0.896	0.97
Yolo	24.5R32	T-Dry	62.05	21.47	0.522	0.143	0.98	0.656	0.902	0.98
Yolo	24.5R32	T-Dry	62.05	27.86	0.499	0.130	0.97	0.628	0.867	0.98
Yolo	24.5R32	T-Dry	82.73	15.56	0.404	0.100	0.96	0.585	0.860	0.96
Yolo	24.5R32	T-Dry	82.73	21.73	0.434	0.126	0.96	0.581	0.879	0.96
Yolo	24.5R32	T-Dry	82.73	27.92	0.490	0.159	0.99	0.608	0.894	0.99
Yolo	24.5R32	T-Dry	103.42	15.51	0.474	0.062	0.96	0.642	0.905	0.97
Yolo	24.5R32	T-Dry	103.42	21.78	0.458	0.101	0.98	0.613	0.876	0.98

Table 2 - Continued

Soil	Tire	Condition	Inflation Pressure kPa	Axle Load KN	Draft Equation			Torque Equation		
					a	c	R ²	a'	b'	R ²
Yolo	24.5R32	T-Dry	103.42	27.60	0.459	0.138	0.99	0.580	0.916	0.98
Yolo	24.5R32	NT-Dry	62.05	15.56	0.508	0.154	0.98	0.657	0.944	0.98
Yolo	24.5R32	NT-Dry	62.05	21.61	0.543	0.157	0.98	0.674	0.924	0.98
Yolo	24.5R32	NT-Dry	62.05	27.80	0.508	0.228	0.99	0.612	0.921	0.99
Yolo	24.5R32	NT-Dry	82.73	15.87	0.488	0.134	0.99	0.643	0.899	0.98
Yolo	24.5R32	NT-Dry	82.73	21.74	0.548	0.156	0.99	0.670	0.920	0.99
Yolo	24.5R32	NT-Dry	82.73	27.74	0.506	0.174	0.98	0.606	0.938	0.98
Yolo	24.5R32	NT-Dry	103.42	15.72	0.476	0.130	0.98	0.652	0.915	0.97
Yolo	24.5R32	NT-Dry	103.42	21.62	0.529	0.131	0.99	0.677	0.936	0.98
Yolo	24.5R32	NT-Dry	103.42	27.94	0.507	0.188	0.99	0.619	0.937	0.99
Yolo	13.6R28	NT-Wet	62.05	13.65	0.608	0.109	0.98	0.710	0.943	0.98
Yolo	13.6R28	NT-Wet	62.05	19.41	0.631	0.122	0.98	0.736	0.939	0.99
Yolo	13.6R28	NT-Wet	62.05	25.65	0.607	0.123	0.99	0.719	0.926	0.99
Yolo	13.6R28	NT-Wet	82.73	13.76	0.627	0.085	0.99	0.748	0.955	0.99
Yolo	13.6R28	NT-Wet	82.73	19.75	0.636	0.109	0.98	0.736	0.938	0.98
Yolo	13.6R28	NT-Wet	82.73	25.76	0.568	0.187	0.99	0.659	0.944	0.99
Yolo	13.6R28	NT-Wet	103.42	13.71	0.622	0.105	0.99	0.739	0.935	0.98
Yolo	13.6R28	NT-Wet	103.42	19.61	0.618	0.110	0.98	0.717	0.951	0.98
Yolo	13.6R28	NT-Wet	103.42	25.70	0.606	0.107	0.97	0.699	0.951	0.98
Yolo	13.6R28	T-Wet	62.05	13.65	0.508	0.140	0.99	0.656	0.870	0.99
Yolo	13.6R28	T-Wet	62.05	19.54	0.515	0.149	0.99	0.650	0.870	0.98
Yolo	13.6R28	T-Wet	62.05	25.54	0.516	0.171	0.99	0.659	0.876	0.98
Yolo	13.6R28	T-Wet	82.73	13.48	0.503	0.113	0.98	0.624	0.926	0.98
Yolo	13.6R28	T-Wet	82.73	19.54	0.518	0.121	0.99	0.636	0.906	0.99
Yolo	13.6R28	T-Wet	82.73	25.69	0.508	0.131	0.99	0.620	0.899	0.99
Yolo	13.6R28	T-Wet	103.42	13.64	0.481	0.105	0.98	0.615	0.891	0.98
Yolo	13.6R28	T-Wet	103.42	19.37	0.515	0.101	0.99	0.637	0.893	0.99

Table 2 - Continued

Soil	Tire	Condition	Inflation Pressure kPa	Axle Load KN	Draft Equation			Torque Equation		
					a	c	R ²	a'	b'	R ²
Yolo	13.6R28	T-Wet	103.42	25.55	0.515	0.121	0.99	0.636	0.909	0.99
Yolo	13.6R28	T-Dry	62.05	13.31	0.473	0.159	0.97	0.632	0.903	0.97
Yolo	13.6R28	T-Dry	62.05	19.36	0.481	0.150	0.98	0.624	0.876	0.97
Yolo	13.6R28	T-Dry	62.05	25.29	0.462	0.146	0.98	0.599	0.874	0.98
Yolo	13.6R28	T-Dry	82.73	13.33	0.439	0.105	0.98	0.591	0.850	0.98
Yolo	13.6R28	T-Dry	82.73	19.30	0.473	0.129	0.98	0.622	0.890	0.98
Yolo	13.6R28	T-Dry	82.73	25.29	0.477	0.170	0.95	0.613	0.915	0.95
Yolo	13.6R28	T-Dry	103.42	13.35	0.426	0.115	0.96	0.566	0.914	0.97
Yolo	13.6R28	T-Dry	103.42	19.37	0.464	0.120	0.98	0.595	0.910	0.98
Yolo	13.6R28	T-Dry	103.42	25.42	0.469	0.138	0.98	0.582	0.911	0.98
Yolo	13.6R28	NT-Dry	62.05	13.70	0.565	0.133	0.98	0.719	0.940	0.99
Yolo	13.6R28	NT-Dry	62.05	19.50	0.574	0.148	0.99	0.720	0.916	0.99
Yolo	13.6R28	NT-Dry	62.05	25.24	0.543	0.147	0.99	0.673	0.910	0.99
Yolo	13.6R28	NT-Dry	82.73	13.80	0.537	0.131	0.99	0.702	0.926	0.99
Yolo	13.6R28	NT-Dry	82.73	19.81	0.560	0.141	0.99	0.706	0.921	0.99
Yolo	13.6R28	NT-Dry	82.73	25.57	0.572	0.162	0.99	0.691	0.925	0.99
Yolo	13.6R28	NT-Dry	103.42	13.51	0.520	0.145	0.99	0.673	0.916	0.99
Yolo	13.6R28	NT-Dry	103.42	19.43	0.555	0.141	0.99	0.696	0.931	0.98
Yolo	13.6R28	NT-Dry	103.42	25.40	0.546	0.168	0.99	0.675	0.933	0.99

Table 3. Soil and tire parameters used in the simulation study.

Number	Tire	Axle Load KN	Infl. Pres. kPa	Soil Type	Soil Cond.	Sinkage (100 mm)		Coh., C kPa	Phi degree	Shear mod mm	CI kPa	Density kg/m ³	MC %
						Const., K	Exp., n						
11	4	19.34	62.05	2	2	295.9	1	22.79	11.3	8.41	283.08	1170	7.82
25	4	13.5	103.42	2	4	256.4	1	13.93	21.3	8.81	194.68	1140	11.5
36	4	25.68	103.42	2	3	679.6	0.9	2.41	36.86	16.7	347.72	1180	16.29
94	3	15.05	82.73	2	2	295.9	1	22.79	11.3	8.41	283.08	1170	7.82
129	2	26.55	62.05	2	1	494.6	0.9	1.54	33.02	9.66	380.27	1150	9.41
135	2	26.54	103.42	2	1	494.6	0.9	1.54	33.02	9.66	380.27	1150	9.41
137	2	20.19	62.05	2	2	295.9	1	22.79	11.3	8.41	283.08	1170	7.82
154	1	14.47	62.05	1	2	304.5	1	3.53	33.42	3.12	164.26	1320	5.82
168	1	26.44	82.73	1	4	177.6	1	11.93	30.96	2.6	122.29	1230	8.6
186	2	26.86	82.73	1	3	3410	0.9	5.22	35.37	6.62	1146.8	1440	16.77
202	2	14.98	82.73	1	2	304.5	1	3.53	33.42	3.12	164.26	1320	5.82
236	3	21.47	62.05	1	2	304.5	1	3.53	33.42	3.12	164.26	1320	5.82
257	4	19.75	82.73	1	3	3410	0.9	5.22	35.37	6.62	1146.8	1440	16.77
258	4	25.76	82.73	1	3	3410	0.9	5.22	35.37	6.62	1146.8	1440	16.77
269	4	19.37	103.42	1	4	177.6	1	11.93	30.96	2.6	122.29	1230	8.6

Tire: 1 - 16.9R38, 2 - 18.4R38, 3 - 24.5R32, 4 - 13.6R28

Soil: 1 - Yolo Loam, 2 - Capay Clay

Soil Cond.: 1 - NT-Dry, 2 - T-Dry, 3 - NT-Wet, 4 - T-Wet

Table 4. Experimentally obtained traction parameters versus those determined using the semi-empirical technique developed in this study.

Number	Inflation Press, kPa	Soil Type	Tire	Soil Cond.	Axle Load, KN	a		a'			b'		c		
						Exp.	Pred.	Exp.	a'W	simple	Exp.	a'b'	simple	Exp.	Pred.
11	62.05	2	4	2	19.34	0.512	0.409	0.627	0.913	0.637	0.891	0.907	0.908	0.135	0.096
25	103.42	2	4	4	13.50	0.485	0.522	0.651	1.294	0.613	0.858	0.896	0.908	0.111	0.080
36	103.42	2	4	3	25.68	0.581	0.602	0.698	0.676	0.697	0.916	0.912	0.908	0.12	0.103
94	82.73	2	3	2	15.05	0.452	0.441	0.559	1.163	0.584	0.863	0.883	0.908	0.095	0.063
129	62.05	2	2	1	26.55	0.569	0.493	0.702	0.674	0.687	0.888	0.921	0.908	0.22	0.118
135	103.42	2	2	1	26.54	0.559	0.505	0.67	0.677	0.678	0.915	0.909	0.908	0.158	0.086
137	62.05	2	2	2	20.19	0.491	0.420	0.628	0.875	0.618	0.868	0.916	0.908	0.15	0.097
154	62.05	1	1	2	14.47	0.487	0.570	0.631	1.229	0.615	0.881	0.907	0.908	0.12	0.125
168	82.73	1	1	4	26.44	0.533	0.525	0.656	0.695	0.655	0.884	0.876	0.908	0.148	0.120
186	82.73	1	2	3	26.86	0.502	0.537	0.592	0.671	0.628	0.931	0.943	0.908	0.303	0.121
202	82.73	1	2	2	14.98	0.495	0.568	0.638	1.189	0.622	0.890	0.897	0.908	0.131	0.089
236	62.05	1	3	2	21.47	0.522	0.513	0.656	0.841	0.645	0.902	0.907	0.908	0.143	0.111
257	82.73	1	4	3	19.75	0.636	0.561	0.736	0.911	0.745	0.938	0.927	0.908	0.109	0.098
258	82.73	1	4	3	25.76	0.568	0.531	0.659	0.704	0.686	0.944	0.937	0.908	0.187	0.116
269	103.42	1	4	4	19.37	0.515	0.587	0.637	0.933	0.639	0.893	0.891	0.908	0.101	0.071

Tire: 1 - 16.9R38, 2 - 18.4R38, 3 - 24.5R32, 4 - 13.6R28

Soil: 1 - Yolo Loam, 2 - Capay Clay

Soil Cond 1 - NT-Dry, 2 - T-Dry, 3 - NT-Wet, 4 - T-Wet

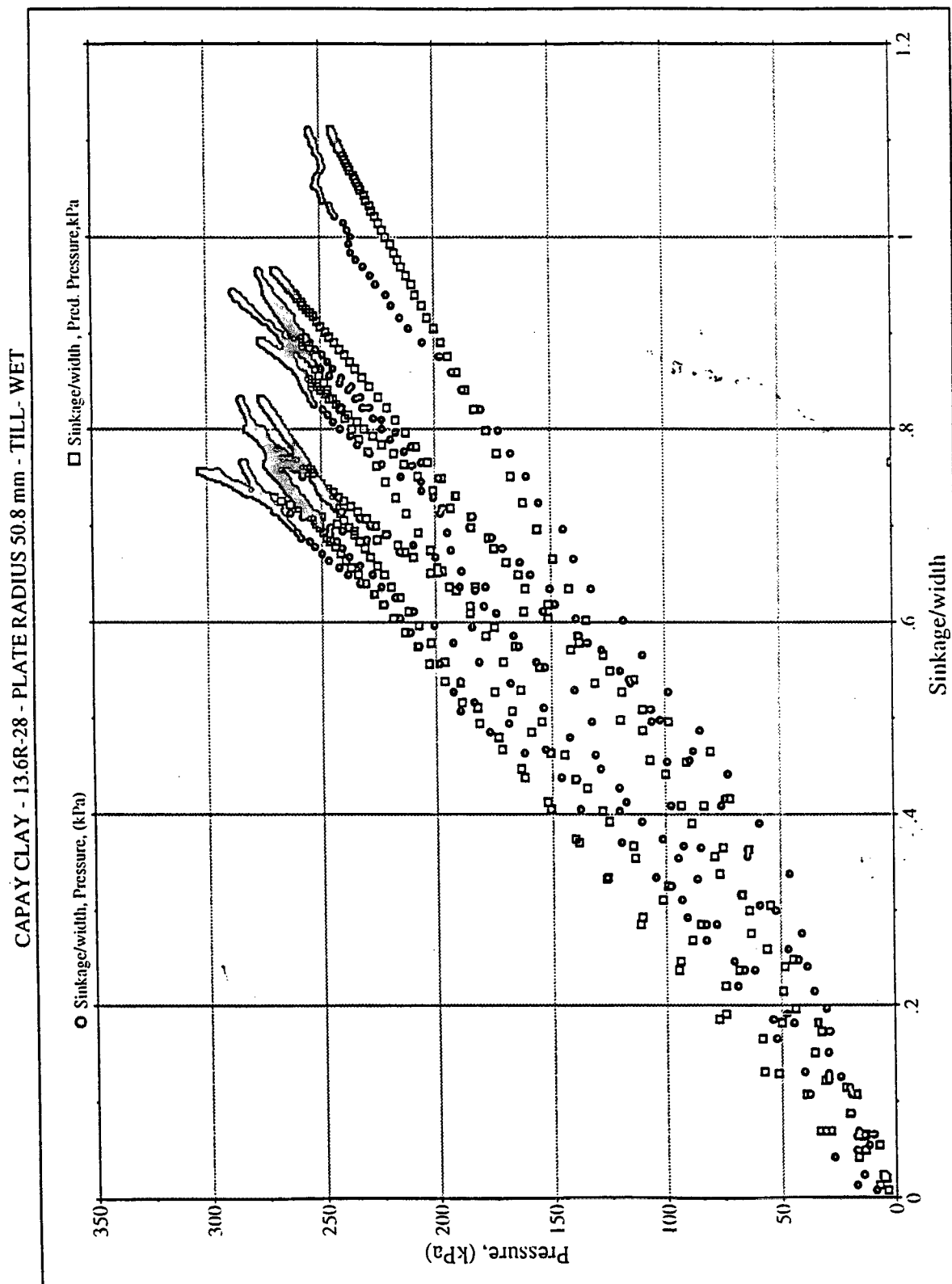


Figure 1. A typical pressure versus sinkage plot for a 50 mm circular plate in a tilled, wet, Capay clay soil.

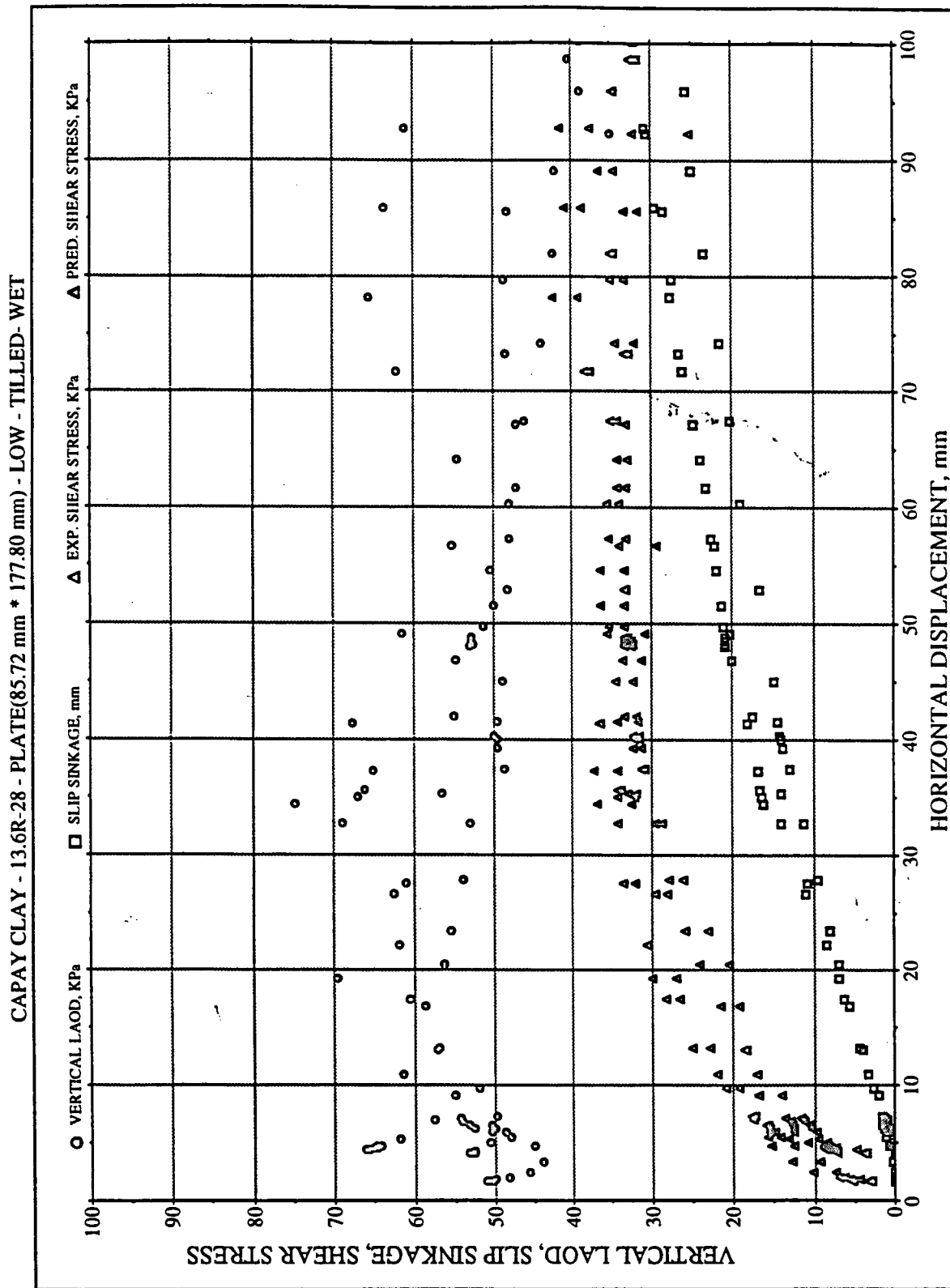


Figure 2. A typical grouser plate test results in a tilled, wet, Capay clay soil at a vertical load of 60 kPa. Variations in vertical load, shear stress, and slip sinkage as a function of shear deformation are plotted.

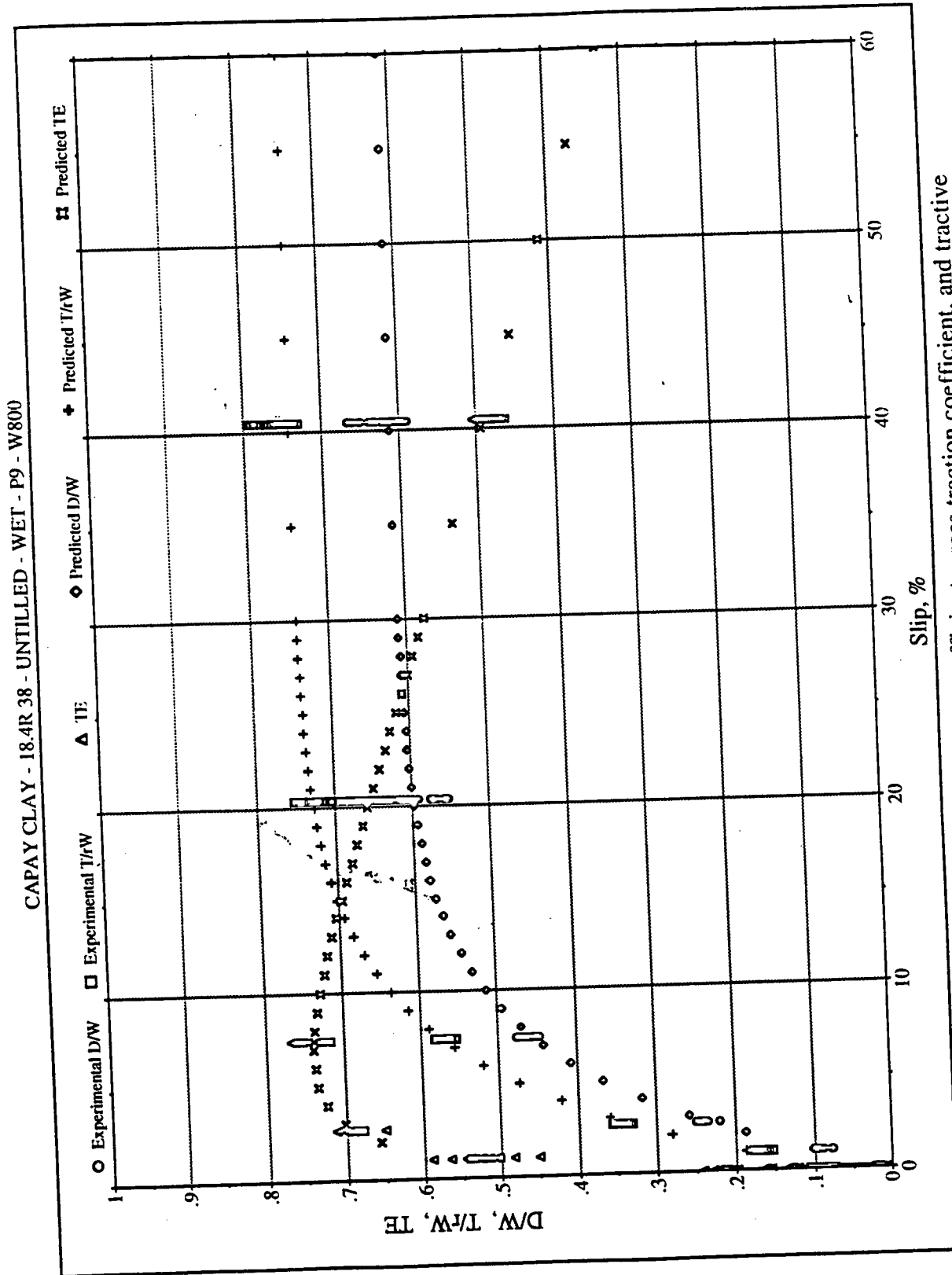


Figure 3. A typical plot of net traction coefficient, gross traction coefficient, and tractive efficiency as a function of slip. This particular test was conducted in an untilled, wet, Capay clay soil using a 18.4R38 tire at 62 kPa inflation pressure and 16 kN axle load.

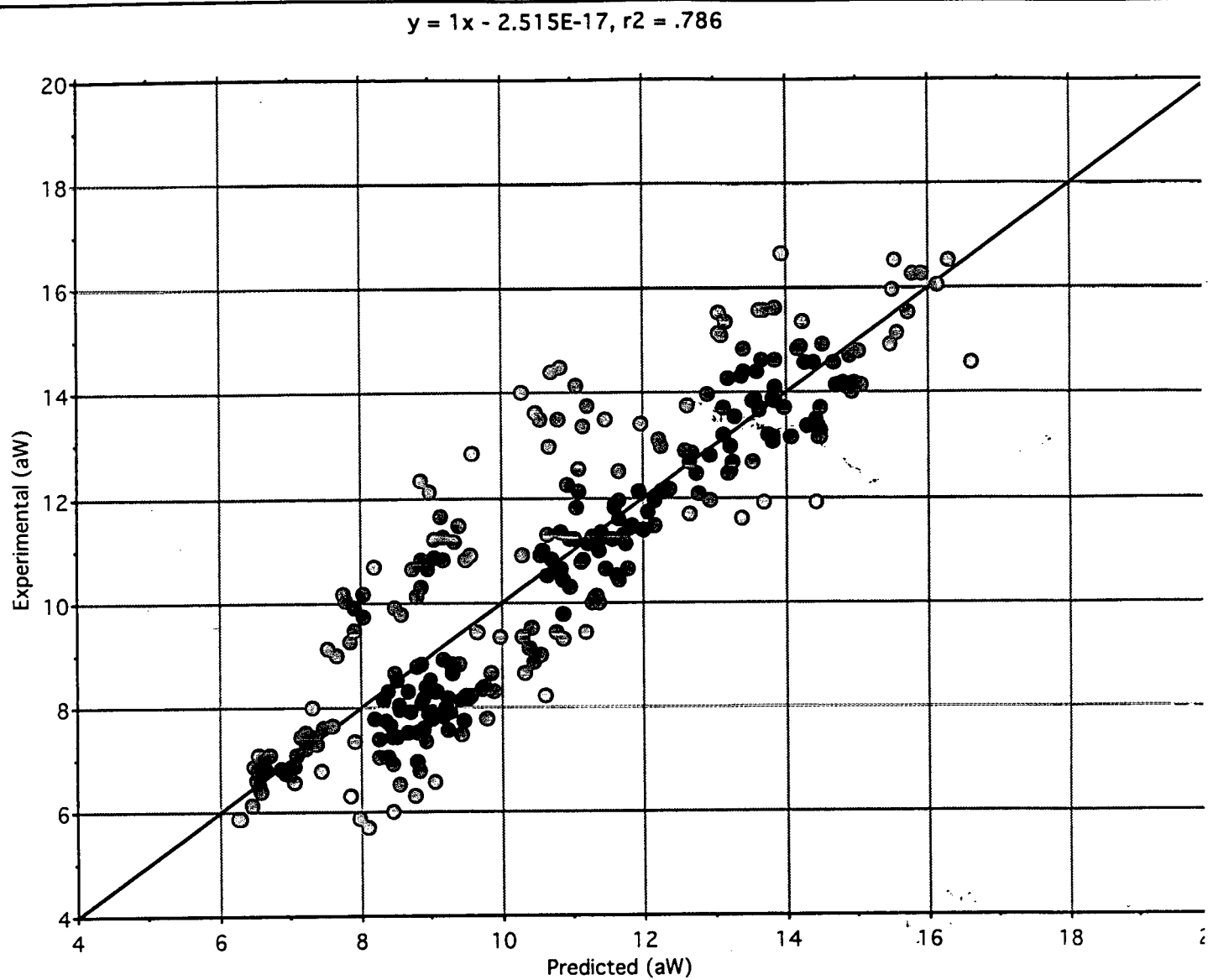


Figure 4. Plot of experimentally determined traction coefficient, aW versus predicted coefficient, aW using a semi-empirical technique.

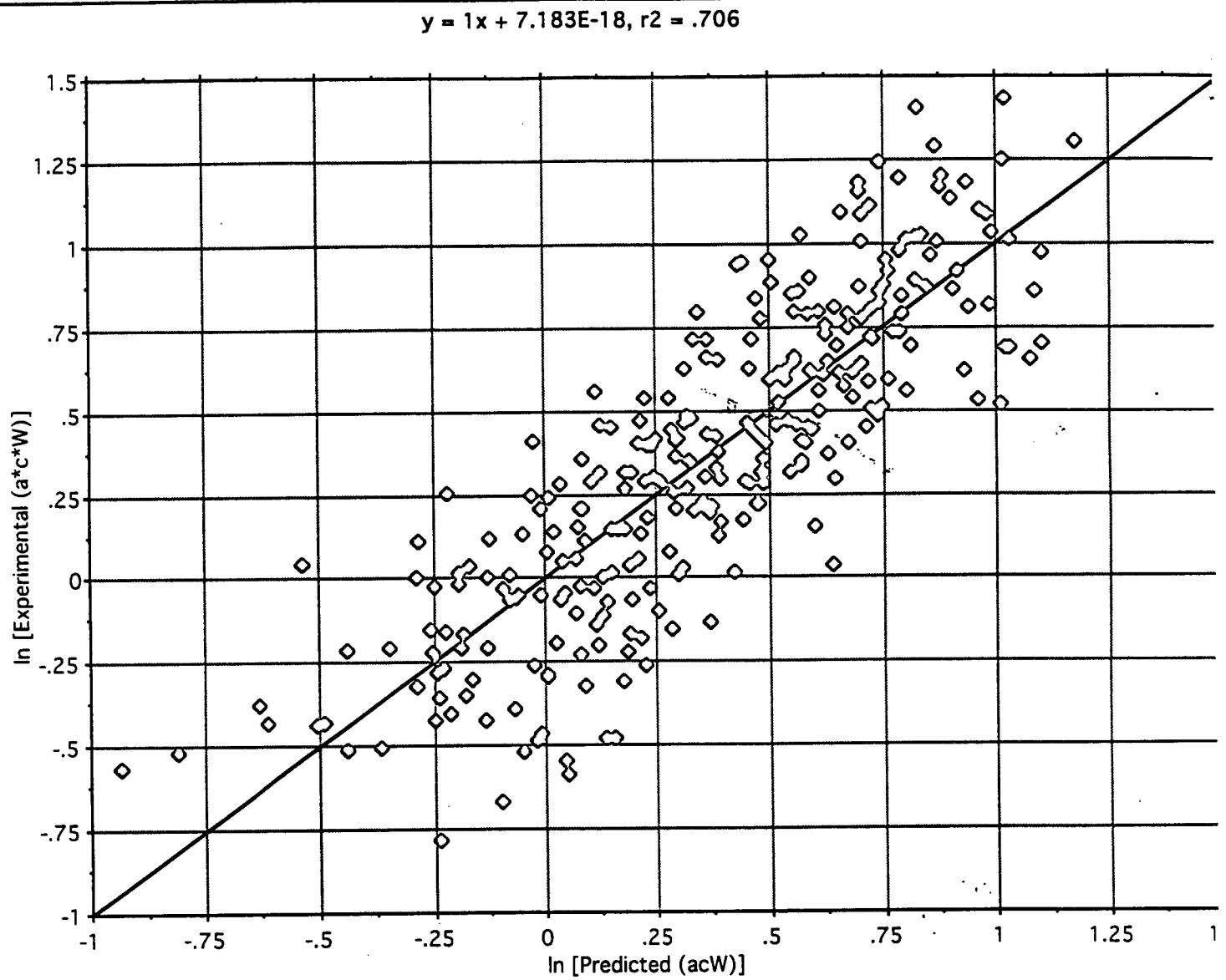


Figure 5. Plot of experimentally determined traction coefficient, acW versus predicted coefficient, acW using a semi-empirical technique.

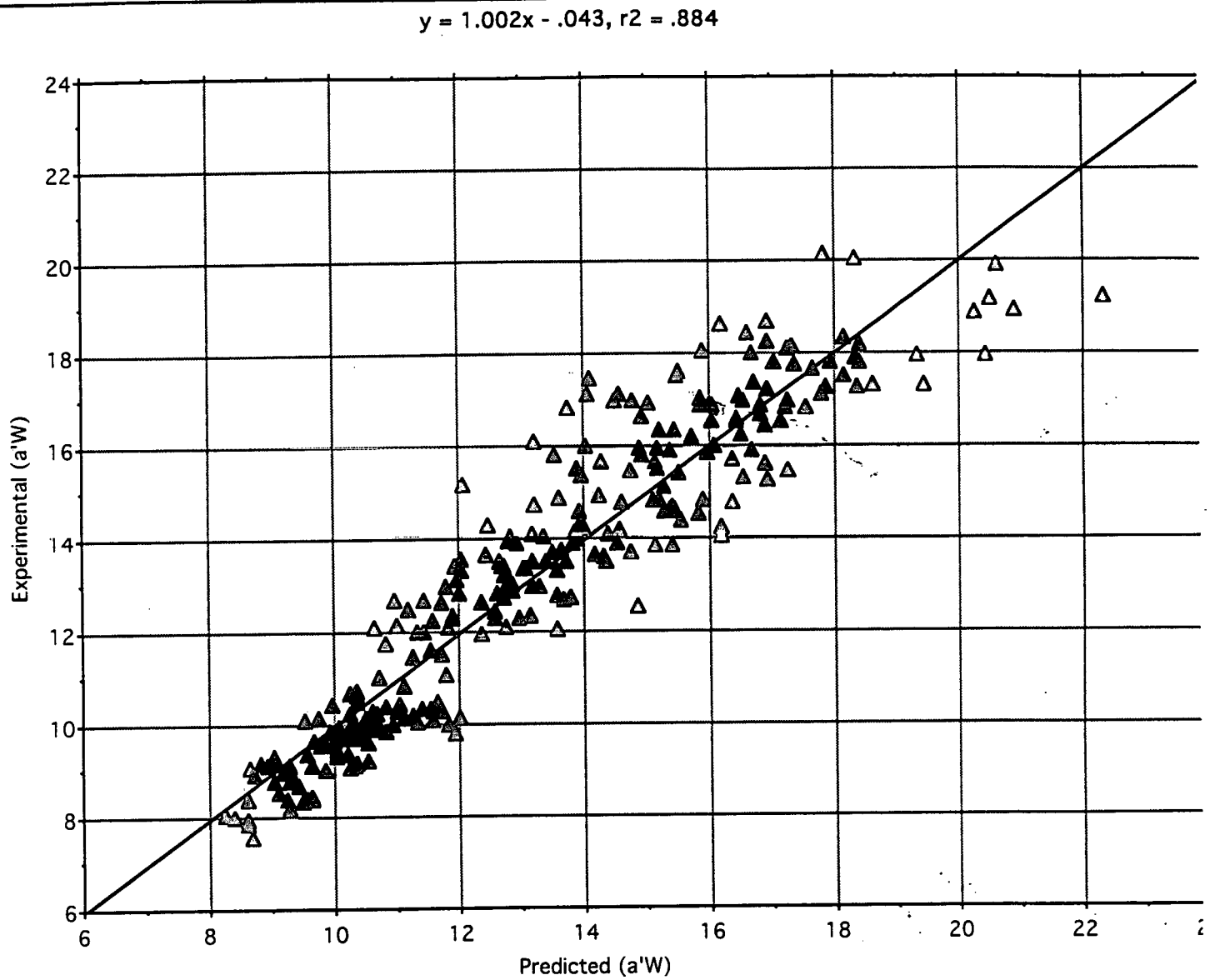


Figure 6. Plot of experimentally determined traction coefficient, $a'W$ versus predicted coefficient, $a'W$ using a semi-empirical technique.

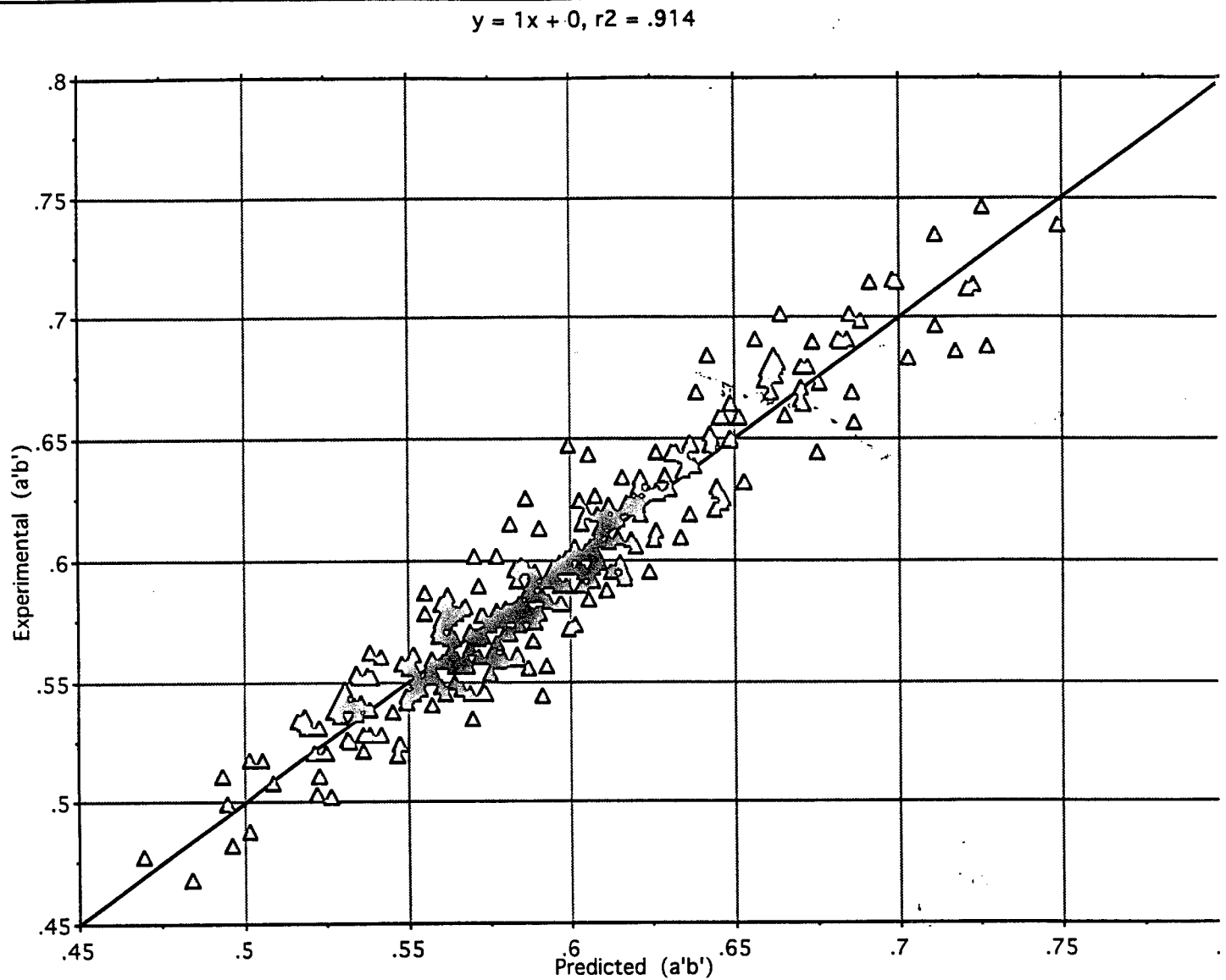


Figure 7. Plot of experimentally determined traction coefficient, $a'b'$ versus predicted coefficient, $a'b'$ using a semi-empirical technique.

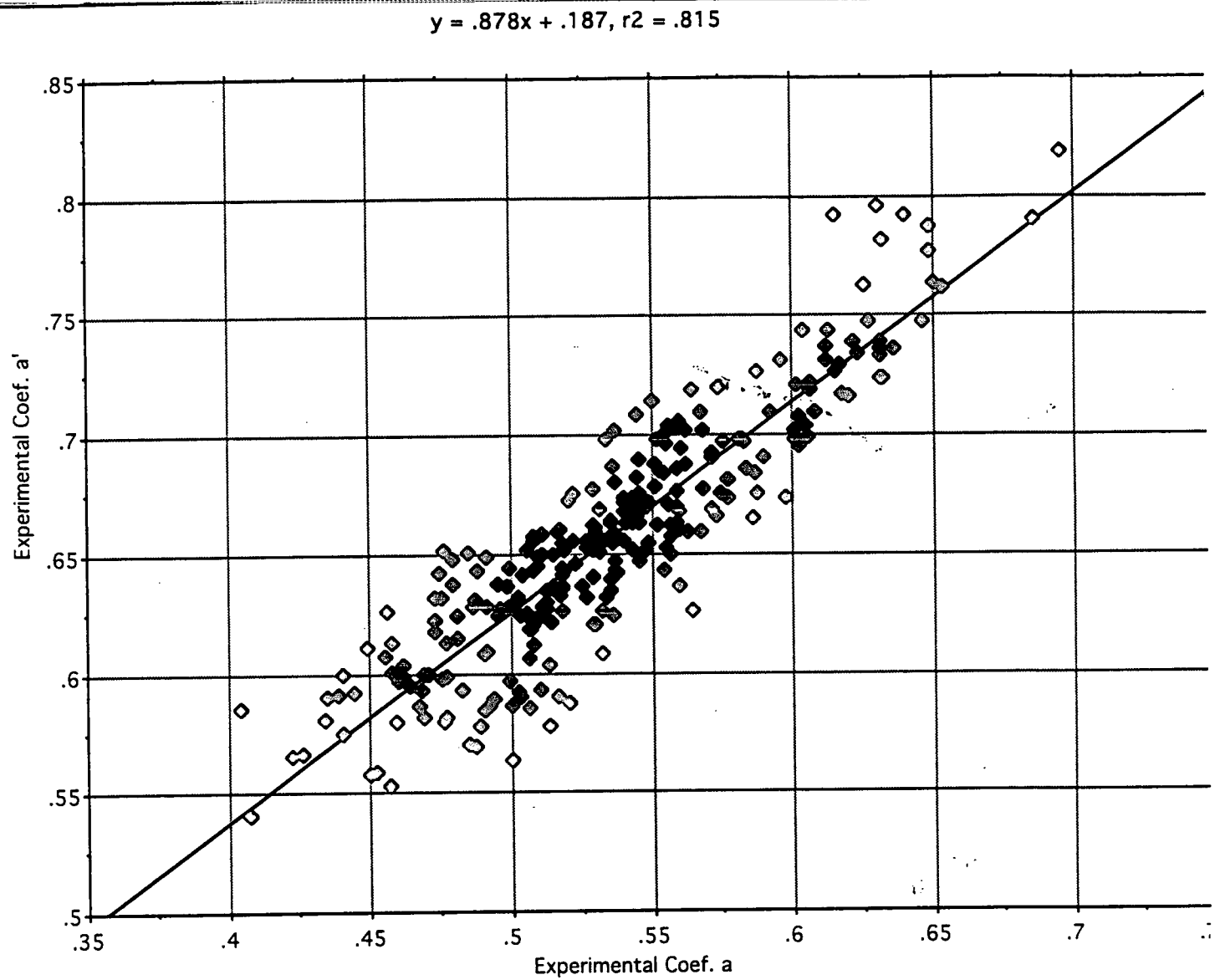


Figure 8. Plot of experimentally determined traction coefficient, a' , versus experimentally determined coefficient, a .

In the final year of this study an axisymmetric, nonlinear elastic, variable moduli soil compaction model was developed. Moreover, a 2-D and a 3-D traction prediction model was also developed. We wrote user friendly computer programs to evaluate traction and soil compaction characteristics of radial ply tires. A paper discussing the preliminary results of this aspect of the study was presented at the Second International Conference on Soil Dynamics in Silsoe, England in 1994. Another paper which dealt with the traction-soil compaction more comprehensively was presented at the 1995 ASAE Summer meeting in Chicago, IL. Based on some suggestion received at the ASAE Summer meeting, the traction-soil compaction model was modified considerably and is presented below. There is still a need to further develop this model especially to improve on 3-D analytical traction prediction and soil compaction prediction. Of the various traction prediction technique included, the semi-empirical technique provides superior results compared to all other methods. An user-friendly, Microsoft QuickBasic traction-soil compaction prediction program is available from the project leader for public use.

Shrini K. Upadhyaya W. J. Chancellor
Biological and Agricultural Engineering Department, University of
California, Davis

I. Shmulevich
Agricultural Engineering Department, Israel Institute of Technology,
Technion

A. Hadas
Institute of Soil and Water, Agricultural Research Organization, Volcani Center

Introduction and Review of Literature:

Tractive ability of off-road vehicles is restricted mainly by the limitations of the traction device (wheels or tracks) imposed by the terrain over which they operate. The tractive efficiency of pneumatic tires ranges from about 90 percent when operating on concrete to less than 50 percent on loose or sandy soils [Wulfsohn, et al., 1988]. A conservative estimate of annual fuel loss due to the poor tractive efficiency of agricultural tractors in the United States alone is about 600 million liters [Gill and VandenBerg, 1968]. Even an increase in the tractive efficiency by a percentage point, amounts to over 25 million dollars saved annually in the U. S. alone.

Soil-pneumatic tire interaction is a complex dynamic process. The geometry of the tire such as its overall diameter, width, section height, and tread type, tire type such as radial ply or bias ply construction, dynamic load on the axle, inflation pressure, and soil type and condition influence the tractive ability of a tire [Upadhyaya et al, 1989; Upadhyaya and Wulfsohn, 1989; Wulfsohn et. al., 1988; Upadhyaya, 1988; Yong et al., 1984; Gill and VandenBerg, 1968]. Adjusting inflation pressure and changing axle load are two simple ways of enhancing tractive ability of pneumatic tires. Zoz and Turner (1994) found that the peak tractive efficiency increased by 4 to 7% when inflation was properly adjusted to the axle load. Wiley et al. (1992) reported that adjusting radial ply tire pressures properly to static loads was a key factor in controlling power hop. Lancas et al. (1995) found that properly adjusting inflation pressures to axle loads led to increased fuel efficiency, productivity, and lower degree of soil compaction under California conditions.

Numerous studies have shown that increased axle load leads to increased tractive performance of tires [Upadhyaya et al., 1989; Wulfsohn et al., 1988; Yong et al., 1984; Wong, 1980; Nowatski and Karafiath, 1978; and Bekker, 1956 and 1960]. However, increased axle load also leads to increased incidence of soil compaction which has implications on water infiltration rate, root penetration, tillage energy requirements,

biological activity in soil, and perhaps crop yield [Hadas, et al. 1983, 1985, 1988; Trowse, 1971; Russell and Goss, 1974; Bowen, 1982; Hadas and Wolf, 1984; Wolf and Hadas, 1983, 1984; LAWR-Cooperative extension, 1984; Hassan and Upadhyaya, 1991]. Therefore benefits of increased tractive ability due to increased axle load should be carefully evaluated with respect to its implications on soil compaction. A joint Binational (United States and Israel) Agricultural Research and Development [BARD] Project was initiated between the University of California, Davis, Israel Institute of Technology, Technion, Agricultural Research Organization, Volcani Center, Israel in 1991. *One key objective of this project was to develop a traction/soil compaction prediction model. This paper discusses the development of a traction/soil compaction prediction model at the University of California, Davis.*

Traction Prediction Equations:

Upadhyaya and Wulfsohn (1990) reviewed various traction prediction equations reported in the literature. In this study we have included five different techniques of predicting traction for radial ply tires. Two of these equations are based on characterizing soil by its cone index value (Brixius equations (1987) as modified by Al-Hamed et al., 1994, and Upadhyaya et al. 1989). The third set of equations are based on the semi-empirical equations developed by Upadhyaya and Wulfsohn (1993) which uses soil sinkage and shear parameters. The fourth set of equations is based on a 2-D contact geometry, soil sinkage and shear properties, and traction mechanics. The last set of equations considers the 3-D nature of the soil-tire contact profile and evaluates tractive ability based on traction mechanics, and soil sinkage and shear properties. We also intend to incorporate a neural network based prediction. However, it is not included in this study. These equations are discussed below:

Cone Index Based Predictions Using the Modified Brixius Equations:

Brixius (1987) reported traction prediction equations for bias ply tires which were improvements on the earlier equations reported by Wismer and Luth (1972). He suggested that these equations could be modified for radial ply tires by changing some of the empirical constants in those equations. Based on Brixius's suggestions, Al-Hamed et al. [1994] used following equations to predict tractive ability of radial ply tires:

$$\mu_{nt} = NT / W = 0.88(1 - e^{-0.1B_n}) * (1 - e^{-9.5S}) - \frac{0.9}{B_n} - \frac{0.5S}{\sqrt{B_n}}$$

$$\mu_{gt} = T / rW = 0.88(1 - e^{-0.1B_n}) * (1 - e^{-9.5S}) + 0.032$$

where

μ_{nt} = net traction coef.

NT = net traction

W = axle load

$$B_n = \left(\frac{C_i b d}{W} \right) \left(\frac{1 + 5\delta / h}{1 + 3b / d} \right)$$

C_i = cone index

b = section width

d = overall diameter

δ = loaded deflection

h = (d - rim diameter) / 2

(1)

$$S = \text{slip} = \left(1 - \frac{V_a}{V_t}\right)$$

V_a = actual travel speed

V_t = Theoretical wheel speed = $r\omega$

r = rolling radius on a hard surface

$$= \frac{2.5(d/2)(\text{static loaded radius})}{1.5(d/2) + (\text{static loaded radius})}$$

ω = angular velocity of wheel

μ_{gt} = gross traction coef.

T = input torque

Cone Index Based Predictions Using the Upadhyaya and Wulfsohn Equations (1989):

Upadhyaya and Wulfsohn (1989) conducted extensive field tests using the UC Davis single wheel tire tester (3 tires x 2 soils x 5 soil conditions x 3 axle loads x 2 inflation pressures). Using a nonlinear regression technique, they found that the traction test results always fitted equations of the following type with very high coefficients of multiple determination (R^2):

$$\mu_{nt} = NT / W = a(1 - e^{-cS}) \quad (2)$$

$$\mu_{gt} = T / (rW) = a'(1 - be^{c'S})$$

where a , c , a' , b , and c' are soil, tire, and loading (inflation pressure and axle load) related empirical coefficients. They found that c was approximately equal to c' in all cases. They used traction mechanics, conservation of energy principle, and dimensional analysis to relate these empirical coefficients to soil, tire, and loading parameters. They had limited success in relating these coefficients to soil parameters when only soil cone index and

moisture content values were used to represent soil type and conditions. They obtained the following empirical equations:

$$a = 0.311 + 0.067 (b/l) + 0.001 (C_i/p) + 1.089 (\theta) - 0.933 (C_i/p) (W/C_i b l)^2$$

$$1/c = -5.376 - 0.764 (aW/l) + 4.923 (b/l) - 211.152 \{W/(C_i b l)\} (\theta) \quad (3)$$

$$+ 101 (a/l) \{W/(C_i b l)\} + 32.646 (\theta) + 30.913 a$$

$$a' = 0.245 + 0.411 (\theta) + 0.474 a + 0.251(a/l) - 0.001 a (aW/l)^2$$

$$b = 0.2993 + 0.5343 (a/a') + 0.1336 \{a/(a'l)\} - 0.0002 (a/a')(aW/l)^2$$

where

l = contact length, m

p = inflation pressure, kPa

θ = moisture content in dry basis, fraction

All quantities in equation (3) are expressed in SI units (i.e. length units are in m, forces are in kN, pressures are in kPa). The coefficients of multiple determination for parameters a , c , a' , and b are respectively 0.61, 0.73, 0.71, and 0.76.

Semi-empirical 2-D Predictions Based on Soil Sinkage and Shear Parameters (Upadhyaya and Wulfsohn, 1993)* :

Realizing the inadequacy of using only soil cone index values to represent soil characteristics (as in equation 2 above), Upadhyaya et al. (1993) developed an instrumented soil test device to measure soil sinkage (sinkage constant, k , and exponent,

* Unfortunately, the original article by Upadhyaya and Wulfsohn (1993) contained some typographical errors in $a'W$ and $a'(1-b)$ equations.

n), and shear (cohesion, C , internal angle of friction, ϕ , and shear modulus, K) parameters. Using these soil parameters, traction mechanics, and conservation of energy principle, Upadhyaya and Wulfsohn (1993) developed empirical equations to predict traction parameters a , c , a' , and b . In deriving the theoretical basis for these equations they assumed the soil-tire contact area to be elliptical in a 2-D space. These prediction equations are of the following form:

$$a = 6.675 + 0.952 A_c \tau_{\max} - 19.208 \tau_{\max} K l_w$$

$$1/c = -4.682 + 413.067 [a (\bar{p} / \tau_{\max})(K/l_c)] + 41.377 [aW/(K_t l_c)] \quad (4)$$

$$a' W = 8.527 - 15.793 (aWK/l_c) + 10.943 [(aW)^2/(K_t l_c)]$$

$$a'(1-b) = 0.921 - 13.269 x_1 + 4.681 x_2 + 48.846 x_1^2 - 19.878 x_2^2 \\ - 23.078 x_1 x_2$$

where

A_c = 2-D contact area, m^2

$\tau_{\max} = C + \bar{p} \tan(\phi)$, kPa

l_w = contact width, m

K = shear modulus, m

K_t = tire stiffness in the tangential direction, kN/m

\bar{p} = average contact pressure, W/A_c , kPa

l_c = contact length, m

$x_1 = \delta_t / l_c$

$x_2 = [\delta_s / (n + 1)] / l_c$

d_s = soil deformation, m

d_t = tire deformation in the vertical direction, m

The coefficients of multiple determination for a , c , a' , and b were respectively 0.82, 0.79, 0.92, and 0.84. However, these equations were based on limited tests.

During the summer of 1993 extensive field tests were conducted using the UCD single wheel tester. Four radial ply tires [13.6R28, 16.9R38, 18.4R38, and 24.5R32] were used in this study. The tests were conducted in a Capay clay and a Yolo loam soil on the UCD campus. In each of these two soils four soil conditions were created. A 240 m x 240 m plot was marked off in each field. This plot was divided into two subplots, one of which was irrigated and the other was left dry. Both the irrigated (wet) and dry subplots were further subdivided into two sub-subplots. One each of these sub-subplots was tilled and the other was left undisturbed. Each tire was tested in each of these soil conditions at three levels of vertical loads (approximately 26, 20, and 14 kN) and three levels of inflation pressures (64, 85, and 106 kPa). This test plan resulted in 288 traction tests. Moreover, in each of these soil condition plate sinkage tests, grouser shear tests, cone penetrometer tests were conducted to obtain soil parameters related to traction. Furthermore, soil density and moisture content data were obtained to quantify soil conditions. All 288 tests were analyzed using the approach outlined by Upadhyaya and Wulfsohn (1993) to obtain the following general empirical equations:

$$\begin{aligned}
 aW &= 1.73 + 0.572 * \tau_{\max} * A_c + 3.589 * \tau_{\max} K * l_w + 5.672 * \left(\frac{\bar{p}}{K_r} \right) \\
 acW &= 0.881 * \left[\frac{\delta_t - \delta_s}{l_c} \right]^{0.183} \left[\frac{\delta_t}{l_c} \right]^{1.346} \left[\frac{l_w}{K} \right]^{-1.717} \left[\frac{l_c}{K} \right]^{1.743} \left[\frac{l_c l_w}{A_c} \right]^{4.198} [\tau_{\max} A_c]^{0.685} \\
 a'W &= 5.843 - 3.697 \left[\frac{aWK}{l_c} \right] + 11.778 \left[\frac{(aW)^2}{294.1 * l_c} \right] \\
 a'b &= 0.053 + 0.865 a' - 1.488 x_1 + 13.496 x_1^2
 \end{aligned} \tag{4a}$$

It was further found that a' and b' may be determined using following simpler equations with out sacrificing much on accuracy. i.e.

$$a' = 0.878 a + 0.187 \quad (4b)$$

$$b' = 0.91$$

where K_r is the Reece's sinkage constant, δ_t (m) is the total deformation (soil+tire), and δ_s (m) is the maximum soil deformation. The coefficients of multiple determination for a , c , a' , and b in equation 4a were respectively 0.79, 0.71, 0.88, and 0.91. The coefficient of determination for a' in equation 4b was 0.81.

From equations 4 and 4a it is clear that equations for coefficients a' and b' are similar for the more general case compared to the one obtained earlier. Equation for coefficient " a " has an additional term which is related to soil sinkage and was found to be necessary to account for different soil type and conditions included in this study. The coefficient c was the hardest to predict and needed several terms to account for various soil type and conditions and tire sizes.

Analytical Model Based on 2-D Contact Area and Traction Mechanics: In this approach the contact area is assumed to be 2-D (i.e. like on a hard surface). This allows us to use the tire-contact information provided by the tire manufacturers to predict tractive characteristics of tires. Information such as load deflection characteristics, contact length, contact width, and contact area can be obtained for any tire from tire engineers associated with tire companies. The 2-D contact length and area were found to vary linearly with tire deflection in all the cases studied (13.6R28, 16.9R38, 18.4R38, and 24.5R32 tires). The contact width was found to vary as a highly nonlinear function of tire deflection as given below for all four tires considered:

$$(1/l_w)^4 = b_0 + b_1 (1/\delta_t)^2 + b_2 (1/\delta_t)^4 \quad (5)$$

where b_0 , b_1 , and b_2 are regression coefficients. This equation makes it possible to change the shape of the footprint from elliptic under low axle load to rectangular with curved edges at high axle loads in a smooth fashion, instead of a need to use piece-wise smooth functions such as the ones used by Upadhyaya and Wulfsohn (1990). Equation (5) can be used to determine the shape of the 2-D contact surface. Once the shape of the contact surface is known, the pressure distribution over the contact area can be estimated. The tire deformation can be estimated from the following equation,

$$d_t = g(x,y) = \frac{\delta_t}{l_w^4} \left[\frac{(l_c^2 - y^2)^2}{c_0 + c_1(l_c^2 - y^2) + c_2(l_c^2 - y^2)^2} - x^4 \right] \quad (6)$$

where xy represents a right handed Cartesian coordinate system in which y coincides with the direction of travel. Note that d_t is the tire deformation at any location (x,y) in the contact surface and $g(x,y)=0$ gives the 2-D contact surface [See Fig. 1]. Moreover, c_0 , c_1 , and c_2 are related to b_0 , b_1 , and b_2 respectively by contact length versus tire deformation relationship.

The net traction is given by:

$$NT = \int_{A_c} [C + p(x,y) \tan(\phi)] [1 - e^{-S\xi/K}] dx dy \quad (7)$$

$$T = \int_{A_c} [C + p(x,y) \tan(\phi)] [1 - e^{-S\xi/K}] r dx dy \quad (8)$$

where

ξ = distance shown in Fig. 1

r = moment arm of elemental shear stress about the axle.

Although $p(x,y)$ varies along the 2-D contact area because of the presence of treads and the edge effect, an average pressure equal to (axle load, W)/(contact area, A_c) was used to evaluate integrals (7) and (8). In addition energy losses due to tire and soil deformation are also accounted for in determining the gross traction coefficient.

Analytical Model Based on 3-D Contact Area and Traction Mechanics: In this model soil is allowed to deform to produce the full 3-D soil/tire interface. The model starts with the 2-D contact model described in Eqn. (7). If tire alone deforms, we have

$$d_t = \delta f(x,y) \quad (9)$$

where $f(x,y) = g(x,y)/\delta$ and δ is maximum tire deformation.

If wheel is rigid and only soil deforms, soil deformation, d_s , can be written as:

$$d_s = \delta f(x,y) \quad (10)$$

If both soil and tire deform, we have,

$$d_t = \delta f(x,y) - d_s \quad (11)$$

or,

$$d_t + d_s = \delta f(x,y) \quad (12)$$

If δ_s is the maximum soil deformation, then the 3-D soil deformation can also be written as,

$$d_s = \delta_s f(x,y) \quad (13)$$

The maximum soil deformation can be estimated from average contact pressure ($\bar{p} = W/A_c$) using Reece's sinkage formula as follows:

$$\delta_s = b (\bar{p}/k_s)^{1/n} \quad (14)$$

Finally, requiring that integral of the vertical stresses over the contact surface should equal to the axle load, we obtain,

$$W = k_s \int_{A_c} \left(\frac{d_s}{b} \right)^n dx dy \quad (15)$$

Equation (15) can be evaluated if 3-D contact area is known. In order, to know the front and rear contact lengths and widths, we need to know δ in equation (9). Using 2-D tire deformation, δ_t , as the initial guess for δ , equation (15) can be evaluated to estimate W . If estimated W is too low, we need to increase δ by an amount equal to the estimated error, and reevaluate equation (15). On the other hand, if W is too high, we decrease δ by an amount equal to the estimated error and once again evaluate equation (15) until W is estimated with desired accuracy. This technique results in a value of δ which estimates W within about 1% accuracy in a few iterations. Note that we assume no rebound in the soil after the wheel passes.

Once the 3-D soil deformation is obtained, soil stress at every point in the contact can be determined. Usually k_s is obtained using a small sinkage device in the field. This k_s value should be modified to account for the larger dimension of the tire. A soil compaction model was developed to estimate the k_s value appropriate for the tire. To evaluate net

traction and input torque a further assumption was made as shown in Fig. 2. The smooth 3-D surface was approximated by steps in the Y-direction so that normal stress became vertical and Reece's sinkage equation could be used.

The net traction, NT is given by,

$$\begin{aligned}
 NT &= \int_{A_c} [C + \sigma \tan(\phi)] (1 - e^{-S\xi/K}) \, dx dy \\
 \sigma &= k_s (d_t / b)^n \\
 T &= \int_{A_c} [C + \sigma \tan(\phi)] (1 - e^{-S\xi/K}) \, r \, dx dy \quad (16)
 \end{aligned}$$

The integration shown in equation (17) is evaluated over the whole 3-D contact surface.

Soil Compaction Model:

An axisymmetric, nonlinear elastic, variable moduli model was developed to predict soil compaction. The zone of influence under the plate was assumed to be a cylindrical column of soil directly under the plate. Moreover, a punch failure was assumed to occur at the edge of the plate. Referring to Fig. 3a, we can write the equation of vertical equilibrium for element (1) as:

$$\frac{d\sigma_z}{dz} + \left(\frac{P}{A}\right)\tau = 0 \quad (17)$$

where

σ_z = vertical stress

τ = shear stress = $[C + \sigma_r \tan(\phi)][1 - e^{-w/K}]$

P = perimeter of the plate

A = plate area

σ_r = radial stress

w = vertical deformation at the edge of the plate

Radial expansion of the soil was incorporated into the model by solving the radial equilibrium equation for the cylindrical soil element using the Galerkin approach. The equation of equilibrium in the radial direction is given by (Reismann, H. and P. S. Pawlik, 1980):

$$\frac{\partial \sigma_r}{\partial r} + \frac{\sigma_r - \sigma_\theta}{r} + \frac{\partial \tau}{\partial z} = 0 \quad (18)$$

From the constitutive relations, we have

$$d\sigma_r = \frac{E}{(1+\nu)(1-2\nu)} [d\epsilon_r + \nu d\epsilon_z] \quad (19a)$$

$$d\sigma_z = \frac{E}{(1+\nu)(1-2\nu)} [2\nu d\epsilon_r + (1-\nu) d\epsilon_z] \quad (19b)$$

where E is the Young's modulus and ν is the Poisson's ratio. If a logarithmic elastic behavior is assumed, then elastic modulus, E can be assumed to be proportional to the hydrostatic stress, p . i.e.:

$$E = E_0 + E_1 p \quad (20)$$

and shear modulus,
$$G = \frac{E}{2(1+\nu)} = \frac{E_0 + E_1 p}{2(1+\nu)} \quad (21)$$

Moreover, from the constitutive laws we can show that, (cf. Reismann and Pawlik, 1980),

$$(\sigma_r - \sigma_\theta) = 2G (\epsilon_r - \epsilon_\theta) \quad (22)$$

For small deformations, shear stress τ may be approximated by (cf. element 2 in Fig. 3)

$$\tau = G w/L = (G_0 + G_1 p) w/L \quad (23)$$

From traction mechanics, we have

$$\tau = (C + \sigma_r \tan(\phi)) (1 - e^{-w/K}) \quad (24)$$

If $\sigma_r = \rho p^*$ and w is small equation (24) becomes,

$$\tau = (C + \rho p \tan(\phi)) w/K \quad (25)$$

From equations (23) and (25) we see that $G_0 = C$, $G_1 = \rho \tan(\phi)$, and $L = K$. The shear stress term in equations (17) and (18) are modeled using equation (23) [alternately equation (25)] until it reaches a maximum value of $[C + \rho p \tan(\phi)]$ and thereafter remains constant at this maximum value. Combining equations (18) through (23) we can rewrite the radial equilibrium equation as:

$$\frac{2}{(1-2\nu)} \left[\frac{\partial \epsilon_r}{\partial r} + \frac{\partial \epsilon_z}{\partial z} \right] + \frac{(\epsilon_r - \epsilon_\theta)}{r} + \frac{\partial w}{\partial z} h(r-R) \quad (26)$$

* This will be verified later.

where $h(r-R)$ represents the unit Heavy-side function. Assuming distribution of radial displacement, u , vertical displacement, w , and shear stress, τ , to be as shown in Figs. 3b, 3c, and 3d over element (1) which is directly under the plate and element (2) which is outside the plate, we get,

$$\begin{aligned} u &= \xi u_r & 0 < r < R \\ u &= (1 - \xi) u_r & R < r < (R+L) \end{aligned} \quad (27)$$

$$\begin{aligned} w &= w(z) & 0 < r < R \\ w &= w(1 - \xi) & R < r < (R+L) \end{aligned} \quad (28)$$

$$\begin{aligned} \text{and} \quad \tau &= 0 & 0 < r < R \\ \tau &= G w/L & R < r < (R+L) \end{aligned} \quad (29)$$

where $\xi = r/R$ in $0 < r < R$ and $\xi = (r - R)/L$ in $R < r < (R+L)$.

Applying Galerkin's technique to equation (26) over elements (1) and (2), we get,

$$\int_0^{R+L} N \left[\frac{2}{(1-2\nu)} \left[\frac{\partial \epsilon_r}{\partial r} + \frac{\partial \epsilon_z}{\partial z} \right] + \frac{(\epsilon_r - \epsilon_\theta)}{r} + \frac{\partial w}{\partial z} h(r-R) \right] 2\pi r \, dr \quad (30)$$

where N = shape function

$$= \xi \quad \text{if } 0 < r < R$$

$$= (1 - \xi) \quad \text{if } R < r < (R+L)$$

$$r = \xi R \quad \text{if } 0 < r < R$$

$$= (1 - \xi) R + \xi (R+L) \quad \text{if } R < r < (R+L)$$

Evaluating equation (30) utilizing equations (27), (28), and (29), we obtain the following expression for u_r upon considerable simplification,

$$u_r = -\alpha \frac{\partial w}{\partial z} \quad (31)$$

$$\text{where } \alpha = \frac{(4\nu R + 2\nu L + 4R + L)}{24 \frac{(R + L)}{L} (1 - 2\nu) \left[\frac{2\nu}{(1 - 2\nu)} + \frac{(R + L)}{L} \ln \left[\frac{(R + L)}{R} \right] \right]}$$

Using the convention that compression is positive, we can represent vertical strain, ϵ_z , as:

$$\epsilon_z = - (dw/dz) \quad (32)$$

Utilizing equations (19b), (23), (31), and (32) in equation (17), we can rewrite the vertical equilibrium equation as,

$$\frac{d^2 w}{dz^2} - \lambda w = 0 \quad (33)$$

$$\text{where } \lambda = \frac{PG'}{2G\beta AL}$$

G' = shear modulus for element (2)

G = shear modulus for element (1)

$$\beta = \frac{1}{(1 - 2\nu)R} [(1 - \nu)R - 2\nu\alpha]$$

Moreover, from equations (19a and b) and 31, we can show that

$$\sigma_r = \rho p \quad (34)$$

and

$$p = \chi \sigma_z$$

$$\rho = \frac{1}{3} \left[\frac{(1 + \nu)(R - 2\alpha)}{R(1 - \nu) - 2\nu\alpha} \right]$$

where

$$\chi = \frac{[\alpha - \nu R]}{[2\nu\alpha - (1 - \nu)R]}$$

Nonlinear equation (33) was solved using a Finite element technique which utilized an updated Lagrange technique to handle large displacements. Following boundary conditions were used during the finite element analysis.

$$w = 0 \quad \text{when } z \Rightarrow \infty$$

$$\text{and } \sigma_z = p_a$$

where p_a = applied pressure.

Applied pressure was implemented in several steps. At each step, every element was checked for shear failure at the edge. When an element failed, it was assumed to become incompressible (i.e. Poisson's ratio approaches 0.5, Chancellor, 1993).

Results and Discussion:

A user friendly computer was written to evaluate tractive ability of radial ply tires. This program currently contains data for 13.6R28, 16.9R38, 18.4R38, and 24.5R32 tires. Tractive ability of any of these tires can be predicted under desired soil and loading conditions using one or more of the methods outlined earlier. The program produces net traction coef., gross traction coef., and tractive efficiency [$TE = (\mu_{nt}/\mu_{gt})(1-S)*100$] estimated by various prediction techniques. Figure 4 is a block diagram which shows the major steps involved in the traction prediction program.

This program was used to evaluate the traction of 15 randomly selected conditions out of the 288 explored during the course of this project. Five of these 15 conditions are presented in figures 5 to 10. These figures in sets of three (a,b,c). For example figure 5a represents prediction of net traction coef., 5b depicts prediction of gross traction coef., and 5c shows the plot of tractive efficiency. Figure 5 represents the tractive ability of 13.6R38 tire operating in a tilled, wet, Capay clay soil at an axle load of 13.5 kN and an inflation of

103 kPa as predicted by the various prediction techniques. For this case semi-empirical technique provided the best prediction. Both 2-D and 3-D analytical techniques tended to over predict its tractive characteristics and the two cone index based technique under-predicted its tractive ability. In general, semi-empirical prediction technique which is based on traction mechanics, dimensional analysis, and conservation of energy principles appears to be the best (Figs. 5 to 10). In general, 2-D and 3-D analytical prediction techniques resulted in similar values for NT/W , but 3-D technique estimated T/rW better since it accounted for 3-D nature of soil-tire interaction. 3-D technique also predicted TE better than 2-D technique. Among the cone index techniques Brixus based technique performed better than the model proposed by Upadhyaya and Wulfsohn (1989). In general, cone index based techniques appeared to work well in a narrow range of soil cone index conditions. Method proposed by Upadhyaya and Wulfsohn (1989) worked reasonably well for high cone index (plots not shown) and low moisture values, and under-predicted tire's tractive ability under all other conditions. This technique seems to have the most limited range of application. The modified Brixus equations worked well for medium range of cone index values. It tended to over predict tire's tractive ability for higher cone index values and under predict its traction characteristics for low cone index values.

Table 1 lists the details of the operating conditions used for simulations shown in figures 5 through 10. The inadequacy of 2-D and 3-D analytical techniques in predicting tire's tractive characteristics is most likely due to the differences in soil parameters (sinkage, shear etc.) estimated using small plates used on the soil test device versus actual values as seen by larger tires. Unfortunately, our attempts to scale up sinkage parameters using our soil compaction model was not successful. It should be noted that semi-empirical technique is similar to 2-D analytical techniques except that the prediction equations have been calibrated against the experimental results. A similar approach with the 3-D analytical technique could be even better. However, this aspect was not investigated in this study.

Although the 3-D analytical technique needs further work, it appears to have a good potential. It not only provides an estimation of tractive characteristics of tires, it also estimates the pressure distribution on the 3-D surface.

Figures 11 and 12 show the effect of inflation pressure on soil deformation. At a low inflation pressure level soil does not deform as much (Fig. 11) compared to soil deformation at a high inflation pressure level (Fig. 12). The qualitative predictions seem quite reasonable.

Figures 13, 14, 15, and 16 show the results of soil-compaction program. Figure 13 shows displacements, Fig. 14 shows vertical stress, Fig. 15 shows the radial stress, and Fig. 16 shows void ratio at four different levels of applied pressure. The results shown are for a sinkage test using a 100 mm plate in a soil with a cohesion of 14 kPa, internal angle of friction of 22 deg., shear modulus of 9mm, previous loading of 25 kPa, and a void ratio of 1.26. The predicted displacements are reasonable compared to the experimental results. It is interesting to see the prediction of void ratio by this model (Fig. 16). The compaction process appears to propagate from the surface down as surface load is increased. There appears to be a zone of active compression ahead of the layer which has been compressed to its critical value. This phenomenon has been observed by Dr. Chancellor, Professor, Biological and Agricultural Engineering Department, UCD in his extensive studies on soil compaction (personal communication). This model needs further experimental verification. This aspects is worthy of further investigation.

Conclusions:

Based on this study we reached the following conclusions:

1. A traction prediction program which estimates the tractive ability of pneumatic tires using several different techniques (2D-semi-empirical, CI-based, Brixius, 2-D analytical, and 3-D analytical) has been developed and a user friendly computer program was developed to evaluate these models for radial ply tires.

2. Our simulation studies indicate that semi-empirical model performed better than all other prediction technique. The 2-D and 3-D analytical techniques tended to over-predict the tractive ability of tires. The cone index based equations developed Upadhyaya and Wulfsohn (1989) under-predicted tractive ability of tires under low soil cone index value conditions. The cone index based technique developed Brixius (1987) as modified by Al-Hamed et al. (1994)] over predicted tractive ability of tires under high soil cone index values and under-predicted under low cone index values. It appears to work reasonably well for mid range of soil cone index values. It should be noted that the semi-empirical technique is similar to 2-D analytical prediction technique, but calibrates model response to experimental results to obtain empirical coefficients. A similar approach with the 3-D analytical model would be useful.

3. A nonlinear elastic, variable moduli, FEM model was developed to predict soil compaction. The qualitative behavior of this model was reasonable and predicts soil sinkage under a 100 mm plate reasonably well. However, this model needs to be verified in the field for predicted stress distribution and void ratio.

Acknowledgments:

Authors are grateful to BARD for their financial support for this project. They are also indebted to the Goodyear Tire and Rubber Co. for their suggestions and support for this project.

References:

- Al-Hamed, S. A., R. D. Grisso, F. M. Zoz, K. Von Bargaen. 1994. Tractor performance spreadsheet for radial tires. *Computers and Electronics in Agriculture*. 10:45-62.
- Bekker, M. G. 1956. *Theory of land locomotion*. The University of Michigan Press. Ann Arbor. 560p.
- Bekker, M. G. 1960. *Off-the-road locomotion*. The University of Michigan Press. Ann Arbor, 220p.
- Brixius, W. W. 1987. Traction prediction equations for bias ply tires. ASAE paper. 87-1622, ASAE St. Joseph, MI 49085.
- Bowen, H. D. 1982. Alleviating mechanical impedance. In Arkin, G. F. and H. M. Taylor (Eds.) *Modifying root environment to reduce stress*. ASAE Monograph, 34. St. Joseph, MI 141-193.
- Chancellor, W. J. 1993. Generalized stress-strain characteristics for cylindrical soil samples during compaction and shear. ASAE Paper 93-1524. ASAE St. Joseph, MI 41085.
- Gill, W.R. and G.E. VandenBerg. 1968. *Soil dynamics in tillage and traction*. Agricultural Handbook No. 316. U. S. Govt. Printing office. Washington, D. C. 511p.
- Hadas, A. and D. Wolf. 1984. Soil aggregates and clod strength dependence on clod size cultivation and stress load rates. *Soil Sci. Soc. Am.* J.43:1157-1164.
- Hadas, A., D. Wolf., and E. Rawitz. 1983. Zoning soil compaction and cotton stand under controlled traffic conditions. ASAE Paper 83-1042. ASAE, St. Joseph, MI 49085.
- Hadas, A., D. Wolf., and E. Rawitz. 1985. Residual compaction effect on cotton stand and yields. *Trans. ASAE*. 28:691-696.
- Hadas, A., W. E. Larson, and R. R. Allmaras. 1988. Advances in modeling machine-soil-plant interactions. *Soil and Tillage Res.* 11:349-372.
- Hassan, A. and S. K. Upadhyaya. 1991. Effect of soil crust and compaction on infiltration in a Yolo loam soil. ASAE Paper. 91-2081. ASAE St. Joseph, MI 49085.
- Lancas, K. P., S. K. Upadhyaya, and M. Sime. 1995. Traction and soil compaction due to low/correct inflation pressure for radial ply tractor tires. *Proc. 5th North American ISTVS Conference/Workshop*, Saskatoon, SK, CANADA. p11-16.
- LAWR - Cooperative Extension. 1984. *Water penetration in California soils*. Technical Report. Joint Infiltration Committee. Dept. of LAWR, UC Davis, CA. 95616.
- Nowatzki, E.A. and L. L. Karafiath. 1978. *Soil mechanics for off-road vehicle engineering*. Trans. Tech. Pub. Aeder Mannsdorf, Switzerland. 515p.
- Reismann, H. and P. S. Pawlik. 1980. *Elasticity: Theory and applications*. John Wiley and sons. NY 425 p.

- Russell, R. S., and M. J. Goss. 1974. Physical aspects of soil fertility: The response of roots to mechanical impedance. *Neth. J. Agr. Sci.* 22:305-318.
- Trause, A. C. 1971. Soil conditions as they affect plant establishment, root development and yields. In Barnes, K. K. et al. (Eds.). *Compaction of Agricultural Soils*. ASAE Monograph #1, St. Joseph, MI 225-276p.
- Upadhyaya, S. K. 1988. Effect of tread design on bias ply tire traction characteristics. *Trans. ASAE*. 31(5):1338-1344.
- Upadhyaya, S. K. and D. Wulfsohn. 1989. An overview of traction research at the University of California, Davis. *California Agriculture* 43(2):15-17.
- Upadhyaya, S. K., D. Wulfsohn, and G. Jubbal. 1989. Traction prediction equations for radial ply tires. *J. Terramechanics*. 26(2):149-175.
- Upadhyaya, S. K. and D. Wulfsohn 1990. Review of traction prediction equations. ASAE Paper. No. 90 -1573., ASAE St. Joseph, MI 49085.
- Upadhyaya, S. K. and D. Wulfsohn. 1990. Relationship between tire deflection characteristics and 2-D tire contact area. *Trans. ASAE*. 33(1):25-30.
- Upadhyaya, S.K. and D. Wulfsohn, 1993. Traction prediction using soil parameters obtained with an instrumented analog device. *J. Terramech*. 30(2):85-100.
- Upadhyaya, S. K., D. Wulfsohn, and J. Mehlschau. 1993. An instrumented device to obtain traction related parameters. *J. Terramech*. 30(1):1-20.
- Wiley, J. C., B. E. Roming, L. V. Anderson, and F. M. Zoz. 1992. Optimizing dynamic stability and performance of tractors with radial tires. ASAE Paper No. 92-1586. ASAE St. Joseph, MI 49085.
- Wisner, R. D. and H. J. Luth. 1972. Off-road traction prediction for wheeled vehicles. *J. Terramech.*, 10:49-61.
- Wolf, D. and A. Hadas. 1983. Conventional vs. controlled traffic and precision tillage systems for cotton. ASAE Paper 83-1040. ASAE, St. Joseph, MI 49085.
- Wolf, D. and A. Hadas. 1984. Soil compaction effects on cotton emergence. *Trans. ASAE*. 27:655-659.
- Wong, J. Y. 1980. *Theory of ground vehicles*. Wiley and Sons, NY, 380p.
- Wulfsohn, D., S. K. Upadhyaya, and W. J. Cahncellor. 1988. Tractive characteristics of radial ply tires in a California soil. *J. Terramechanics*. 25(2):111-134.
- Yong, R. N., E. A. Fattah, and N. Skiadas. 1984. *Vehicle traction mechanics*. Elsevier, Amsterdam, 307p.
- Zoz, F. M. and R. J. Turner. 1994. Effect of "correct" pressure on tractive efficiency of radial ply tires. ASAE Paper No. 94-1051., ASAE St. JOseph, MI 49085.

Table 1. Soil and tire parameter used in predicting tractive ability of tires.

Number	Tire	Axle Load KN	Infl. Pres. kPa	Soil Type	Soil Cond.	Sinkage (100 mm)		Coh., C kPa	Phi degree	Shear mod mm	CI kPa	Density kg/m ³	MC %
						Const., K	Exp., n						
11	4	19.34	62.05	2	2	295.9	1	22.79	11.3	8.41	283.08	1170	7.82
25	4	13.5	103.42	2	4	256.4	1	13.93	21.3	8.81	194.68	1140	11.5
36	4	25.68	103.42	2	3	679.6	0.9	2.41	36.86	16.7	347.72	1180	16.29
94	3	15.05	82.73	2	2	295.9	1	22.79	11.3	8.41	283.08	1170	7.82
129	2	26.55	62.05	2	1	494.6	0.9	1.54	33.02	9.66	380.27	1150	9.41
135	2	26.54	103.42	2	1	494.6	0.9	1.54	33.02	9.66	380.27	1150	9.41
137	2	20.19	62.05	2	2	295.9	1	22.79	11.3	8.41	283.08	1170	7.82
154	1	14.47	62.05	1	2	304.5	1	3.53	33.42	3.12	164.26	1320	5.82
168	1	26.44	82.73	1	4	177.6	1	11.93	30.96	2.6	122.29	1230	8.6
186	2	26.86	82.73	1	3	3410	0.9	5.22	35.37	6.62	1146.8	1440	16.77
202	2	14.98	82.73	1	2	304.5	1	3.53	33.42	3.12	164.26	1320	5.82
236	3	21.47	62.05	1	2	304.5	1	3.53	33.42	3.12	164.26	1320	5.82
257	4	19.75	82.73	1	3	3410	0.9	5.22	35.37	6.62	1146.8	1440	16.77
258	4	25.76	82.73	1	3	3410	0.9	5.22	35.37	6.62	1146.8	1440	16.77
269	4	19.37	103.42	1	4	177.6	1	11.93	30.96	2.6	122.29	1230	8.6

Tire: 1 - 16.9R38, 2 - 18.4R38, 3 - 24.5R32, 4 - 13.6R28

Soil: 1 - Yolo Loam, 2 - Capay Clay

Soil Cond.: 1 - NT-Dry, 2 - T-Dry, 3 - NT-Wet, 4 - T-Wet

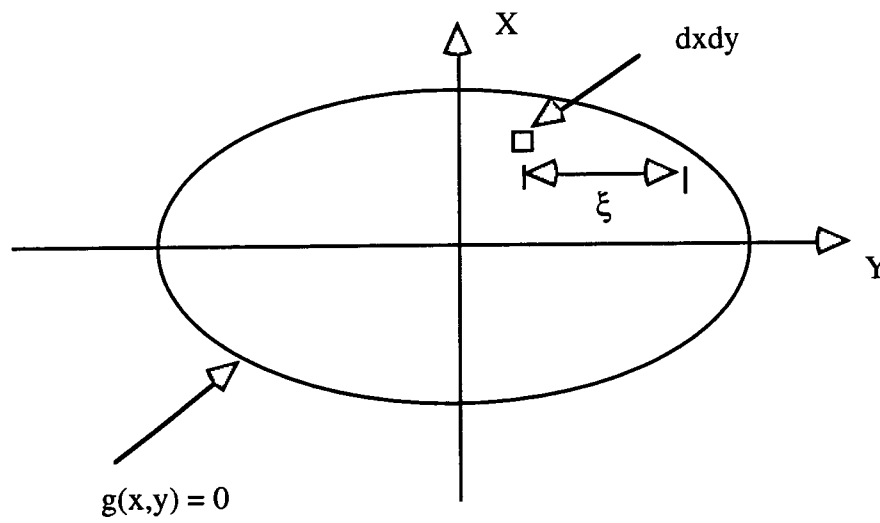


Figure 1. Evaluation of net traction and input torque for the case of 2-D analytical model.

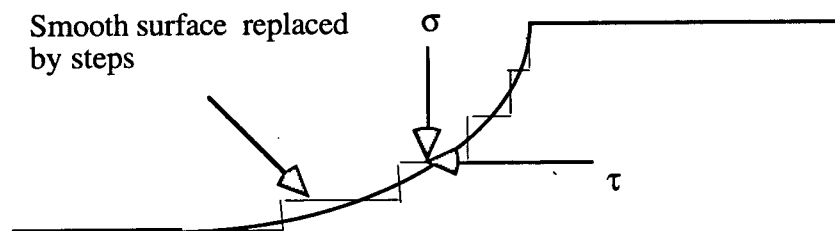


Figure 2. Approximating the smooth 3-D surface by steps.

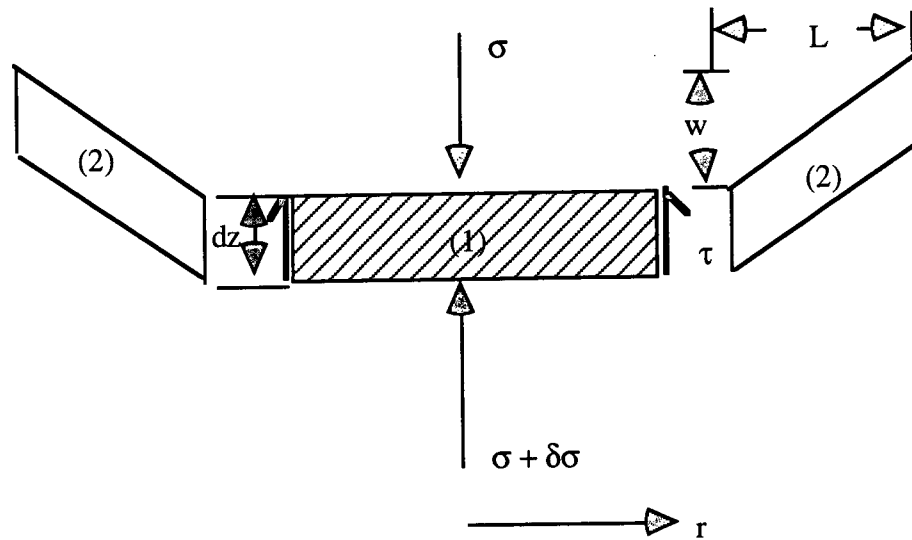


Figure 3a. Soil mass in vertical equilibrium

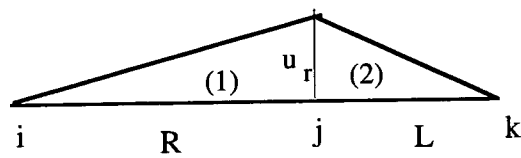


Fig. 3b. Radial deformation

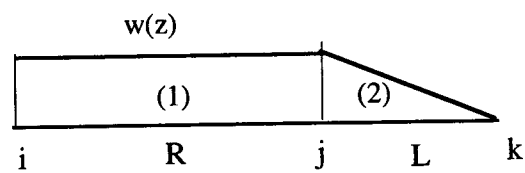


Fig. 3c. Vertical deformation

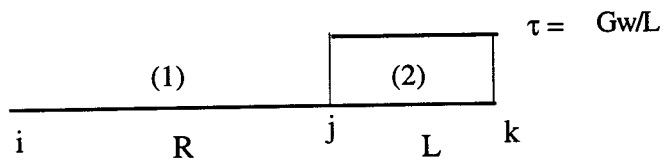


Fig 3d. Shear stress distribution

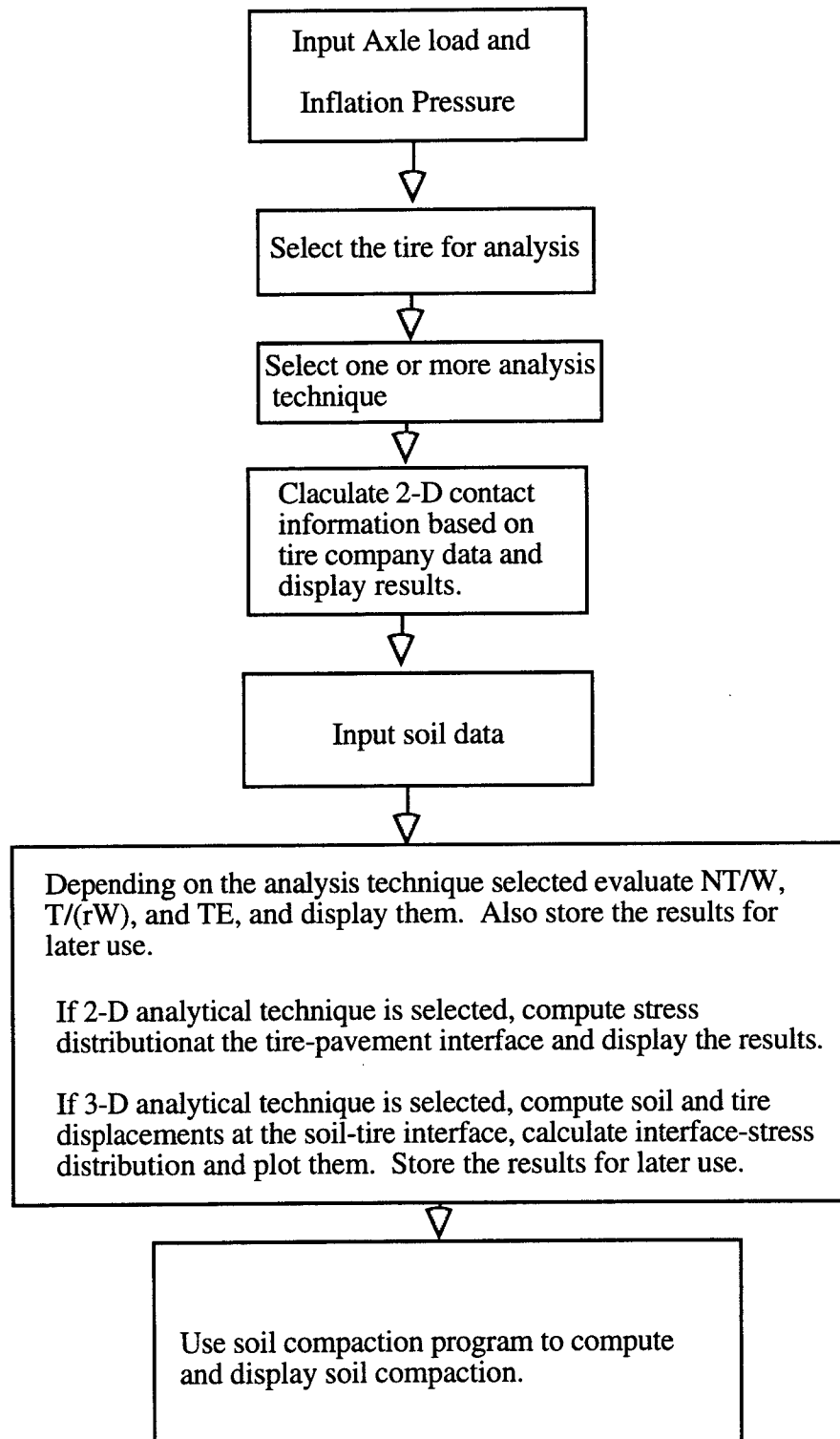


Figure 4. Block diagram of the traction-soil compaction prediction program.

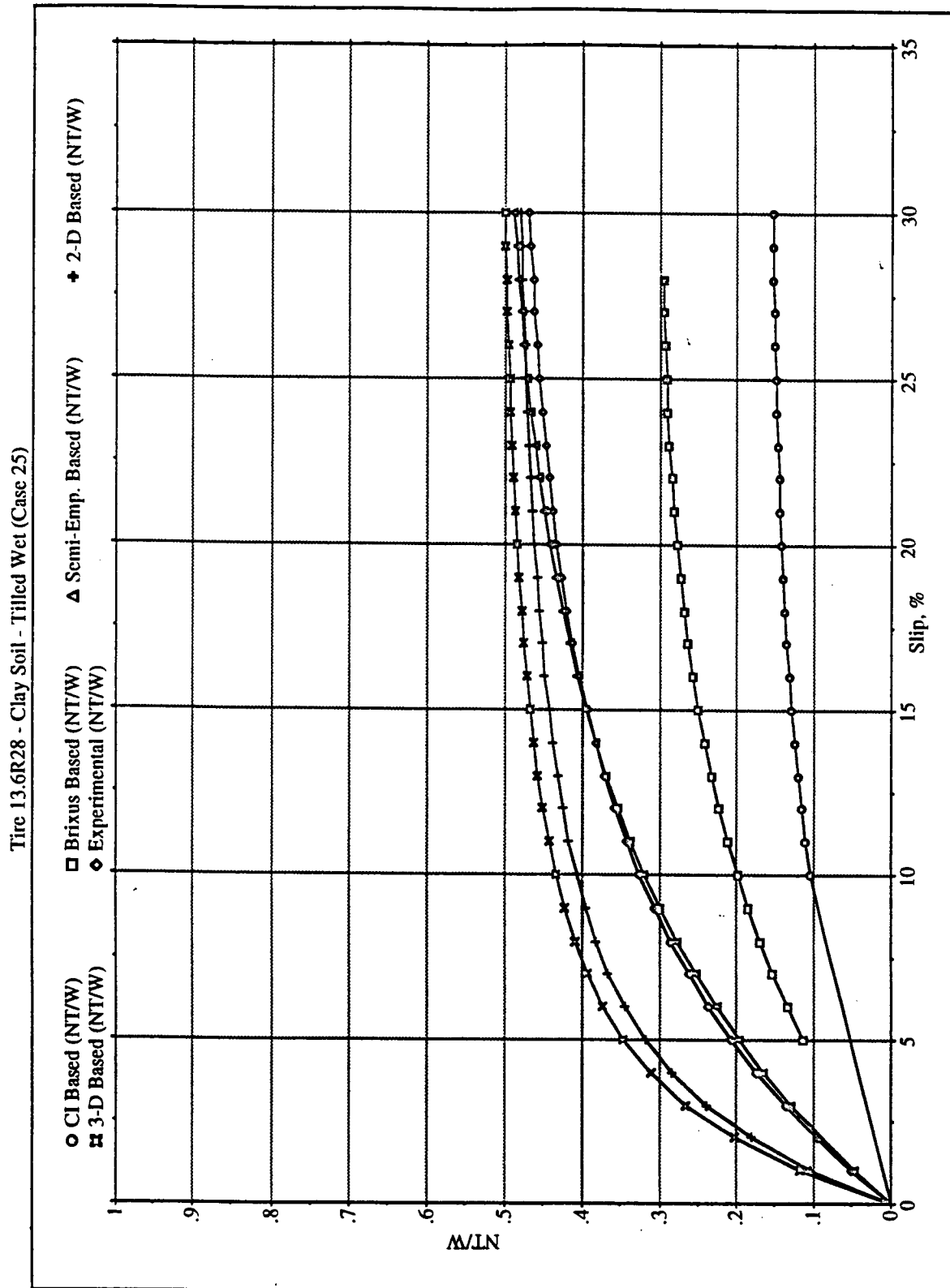


Figure 5a: Comparison of net traction coefficient for a 13.6R28 tire in a wet, tilled Capay clay soil at 13.5 kN axle load and 103 kPa inflation pressure.

Tire 13.6R28 - Clay Soil - Tilled Wet (Case 25)

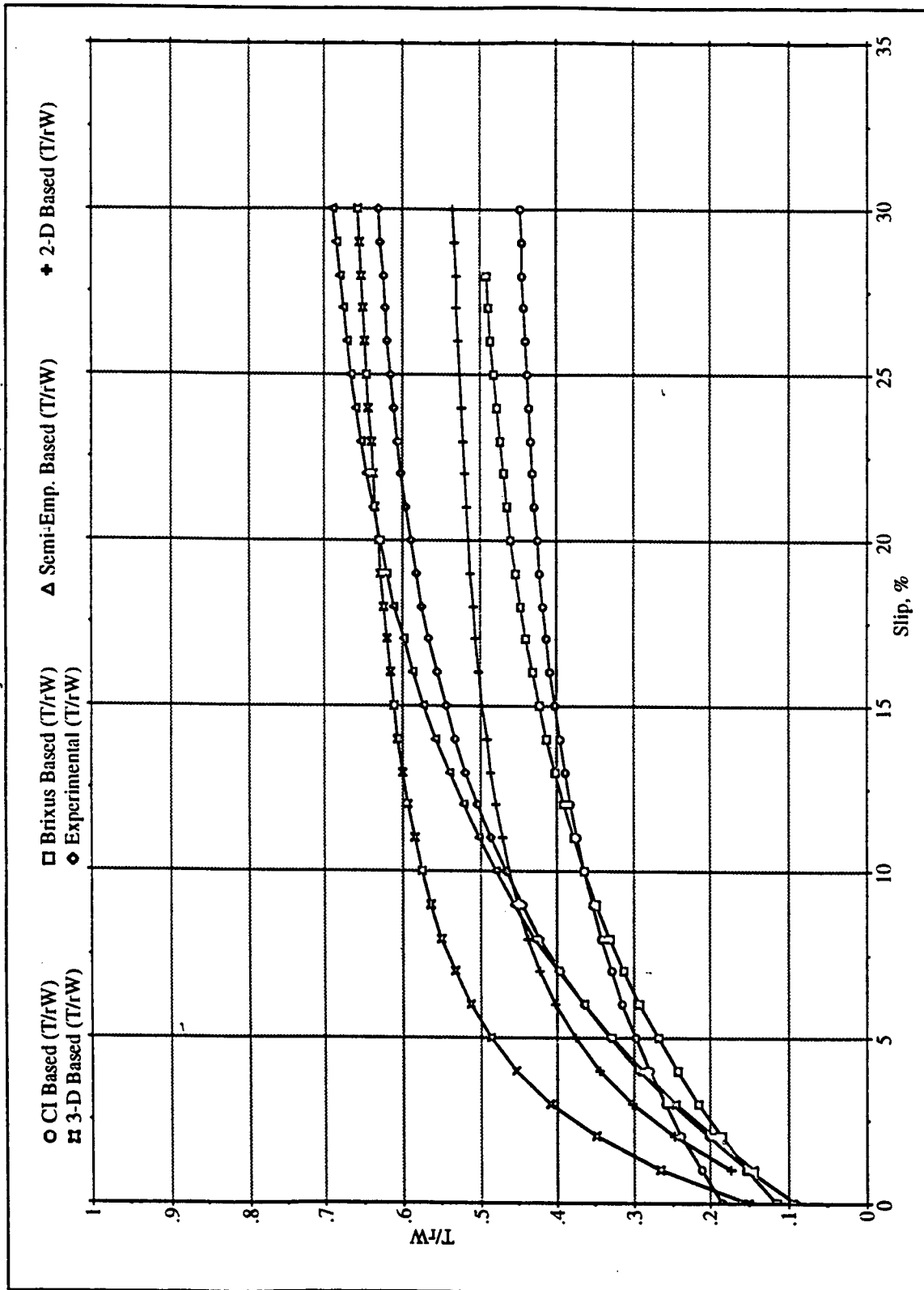


Figure 5b: Comparison of gross traction coefficient for a 13.6R28 tire in a wet, tilled Capay clay soil at 13.5 kN axle load and 103 kPa inflation pressure.

Tire 13.6R28 - Clay Soil - Tilled Wet (Case 25)

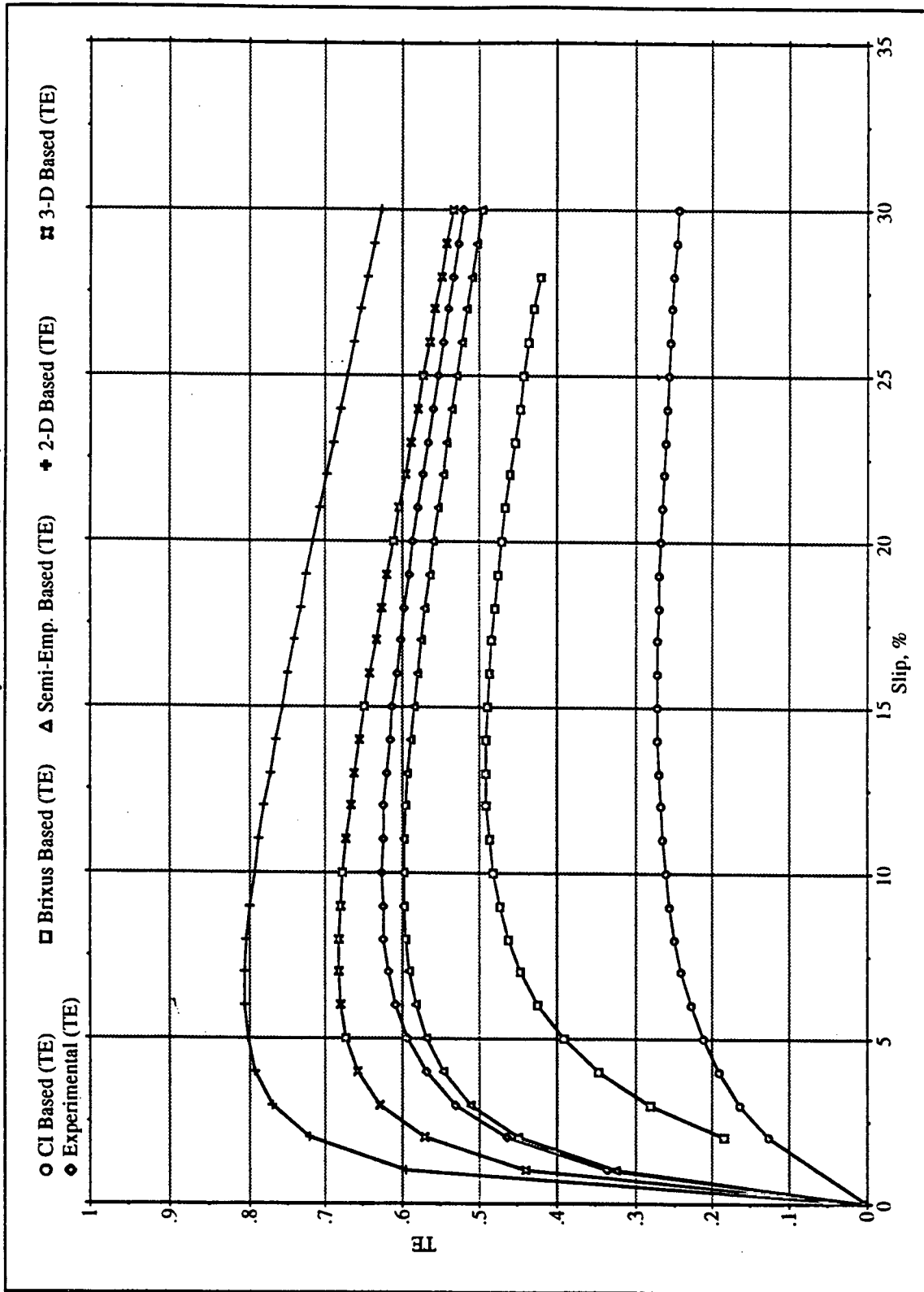


Figure 5c: Comparison of tractive efficiency for a 13.6R28 tire in a wet, tilled Capay clay soil at 13.5 kN axle load and 103 kPa inflation pressure.

Tire 24.5R32 - Clay Soil - Tilled Dry (Case 94)

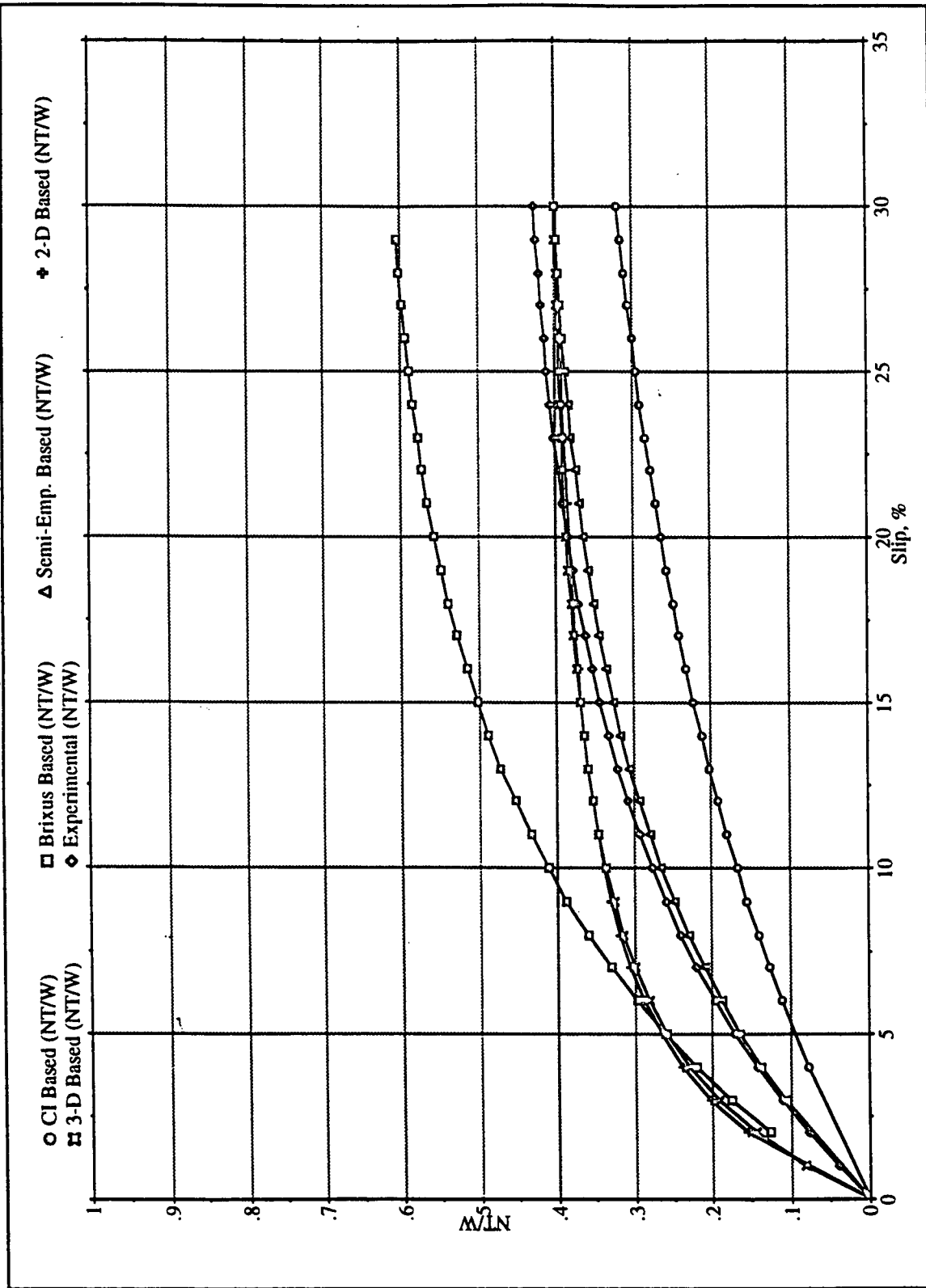


Figure 6a: Comparison of net traction coefficient for a 24.5R32 tire in a dry, tilled Capay clay soil at 15 kN axle load and 83 kPa inflation pressure.

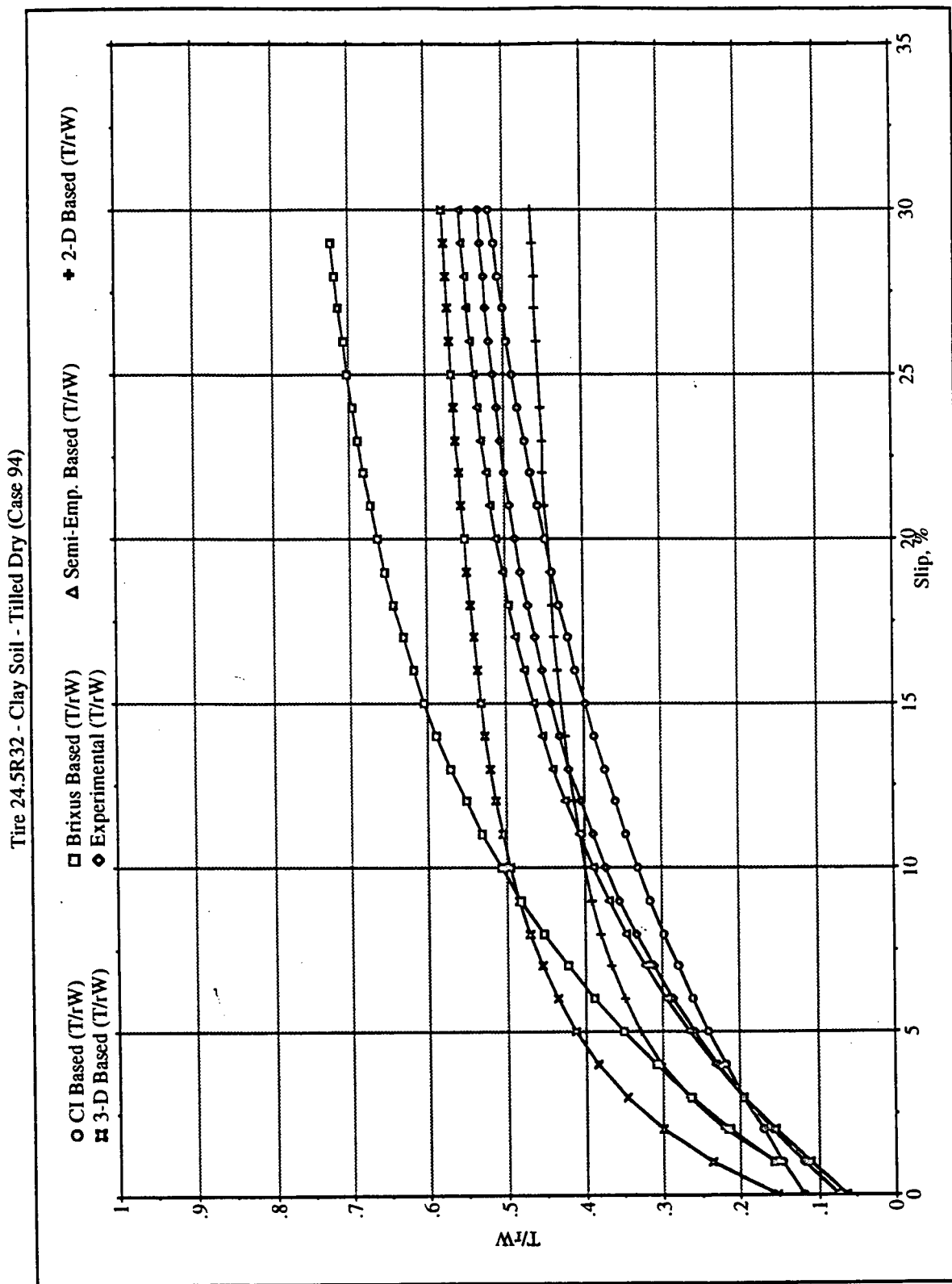


Figure 6b: Comparison of gross traction coefficient for a 24.5R32 tire in a dry, tilled Capay clay soil at 15 kN axle load and 83 kPa inflation pressure.

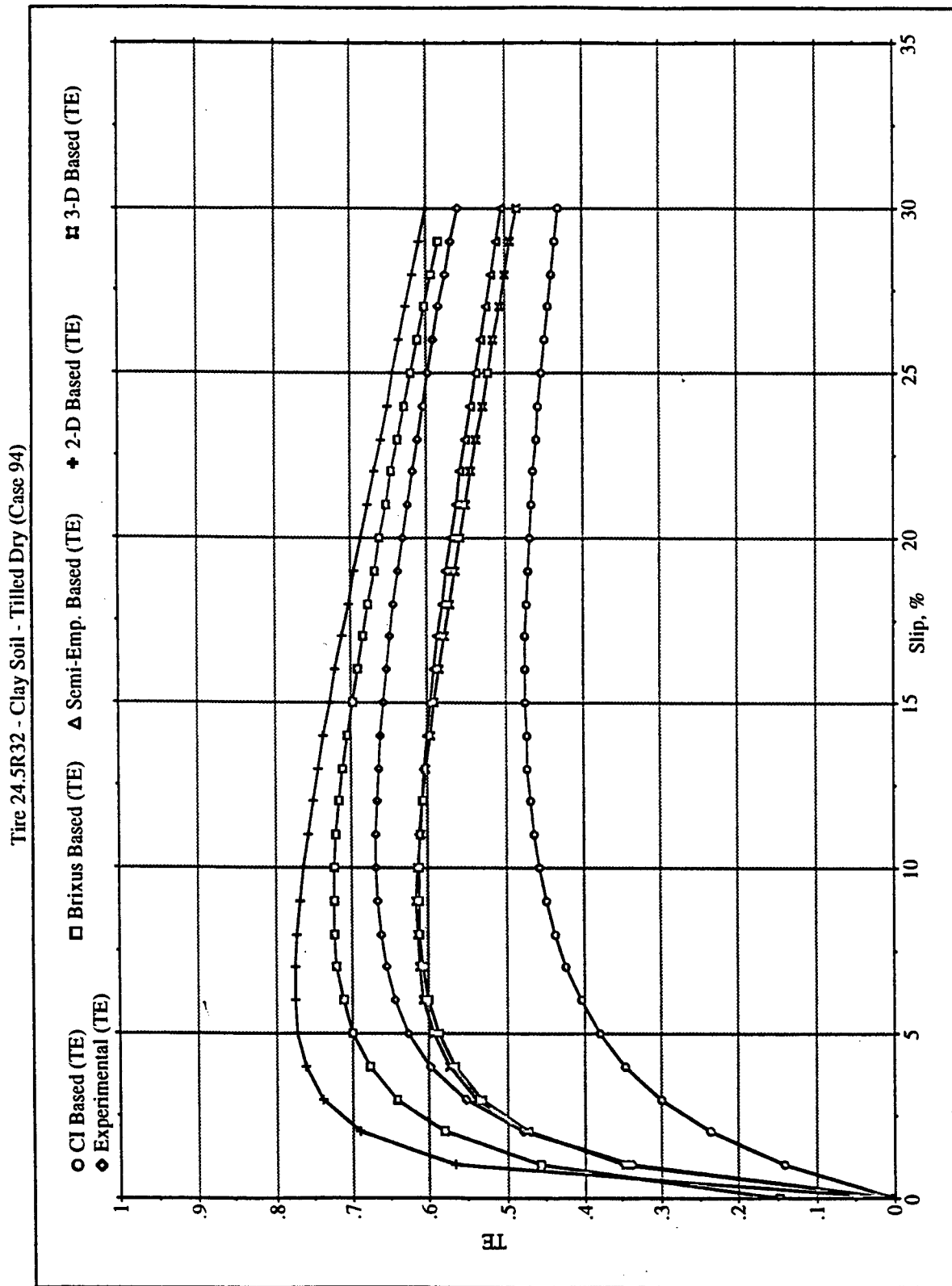


Figure 6c: Comparison of tractive efficiency for a 24.5R32 tire in a dry, tilled Capay clay soil at 15 kN axle load and 83 kPa inflation pressure.

Tire 18.4R38 - Clay Soil - Untilled Dry (Case 135)

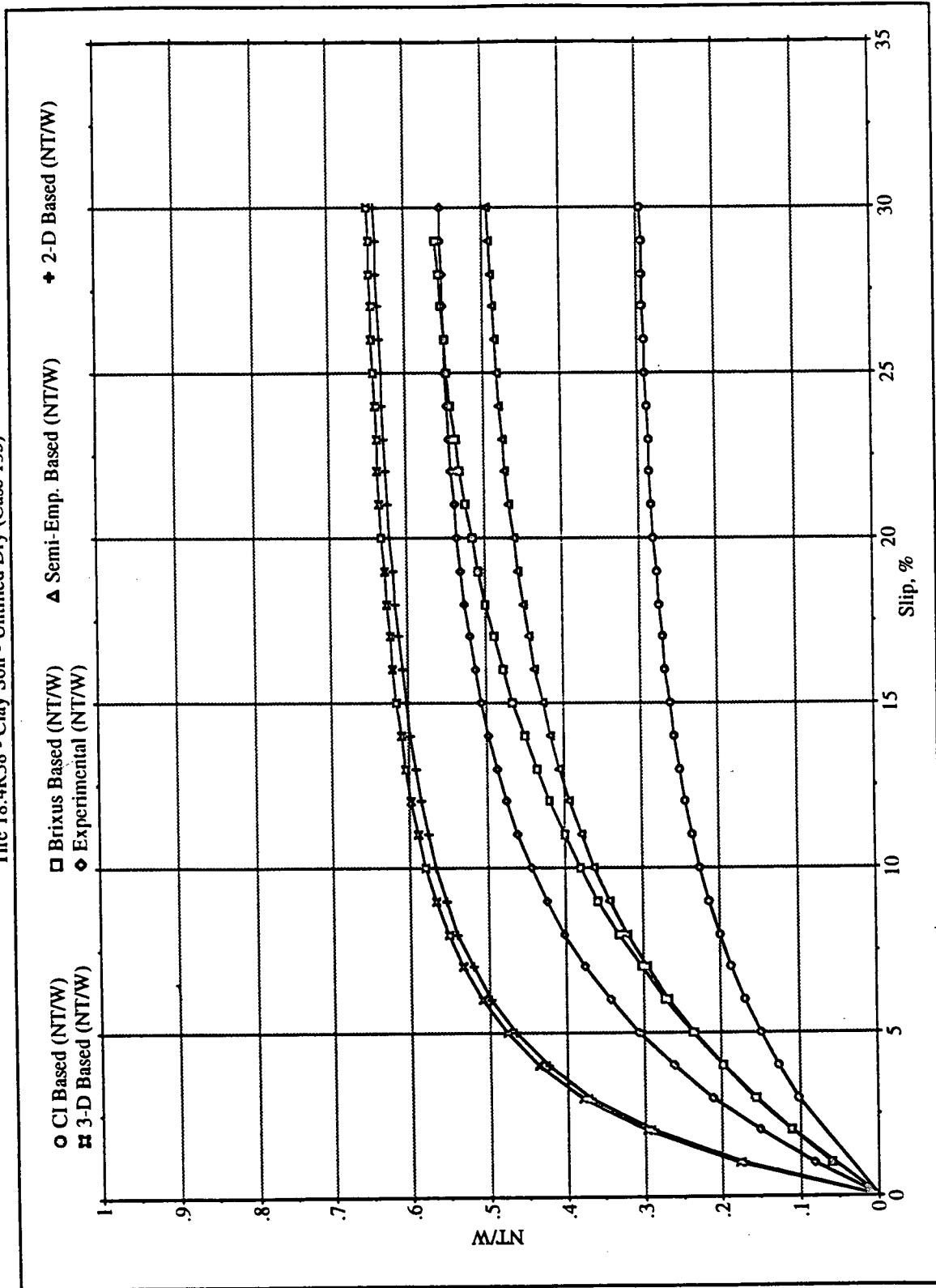


Figure 7a: Comparison of net traction coefficient for a 18.4R38 tire in a dry, untilled Capay clay soil at 26.5 kN axle load and 103 kPa inflation pressure.

Tire 18.4R38 - Clay Soil - Untilled Dry (Case 135)

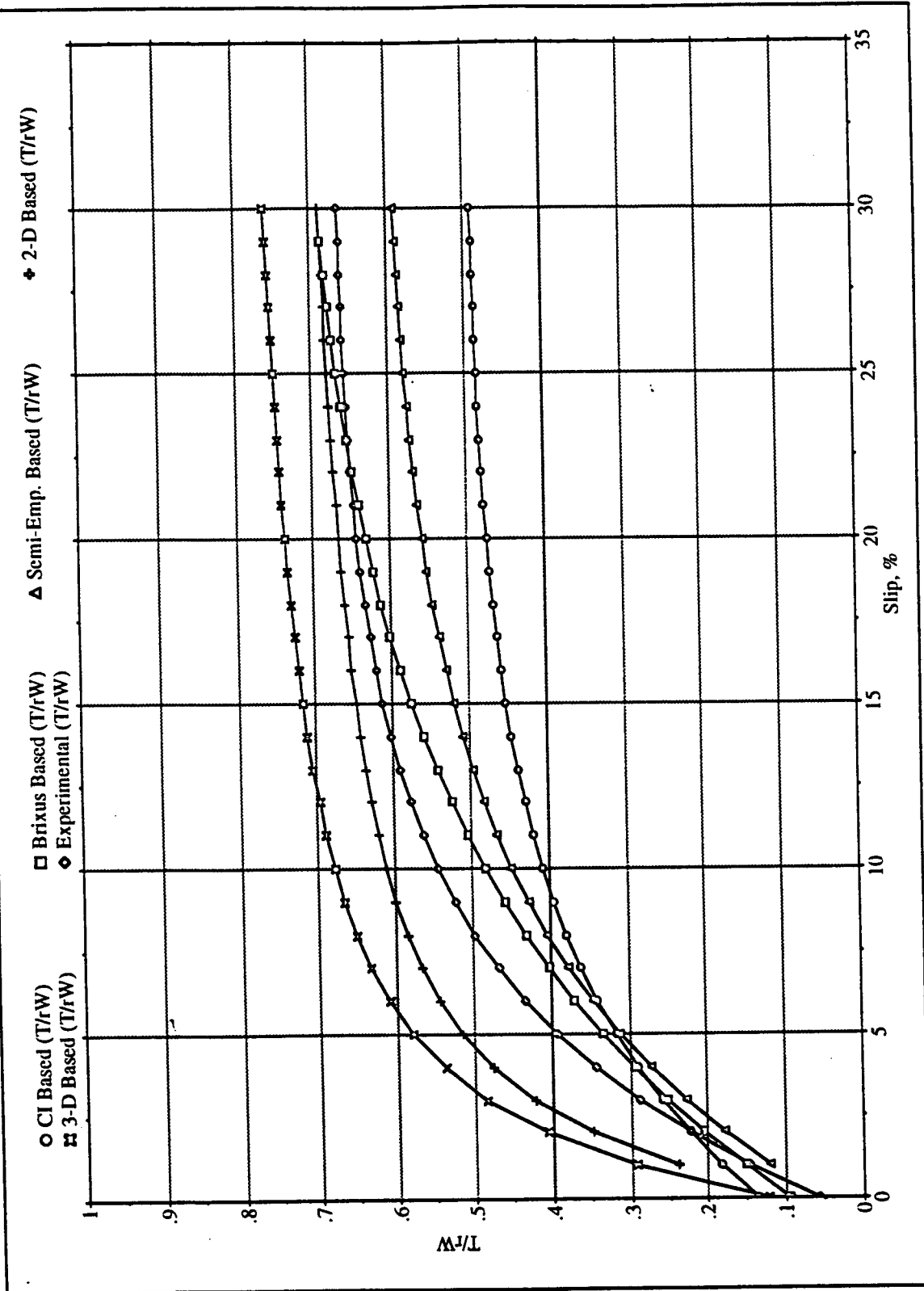


Figure 7b: Comparison of gross traction coefficient for a 18.4R38 tire in a dry, untilled Capay clay soil at 26.5 kN axle load and 103 kPa inflation pressure.

Tire 18.4R38 - Clay Soil - Untilled Dry (Case 135)

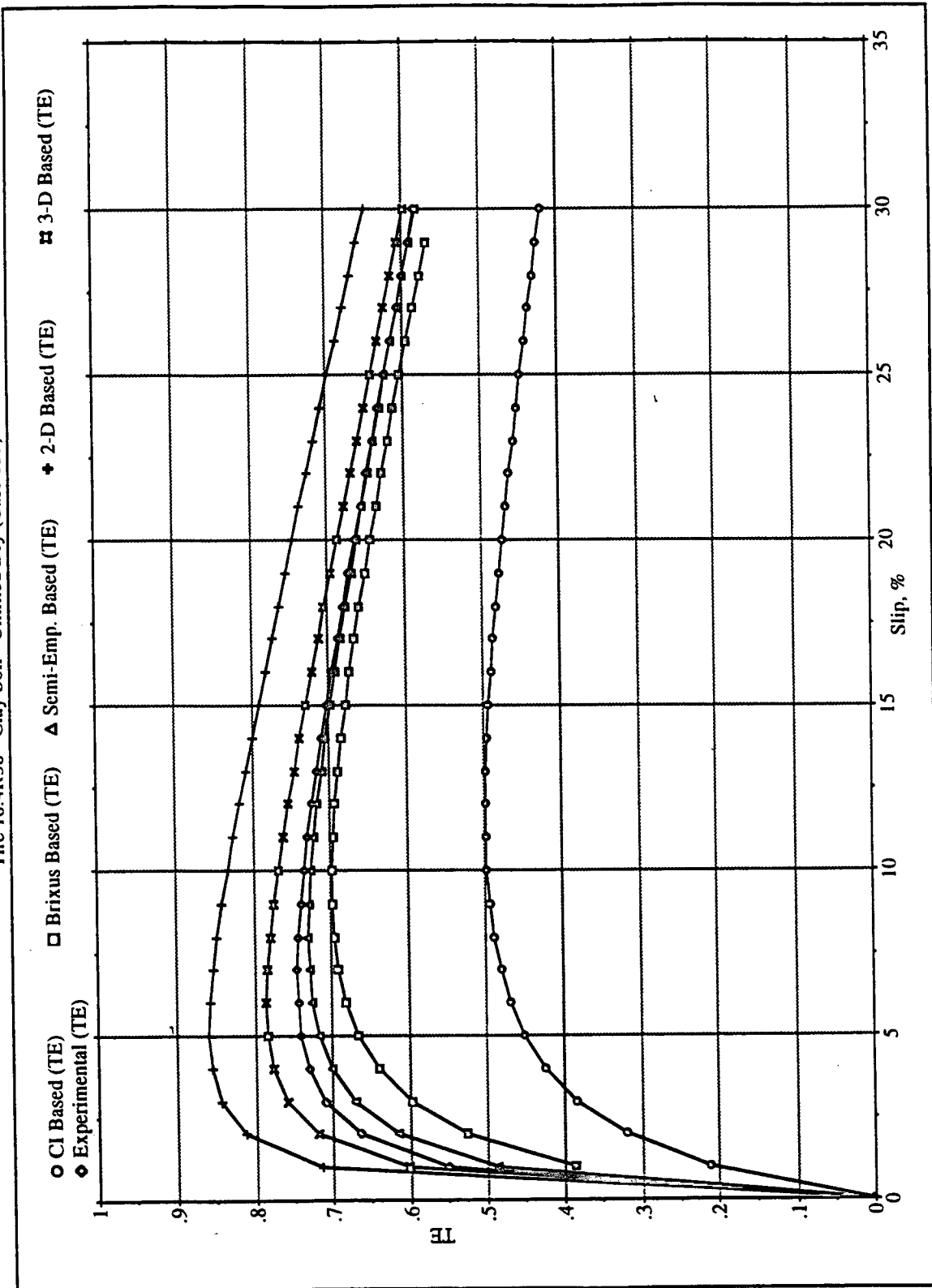


Figure 7c: Comparison of tractive efficiency for a 18.4R38 tire in a dry, untilled Capay clay soil at 26.5 kN axle load and 103 kPa inflation pressure.

Tire 16.9R38 - Yolo Loam Soil - Tilled Wet (Case 168)

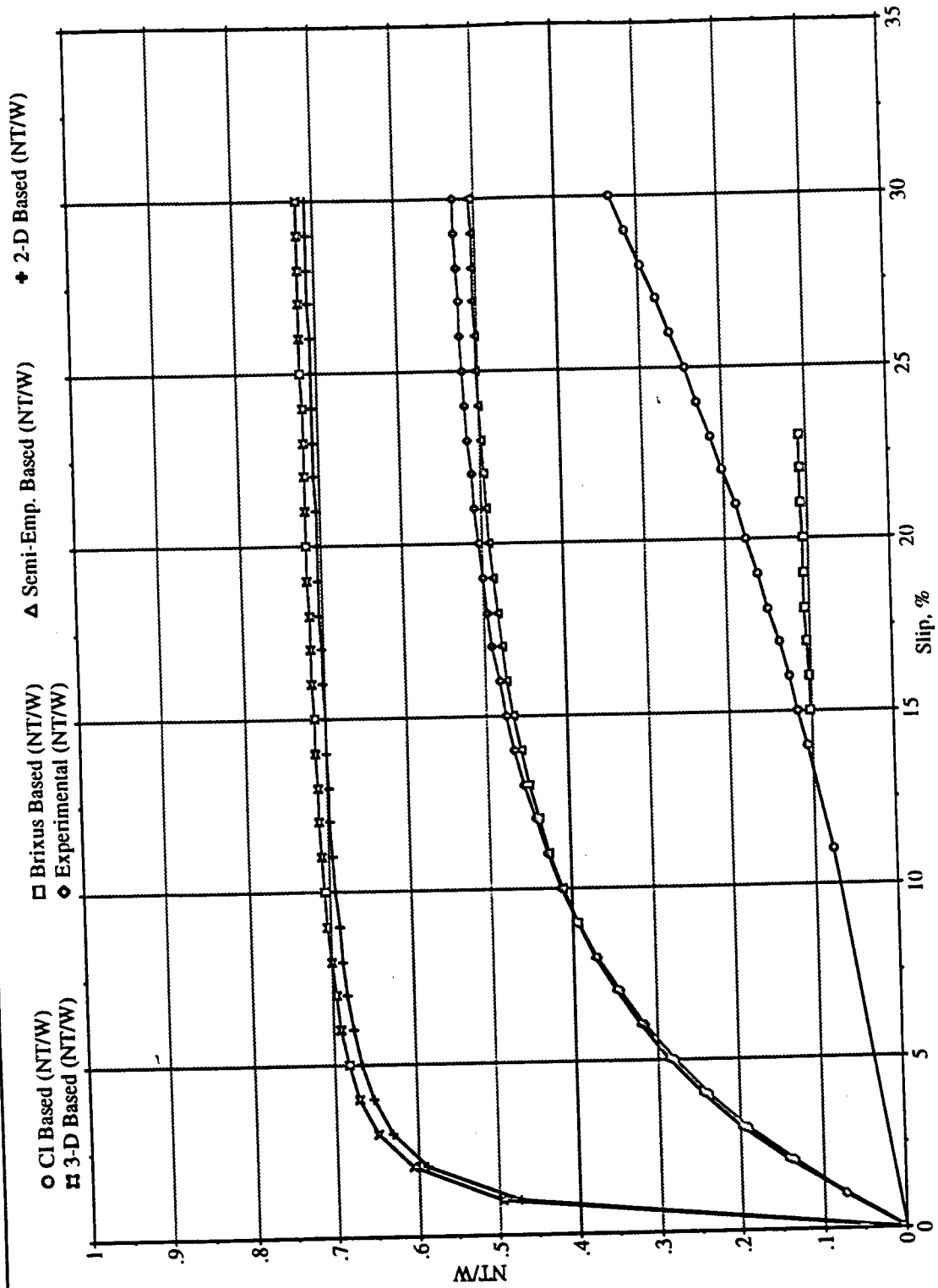


Figure 8a: Comparison of net traction coefficient for a 16.9R38 tire in a wet, tilled Yolo loam soil at 26.4 kN axle load and 83 kPa inflation pressure.

Tire 16.9R38 - Yolo Loam Soil - Tilled Wet (Case 168)

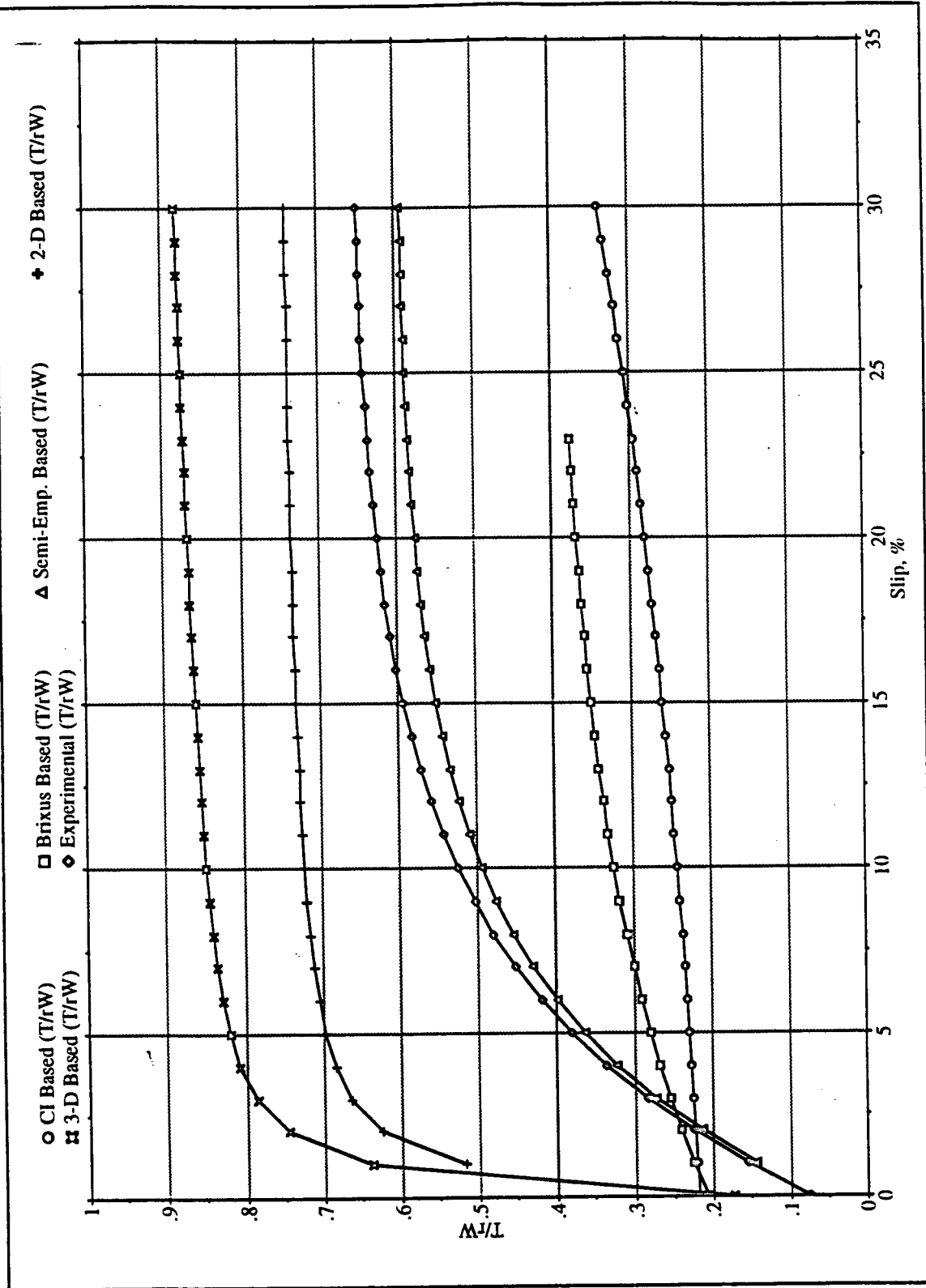


Figure 8b: Comparison of gross traction coefficient for a 16.9R38 tire in a wet, tilled Yolo loam soil at 26.4 kN axle load and 83 kPa inflation pressure.

Tire 16.9R38 - Yolo Loam Soil - Tilled Wet (Case 168)

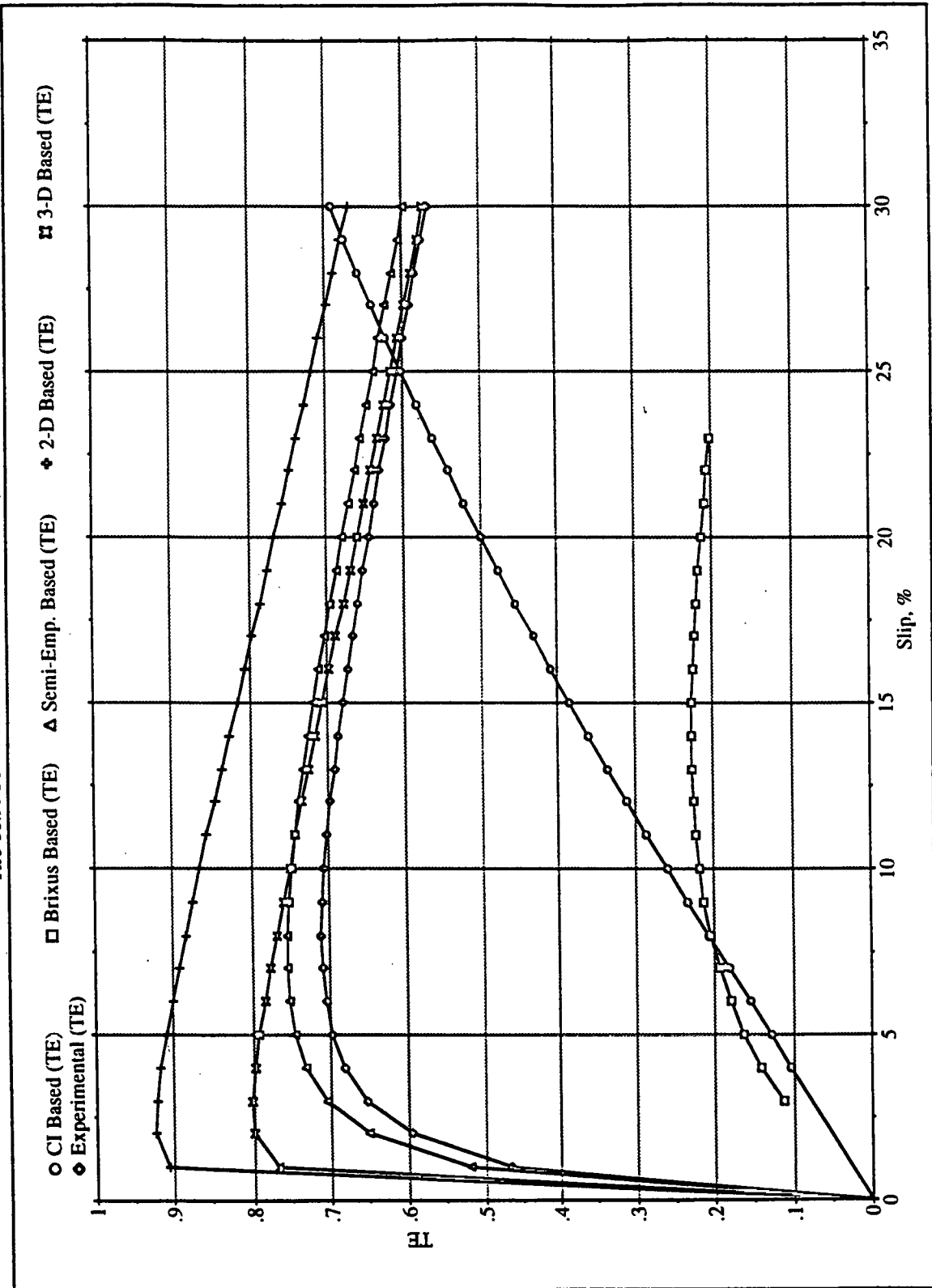


Figure 8c: Comparison of tractive efficiency for a 16.9R38 tire in a wet, tilled Yolo loam soil at 26.4 kN axle load and 83 kPa inflation pressure.

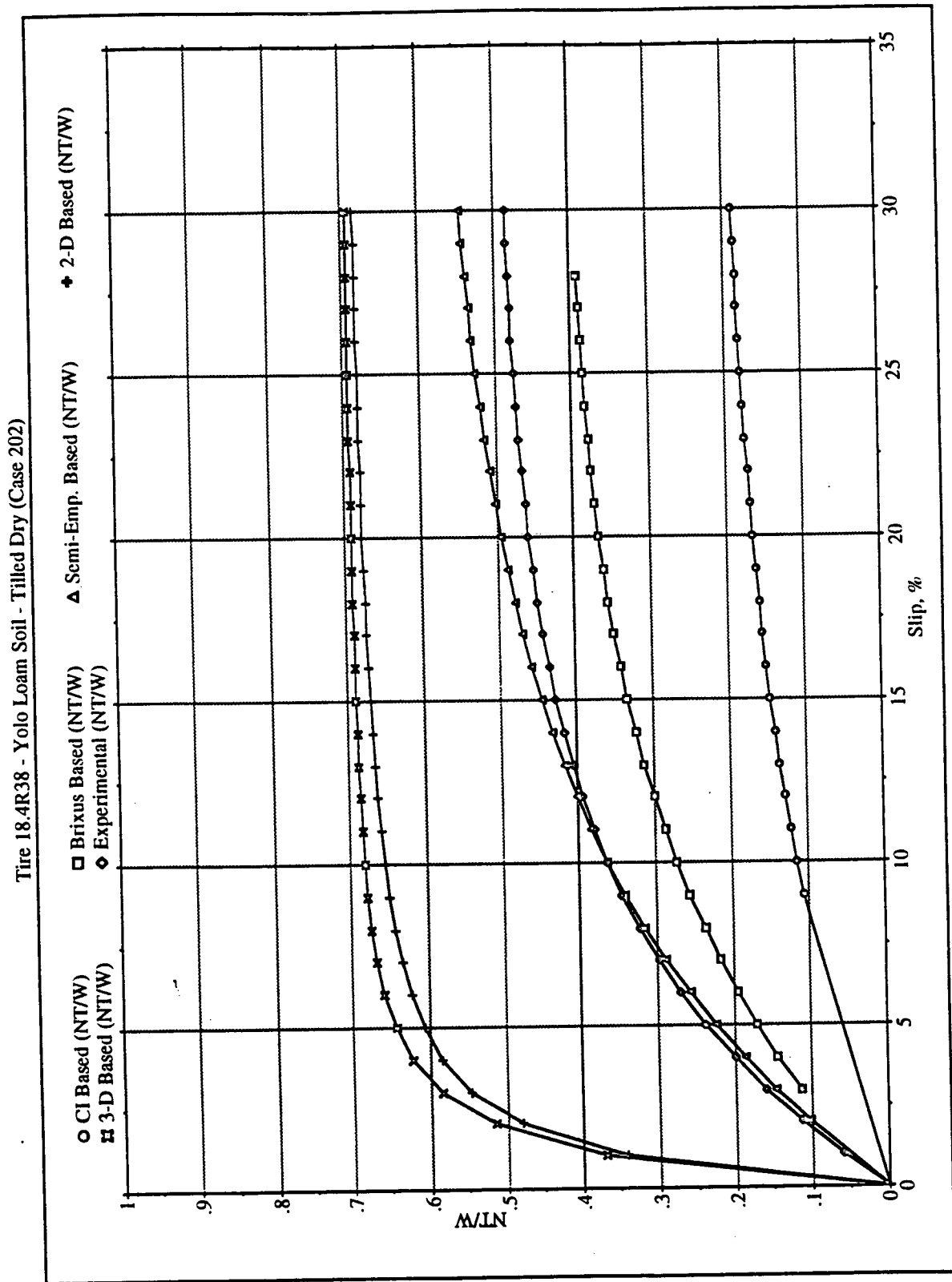


Figure 9a: Comparison of net traction coefficient for a 18.4R38 tire in a dry, tilled Yolo loam soil at 15 kN axle load and 83 kPa inflation pressure.

Tire 18.4R38 - Yolo Loam Soil - Tilled Dry (Case 202)

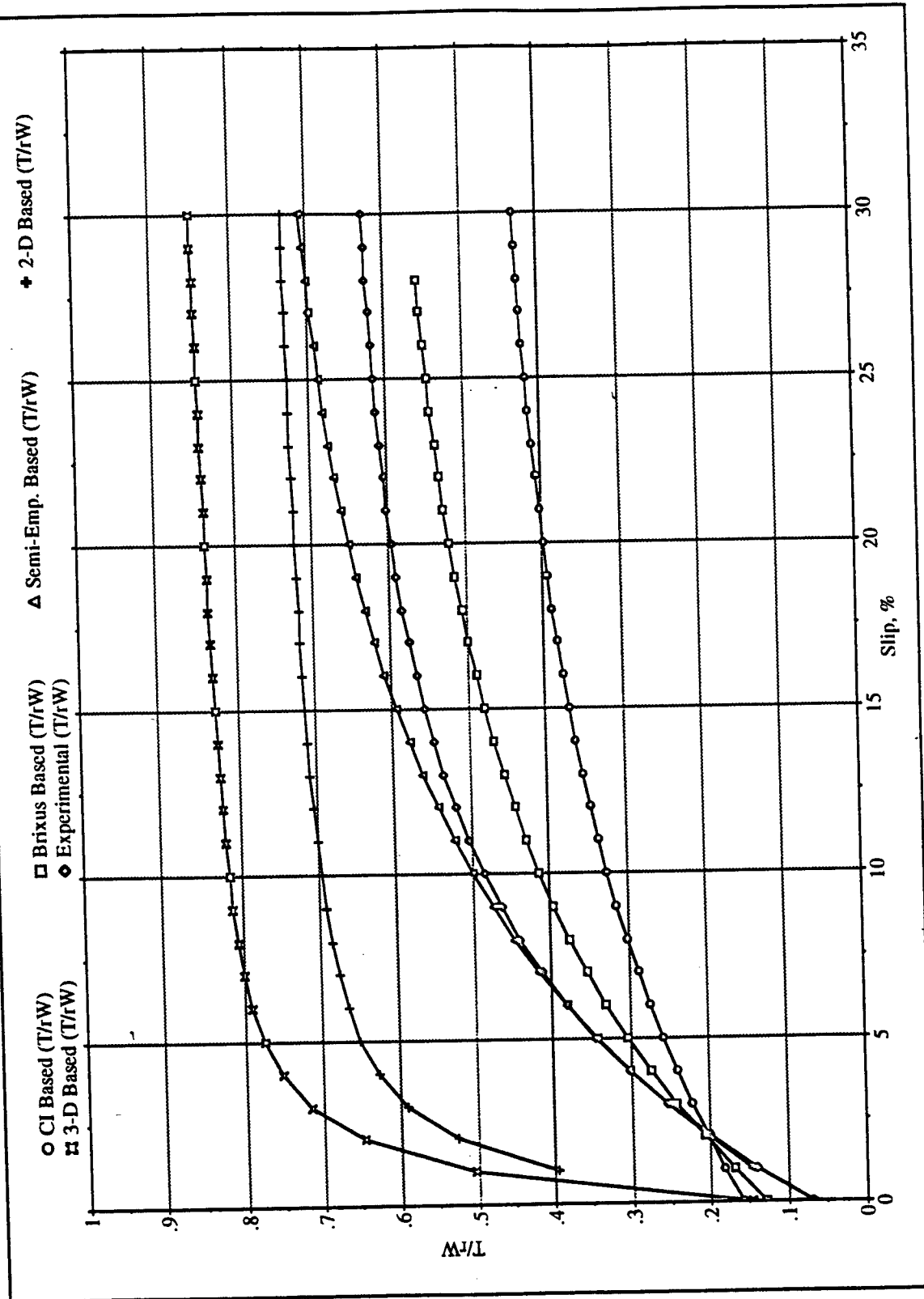


Figure 9b: Comparison of gross traction coefficient for a 18.4R38 tire in a dry, tilled Yolo loam soil at 15 kN axle load and 83 kPa inflation pressure.

Tire 18.4R38 - Yolo Loam Soil - Tilled Dry (Case 202)

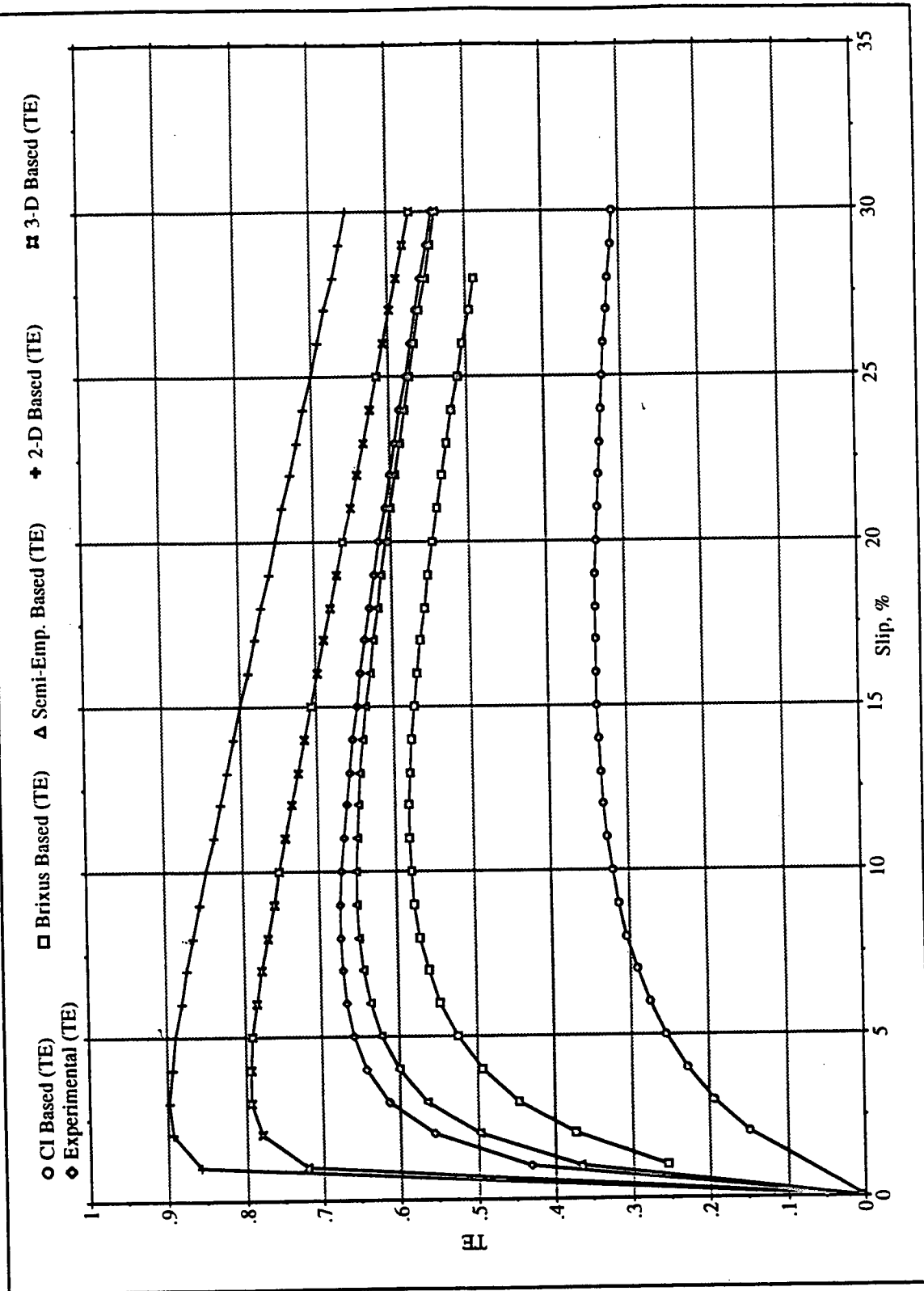


Figure 9c: Comparison of tractive efficiency for a 18.4R38 tire in a dry, tilled Yolo loam soil at 15 kN axle load and 83 kPa inflation pressure.

Tire 13.6R28 - Yolo Loam Soil - Untilled Wet (Case 257)

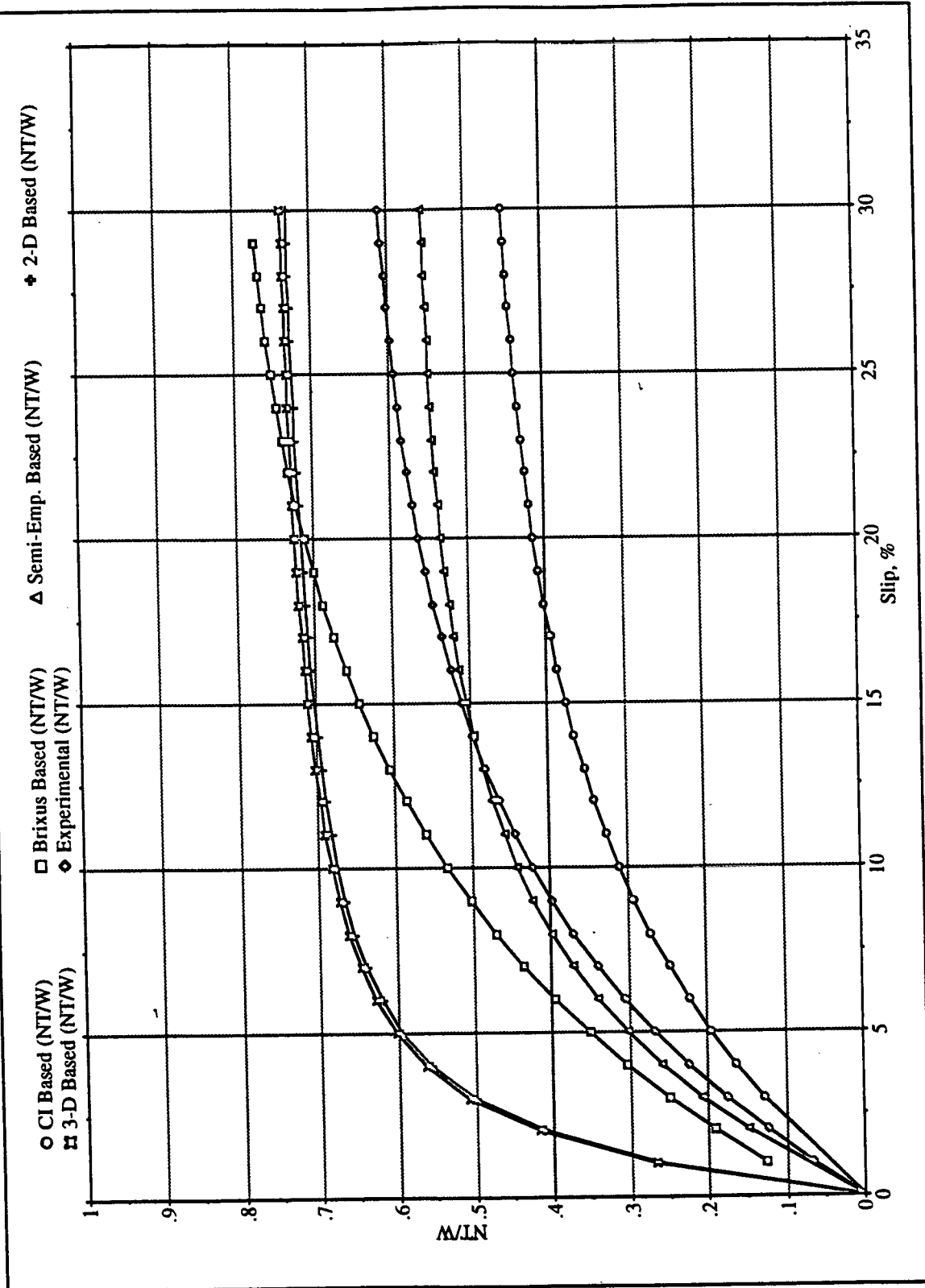


Figure 10a: Comparison of net traction coefficient for a 13.6R28 tire in a wet, untilled Yolo loam soil at 19.8 kN axle load and 83 kPa inflation pressure.

Tire 13.6R28 - Yolo Loam Soil - Untilled Wet (Case 257)

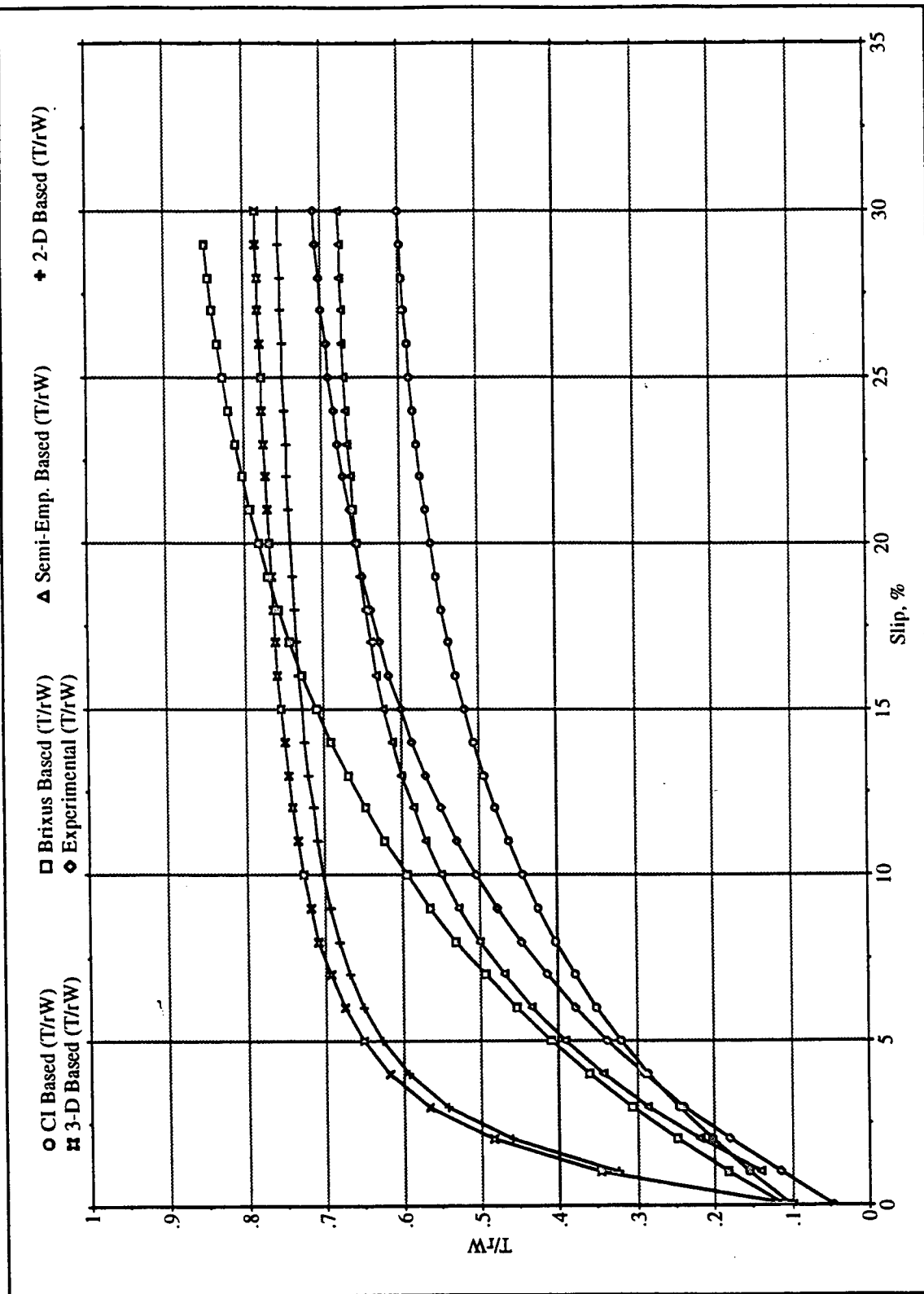


Figure 10b: Comparison of gross traction coefficient for a 18.4R38 tire in a dry, tilled Yolo loam soil at 15 kN axle load and 83 kPa inflation pressure.

Tire 13.6R28 - Yolo Loam Soil - Untilled Wet (Case 257)

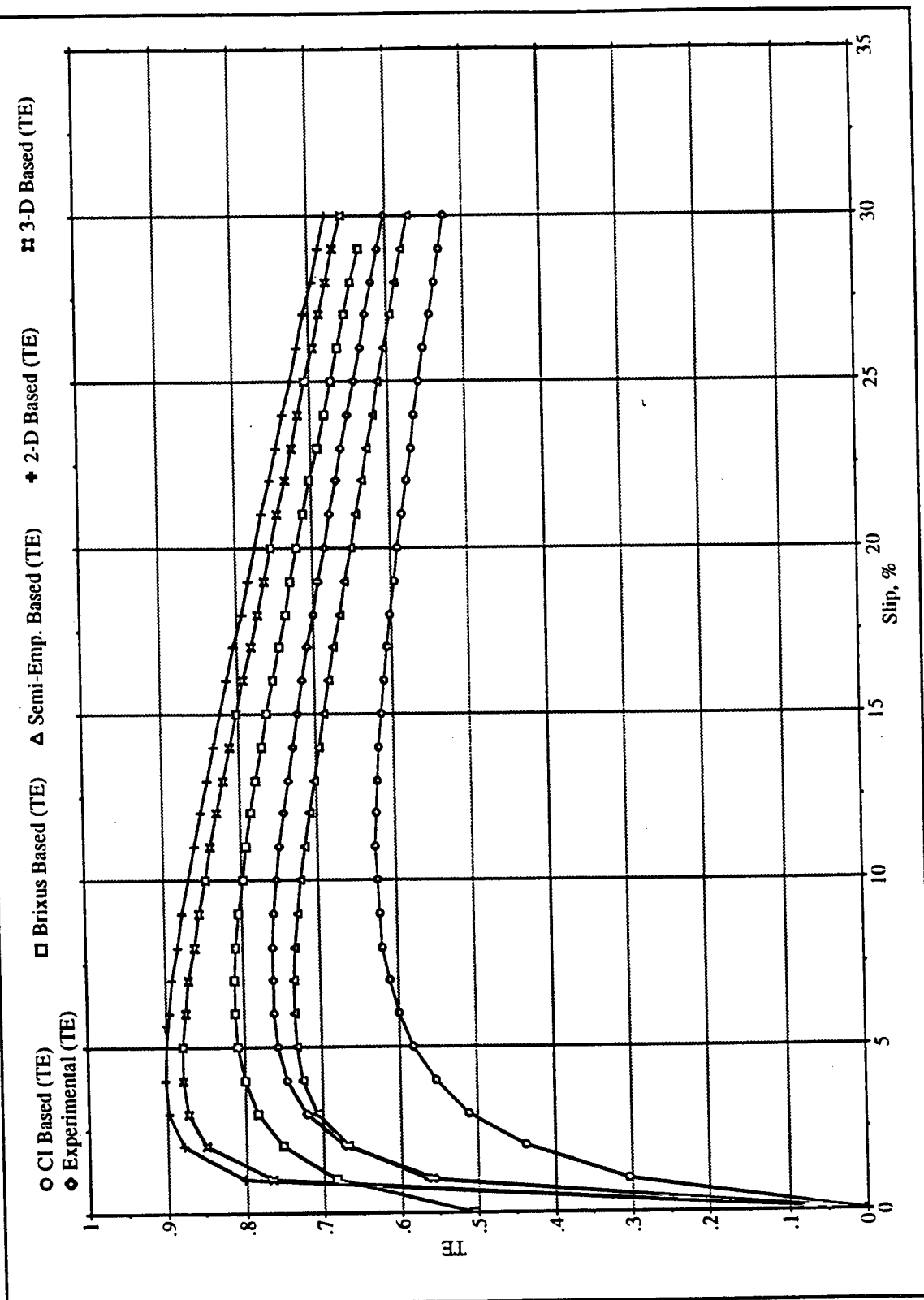


Figure 10c: Comparison of tractive efficiency for a 18.4R38 tire in a dry, tilled Yolo loam soil at 15 kN axle load and 83 kPa inflation pressure.

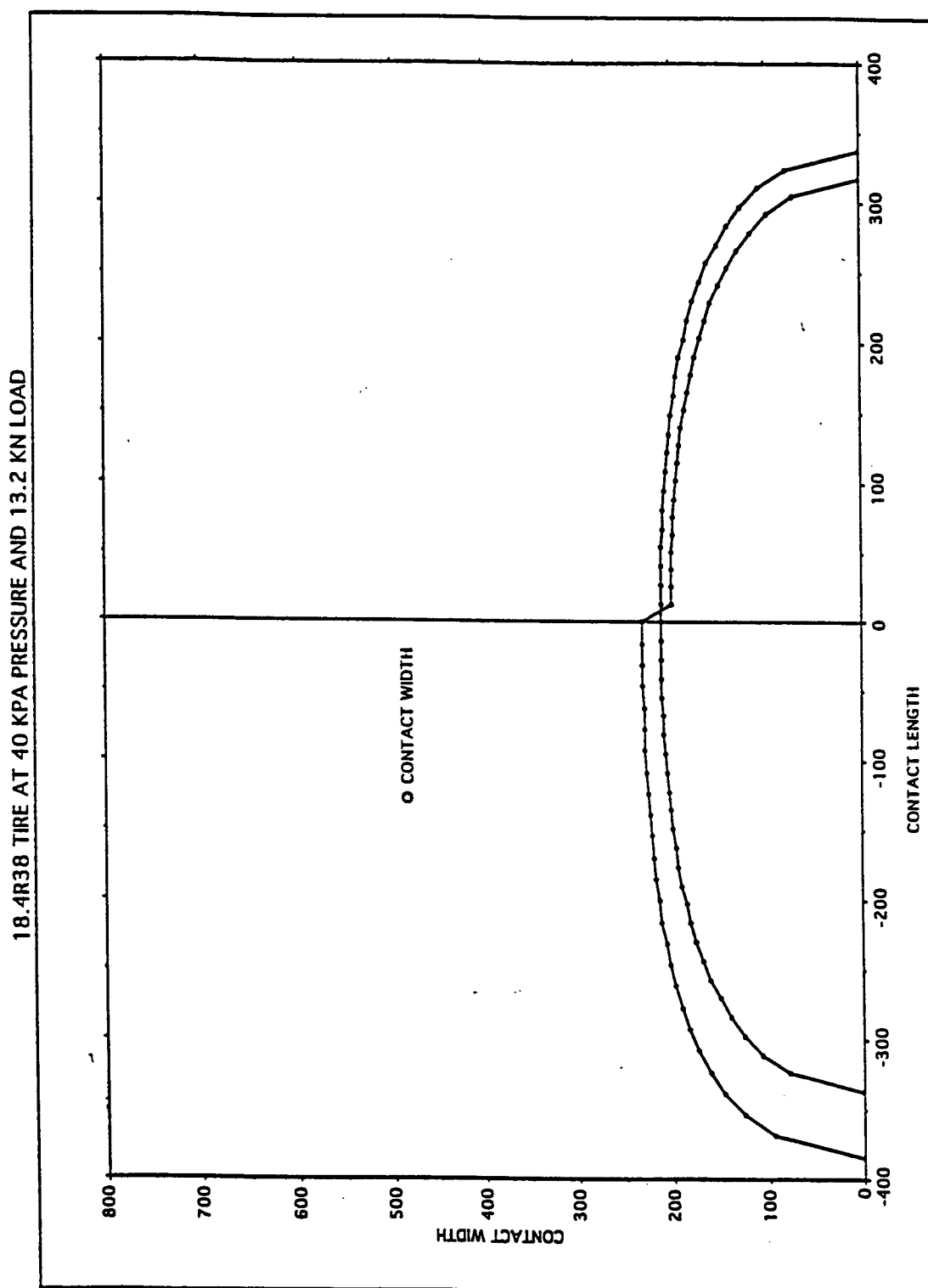


Figure 11. The footprint of a 18.4 R 38 tire on a hard surface as well as soil surface at 40 kPa inflation pressure and 13.2 kN axle load.

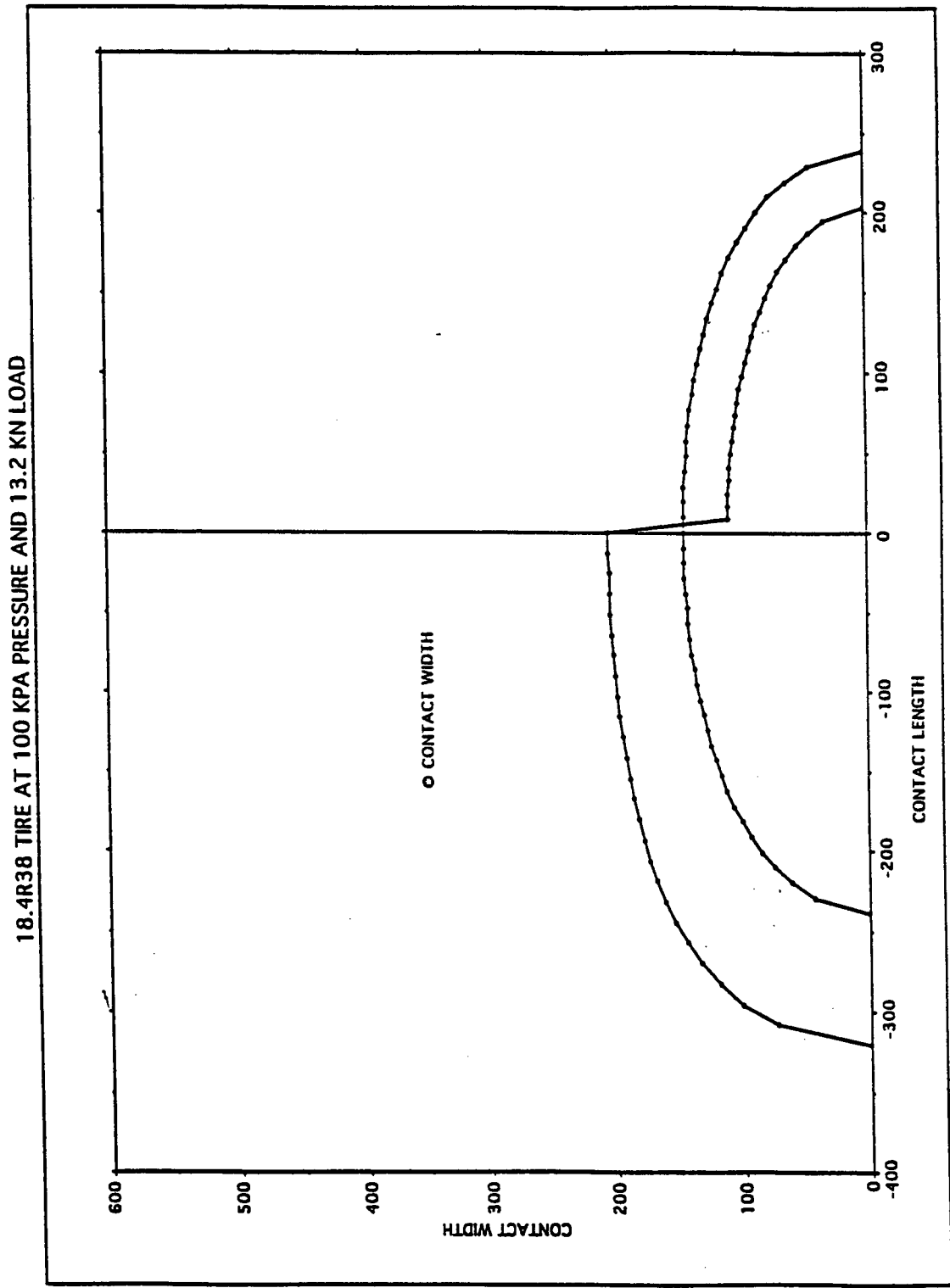


Figure 12: The footprint of a 18.4 R 38 tire on a hard surface at 100 kPa inflation pressure and 13.2 kN axle load.

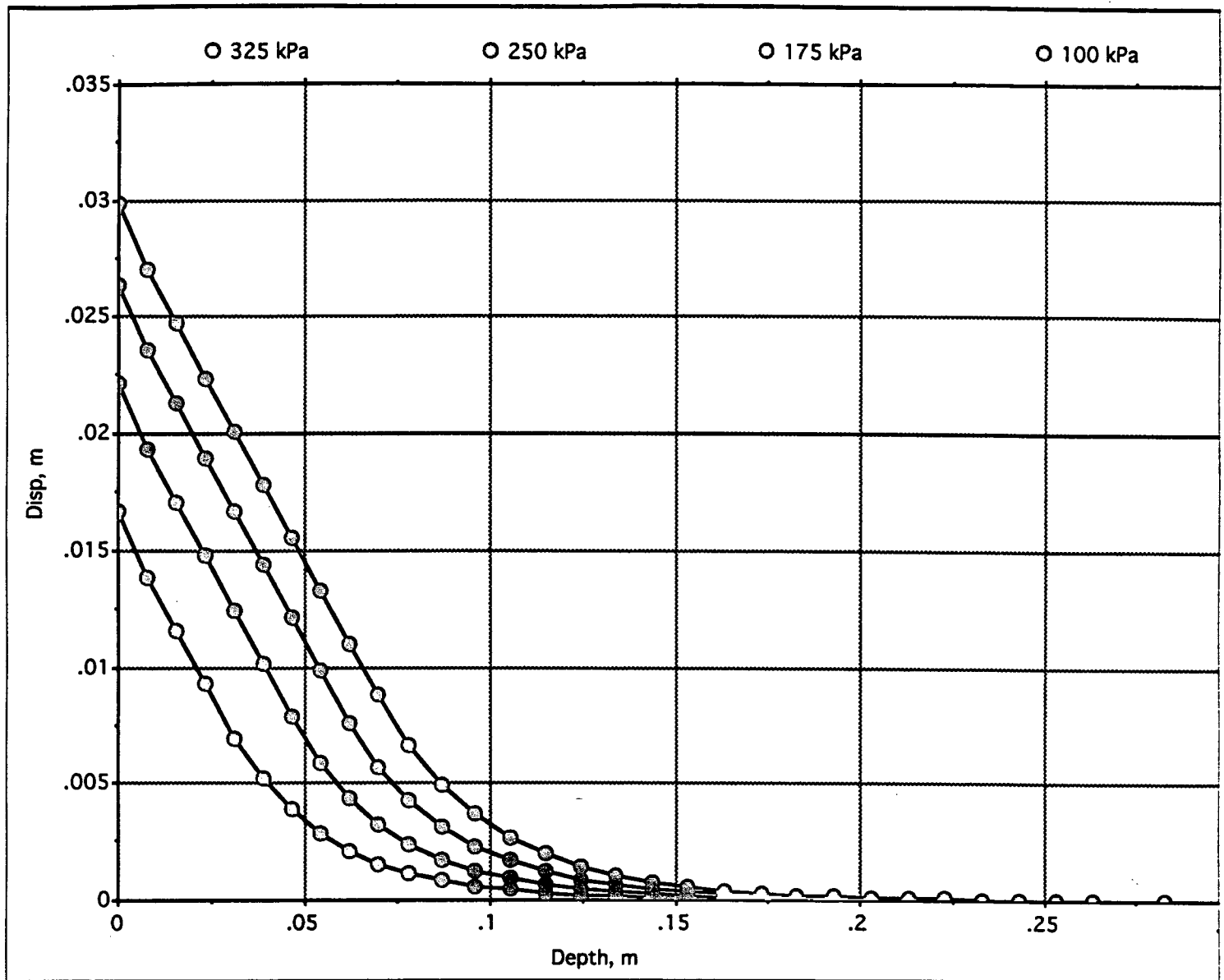


Figure 13: Effect of plate load on soil displacement as a function of depth.

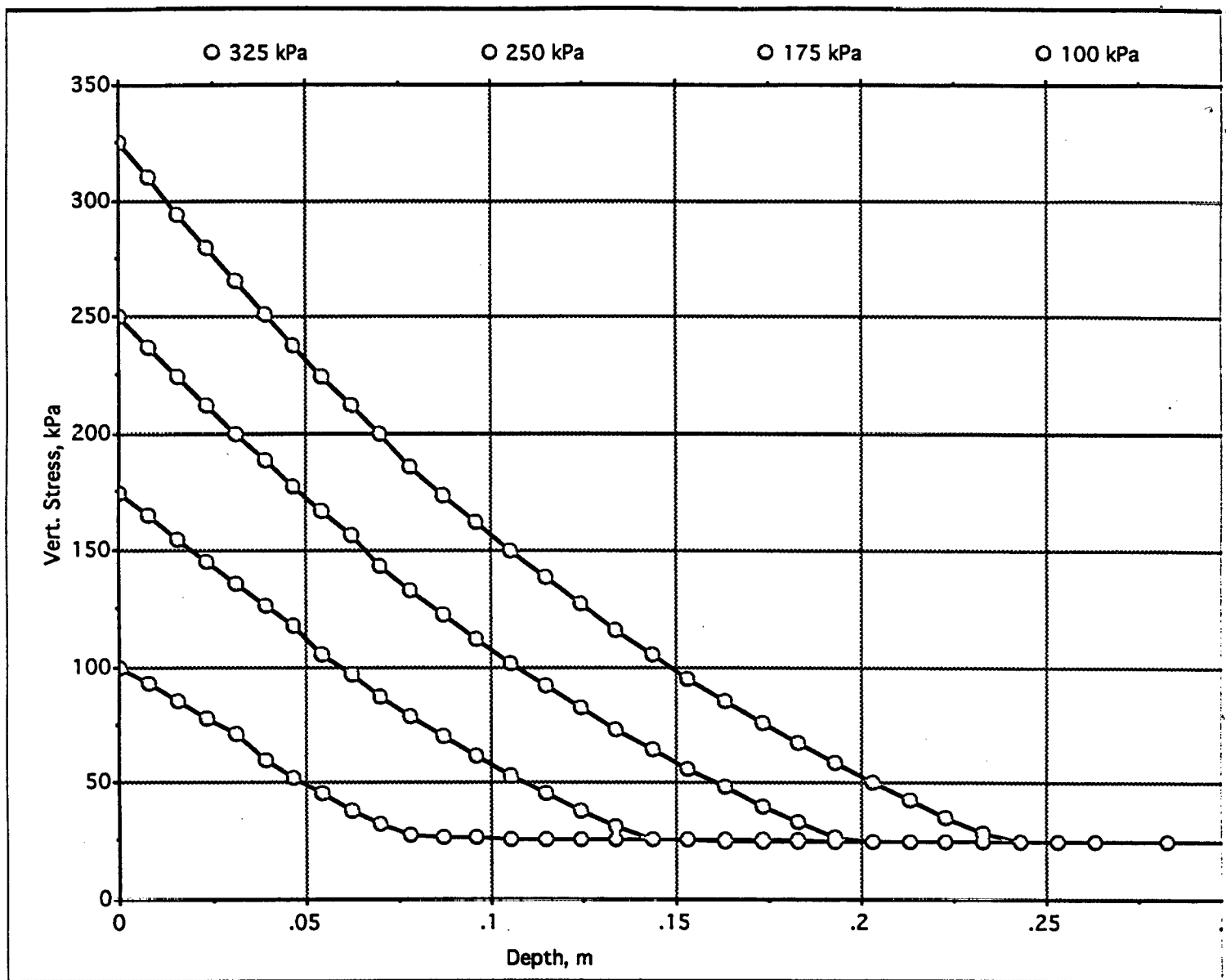


Figure 14: Effect of plate load on the vertical stress as a function of depth.

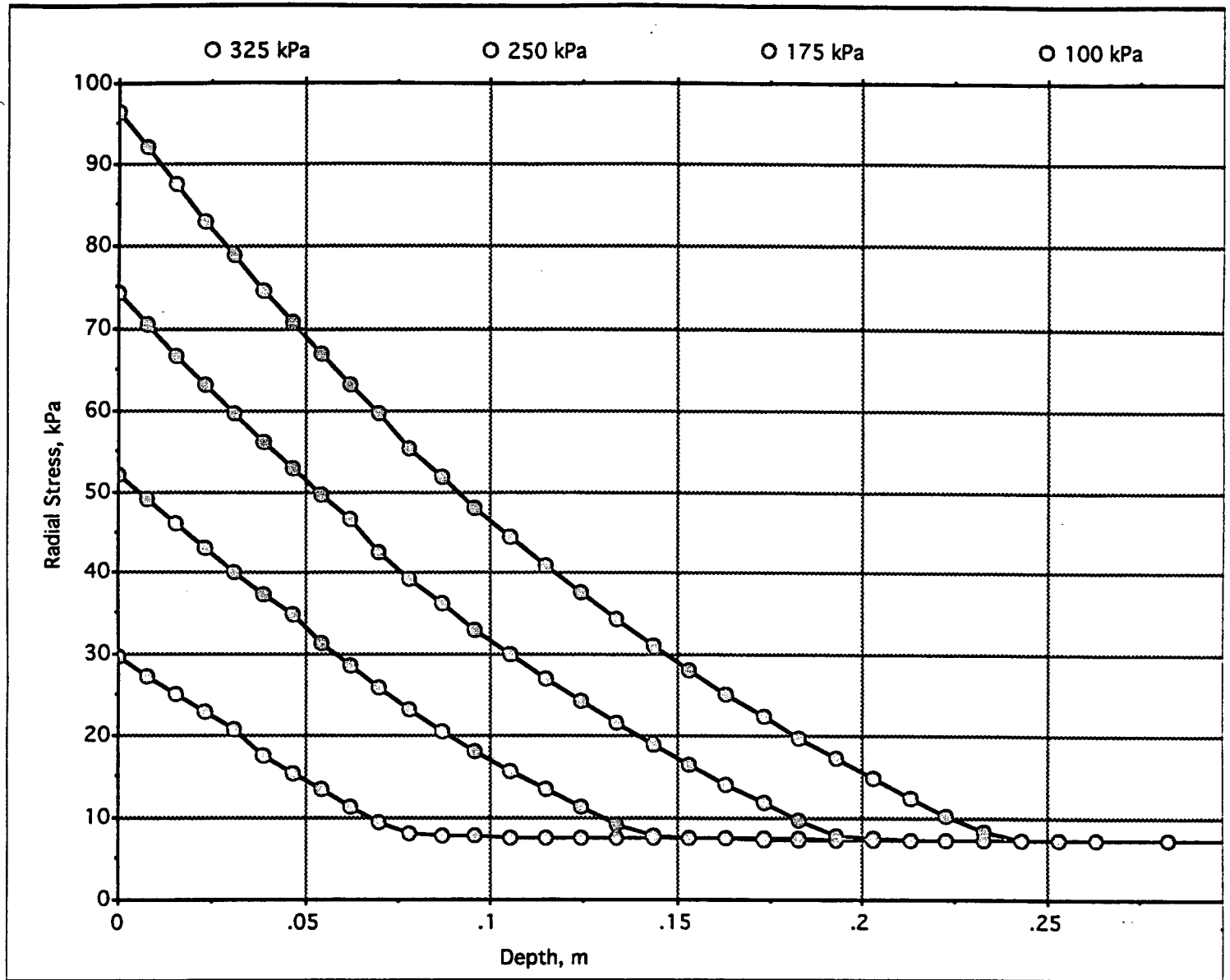


Figure 15: Effect of plate load on the radial stress as a function of depth.

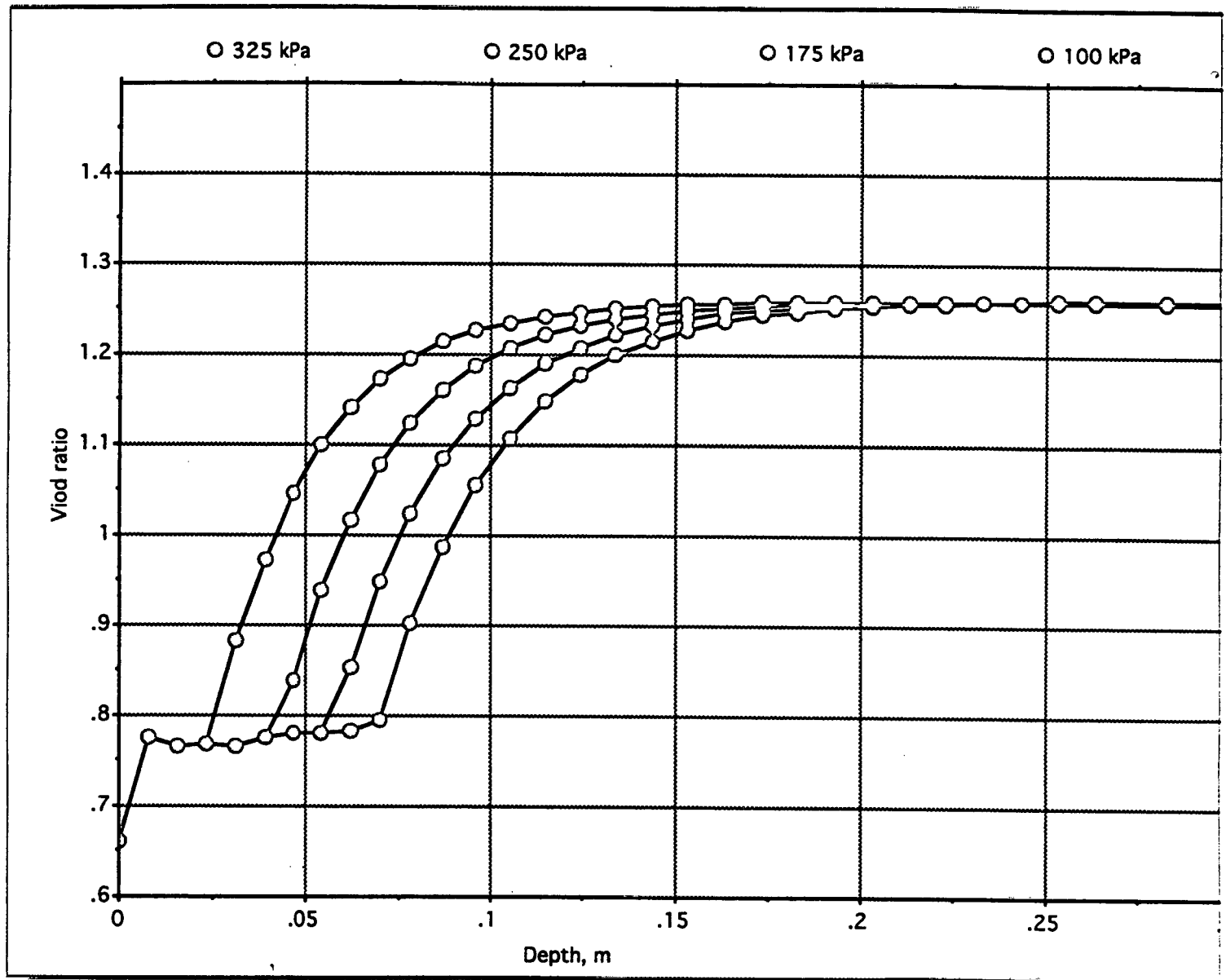


Figure 16: Effect of plate load on the void ratio as a function of depth.

VI. DESCRIPTION OF COOPERATION:

We tried to achieve cooperation between U. S. and Israeli investigators by several means.

These were:

1. Exchange of information by e-mail, FAX, air-mail, and telephone.
2. Meeting held in Israel during Dr. Shrini K. Upadhyaya's visit to Israel.
3. Meeting between investigators during the ICCPAM conference in Bonn, Germany.
4. Meeting held in U.S. during Dr. Wolf and Shmulewich's visit to U. S.
5. Meetings held in Silsoe, U.K. during the International Soil Dynamics Conference.
6. Meetings held between investigators during semi-annual ASAE meeting in the U. S.
7. Dr. Rubinstein visited U.S. and worked on this project with Dr. Upadhyaya and returned to Technion as a faculty member and continued to interact with both UC Davis and Israeli investigators.

VII. EVALUATION OF THE RESEARCH ACHIEVEMENT WITH RESPECT TO THE ORIGINAL RESEARCH PROPOSAL AND ITS OBJECTIVES:

Both Israeli and U. S. investigators have made concerted effort to address all the objectives of the project as originally proposed except the development of an expert system to predict traction-soil compaction tradeoff. As the reviewers of our proposal had suggested we realized that we were overambitious in some of our objectives. At the initial meeting between the U.S. and Israeli investigators it was decided that U.S. investigators will concentrate on the determination of in-situ determination engineering soil properties (secondary objectives 1a and part of 1b), determination of 3-D soil-tire contact profile (secondary objective #2), development of traction prediction models (secondary objective #3), and the Israeli investigators will concentrate on the dynamic aspects of traction

prediction (part of secondary objective #1b), and developing a soil compaction model (secondary objective #4). At the end of second year of the study when Dr. Upadhyaya visited Israel the project status was evaluated and it was decided that dynamic effects were extremely complex and would require much more time and effort to bring to meaningful conclusions. Since even the quasi-static aspects of traction and soil compaction are not well understood, it was thought to be worthwhile to concentrate on the quasi-static aspects. We felt that since most of the agricultural heavy draft operations fall under this category (0 to 5 kmph range), this is an appropriate compromise to make. In view of this, only limited studies were conducted in Israel on the effect of strain rate on soil-tire interaction. It was decided that Israeli investigators will concentrate on the development of traction and soil property test devices (single wheel tester and in-situ soil sinkage and shear tester) and the development of a quasi-static soil compaction model. Rather than critical state concept based soil compaction model which requires a large computer to simulate, a simpler model that can be implemented on a PC would be developed by the U.S. researchers. Moreover, secondary objective #5 would be accomplished by integrating the traction model with the soil compaction. It was also felt that we would not have enough time to accomplish objective #6 as it stands. Instead of an expert system, an user friendly computer program that predicts tractive ability of pneumatic tires would be developed at U. C. Davis. When coupled with the soil compaction program, this results in a traction-soil compaction prediction program. With these in mind, our research evaluation may be summerized as follows:

1. Development and verification of a response surface methodology to determine engineering properties of soil in-situ based on both Drucker-Prager and Critiacl State (Modified Cam clay) soil constitutive model.

2. Development of a semi-empirical traction prediction model for radial ply tires based on extensive field tests in the U.S.
3. Development of a traction prediction model which takes into account dynamic effects (Israel).
4. Development of a single wheel tester and a soil test device which will greatly assist the traction-soil compaction studies in Israel.
5. Development a soil compaction model to predict stresses within the soil as well as changes in the void ratio. The qualitative behavior of this model is fine, however, quantitative behavior needs additional verification.
6. Development of a user friendly traction-soil compaction prediction program which provides several alternatives to predict traction (empirical cone index based to semi-empirical based on traction mechanics and conservation of energy principle to analytical technique). The 3-D analytical traction prediction model is quite intriguing, however, it tends to over predict tractive characteristics of tires. There is a need to develop a calibration technique for this method. The semi-empirical prediction is reasonably good at this point in time.

VIII. CONCLUSIONS:

We have listed our conclusions in the body of the report under each topic addressed. The major accomplishments of this project are the development and verification of the response surface method to determine engineering properties of soil in-situ; development of the semi-empirical traction prediction equations; a traction prediction model that takes into account dynamic effects; developments of a single wheel tester and soil test device in Israel;

development of user friendly traction-soil compaction prediction program which is available for public use.

IX LIST OF PUBLICATIONS:

Presented and published papers:

1. Upadhyaya, S. K., D. Rubinstein, and M. Sime. 1993. An inverse solution technique to determine engineering properties of materials. ASAE Paper 93-1084. ASAE St. Joseph, MI 49085.
2. Rubinstein, D. S. K. Upadhyaya, and M. Sime. 1993. Determination of in-situ engineering properties of soil using response surface methodology. Proceedings of the 11th International Conference of ISTVS, Vol II, page 634-646.
3. Rubinstein, D., S. K. Upadhyaya, and M. Sime. 1993. A response surface methodology for determination of engineering properties of soil in-situ. 5th ICCPAM International Conference, Sept. 6-8, 1993, Bonn, Germany.
4. Rubinstein, D., S. K. Upadhyaya, and M. Sime. 1994. Determination of in-situ engineering properties of soil using a response surface methodology. J. Terramechanics. Vol 31. p67-92.
5. Rubinstein, D., S. K. Upadhyaya, 1994. A response surface methodology for determination of engineering properties of soil in-situ. J. Agrophysics. 8:113-130.
6. Upadhyaya, S. K. 1994. Determination of engineering properties of soil in-situ. Proceedings of the workshop on "modeling the mechanics of off-road mobility" held at the Waterways Experiment Station, Vicksburg, Mississippi, April 5-6, 1994.
7. Sime, M, S. K. Upadhyaya, 1994. Experimental verification of an inverse solution technique developed for parameter estimation. ASAE Paper. 94-1565. ASAE St. Joseph, 49085.
8. Sime, M. and S. K. Upadhyaya. 1995. Development and evaluation of parameter estimation technique using response surface method. Proceedings of the 5th North American ISTVS Conference, May10-12, Saskatoon, SK, Canada. p 249-258.
9. Upadhyaya, S. K., W. J. Chancellor, I. Shmulevich, A. Hadas, and D. Wolf. 1994. A traction soil compaction tradeoff model. Proceedings of the Second International Conference on Soil dynamics, Silsoe, England, p98-100.
10. Upadhyaya, S. K., W. J. Chancellor, I. Shmulevich, A. Hadas, and D. Wolf. 1994. A traction-soil compaction prediction model. ASAE Paper 95-1329. ASAE, St. Joseph, MI 49085.

Manuscript in Preparation:

1. Rubinstein, D., W., S. K. Upadhyaya, and M. Sime. 1995. Evaluation of engineering properties of field soil in-situ using the inverse solution technique. For publication in the J. Terramechanics.
2. Sime, M. and S. K. Upadhyaya. 1995. Experimental verification of the response surface methodology for a Critical State soil constitutive model. For publication in the J. Terramechanics.
3. Upadhyaya, S. K. 1995. Traction-soil compaction prediction model. For publication in Trans. ASAE.

Publications of Israeli Investigators:

Presented Papers:

1. Mussel, U., I. Shmulevich and D. Wolf. 1992. "The effect of dynamically varying velocity on wheel traction". ASAE Summer Meeting, Charlotte, North Carolina. Paper No. 92-1013.
2. Wolf, D., I. Shmulevich and U. Mussel. 1992. "Wheel traction losses on hard soil". ASAE Summer Meeting, Charlotte, North Carolina.
3. Ronai, D., I. Shmulevich, A. Hadas. 1993. "Influence of tire action on top soil compaction". ASAE winter meeting. Chicago, Illinois. Paper No. 93-1540.
4. Ronai, D., I. Shmulevich and Wolf D. 1994. "A new Technion Field Single Wheel Tester". The 25th Israel Conference on Mechanical Engineering, Technion City, Haifa, Israel.
5. Ronai, D., I. Shmulevich and Wolf D. 1994. "A new Technion Field Single Wheel Tester". 2nd International Conference on Soil Dynamics. Silsoe College, Silsoe, Bedford, United Kingdom.
6. Shmulevich, I., Ronai D., and Wolf D. 1994. "A new field single-wheel tester". XII Congress on Agricultural Engineering, World Congress. Milan, Italy. Paper No 94-D-034.
7. Shmulevich, I., U. Mussel and D. Wolf. 1994. "The effect of velocity on wheel performances". XII Congress on Agricultural Engineering, World Congress. Milan, Italy. Paper No 94-D-056.

Accepted papers:

1. Ronai, D., I. Shmulevich. 1995. "Comparative analysis of some soil compaction measurement techniques", International Agrophysics